Hydrodynamic Stability of Boundary-Layer Flows in the Presence of Mass Transfer

Iordan Atanassov Halatchev

Thesis submitted for the degree of

Doctor of Philosophy
in
Applied Mathematics

at

The University of Adelaide

(School of Mathematical and Computer Sciences)

Department of Applied Mathematics

ADELAIDE
UNIVERSITY
AUSTRALIA

December 5, 2000

Dedicated to my parents Anna and Athanas
who taught me the value of knowledge,
and to my brother Krum
for also being one of my dearest friends

Contents

Abstract

The kinetics of non-linear mass transfer and its effect on the hydrodynamic stability of fluid–solid permeable surface, gas–liquid and liquid–liquid systems is presented. A comparative theoretical analysis of the influence of non-linear mass transfer and the Marangoni effect on the heat and mass transfer and the hydrodynamic stability is discussed.

A linear analysis of the hydrodynamic stability of gas–permeable surface systems is undertaken. The problem can be reduced to an eigenvalue one, consisting of an Orr-Sommerfeld type equation coupled to the convection-diffusion equation through the boundary conditions at the permeable surface. Previous studies have ignored the effect of this coupling. The effect of coupling on the stability is studied at different values of the mass-transfer rate and Schmidt number. Comparison with approximate solutions is presented.

The natural asymptotic limit of large Reynolds number and "small" amplitude disturbances of fixed frequency are also considered. Under these assumptions the linearised disturbance equations are governed by the standard triple-deck structure of Smith, and others. The eigenrelation, which determines the stability of the flow, is derived by solving a series of equations in each layer of the triple-deck. Due to the different scales in hydrodynamic and concentration boundary layers the resulting eigenvalue problem must be tackled numerically.

The problem of diffusion induced separation of boundary-layer flows under conditions of interfacial mass transfer is also investigated. A semi-implicit marching algorithm is used to solve the boundary-layer equations over a permeable "slot" through which species diffusion occurs. A simple representation for the mass-transfer parameter is constructed in order to model the presence of the slot (the region of active diffusion) and to ensure that no discontinuities are introduced into the calculations.

It is shown that in the case of diffusion driven boundary-layer flows the streamwise velocity develops an inflection point at some streamwise location downstream, which may result in an early transition from laminar to turbulent flow over the "slot". An inviscid Rayleigh instability analysis over the "slot" is carried out. The magnitude of the mass-transfer parameter required to render an otherwise stable flow inviscidly unstable is determined.

Statement

This work contains no material which has been accepted for the award of any other degree or diploma in any university and that, to the best of my knowledge and belief, contains no material previously published or written by another person, except where due reference has been made in text.

I give consent to this copy of my thesis, when deposited in the University Library, being available for loan and photocopying.

Iordan Atanassov Halatchev
December 5, 2000

List of Publications

The following is a list of publications related to the subject of this thesis along with an article in conference proceedings which has been written during the author's PhD study. The list has been divided into three categories: articles that have been published, articles that are to be submitted and articles which have been printed in the refereed conference proceedings.

Publications in International Journals:

1. C. Boyadjiev, I. Halatchev, B. Tchavdarov, The linear stability in systems with intensive inter-phase mass transfer. Part 1. Gas (liquid) - solid, *Int. J. Heat Mass Trans.*, **39** (1996) 2571-2580.

2. C. Boyadjiev and I. Halatchev, The linear stability in systems with intensive inter-phase mass transfer. Part 2. Gas-liquid, *Int. J. Heat Mass Trans.*, **39** (1996) 2581-2585.

3. I. Halatchev and C. Boyadjiev, The linear stability in systems with intensive inter-phase mass transfer. Part 3. Liquid - liquid, *Int. J. Heat Mass Trans.*, **39** (1996) 2587-2592.

4. C. Boyadjiev and I. Halatchev, The linear stability in systems with intensive inter-phase mass transfer. Part 4. Gas-liquid film flow, *Int. J. Heat Mass Trans.*, **39** (1996) 2593-2597.

5. C. Boyadjiev and I. Halatchev, The mass transfer and stability in systems with large concentration gradients. 1. Mass transfer kinetics, *Int. J. Heat Mass Trans.*, **41** (1997) 936-944.

6. I. Halatchev and C. Boyadjiev, The mass transfer and stability in systems with large concentration gradients. 2. Hydrodynamic stability, *Int. J. Heat Mass Trans.*, **41** (1997) 945-949.

7. C. Boyadjiev and I. Halatchev, Non-linear mass transfer and Marangoni effect in gas-liquid systems, *Int. J. Heat Mass Trans.*, **41** (1997) 197-202.

8. I. Halatchev and J. Denier, Stability of boundary-layer flows under conditions of intensive interfacial mass transfer: the effect of interfacial coupling, *Int. J. Heat Mass Trans.*, (2000) (*accepted*).

In Preparation:

1. I. Halatchev and J. Denier, On diffusion induced separation and inviscid instabilities, *Int. J. Heat Mass Trans.*, (*to be submitted*).

Articles in Conference Proceedings:

1. V. Stamatov, J. Denier, I. Halatchev, K. King and D-K. Zhang, *Mathematical Modelling of Methane Oxidation Caused by a Laser Heated Inert Particle*, In the

Proceedings of The 17th International Colloquium on the Dynamics of Explosions and Reactive Systems (ICDERS 99), July 25 - 30, 1999, Heidelberg, Germany.

Acknowledgement

My supervisor, Dr James Denier, has been guiding me for the past few years. He has been a real inspiration, providing me with knowledge, new ideas and careful criticism. I would like to thank him for his patience, enthusiasm, for being always available for consultation, answering all my questions and for funding my participation at conferences.

During the course of my research, I have attended a number of conferences, workshops and seminars. Thanks particularly to The Department of Applied Mathematics and The Duncan Trust for their financial assistance. I must also acknowledge The University of Adelaide, arguably the best theoretical fluid dynamics environment in Australia, for granting me a University of Adelaide Scholarship for Research and making this research possible.

I would especially like to thank Dr. Peter Gill, the Head of the Applied Mathematics Department at Adelaide University, for his benevolence and friendliness, who has always been willing to help. I am especially grateful to Dianne Parish, for her advice and assistance with administrative matters. I was fortunate to have my fellow students who have been invaluable in helping to sort out computing problems and making the atmosphere at work breathable. My personal gratitude to Dr Paul McCann and Mr David Beard for keeping the workstations steaming. My first mentor on this topic has been Professor Christo Boyadjiev. For his ardent affection for science, lively and uncompromising feedback he must be thanked.

Finally, thanks to my close friends and my long-suffering family who have endured neglect as cheerfully during this project as they have with others in the past. Thank you for your encouragement and support.

Introduction

The latest developments in the chemical engineering, bio-technological and medical equipment industries and the study of kinetics of all processes based on fluid flows through porous media pose the task of devising instruments with high power-to-weight ratio along with the requirement of reducing the equipment size. The most natural way of achieving these goals is the implementation of high mass and heat-transfer rate processes. This can only be achieved through an understanding of the nature of transport phenomena and consequently flow instabilities.

The basic problem of transport phenomena in fluids is usually considered by setting up a macroscopic framework based upon the principles of hydrodynamics and thermodynamics. Any system not in equilibrium will naturally tend towards an equilibrium state. This results in a transport of heat (in the case of thermal equilibrium) or mass (in the case of concentration equilibrium). Since the equilibrium state is characterised by the absence of gradients of the system parameters, a spontaneous process of mass transfer[1] in the non-equilibrium state is due to a concentration gradient acting within the system. The concentration gradient then induces a mass flux through the interface.

The optimal design of equipment which operate under conditions of intense interfacial mass transfer has not been an easy task due to the significant discrepancies between experimentally measured process rates and the rates predicted by the linear theory of mass transfer. The linear theory of mass transfer is characterised by three basic features:

1. The mass-transfer rate does not depend on the direction of mass exchange between phases (for example absorption and desorption rates are equal);
2. The Sherwood number[2] does not depend on concentration;
3. Mass transfer does not influence the hydrodynamics.

The basic reasons for the deviations from the linear theory are the occurrence of several non-linear effects as a result of the gradients of pressure (Stefan flow[3], that is a vapour (gas) flux generated from the gradient of pressure on the interface). This gradient can be considered as a result of phase transition - evaporation, condensation etc. During the phase transition the phase volume changes. The other cause for the pressure gradient can be a chemical reaction on the interface if the volumes of the reactive species and the products of reaction are not equal, i.e. $3H_2 + N_2 = 2NH_3$ (where four volumes give two), density (natural convection), concentration (non-linear mass transfer), and surface tension (Marangoni effect[4]), that is a secondary flow as a result of the gradient

[1]Mass transfer considered as mass in transit as a result of a species concentration difference in a mixture (see Incropera & DeWitt (1990)).

[2]The Sherwood number $Sh = kL/D$ is the dimensionless concentration gradient at the surface and a measure of the convection mass transfer occurring at the surface. Here k is the mass-transfer coefficient, L the characteristic length and D the diffusivity coefficient.

[3]Stefan flow is a special case of diffusiophoresis, with particle motion towards or away from evaporating or condensing surfaces.

[4]The Marangoni effect is a phenomenon whereby movement of the surface of liquid occurs due to

of the surface tension on the gas–liquid or liquid–liquid interface. The cause for this gradient is local differences in surface tension, temperature and/or concentration of the transferred substances. The existence of the temperature and concentration dependencies of the parameters in the equations of momentum, mass and heat transfer, as well as the chemical reactions (especially those of higher order), leads to other types of non-linear effects. All these effects represent the influence of the temperature and concentration on the flow rate of a fluid, in which heat and/or mass transfer takes place. They may occur in two ways. First, the changes in the velocity field lead to changes in the concentration and temperature fields, and therefore to changes in the kinetics of the mass and heat transfer. Second, the change in the velocity field can lead to a loss of stability[5] of the flow, and consequently to the appearance of stable dissipative or turbulent structures. These in turn lead to new mechanisms of heat and mass transfer and to an essential increase of the heat and mass-transfer rate. In most cases, existing models of non-linear processes are treated as a superposition of the linear theory and the separate non-linear effects such as the induction of secondary mass fluxes normal or tangential to the interface and the non-linear effects due to high concentrations and chemical reactions

Mass transfer through an interface is always connected with momentum transfer. In the case of intense interfacial mass transfer however, this momentum transfer is comparable with the basic flow momentum transfer. Thus, the intense interfacial mass transfer induces secondary flow through the surface. According to the non-linear theory of mass transfer the local mass flux I across the interface has both diffusive and convective components

$$I = -MD\frac{\partial c^*}{\partial n} + Mc^* v_n = -\frac{MD\rho^*}{\rho_0^*}\frac{\partial c^*}{\partial n}, \tag{1}$$

where $\rho^* = \rho_0^* + Mc^*$ and c^* are the density and the concentration of the transferred substance through the phase boundary. The derivation of this fundamental equation of mass transport phenomena theory can be found in Bird, Stewart & Lighfoot (1966) (see equation 17.0-1). In (1) the normal component of the velocity of the induced flow on the interface v_n can be defined by the mass flux through the surface as follows (see Incropera & DeWitt (1990))

$$v_n = -\frac{MD}{\rho_0^*}\frac{\partial c^*}{\partial n}, \tag{2}$$

where M is the molecular mass, D is the diffusion coefficient, ρ_0^* is the density of the fluid, $\partial/\partial n$ denotes the derivative normal to the interface. In (2) v_n can be considered as the rate of the Stefan flux but it does not result from a phase transition (see Boyadjiev & Vulchanov (1990)). It has an effect of "suction" or "blowing" from/into the flow depending on the direction of the induced mass flux.

Expression (1) shows that the mass-transfer rate depends on the mass concentration and the concentration gradient on the interface. The influence of the mass concentration at

local differences in the surface tension of the liquid.

[5] Antonyms stability and instability are interchangeable as terms.

the interface in the case of reversible processes is expressed by

$$\frac{\rho^*}{\rho_0^*} = 1 + \frac{Mc^*}{\rho_0^*}. \tag{3}$$

The effect described above is of particular significance when $Mc^*/\rho_0^* > 10^{-2}$. Therefore when the processes are irreversible (i.e. once having taken place they cannot be reversed and in doing so leave no change in either the system or its surrounding) this effect is theoretically absent and in a number of cases (all the processes that cannot be studied as quasi-equilibrium ones) can be considered as negligible.

The new velocity component v_n (in the linear theory of mass transfer $v_n = 0$ on the interface) can then influence both the dynamics and stability of the flow. In this case the velocity vector $\boldsymbol{v}$ depends on the concentration distribution, and the left-hand-side of the convection-diffusion equation

$$\boldsymbol{v}\nabla c = \nabla \cdot (D\nabla c) \tag{4}$$

will be non-linear[6].

The theory of non-linear mass transfer is of practical interest in high intensity heat and mass-transfer processes. Hence, fluid–solid permeable surface, gas–liquid, and liquid–liquid systems will be examined. The results that will be obtained will be of use in the clarification of the physical models and the kinetics of a number of practically interesting processes. For instance, in the cases of intense interfacial mass transfer in electro-chemical systems with high current density, an example of which is the process involving metals in the electrolyte flow, the anode dissolution can increase substantially because of flow turbulation at relatively small values of the Reynolds number[7], while the electro-separation of metals out of concentrated solutions can be implemented under laminar flow conditions at high values of Reynolds number. Intense interfacial mass transfer is also of interest for the process of ablation (for example, a spacecraft descending through the denser atmospheric layers). Intense evaporation of a substance from a solid surface leads to an increase of the heat-transfer coefficients, i.e. to a decrease of the "undesired" heat flux toward the spacecraft (missile) rounded fuselage nose.

The suggestion by Prandtl in 1904 that the fluid motion around objects could be divided into two regions: a thin transition layer close to the object where frictional effects are important, and an outer region where viscosity effects can be neglected, was one of the most important advances in fluid dynamics. This thesis will focus on low-viscosity flows ($\nu \ll 1$) and hence large Reynolds numbers. Therefore, we shall concern ourselves with boundary-layer flows. There are several implications as a result. Firstly, environmental disturbances are present in any flow and these can amplify so as to produce turbulent flow. For small Reynolds numbers viscous effects are sufficient to prevent the amplification of disturbances and a laminar flow is maintained. By increasing the Reynolds number even

[6]Here $\nabla = \partial/\partial x\boldsymbol{i} + \partial/\partial y\boldsymbol{j} + \partial/\partial z\boldsymbol{k}$ is the usual gradient operator in Cartesian coordinates.

[7]Reynolds number $Re = U_\infty L/\nu$ is the ratio of the inertia and viscous forces, i.e. a measure of the relative importance of inertia and viscous forces. Here U_∞ is the free-stream velocity, L the characteristic length and ν the kinematic viscosity.

small disturbances can be amplified to a point where the flow undergoes a transition to turbulence. Secondly, the magnitude of the Reynolds number influences the momentum boundary-layer thickness $\delta_m = O(Re^{-1/2})$. In addition to the momentum boundary layer which determines wall friction, the presence of mass transfer in our studies requires the consideration of the concentration boundary layer. The thickness of the concentration boundary layer is of order $O(Sc^{-1/2}Re^{-1/2})$ where the Schmidt number $Sc = \nu/D$ is the ratio of the momentum and mass diffusivities. The physical interpretation of the Schmidt number is as a measure of the relative effectiveness of momentum and mass transfer by diffusion in the momentum and concentration boundary layers. For gases the value of the Schmidt number is near unity, in which case momentum transfer and mass transfer by diffusion are comparable. It is evident that for liquids where $Sc > 1$ the momentum transfer exceeds the mass transfer by diffusion. In a manner similar to the role of the Reynolds number, the Schmidt number determines the relative thickness of the momentum and concentration boundary layers - for gases they are comparable and for liquids the momentum boundary-layer thickness is larger than the concentration boundary-layer thickness $\delta_c = O(Sc^{-1/2}Re^{-1/2})$.

Broadly speaking, we say that instability problems are concerned with the behaviour of systems when there is some disturbance to their equilibrium state (equilibrium of the external forces, inertia and viscous stresses of a fluid). The behaviour then depends on the system's stability. In the case of mass transfer dominated systems the induction of the secondary flow changes the velocity profiles in the boundary layer, and hence its hydrodynamic stability properties.

In this thesis, the problems to be considered are set up by studying the laminar flow of a viscous incompressible fluid over a flat, semi-infinite, permeable plate across which a concentration gradient exists or across a movable interface in the case of a two-phase system. The problem of the onset of instability will be examined by making one simplification. First, the physical mechanism regarding mass fluxes and concentration gradients will be somewhat simplified. Certainly the most important contribution to the mass flux is that resulting from the concentration gradient (see Bird, Stewart & Lightfood (1966)). We shall neglect the other two "mechanical driving forces" - the pressure gradient and external forces, such as gravity, electro-magnetic field etc., acting unequally on the various chemical species. According to the theory of the thermodynamics of the irreversible processes, the whole mechanism is not as simple as stated above and there will be a contribution to each flux due to each driving force in the system. In this sense we shall base our work on the assumption that the mass flux is a result only of a concentration gradient. This allows us to simplify our discussions and to focus upon the most important effect, namely the effect of the diffusion induced, normal flux on the hydrodynamic stability of the boundary-layer flow.

The influence of intense interfacial mass transfer on the hydrodynamic stability of the boundary-layer flow is even more interesting for systems with movable interface (gas–liquid, liquid–liquid). A study to examine the effect of such a movable interface will be done. Interaction between boundary-layer flows in gas and liquid will be considered; we shall focus on the dominant effect of the diffusion induced mass transfer, i.e. excluding

the interfacial instabilities. Here the effect of induction of secondary flows as a result of intense interfacial mass transfer in the gas–liquid system will be studied, together with the hydrodynamic interaction between the above mentioned two phases (only through the basic velocity and concentration fields). In the case of liquid–liquid systems the influence of the mass transfer on the hydrodynamic stability is analogous to the case of a motionless interface, but now depending on the distribution of the diffusive resistance in both phases. The mass-transfer kinetics and instabilities of the flow under these conditions is not only of theoretical interest, but also of practical interest in view of the fact that they define the rate of a number of industrial absorption and desorption processes, for example the absorption of pure CO_2 in H_2O.

Experimental studies of systems under conditions of large concentration gradients show that the density, viscosity and diffusivity coefficients are functions of the concentration. The effect of these functional dependencies upon the mass-transfer kinetics and flow stability will be evaluated.

A comparative analysis of the influence of the effects of the mass transfer and the Marangoni effect on the transfer kinetics and hydrodynamic stability of the flow will be investigated. As has been mentioned above the Marangoni effect is a phenomenon where a normal mass flux occurs on the interface due to local differences in the surface tension of the liquid. Co-current gas and liquid flows in a laminar boundary layer along a flat semi-infinite interface surface will be considered. The gas component is absorbed by the liquid and reacts with the liquid component. The chemical reaction rate will be taken to be of first-order. The heat effect from the chemical reaction creates a temperature gradient, so that the mass transfer is accompanied by heat transfer. Data for heat and mass-transfer coefficients will be obtained as well as the critical Reynolds numbers and the corresponding critical wave-numbers and frequencies (or wave-speeds).

A further study of fluid–permeable surface systems is proposed which is mainly motivated by a desire to remove a simplification made in the aforementioned studies (see Boyadjiev & Halatchev (1996a,b,c) and Halatchev & Boyadjiev (1996)). This simplification employed in earlier works was based upon the fact that the inhomogeneous boundary condition on the vertical disturbance velocity component contains a term proportional to the mass-transfer parameter and the reciprocal of the Reynolds number. It was argued that even for moderate values of the Reynolds number and "small" mass-transfer parameter, this term would be small and hence that the inhomogeneity could be ignored. In this case, the only way the mass transfer can affect the boundary-layer flow is through its influence on the basic flow, changing the shape of the velocity profile and hence its stability properties. We shall determine the realm of validity of this assumption, and the range of critical parameters (namely the Schmidt number) where it cannot be applied. Thus, the correct critical values of Reynolds number will be obtained.

Further we will obtain an analytic solution to the problem which presents itself in the high Reynolds number limit. We shall restrict our attention to "small" amplitude disturbances of fixed frequency. Under this assumption the linearised disturbance equations are governed by the standard triple-deck structure (see Smith (1979a)). By solving a se-

ries of equations in each layer of the triple-deck, the eigenrelation (which determines the stability of the flow or the position of neutral stability) will be derived. A close examination of the equations, and the corresponding boundary conditions, within the lower deck of the triple-deck, will demonstrate that the vertical momentum and concentration are coupled, the magnitude of this coupling being dependent upon the magnitude of the concentration gradient across the permeable boundary. The curves of neutral stability will be obtained. The first-order correction to the neutral stability frequency and wavenumber, as functions of the mass-transfer parameter, will be determined for different values of the Schmidt number.

In order to maintain unseparated (or attached) flow severe restrictions must usually be placed upon the flow parameters; in many cases these restrictions lay outside the normal operating envelope of the particular device. The early onset of flow separation, resulting in a closed region of re-circulating fluid, can have a significant detrimental effect in devices where mixing is the desired outcome. Typically, fluid is entrained within the separation bubble (that is, the zone of flow recirculation) that can arise when a boundary-layer flow separates and as such it does not mix with the bulk of the flow. The problem of the onset of flow separation is of vital importance in the study of boundary-layer flows which arise in modern industrial applications. For example, in areas such as electro-dialysis applications, the early onset of flow separation must be controlled in order to adequately control mixing within the flow. Another interesting practical aspect is the use of diffusion induced "blowing" as a means of effecting an increase in heat transfer from a hot surface to a cooler fluid. Our concern is with the effect of diffusion driven secondary fluxes, induced by the presence of large concentrations gradients, on the boundary-layer flow which arises when an almost inviscid fluid flows over a permeable surface through which another fluid (or gas) diffuses.

In general, separation occurs in boundary-layer flows under an imposed adverse pressure gradient (see Chang (1970)). Under the influence of the adverse pressure gradient the fluid elements moving inside the boundary layer, having a smaller amount of kinetic energy than the elements of the outer flow, decelerate more strongly, leading to a gradual change in the velocity profile in the boundary layer. At some local streamwise position the skin friction becomes zero and further downstream a region of slow reversed flow appears, which expands rapidly, moving fluid elements from the boundary layer to finite distances from the body surface.

We shall consider the problem of diffusion driven boundary-layer flow separation, excluding from our study one of the causes of flow separation, the pressure gradient. Therefore we focus our attention on a boundary-layer flow under conditions of intense interfacial mass transfer with zero pressure gradient. This will be done not only for the purpose of simplifying the problem, but to study the effect of the induced secondary flow, due to a concentration gradient (diffusion in our case), acting normal to the streamwise direction of the boundary-layer flow. To overcome the inevitable difficulties connected with the presence of different scales, within which the relative importance of diffusivity over viscosity is to be accounted for, we shall consider only the case of flow separation along a gas–permeable surface for which the Schmidt number $Sc = 1$. In contrast to previous

studies of a boundary-layer flow under conditions of intense interfacial mass transfer (see Hartnett & Eckert (1957), Boyadjiev, Halatchev & Tchavdarov (1996) and Halatchev & Denier (2000)) we consider a finite mass-transfer region, this being a more realistic model for many mass-transfer (diffusion) dominated flows. The detachment of the boundary-layer flow is a result of the shifting of the fluid elements in the boundary layer far from the surface (membrane) due to the diffusion induced vertical velocity component on the surface.

Prior to separation the diffusion driven flow develops (what is termed) a point of inflexion and as such will become susceptible to the high frequency, short wavelength, instabilities known as Rayleigh waves. These waves are known to provide one route for the rapid onset of turbulence in the flow. We will study the level of diffusion required to render an otherwise stable flow inviscidly unstable. The stability aspects of this flow will be considered by solving the Rayleigh pressure equation numerically, employing a global solver for complex eigenvalue problems, to determine the growth rate at selected streamwise locations over the slot region. This will allow us to determine the point at which the flow becomes unstable in terms of the level of mass transfer through the slot. Ultimately the outcome of this study will be the development of techniques which will allow for the prediction and active control of instability in the flow.

Finally, we should draw our attention back to the two-fluid problem. The linear stability analysis of two-fluid systems in this thesis is limited to an immobile interface and the criteria for flow instability of a horizontal interface between two liquids is not firmly established in Chapter 2. This limitation was motivated firstly by the complexity of the real problem and secondly by a desire focus on the dominant effect of intense interfacial mass transfer. There are several attempts, from the hydrodynamic point of view, to examine some aspects of the boundary-layer flow instabilities in the cases of gas–liquid (see Boyadjiev & Halatchev (1996b)), liquid–liquid (see Halatchev & Boyadjiev (1996)) and gas–liquid film–solid surface systems (see Boyadjiev & Halatchev (1996c)). The full, complete solution of these problems is yet to be presented; the interface has been considered rigid, thus restricting attention to the effect of mass transfer and not considering the possibility of interfacial instabilities. However, in the last section of this thesis (see Future Work) the governing disturbance equations and their boundary conditions are derived for the general problem of interfacial instabilities. Their solution, is however, outside the scope of this thesis. Such a study provides a good starting point for future analysis.

Historical Survey

Many experimental studies show that the linear models of mass transfer fail to capture the true physics of mass transfer processes. Several references (see Grassman & Anders (1959), Sterling & Scriven (1959), Ruckenstein & Berbente (1964), Linde, Schwartz & Gröeger (1967), Thomas & Nicholl (1969) and Ramm (1976)) indicate an influence of the direction of interfacial mass transfer on the mass-transfer rate at the interface. The dependence of the Sherwood number on the concentration has been noted in a number of cases, particularly when the mass transfer is accompanied by a chemical reaction (see Astarita (1967)). Most often the deviations of the experimental data from the linear theory arise in cases when the mass-transfer rate increases, which can be partially explained by spontaneous (surface, or interfacial) turbulence, the Marangoni effect, or self-organising dissipative structures (see Sterling & Scriven (1959), Brian, Vivian & Matiatos (1967), Linde, Schwartz & Groeger (1967), Thomas & Nicholl (1969) and Porter, Cantwell & McDermott (1971)). All deviations of the experimental data from the predictions of the linear theory of mass transfer, mentioned above, are a result of different non-linear effects. The problem of non-linear mass transfer appears in connection with the examination of systems with intense mass transfer. A series of non-linear effects in the mass-transfer kinetics occur under these conditions as a result of the development of large concentration gradients in the transferred substance. These effects have various manifestations, but their influence on the mass-transfer rate can always be regarded as interconnected. Theoretical analysis of the mass-transfer kinetics permits the identification of a number of main effects, which differ from one another in principle. According to Boyadjiev & Babak (2000) some of them can be regarded as quantitative only, i.e. having an impact on the mass-transfer rate, and qualitative effects which are of greatest interest because they influence the mass-transfer mechanism.

The case when the dependence of the mass flux density on the concentration gradient of the transferred substance is non-linear could be considered as the first example of a non-linear effect. Under these conditions models are usually used, where the diffusivity coefficient depends on the concentration of the transferred material (see Bird, Stewart & Lightfoot (1966)), i.e. the Fick's law[8] is non-linear. This non-linear effect is significant in liquid systems, but not in gases because the diffusivities of gases at low densities are almost composition independent, increase with temperature, and vary inversely with pressure, while liquid diffusivities are strongly concentration dependent and generally increase with temperature (see Bird, Stewart & Lightfood (1966)). For the purposes of engineering calculations this effect can be accounted for by the relationship between the chemical reactivity and the concentration of the transferred substance, if the chemical potential gradient is added into Fick's equation (see Sherwood, Pigford & Wilke (1975)).

Another non-linear effect, which also shows up when the concentration gradients are not

[8]Fick's first law of diffusion, written in terms of molar diffusion flux ($J_A^* = -kD_{AB}\nabla c_A$), where k is a proportionality coefficient and c is concentration, states that species A diffuses in the direction of decreasing mole fraction of A, just as heat flows by conduction in the direction of decreasing temperature; Fick's second law of diffusion is simply the diffusion equation (see Bird, Stewart & Lightfood (1966)).

very large, is connected with the dependence of the viscosity on the concentration of the transferred material. This effect influences the convective mass transfer in liquids (including those with complex rheology), but its impact on the mass-transfer rate is not strong enough to change the mass-transfer kinetics in a qualitative way. Thus, for instance, it has been shown in Boyadjiev (1984) that taking into account the dependence of the viscosity and the diffusivity coefficients on the concentrations does not lead to a change in the mass-transfer mechanism.

From theoretical and practical points of view the most interesting non-linear effect is associated with the initiation of a secondary flow under conditions of intense interfacial mass transfer, that is of a new mass flux which takes part in the overall balance of the transferred substance, thus changing the mass-transfer mechanism (see Boyadjiev & Beshkov (1984)). This non-linear effect has various manifestations, the most interesting being the impact of the direction of the intense interfacial mass transfer on the rates of mass transfer, heat transfer and multi-component mass transfer. The secondary flows at the phase boundary can be normal (non-linear mass-transfer effect) or tangential (the Marangoni effect).

Another effect of interest is connected with the existence of a non-linear source or sink of the diffusing substance as a result of chemical reactions in the volume of the phases (liquid, gas). The influence of this non-linearity can be regarded as a qualitative effect, so far as the non-linearity of the chemical reactions kinetics changes the mass-transfer mechanism significantly as in an Arrhenius reaction, as occurs in the case of combustion.

The non-linear effects in systems with intense interfacial mass transfer lead to changes in the hydrodynamics of the systems and their stability. In work by Boyadjiev, Halatchev & Tchavdarov (1996a) the hydrodynamic stability of systems under conditions of intense interfacial mass transfer, in fluid–solid permeable surface systems, was studied. A laminar flow of a viscous incompressible fluid over a flat, semi-infinite, permeable plate across which a concentration gradient exists, was considered. A simplified assumption that the mass transfer is a result only of a concentration gradient was employed. The concentration gradient induces mass flux through the interfacial boundary which has an effect of "blowing", or "suction", in/from the boundary layer depending on the direction of the mass transfer. The flow was assumed to be nearly parallel and the stability properties governed by the classical Orr-Sommerfeld eigenvalue problem. The Orr-Sommerfeld equation was solved numerically to determine the critical Reynolds number and wave-numbers of the flow at different mass-transfer rates and Schmidt numbers.

The extension to gas–liquid and liquid–liquid systems was considered in the studies by Boyadjiev & Halatchev (1996b,c). In the former, the diffusion acts from the gas to the liquid whereas in the latter diffusion of different species can occur between both liquid phases. The onset of instability was examined and the critical system parameters were determined. Results for the flow in a gas-liquid film–solid surface systems were presented in the work by Halatchev & Boyadjiev (1996). This work demonstrated that the influence of a tangential velocity at the interface on the stability of the gas phase (that is, the upper, less dense fluid) was significant.

A theoretical analysis of the effect of a large concentration gradient on mass-transfer kinetics was done in the study by Boyadjiev & Halatchev (1998b). Under conditions of large active concentration gradients the density, the viscosity and diffusivity coefficients are functions of the concentration. The results show that the change in the density with the concentration affects the stability of the flow in gases and liquids but has no impact on the mass transfer in gases. The change in the viscosity with the concentration influences the stability and the mass transfer in both gases and liquids. It was shown that the non-linear theory of mass transfer, at constant values of the density, viscosity and diffusivity, is of sufficient accuracy to describe the mass-transfer kinetics in gases and liquids if the densities of the transfered substance and the gas (or liquid) mixture do not differ significantly. An analysis of the influence of large concentration gradients on the stability[9] of systems under conditions of intense interfacial mass transfer was considered in the work by Halatchev & Boyadjiev (1998). The results show that the inclusion of the dependence of the density on concentration acts to stabilise the flow. The decrease in the concentration gradient leads to a decrease of stability. It was shown that in the cases where an increase of concentration leads to an increase of viscosity one can observe an increase in the stability of the flow, while changes in diffusivity do not influence the stability of the flow. This was extended by Boyadjiev & Halatchev (1998a) to consider the effect of surface tension.

In the aforementioned studies on flow instability the effect of coupling between the momentum and concentration disturbance equations was largely ignored. This was done on the supposition that, even for moderate values of the Reynolds number and small mass-transfer parameter, the inhomogeneity in the wall boundary condition for the vertical disturbance velocity could be safely ignored. Also the mass-transfer parameter in this term was considered to be "small" while still regarding the mass-transfer processes as intense. In essence this assumes that mass transfer can affect the boundary-layer flow through its influence on the basic flow, changing the shape of the velocity profile and hence its stability properties. In the study by Halatchev & Denier (2000) (see Chapter 4) we remove this approximation by solving the fully coupled system describing the disturbance amplitude; this consists of a fourth-order Orr-Sommerfeld equation and second-order concentration equation. This was done by developing a new numerical scheme that was able to account for the coupling in these equations in the boundary conditions at the permeable surface. We were able to determine the correct values of the critical Reynolds number and wavenumber and carry out an exhaustive parameter study, in terms of Schmidt number and mass-transfer rate. Comparison with the earlier approximate solutions suggests that they do remain valid for a relatively large Schmidt number; at $Sc = 100$ the difference between the exact and approximate being less than a few percent and therefore provide a useful engineering approximation for these complex flows.

Although there are numerous studies into the phenomenon of flow separation, either self-induced or by blowing into the boundary layer, little has been done on the problem of flow separation induced by diffusion through a permeable surface. Early work

[9] Stability with respect to Tollmien-Schlichting waves and not interfacial instabilities.

on the problem of mass transfer, or transpiration, induced cooling was reported by Hartnett & Eckert (1957). They considered solutions of the Falkner-Skan equations, which describe the self-similar boundary-layer flow over a wedge whose angle β is given by $\pi\beta = 2m/(m+1))$ with corresponding streamwise velocity x^m. They were able to demonstrate that there is a critical level of mass transfer at which the boundary layer will "blow-off" from the surface; in this case the similarity solution satisfies $\overline{u}_y = 0$ at $y = 0$ and $u = 0$ for any finite y. Of course, such a result indicates that the similarity form of solution to the boundary-layer equation does not adequately describe the state of the boundary layer as the level of mass transfer approaches its critical value. This early work was also summarised by Gadd, Jones & Watson (1963).

The restriction to self-similar flows was removed in Catherall, Stewartson & Williams (1965) where the boundary-layer equations were solved in their primitive, partial differential equation form, for the case of a constant blowing velocity prescribed on the surface of a flat plate. In this case the flow separates at a particular streamwise location, and associated with the point of separation is a singularity in the boundary-layer equations. Klemp & Acrivos (1972) provided a rational expansion to describe the injection region. A very systematic account of more recent studies can be found in surveys by Stewartson (1974), Smith (1982), Brown (1996) and Sychev, Ruban & Sychev (1998). In the recent work of Roy (2000), a non-uniform slot injection into a compressible flow was studied, where mass injection occurs in a small porous section of the body surface. Here, we focus our attention on a boundary-layer flow under conditions of intense interfacial mass transfer with zero pressure gradient. We choose the case of the flat plate (zero streamwise pressure gradient) boundary layer in order to allow us to focus on the effect of the secondary fluxes induced by a concentration gradient (i.e. diffusion in our case), acting normal to the streamwise direction of the boundary-layer flow. We consider only the case of gas–permeable surface ($Sc = 1$). In contrast to the previous studies of a boundary-layer flow under conditions of intense interfacial mass transfer Hartnett & Eckert (1957), Boyadjiev *et. al.* (1996a), Halatchev & Denier (2000) we consider a finite mass-transfer region. It is shown that diffusion induced boundary-layer separation can occur if the level of mass transfer is suitably large (see Chapter 6).

The Structure of This Thesis

This thesis presents studies of the non-linear mass-transfer kinetics and a linear analysis of the hydrodynamic stability of systems under conditions of intense interfacial mass transfer. The thesis has been divided into two parts.

Part I presents my previous studies on this problem. It is concerned with the kinetics of the non-linear mass transfer of systems under conditions of intense interfacial mass transfer and a linear analysis of the hydrodynamic stability of these systems.

The asymptotic theory of non-linear mass transfer is presented in Chapter 1. It gives a brief introduction to the mathematical models used in the theory of non-linear mass-transfer kinetics of fluid–solid permeable surface, gas–liquid, liquid–liquid systems and multi-component interfacial mass transfer. The presence of a large concentration gradient through the phase boundary induces a normal secondary flow (having an effect of "suction", or "blowing", from or into the boundary-layer flow). Its influence on the mass-transfer kinetics is discussed. A comparative analysis of the linear and non-linear mass-transfer theories is done.

The above mentioned secondary flow affects the basic velocity profiles of the boundary layer, serving to stabilise or destabilise the flow. In Chapter 2 this effect is studied under the approximation of the linear theory of hydrodynamic stability. Here we make use of the simplifying assumption that a linearisation in the boundary condition for the vertical velocity component of the disturbance at the interface is appropriate. This leads to a decoupling of the disturbance equations, leaving the need to solve the classical Orr-Sommerfeld eigenvalue problem. The effect of the mass transfer on the hydrodynamic stability of the flow is therefore present only through its influence on the basic flow. The fluid–solid permeable surface is studied as well as gas–liquid, liquid–liquid systems.

The work of Chapter 2 also employs the assumption that the density, viscosity and diffusivity do not depend on the concentration. However, it is very well known that when there is a significant variation in concentration the dependences of fluid properties on the concentration of introduced species should not be ignored. This additional effect is taken into account in a first-order approximation in Chapter 3. The first part ends with some conclusions drawn from the results presented.

Part II of this thesis consists of a further analysis of the linear stability of fluid–permeable systems, a study of flow separation of diffusion driven boundary layers and the inviscid Rayleigh instability analysis of this boundary-layer flow. The transport phenomena is studied in terms of permeability.

The simplification which led to decoupling of the disturbance equations is removed in Chapter 4. The numerical algorithm to solve the fully coupled disturbance equations, consisting of the Orr-Sommerfeld equation and the convection-diffusion equation, is presented. The critical Reynolds numbers are obtained and these are compared with the results of early chapters, showing the realm of validity of the previous approach.

The linear lower-branch stability of a Blasius boundary-layer flow under conditions of

intense interfacial mass transfer is discussed in Chapter 5. The natural asymptotic limit of large Reynolds number is considered. The linearised disturbance equations are governed by the triple-deck structure of Smith. The modified eigenrelation for this problem is obtained.

A different aspect of boundary-layer theory, namely the effect of mass transfer on flow separation, is studied in Chapter 6. We examined a Blasius boundary-layer flow over a semi-infinite plate with a porous section. The mass transfer acts in a finite region (throughout this thesis we will employ the term "slot"). A semi-implicit marching algorithm and a simple mass-transfer parameter representation were employed. The level of mass transfer at which this diffusion driven flow separates is investigated. Also the inviscid instability analysis of this flow is presented and the stability properties determined. The second part concludes with a discussion of the results obtained together with some suggestions for future work on these interesting problems.

Part I

MASS TRANSFER AND STABILITY

Chapter 1

Boundary-Layer Flows and the Asymptotic Theory of the Non-linear Mass Transfer

Many experimental studies (see Linde, Schwartz & Gröeger (1967), Thomas & Nicholl (1969) and Ramm (1976)) of systems under conditions of intense interfacial mass transfer show significant deviations from the linear theory of mass transfer, which assumes the independence of the velocity field from the concentration and temperature fields. These deviations have usually been considered as Marangoni type effects (see Sorensen (1979), Boyadjiev & Toshev (1989)), i.e. the appearance of tangential secondary flows at the interface boundary, induced by the gradient of surface tension due to local differences in surface tension, concentration or temperature.

Theoretical studies of systems under conditions of intense interface mass transfer as a result of large concentration gradients (see Vulchanov & Boyadjiev (1990), Boyadjiev & Babak (2000)) show that large concentration gradients induce secondary flows normal to the interface. On this basis, a non-linear theory of mass transfer has been constructed. This theory provides a satisfactory explanation of the deviations of the experimental results from the linear theory of mass transfer.

In the limit of large Reynolds numbers $Re \gg 1$, as naturally occurs in the flow of an almost inviscid fluid over a rigid surface, the flow develops a boundary layer. Historically, the boundary layer concept evolved from the attempts to solve the Navier-Stokes equations for general flows, by assuming reasonable simplifications. Neglecting the terms with the Reynolds number Re in the Navier-Stokes equations, which seems the easiest and safest approach leads back to the inviscid flow equations, which cannot predict drag or mass and heat transfer. Prandtl (1904) was the first to realise that for high-Reynolds-number flows, viscous effects are confined to a thin layer along a solid surface. This boundary layer is necessary to allow the velocity to adjust from relatively high values out in the free-stream down to zero on the surface (the no-slip condition). This produces large gradients and therefore significant shear forces even for low-viscosity flows. Outside the boundary layer

the flow behaves in an essentially inviscid manner. By analogy a concentration boundary layer must develop if the free-stream and surface concentrations differ; the same applies to the thermal boundary layer. Although these layers are very thin relative to the total flow field they cannot be neglected because all momentum, heat and mass transfer take place through them.

1.1 Mass transfer in fluid–solid permeable surface systems

The kinetics of non-linear mass transfer will be demonstrated for the case of a Blasius boundary-layer flow over a semi-infinite, flat, permeable plate across which a concentration gradient exists (see Boyadjiev & Vulchanov (1988)). This model can describe, for example, the flow of species with different surface and free-stream concentrations, as occurs in a binary mixture of chemical species A and B flowing over a porous surface. For simplicity, we assume that there is no chemical reaction and no external forces acting on the flow, and we neglect emission and absorption of radiant energy into the boundary layer (see Bird, Stewart & Lightfoot (1966)).

A schematic picture of the flow is given in Figure 1.1. In the absence of disturbances a steady concentration boundary layer develops along with the steady velocity (or momentum) boundary layer. The governing equations describing the problem consists of the steady Navier-Stokes equations coupled to the convection-diffusion equation

$$\begin{aligned}
\frac{\partial U_0}{\partial x}+\frac{\partial V_0}{\partial y} &= 0,\\
U_0\frac{\partial U_0}{\partial x}+V_0\frac{\partial U_0}{\partial y} &= -\frac{1}{\rho_0^*}\frac{\partial P_0}{\partial x}+\nu\left(\frac{\partial^2}{\partial x^2}+\frac{\partial^2}{\partial y^2}\right)U_0,\\
U_0\frac{\partial V_0}{\partial x}+V_0\frac{\partial V_0}{\partial y} &= -\frac{1}{\rho_0^*}\frac{\partial P_0}{\partial y}+\nu\left(\frac{\partial^2}{\partial x^2}+\frac{\partial^2}{\partial y^2}\right)V_0,\\
U_0\frac{\partial C_0}{\partial x}+V_0\frac{\partial C_0}{\partial y} &= D\left(\frac{\partial^2}{\partial x^2}+\frac{\partial^2}{\partial y^2}\right)C_0,
\end{aligned} \tag{1.1}$$

with the initial and boundary conditions

$$(U_0,V_0)=(U_\infty,0),\ C_0=\bar{C}_\infty,\ P_0=0 \ \text{ at } x=0; \tag{1.2a}$$

$$U_0=0,\ V_0=-\frac{MD}{\rho_0^*}\frac{\partial C_0}{\partial y},\ C_0=\bar{C}_0^* \ \text{ at } y=0; \tag{1.2b}$$

$$U_0\to U_\infty,\ C_0=\bar{C}_\infty \ \text{ as } y\to\infty. \tag{1.2c}$$

We shall focus our attention on the boundary-layer flow, thus the following momentum

and concentration boundary-layer approximations will be substituted into (1.1) and (1.2):

$$\begin{aligned} U_0 &\gg V_0, \\ \frac{\partial U_0}{\partial y} &\gg \frac{\partial U_0}{\partial x}, \frac{\partial V_0}{\partial y}, \frac{\partial V_0}{\partial x}, \\ \frac{\partial^2 V_0}{\partial x \partial y} &\approx \frac{\partial^2 U_0}{\partial x^2} \ll \frac{\partial^2 U_0}{\partial y^2}, \\ \frac{\partial^2 V_0}{\partial x^2} &\ll \frac{\partial^2 V_0}{\partial y^2}, \\ \frac{\partial C_0}{\partial y} &\gg \frac{\partial C_0}{\partial x}. \end{aligned} \tag{1.3}$$

The mathematical model for this case reduces to

$$\frac{\partial U_0}{\partial x} + \frac{\partial V_0}{\partial y} = 0, \tag{1.4a}$$

$$U_0 \frac{\partial U_0}{\partial x} + V_0 \frac{\partial U_0}{\partial y} = \nu \frac{\partial^2 U_0}{\partial y^2}, \tag{1.4b}$$

$$\frac{\partial P_0}{\partial y} = 0, \tag{1.4c}$$

$$U_0 \frac{\partial C_0}{\partial x} + V_0 \frac{\partial C_0}{\partial y} = D \frac{\partial^2 C_0}{\partial y^2}, \tag{1.4d}$$

with the initial and boundary conditions

$$x = 0: \quad U_0 = U_\infty, \; C_0 = \bar{C}_\infty; \tag{1.5a}$$

$$y = 0: \quad U_0 = 0, \; V_0 = -\frac{MD}{\rho_0^*} \frac{\partial C_0}{\partial y}, \; C_0 = \bar{C}^*; \tag{1.5b}$$

$$y \to \infty: \quad U_0 \to U_\infty, \; C_0 = \bar{C}_\infty, \tag{1.5c}$$

where U_∞ is the free-stream velocity, $\bar{C}_\infty$ the concentration of the free-stream and $\bar{C}^*$ the concentration on the interface. Let us suppose that there is a rapid establishment of thermodynamic equilibrium so that the concentration $\bar{C}^*$ is always a constant on the solid, permeable surface. The thickness of the concentration boundary layer δ_c is typically defined as $(\bar{C}^* - C_0)/(\bar{C}^* - \bar{C}_\infty) = 0.99$. Species transfer by diffusion between the surface and free-stream fluid is determined by conditions in this boundary layer. The molar flux associated with species transfer by diffusion is given by Fick's law, hence, the normal component of the velocity at the interface is determined from the equation (2 p.xv), corresponding to an intense interfacial mass transfer

$$V_0(x, 0) = -\frac{MD}{\rho_0^*} \left(\frac{\partial C_0}{\partial y} \right)_{y=0}. \tag{1.6}$$

The average rate of mass transfer for a plate of length L can be determined from the average mass flux

$$J = Mk(\bar{C}^* - \bar{C}_\infty) = \frac{1}{L} \int_0^L I \, \mathrm{d}x, \tag{1.7}$$

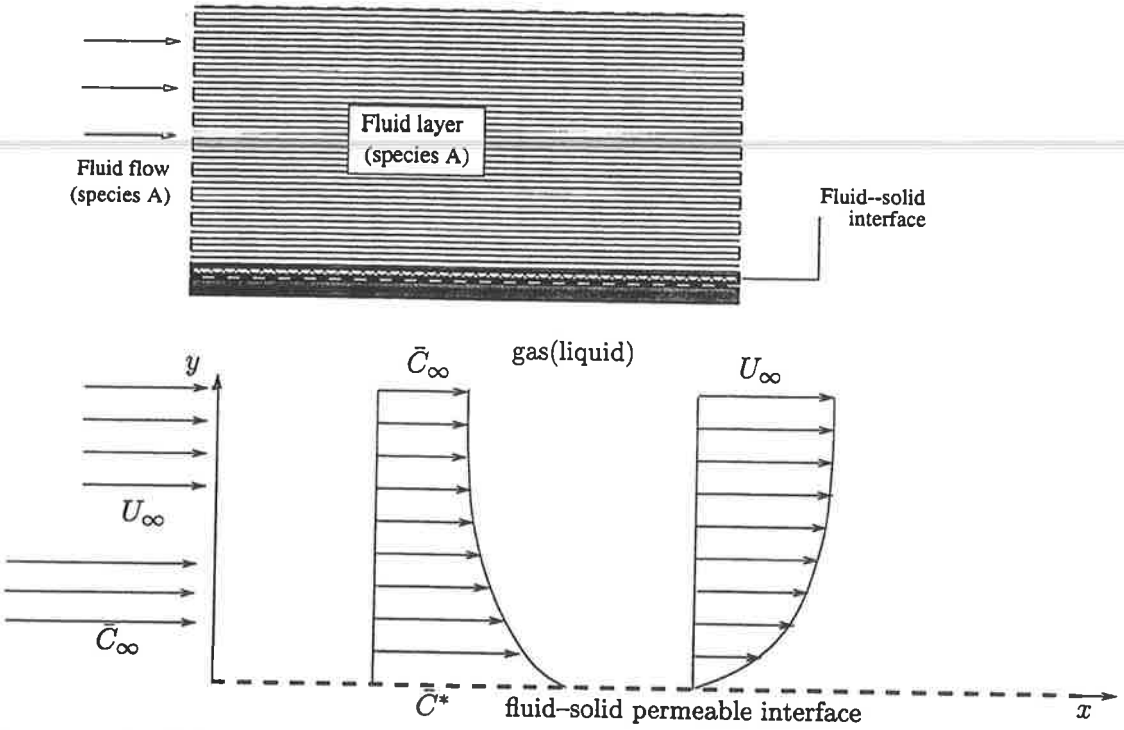

Figure 1.1: Schematic describing a flow of species with different free surface and free-stream concentrations.

where k is the mass-transfer coefficient and I can be derived from (1 p.xv) as follows:

$$I = -\frac{MD\rho^*}{\rho_0^*}\left(\frac{\partial C_0}{\partial y}\right)_{y=0}.$$

In what follows we will consider the Blasius similarity solution. In order to solve system (1.4) with boundary conditions (1.5), it is useful to introduce similarity variables

$$U_0 = \frac{1}{2}U_\infty \varepsilon \Phi', \quad V_0 = \frac{1}{2}\left(\frac{U_\infty \nu}{x}\right)^{1/2}(\eta\Phi' - \Phi), \tag{1.8}$$
$$C_0 = \bar{C}_\infty + (\bar{C}^* - \bar{C}_\infty)\Psi, \quad \eta = y\left(\frac{U_\infty}{4Dx}\right)^{1/2},$$

where $\varepsilon = Sc^{1/2}$, $Sc = \nu/D$ is a non-dimensional parameter - the Schmidt number, $\Phi = \Phi(\eta)$ the stream-function, $\Psi = \Psi(\eta)$ the non-dimensional concentration. The most important feature of the similarity solution is that despite the growth of the velocity (hydrodynamic) and concentration boundary layers with distance x from the leading edge, the velocity U_0/U_∞ and concentration $C_0/[\bar{C}_\infty + (\bar{C}^* - \bar{C}_\infty)]$ profiles remain geometrically similar.

As a result of these substitutions the boundary-layer equations (1.4) and boundary conditions (1.5) reduce to

$$\begin{aligned} &\Phi''' + \varepsilon^{-1}\Phi\Phi'' = 0, \quad \Psi'' + \varepsilon\Phi\Psi' = 0, \\ &\Phi(0) = \Theta\Psi'(0), \ \Phi'(0) = 0, \ \Psi(0) = 1; \\ &\Phi'(\infty) = 2\varepsilon^{-1}, \ \Psi(\infty) = 0, \end{aligned} \tag{1.9}$$

where

$$\Theta = \frac{M(\bar{C}^* - \bar{C}_\infty)}{\varepsilon \rho_0^*} \tag{1.10}$$

is a parameter which reflects the effect of the intensity of non-linear mass transfer. Further in this chapter we shall consider the parameter Θ as small. In the linear theory of mass transfer $\Theta = 0$.

We can substitute (1 p.xv) into (1.7) for the fluid phase to obtain an expression for the Sherwood number in terms of our new variables

$$Sh = \frac{kL}{D} = -\frac{\rho^*}{\rho_0^*} Pe^{1/2} \Psi'(0), \quad Pe = \frac{U_\infty L}{D}, \tag{1.11}$$

where Pe is the Peclet number[1].

It is seen from (1.11) that the mass-transfer kinetics is determined by the dimensionless diffusion flux $\Psi'(0)$, which can be obtained by solving the system of equations (1.9). The solution has been found by Boyadjiev & Toshev (1989) by expanding Φ and Ψ in power series in terms of the small parameter Θ

$$\begin{aligned} \Phi &= \Phi_0 + \Theta\Phi_1 + \Theta^2\Phi_2 + \dots, \\ \Psi &= \Psi_0 + \Theta\Psi_1 + \Theta^2\Psi_2 + \dots. \end{aligned} \tag{1.12}$$

It was demonstrated that $\Psi'(0)$ could be determined as follows:

$$\Psi'(0) = -\frac{2}{\varepsilon\varphi_0} + \Theta\frac{2\varphi_3}{\varphi_0^3} + \Theta^2\left(-\frac{4\varepsilon\varphi_3^2}{\varphi_0^5} + \frac{\varepsilon\varphi_{33}}{\varphi_0^4} + \frac{4\varepsilon\bar{\varphi}_{33}}{\varepsilon\varphi_0^4}\right) + O(\Theta^3), \tag{1.13}$$

where the parameters φ_0, φ_3, φ_{33} and $\bar{\varphi}_{33}$ are functions of the Schmidt number given by

$$\begin{aligned} \varphi_0 &= \int_0^\infty E(\varepsilon,p)\mathrm{d}p \approx \begin{cases} 3.01Sc^{-0.35} & - \text{ for gases} \\ 3.12Sc^{-0.34} & - \text{ for liquids,} \end{cases} \\ \varphi_3 &= \int_0^\infty \left[\int_0^p \varphi(s)\mathrm{d}s\right] E(\varepsilon,p)\mathrm{d}p \approx \begin{cases} 6.56Sc^{-0.80} & - \text{ for gases} \\ 5.08Sc^{-0.67} & - \text{ for liquids,} \end{cases} \\ \varphi_{33} &= \int_0^\infty \left[\int_0^p \varphi(s)\mathrm{d}s\right]^2 E(\varepsilon,p)\mathrm{d}p \approx \begin{cases} 24.0Sc^{-1.3} & - \text{ for gases} \\ 12.2Sc^{-1.0} & - \text{ for liquids,} \end{cases} \\ \bar{\varphi}_{33} &= \int_0^\infty \left[\int_0^p \bar{\varphi}(s)\mathrm{d}s\right] E(\varepsilon,p)\mathrm{d}p \approx \begin{cases} 0.326Sc^{-1.6} & - \text{ for gases} \\ 0.035Sc^{-1.1} & - \text{ for liquids.} \end{cases} \end{aligned}$$

Here

$$E(\varepsilon,p) = \exp\left[-\frac{\varepsilon^2}{2}\int_0^p f(p)\mathrm{d}p\right],$$

[1]This definition of the Peclet number slightly differs from the standard definition in textbooks $Pe_L = U_\infty L/\alpha$, where α is the thermal diffusivity.

and $p = (2/\varepsilon)\eta$, f, φ and $\bar{\varphi}$ are solutions of the following boundary value problem

$$
\begin{aligned}
&2f''' + f'' = 0,\\
&2\varphi''' + f\varphi'' + f''\varphi = 0,\\
&2\bar{\varphi}''' + f\bar{\varphi}'' + f''\bar{\varphi} = \varphi\varphi'',\\
&f(0) = 0,\ f'(0) = 0;\ f'(\infty) = 1;\\
&\bar{\varphi}(0) = 1,\ \bar{\varphi}'(0) = 0;\ \bar{\varphi}(\infty) = 1.
\end{aligned}
$$

A full derivation of these parameters can be found in Boyadjiev & Toshev (1989).

In order to verify the asymptotic theory the problem (1.9) has been solved numerically. A quantitative analysis of the influence of the direction of mass transfer on the mass-transfer rate by numerical integration of the two-point boundary-value problem (1.9) is presented in Boyadjiev & Vulchanov (1990). The result of this work demonstrated that if the Schmidt number Sc is increased, the concentration gradient at the interface, i.e. the Sherwood number, decreases. This is a natural response as it corresponds to a decrease of the diffusivity or an increase of the viscosity. It was shown that a change in the direction of mass transfer will affect the magnitude of the concentration gradient on the interface (Sh respectively). The change of the mass-transfer parameter Θ does not affect the concentration boundary layer and the effect of the induced secondary flow is confined in a sub-layer, termed the "layer of non-linear mass transfer", and is approximately one-third of the thickness of the concentration boundary layer. The influence of the direction of mass transfer on the velocity field was also studied in Boyadjiev & Vulchanov (1990). It was shown that $\Phi'(0)$ has higher values at $\Theta > 0$ (mass transfer directed from the surface to the free stream), i.e the non-linear effect is due to the normal velocity component.

The results obtained through numerical calculations ($\Psi'_N(0)$) are compared with the data from the asymptotic theory ($\Psi'(0)$) in Table 1.1. Note that the missing data is due to numerical difficulties arising from the different scales of the hydrodynamic and concentration boundary-layer thicknesses in the case of $\varepsilon = \sqrt{Sc} = 10$. The results demonstrate that the direction of the intense interfacial mass transfer significantly influences the kinetics of mass transfer as is evident by the change of $\Psi'(0)$ for the respective cases of Θ positive or negative. This fact is not valid in the linear theory approximation ($\Theta = 0$). The results obtained show that intense mass transfer from the volume toward the solid surface ($\Theta < 0$) leads to an increase in the mass-transfer rate, in comparison to the prediction of linear theory. When the mass transfer is directed from the solid surface toward the volume ($\Theta > 0$), its rate decreases.

The hydrodynamic nature of the non-linear effect in the mass-transfer kinetics under conditions of intense mass transfer suggests that analogous effects may take place under conditions of multi-component mass transfer for all components.

Θ	$\varepsilon = 1$		$\varepsilon = 10$	
	$-\Psi'_N(0)$	$-\Psi'(0)$	$-\Psi'_N(0)$	$-\Psi'(0)$
0.00	0.664	0.664	0.314	0.305
0.05	0.641	0.641	0.248	0.250
-0.05	0.689	0.689	0.459	0.415
0.10	0.620	0.620	0.207	0.250
-0.10	0.716	0.716	–	0.581
0.20	0.581	0.581	0.160	0.418
-0.20	0.779	0.779	–	1.080
0.30	0.548	0.555	–	1.808
-0.30	0.855	0.843	–	1.800

Table 1.1: Comparison of the results obtained from the asymptotic theory ($\Psi'(0)$) with the data obtained through direct numerical calculations ($\Psi'_N(0)$) in the case of mass transfer in fluid-solid surface systems.

1.2 Multi-component mass transfer

Let us now consider diffusion in multi-component mixtures, for example, binary, ternary or n-component systems. In the case of gases two problems have been studied (see Sherwood, Pigford & Wilke (1975)): first only one component is diffusing (diffusion of species A through a stagnant mixture containing n components, including A) and second n components diffusing leading to n independent equations (analogous to the first problem) describing the diffusion phenomena. For liquids the mechanism is somewhat more complicated. It is customary in the case of liquid flows to use multi-component diffusion equations that are derived from experimental measurements of the diffusion process by employing a semi-empirical approach. This is not done in the case of gases. Throughout this work the non-empirical approach will be used.

Analysis (see Sherwood, Pigford & Wilke (1975)) shows that the transfer of the components with large concentration gradients can be considered independently from the transfer of other components with low concentration gradients c_i $(i = 1, \ldots, n)$. The theory of diffusion in multi-component systems demonstrates that the independent diffusion approximation is valid in two cases: firstly, when the concentrations of the components are low and secondly when their mass flux diffusion components do not considerably differ from each other. This provides a sufficient basis to solve the problem of the influence of non-linear mass transfer on the multi-component mass transfer in the independent diffusion approximation. Thus, the following system of convection-diffusion equations for the lower concentration gradients species and corresponding boundary conditions should

be added to the system of equations (1.4):

$$
\begin{aligned}
&U_0\frac{\partial C_{0i}}{\partial x}+V_0\frac{\partial C_{0i}}{\partial y}=D_i\frac{\partial^2 C_{0i}}{\partial y^2},\\
&x=0:\ \ C_{0i}=\bar{C}_{\infty i};\\
&y=0:\ \ C_{0i}=\bar{C}_i^*;\\
&y\to\infty:\ \ C_{0i}=\bar{C}_{\infty i},\ \ i=1,\ldots,n.
\end{aligned}
\tag{1.14}
$$

The introduction of the similarity variables (1.8) into the above equations, for all of the components, yields

$$
\begin{aligned}
&\Phi'''+\varepsilon^{-1}\Phi\Phi''=0,\\
&\Psi''+\varepsilon\Phi\Psi'=0,\\
&\Psi_i''+\varepsilon_i\Phi\Psi_i'=0,\\
&\Phi(0)=\Theta\Psi'(0),\ \Phi'(0)=0,\ \Psi(0)=1,\ \Psi_i(0)=1;\\
&\Phi'(\infty)=2\varepsilon^{-1},\ \Psi(\infty)=0,\ \Psi_i(\infty)=0,\ \ i=1,\ldots,n,
\end{aligned}
\tag{1.15}
$$

where

$$
\begin{aligned}
&\varepsilon_i=Sc_i^{1/2},\quad Sc_i=\frac{\nu}{D_i},\\
&\Psi_i(\eta)=\frac{C_{0i}-\bar{C}_{\infty i}}{\bar{C}_i^*-\bar{C}_{\infty i}},\ \ i=1,\ldots,n.
\end{aligned}
$$

The rate of the multi-component mass transfer for a plate with length L can be determined from the average mass flux

$$
J_i=M_iD_i(\bar{C}_i^*-\bar{C}_{\infty i})=\frac{1}{L}\int_0^L I_i\,\mathrm{d}x_i,\quad i=1,\ldots,n,
\tag{1.16}
$$

where the mass flux has convective and diffusive (resulting from the induced flow) components

$$
\begin{aligned}
I_i\ \ =\ \ &-M_iD_i\left(\frac{\partial C_{0i}}{\partial y}\right)_{y=0}+M_i(C_{0i}v_n)=\\
&-M_iD_i\left[\left(\frac{\partial C_{0i}}{\partial y}\right)_{y=0}+\frac{M_i\alpha_i}{\rho_0^*}\left(C_{0i}\frac{\partial C_{0i}}{\partial y}\right)_{y=0}\right],\ \ i=1,\ldots,n,
\end{aligned}
\tag{1.17}
$$

where $\alpha_i=\varepsilon_i/\varepsilon$.

An expression for the Sherwood number in terms of the similarity variables can be obtained directly from (1.16) and (1.17) as follows:

$$
Sh_i=\frac{kL}{D_i}=Pe^{1/2}\left[\Psi_i'(0)+\Theta\varepsilon_i\frac{\bar{C}_{0i}^*}{\bar{C}_{0i}^*-\bar{C}_{\infty i}}\Psi'(0)\right],\ \ i=1,\ldots,n,
$$

where $\Psi'(0)$ is determined from (1.13), while $\Psi_i'(0)$ are determined directly from the system of equations (1.15). The solution has been obtained asymptotically, using series expansions for $\Psi_i'(0)$ $(i = 1, \ldots, n)$ in powers of Θ (see Boyadjiev (1990b)); they are the same as (1.12). One can express $\Psi'(0)$ in the following form:

$$\Psi'(0) = -\frac{2}{\varepsilon\varphi_{0i}} + \Theta\frac{2\varepsilon_i\varphi_{3i}}{\varepsilon\varphi_0\varphi_{0i}^2} - \Theta^2\left[\frac{2\varepsilon_i\varphi_{3i}}{\varepsilon\varphi_0\varphi_{0i}^2}\left(\frac{\varphi_3}{\varphi_0} + \frac{\varepsilon_i\varphi_{3i}}{\varepsilon\varphi_{0i}}\right) - \frac{\varepsilon_i^2\varphi_{33i}}{\varepsilon\varphi_0^2\varphi_{0i}^2} - \frac{\varepsilon_i\varphi_{33i}}{\varepsilon^2\varphi_0^2\varphi_{0i}^2}\right] + O(\Theta^3),$$
$$i = 1, \ldots, n,$$

where the parameters are functions of the Schmidt number

$$\varphi_{0i} = \varphi_0(Sc_i), \quad \varphi_{3i} = \varphi_3(Sc_i), \quad \varphi_{33i} = \varphi_{33}(Sc_i), \quad \bar{\varphi}_{33i} = \bar{\varphi}_{33}(Sc_i),$$
$$i = 1, \ldots, n.$$

The accuracy of the asymptotic theory of the multi-component mass transfer (under conditions of interfacial mass transfer for one of the components) has been verified by comparison with the results obtained from a numerical solution of system (1.15). The comparison of the results obtained through the numerical calculations, $\Psi_{1N}'(0)$, with the asymptotic theory data, $\Psi_1'(0)$, is shown in Tables 1.2 and 1.3. It can be clearly seen that

$\varepsilon = 1$, α_i=2, $\varepsilon_i = 2$		
Θ	$-\Psi_{1N}'(0)$	$-\Psi_1'(0)$
0.0	0.845	0.847
0.1	0.762	0.765
-0.1	0.943	0.945
0.2	0.689	0.700
-0.2	1.060	1.061
0.3	0.633	0.652
-0.3	1.212	1.190

Table 1.2: Comparison of the results obtained from the asymptotic theory ($\Psi_1'(0)$) with the data obtained through direct numerical calculations ($\Psi_{1N}'(0)$) in the case of mass transfer in gas-solid surface systems.

the intense interfacial mass transfer of one of the components, directed from the volume toward the solid surface ($\Theta < 0$), increases the diffusion-mass-transfer rate for all of the components. In the cases where the direction of the intense interfacial mass transfer is from the permeable surface towards the volume ($\Theta > 0$) the diffusion mass transfer decreases for all of the components. These effects do not depend on the change in the direction of the interfacial mass transfer for components with low concentration gradients and can be used in the control of the kinetics of the multi-component mass transfer. The analysis of the multi-component mass-transfer kinetics in the case of non-linear mass transfer of one of the components (as a result of its larger concentration gradient than the rest of the components) shows that the mass-transfer kinetics is influenced not only by the component with the largest concentration gradient but by the direction of the mass transfer of the other components (see Boyadjiev (1990b)).

$\varepsilon = 20$, α_i=0.5, $\varepsilon_i = 10$		
Θ	$-\Psi'_{1N}(0)$	$-\Psi'_1(0)$
0.00	0.198	0.194
0.03	0.167	0.169
-0.03	0.275	0.250
0.05	0.154	0.170
0.10	0.132	0.234

Table 1.3: Comparison of the results obtained from the asymptotic theory ($\Psi'_1(0)$) with the data obtained through direct numerical calculations ($\Psi'_{1N}(0)$) in the case of mass transfer in liquid-solid surface systems.

If we examine equations (1.4b), (1.4c) and the heat-transfer equation that will be introduced in the next section, we readily note a strong similarity. They are characterised by convection terms on the left-hand side and a diffusion term on the right side. The transport phenomena nature of heat transfer implies that analogous effects will be observed. Actually in the decoupled theories, the heat and mass-transfer relations for a particular geometry are interchangeable.

1.3 Heat transfer in fluid–solid permeable surface systems

The theoretical analysis of heat-transfer kinetics accompanied by non-linear mass transfer was studied by Boyadjiev (1990a). The influence of the non-linear mass transfer on the kinetics of heat transfer is considered on the basis of the macroscopic irreversible thermodynamics, i.e. by excluding thermal diffusion. The following model describes, for example, situations where a flow of species A with different free-stream and surface concentrations and free-stream and surface temperatures differ. In this case a thermal boundary layer will develop (see Figure 1.2) along with velocity (hydrodynamic) and concentration boundary layers. Since the dimensionless parameters Prandtl number[2] Pr and Schmidt number Sc have analogous roles in the heat-transfer equation and convection-diffusion equation respectively, the dimensionless relations that govern thermal boundary layer behaviour must be the same as those governing concentration boundary layer, i.e. the boundary-layer temperature and concentration profiles must have the same functional form (see Incropera & DeWitt (1990)).

In the boundary-layer approximation, the system of equations (1.4) has to be supplemented with the following heat-transfer equation and appropriate initial and boundary

[2]The Prandtl number $Pr = \nu/\alpha_T$, where ν is the kinematic viscosity and α_T is the thermal diffusivity, is the ratio of momentum and thermal diffusivities.

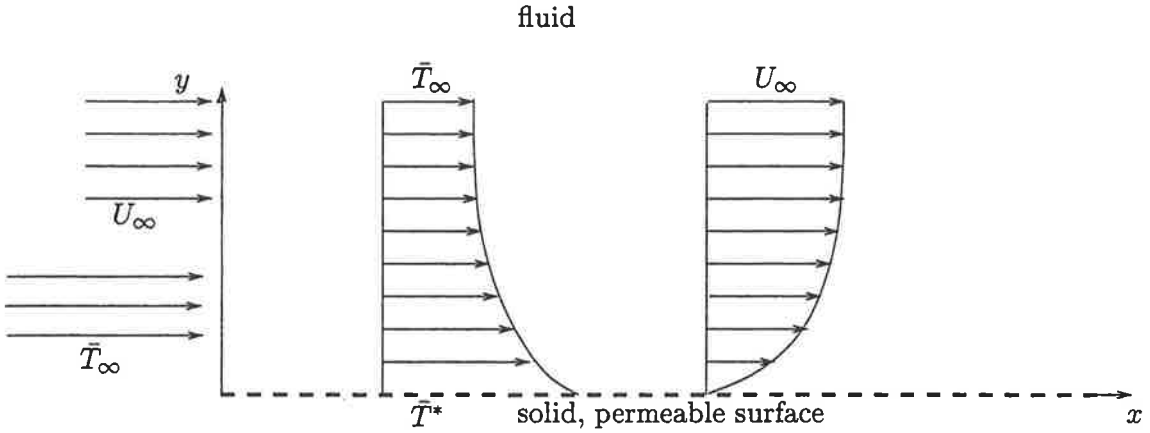

Figure 1.2: Schematic describing only the velocity (hydrodynamic) and thermal boundary layers.

conditions:

$$\begin{aligned} &U_0\frac{\partial T_0}{\partial x}+V_0\frac{\partial T_0}{\partial y}=\alpha_T\frac{\partial^2 T_0}{\partial y^2},\\ &x=0:\ \ T_0=\bar{T}_\infty;\\ &y=0:\ \ T_0=\bar{T}^*;\\ &y\to\infty:\ \ T_0=\bar{T}_\infty, \end{aligned} \tag{1.18}$$

where $\bar{T}_\infty$ and $\bar{T}^*$ are temperatures in the fluid free-stream and on the permeable surface, respectively, and α_T is the thermal diffusivity coefficient.

The average heat-mass-transfer rate for a plate of length L is determined from the average heat flux

$$J_T=k_T(\bar{T}^*-\bar{T}_\infty)=\frac{1}{L}\int_0^L I_T\,\mathrm{d}x, \tag{1.19}$$

which as a result of the induced flow has a convective component as well as a diffusive component

$$I_T=-\lambda\left(\frac{\partial T_0}{\partial y}\right)_{y=0}+\rho_0^* c_p(T_0 v_n)_{y=0}; \tag{1.20}$$

here λ is the heat conductivity coefficient, k_T the heat-transfer coefficient and c_p is the heat capacity of the mixture.

The introduction of the similarity variables (1.8) into equation (1.18) and the boundary conditions leads to the following two-point boundary-value problem:

$$\begin{aligned} &\Phi'''+\varepsilon^{-1}\Phi\Phi''=0,\\ &\Psi''+\varepsilon\Phi\Psi'=0,\\ &T''+\bar{\varepsilon}_T\Phi T'=0,\\ &\Phi(0)=\Theta\Psi'(0),\ \Phi'(0)=0,\ \Psi(0)=1,\ T(0)=1;\\ &\Phi'(\infty)=2\varepsilon^{-1},\ \Psi(\infty)=0,\ T(\infty)=0, \end{aligned} \tag{1.21}$$

where

$$T(\eta) = \frac{T_0 - \bar{T}_0}{\bar{T}^* - \bar{T}_0}, \quad \bar{\varepsilon}_T = \varepsilon \bar{\alpha}_T, \quad \bar{\alpha}_T = \frac{D}{\alpha_T} = Le^{-1};$$

here the parameter Le is termed the Lewis number, defined as a ratio of the thermal and mass diffusivities. It is relevant to any situation involving simultaneous heat and mass transfer and is therefore a measure of the relative thermal and concentration boundary-layer thicknesses.

In order to study the heat-transfer kinetics, the Nusselt number[3] has to be determined from (1.19), (1.20) and (1.21)

$$Nu = \frac{k_T L}{\lambda} = -Pe^{1/2} \left[T'(0) + \Theta \bar{\varepsilon}_T \frac{\bar{T}^*}{\bar{T}^* - \bar{T}_0} \Psi'(0) \right],$$

where the dimensionless temperature gradient $T'(0)$ is determined from the solution of system (1.21). The solution can be obtained through an asymptotic method

$$\begin{aligned} T'(0) \;=\; & -\frac{2}{\varepsilon \varphi_{0T}} + \Theta \frac{2 \bar{\alpha}_T \varphi_{3T}}{\varepsilon \varphi_0 \varphi_{0T}^2} \\ & -\Theta^2 \left[\frac{2 \bar{\varepsilon}_T \varphi_{3T}}{\varepsilon \varphi_0 \varphi_{0T}^2} \left(\frac{\varphi_3}{\varphi_0} + \frac{\bar{\alpha}_T \varphi_{3T}}{\varepsilon \varphi_{0T}} \right) - \frac{\alpha \bar{\varepsilon}_T \varphi_{33T}}{\varepsilon \varphi_0^2 \varphi_{0T}^2} - \frac{\bar{\alpha}_T \bar{\varphi}_{33T}}{\varepsilon^2 \varphi_0^2 \varphi_{0T}^2} \right] + O(\Theta^3), \end{aligned}$$

where

$$\begin{aligned} & \varphi_{0T} = \varphi_0(\varepsilon \bar{\varepsilon}_T), \quad \varphi_{3T} = \varphi_3(\varepsilon \bar{\varepsilon}_T), \\ & \varphi_{33T} = \varphi_{33}(\varepsilon \bar{\varepsilon}_T), \quad \bar{\varphi}_{33T} = \bar{\varphi}_{33}(\varepsilon \bar{\varepsilon}_T). \end{aligned}$$

The asymptotic solution can be compared with the numerical solution of the governing equations (see Vulchanov & Boyadjiev (1988)). Comparison of the results (for a dimensionless heat flux $T'(0)$) obtained from the asymptotic method with the data from the numerical calculations $T'_N(0)$, is presented in Table 1.4. It can be seen that the non-linear mass transfer can increase or decrease the heat-transfer rate depending on the direction of the interfacial mass transfer. It is evident that under conditions of intense mass transfer the non-linear mass and heat transfer are not independent, as is the case for linear mass-transfer theory ($\Theta = 0$) for small concentration gradients.

In the cases when the non-linear mass transfer is toward the solid, permeable wall ($\Theta < 0$), the rate of the heat transfer increases with an increase of the concentration gradient. The rate of the heat transfer decreases when the intense interfacial mass transfer is from the surface toward the fluid ($\Theta > 0$).

The influence of the direction of intense mass transfer on the heat-transfer coefficient and on the non-linear mass transfer can be used in the control of the heat-transfer processes rate in gas–solid permeable surface systems. It was shown by Boyadjiev & Babak (2000) that non-linear effects (as a result of intense interfacial mass transfer), when compared

[3]The Nusselt number is defined as the total heat transfer normalised by the diffusive heat transfer.

$\varepsilon = 1$, $\bar{\alpha}_T$=2, $\bar{\varepsilon}_T = 2$		
Θ	$-T'_N(0)$	$-T'(0)$
0.0	0.864	0.847
0.1	0.762	0.765
-0.1	0.943	0.945
0.2	0.689	0.700
-0.2	1.060	1.061
0.3	0.633	0.652
-0.3	1.212	1.190

Table 1.4: Comparison of the results obtained from the asymptotic theory ($T'(0)$) with the data obtained through direct numerical calculations ($T'_N(0)$) in the case of mass transfer in gas-solid surface systems.

to the results from the linear mass-transfer theory, lead to a rise in the heat-transfer rate, when mass and heat transfer are co-directional and to a decrease in the heat-transfer rate when these two processes are not co-directional.

In the case of liquids, the non-linear mass transfer does not influence the heat transfer, because the Lewis number Le has large values ($\bar{\alpha}_T \approx 10^{-2}$). In other words, the mass transfer in the thin diffusion boundary layer cannot disturb the "thick" temperature boundary layer.

The interfacial mass transfer in the gas–liquid and liquid–liquid systems is associated primarily with industrial absorption and extraction processes. The process intensification through generation of large concentration gradients in the gas and liquid leads to occurrence of non-linear effects in the mass-transfer kinetics in the gas and liquid phases. In this way the interfacial mass transfer in the gas–liquid and the liquid–liquid systems becomes non-linear. The subject of the next section is the interfacial mass transfer in gas–liquid systems.

1.4 Interfacial mass transfer in gas–liquid systems

Industrial gas absorption is most frequently utilised in packed bed columns. The size of these packings is usually small, and the interfacial transfer of the absorbed material is effected through the thin layers attached to the interface between the gas and liquid phases. The main change in the absorbed material concentration takes place in these layers, which allows the theoretical analysis of non-linear interfacial mass-transfer kinetics to be carried out by employing the concentration boundary-layer approximation.

The kinetics of non-linear interfacial mass transfer in gas–liquid systems is considered in the case of co-current gas and liquid flows over a semi-infinite flat interface. The gas and liquid are designated as a first (species A) and second (species B) phase, respectively (see Figure 1.3). Under the boundary-layer approximation the governing equations take

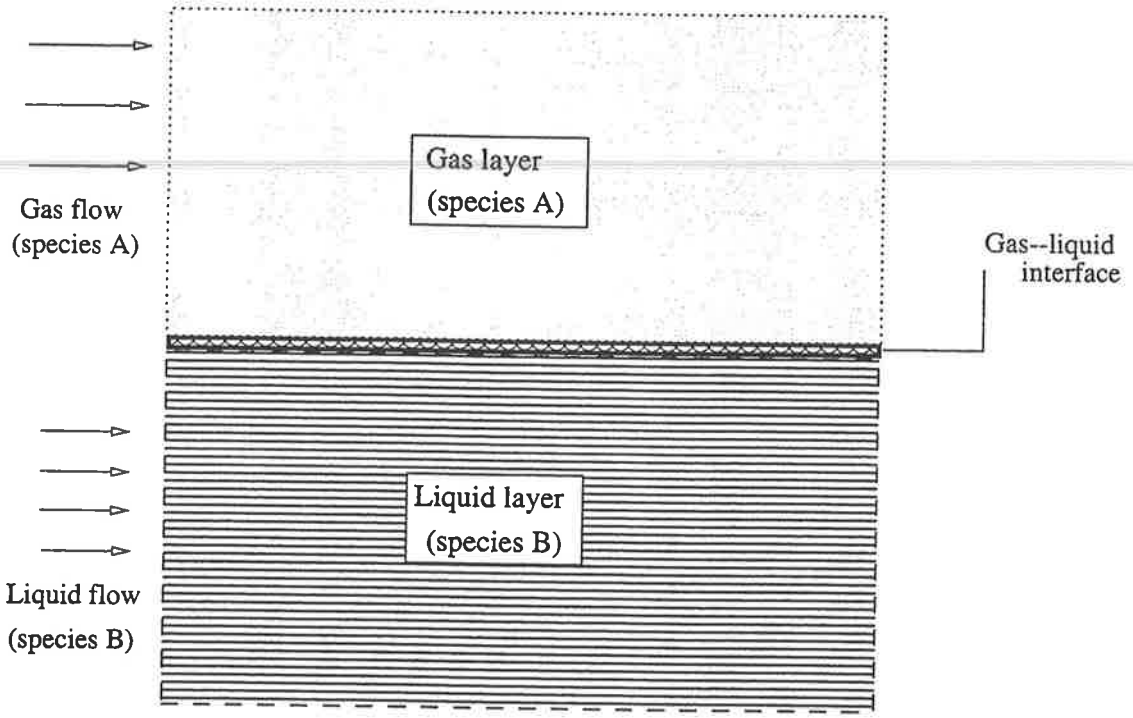

Figure 1.3: Schematic of the describing gas–liquid two-phase system.

a form similar to (1.4) (see Vulchanov & Boyadjiev (1990))

$$\frac{\partial U_{0j}}{\partial x} + \frac{\partial V_{0j}}{\partial y} = 0, \tag{1.22a}$$

$$U_{0j}\frac{\partial U_{0j}}{\partial x} + V_{0j}\frac{\partial U_{0j}}{\partial y} = \nu_j \frac{\partial^2 U_{0j}}{\partial y^2}, \tag{1.22b}$$

$$U_{0j}\frac{\partial C_{0j}}{\partial x} + V_{0j}\frac{\partial C_{0j}}{\partial y} = D_j \frac{\partial^2 C_{0j}}{\partial y^2}, \quad j = 1,\, 2, \tag{1.22c}$$

with the initial and boundary conditions accounting for the continuity of stress, momentum and mass transfer on the interface

$$x = 0: \quad U_{0j} = U_{\infty j},\ C_{0j} = \bar{C}_{\infty j}; \tag{1.23a}$$

$$y = 0: \quad U_{01} = U_{02},\ \mu_1 \frac{\partial U_{01}}{\partial y} = \mu_2 \frac{\partial U_{02}}{\partial y},\ V_{0j} = -\frac{M D_j}{\rho^*_{0j}} \frac{\partial C_{0j}}{\partial y}, \tag{1.23b}$$

$$C_{01} = \chi C_{02},\ \frac{D_1 \rho_1^*}{\rho_{01}^*} \frac{\partial C_{01}}{\partial y} = \frac{D_2 \rho_2^*}{\rho_{02}^*} \frac{\partial C_{02}}{\partial y}; \tag{1.23c}$$

$$y \to \infty: \quad U_{01} = U_{\infty 1},\ C_{01} = \bar{C}_{\infty 1}; \tag{1.23d}$$

$$y \to -\infty: \quad U_{02} = U_{\infty 2},\ C_{02} = \bar{C}_{\infty 2}. \tag{1.23e}$$

Here $U_{\infty 1}$, $U_{\infty 2}$ are free-stream velocities of the phases, $C_{\infty 1}$, $C_{\infty 2}$ concentrations in the free-stream, μ_1 and μ_2 dynamic viscosities and D_j, $(j = 1,\, 2)$ the diffusion coefficient of the ith phase.

It is useful to introduce the following similarity variables

$$U_{0j} = \frac{1}{2} j U_{\infty j} \varepsilon_j \Phi_j', \quad V_{0j} = (-1)^{j-1} \frac{1}{2} j \left(\frac{U_{\infty j} \nu_j}{x} \right)^{1/2} (\zeta_j \Phi_j' - \Phi_j), \quad \zeta_j = \frac{2}{\varepsilon_j} \eta_j, \tag{1.24}$$

$$C_{0j} = \bar{C}_{\infty j} + (\bar{C}_{\infty 1} - \chi \bar{C}_{\infty 2}) \Psi_j, \quad \eta_j = (-1)^{j-1} y \left(\frac{U_{\infty j}}{4 D_j x} \right)^{1/2}, \quad j = 1, 2,$$

where $\varepsilon_j = Sc_j^{1/2}$ and $Sc = \nu_j / D_j$ $(j = 1, 2)$.

After introduction of similarity variables (1.24), the system (1.22) and its boundary conditions (1.23b) - (1.23e) become

$$\Phi_j''' + j \varepsilon_j^{-1} \Phi_j \Phi_j'' = 0, \quad \Psi_j'' + j \varepsilon_j \Phi_j \Psi_j' = 0, \tag{1.25a}$$

$$\Phi_j(0) = (-1)^j \theta_{j+2} \Psi_j'(0), \ \Phi_j'(\infty) = \frac{2}{j \varepsilon_j}, \ \Psi_j(\infty) = 0, \tag{1.25b}$$

$$\Phi_1'(0) = 2\theta_1 \frac{\varepsilon_2}{\varepsilon_1} \Phi_2'(0), \quad \Phi_2''(0) = -0.5 \theta_2 \left(\frac{\varepsilon_1}{\varepsilon_2} \right)^2 \Phi_1''(0), \tag{1.25c}$$

$$\Psi_2'(0) = \frac{\chi}{\varepsilon_0} \Psi_1'(0), \quad \Psi_1(0) + \Psi_2(0) = 1, \ j = 1, 2, \tag{1.25d}$$

where

$$\theta_1 = \frac{U_{\infty 2}}{U_{\infty 1}}, \quad \theta_2 = \frac{\mu_1}{\mu_2} \left(\frac{\nu_1}{\nu_2} \right)^{1/2} \left(\frac{U_{\infty 1}}{U_{\infty 2}} \right)^{3/2}, \quad \theta_3 = \frac{M(\bar{C}_{\infty 1} - \chi \bar{C}_{\infty 2})}{\varepsilon_1 \rho_{10}^*}, \tag{1.26}$$

$$\theta_4 = \frac{M(\bar{C}_{\infty 1} - \chi \bar{C}_{\infty 2})}{2 \varepsilon_2 \chi \rho_{20}^*}, \quad \varepsilon_0 = \frac{\rho_{01}^* \rho_2^*}{\rho_{02}^* \rho_1^*} \left(\frac{D_2 U_{\infty 2}}{D_1 U_{\infty 1}} \right)^{1/2},$$

here χ is the Henry's constant (see Incropera & DeWitt (1990)). The parameters θ_1 and θ_2 account for the kinematic and dynamic interactions between the gas and liquid phases respectively, while θ_3 and θ_4 characterise the levels of mass transfer in the gas and liquid phases respectively.

The new expression for the Sherwood number Sh takes the form:

$$Sh_j = -\frac{\rho_j^*}{\rho_{0j}^*} Pe_j^{1/2} \Psi_j'(0), \quad Pe_j = \frac{U_{\infty j} L}{D_j}, \quad j = 1, 2. \tag{1.27}$$

For a quantitative evaluation of the non-linear interfacial mass transfer it is necessary that $\Psi_j'(0)$ $(j = 1, 2)$ in (1.27) be given thus necessitating the solution of system (1.25). We shall limit our attention to the cases, such as the absorption of ammonia into water, where $\theta_k \ll 1$ $(k = 1, \ldots, 4)$. The solution is obtained through a perturbation method after expanding the unknown functions in series of the small parameters θ_k. The first

order approximation yields

$$\begin{aligned}
\Psi_1'(0) &= -\frac{2}{\varepsilon_1\varphi_{10}}\frac{1}{1+a_0} - \frac{2\theta_1}{a\varepsilon_1\varphi_{10}^2}\frac{1}{(1+a_0)^2} \\
&\quad -\frac{8\theta_2 a\varepsilon_2\bar{\varphi}_2}{\varepsilon_1\varphi_{10}}\frac{a_0}{(1+a_0)^2} - \frac{2\theta_3\varphi_{13}}{\varphi_{10}^3}\frac{1}{(1+a_0)^2} + \frac{8\theta_4\varepsilon_2}{\pi\varepsilon_1\varphi_{10}}\frac{a_0^2}{(1+a_0^2)^3}, \qquad (1.28)\\
\Psi_2'(0) &= -\frac{2}{\sqrt{\pi}}\frac{a_0}{1+a_0} - \frac{2\theta_1}{\sqrt{\pi}a\varphi_{10}}\frac{a_0}{(1+a_0)^2} \\
&\quad -\frac{8\theta_2 a\varepsilon_2\bar{\varphi}_2}{\sqrt{\pi}}\frac{a_0^2}{(1+a_0)^2} - \frac{2\theta_3\varepsilon_1\varphi_{13}}{\varphi_{10}^3}\frac{a_0}{(1+a_0)^2} + \frac{8\theta_4\varepsilon_2}{\pi^{3/2}}\frac{a_0^3}{(1+a_0)^3}.
\end{aligned}$$

In the cases when the interfacial mass-transfer rate is limited by diffusive resistance[4] in the gas phase, it follows from (1.25d) that $\chi/\varepsilon_0 \to 0$, i.e. $a_0 \to 0$, and thus the Sherwood number in the gas phase can be expressed as

$$Sh_1 = -\frac{\rho_1^*}{\rho_{01}^*} Pe_1^{1/2}\left(\frac{2}{\varepsilon_1\varphi_{10}} + \frac{2\theta_1}{a\varepsilon_1\varphi_{10}^2} + \frac{2\theta_3\varphi_{13}}{\varphi_{10}^3}\right). \qquad (1.29)$$

When the process is limited by diffusive resistance in the liquid phase, $\chi/\varepsilon_0 \to \infty$, i.e. $a_0 \to \infty$ and we have

$$Sh_2 = -\frac{\rho_2^*}{\rho_{02}^*} Pe_2^{1/2}\left(\frac{2}{\sqrt{\pi}} + \frac{8\theta_2}{a\varepsilon_2\varphi_2} + \frac{8\theta_3\varepsilon_2}{\pi^{3/2}}\right). \qquad (1.30)$$

The comparison of the non-linear effects in gases with those in liquids (see Vulchanov & Boyadjiev (1990)) shows that the ratio between parameters θ_3 and θ_4 is

$$\frac{\theta_3}{\theta_4} = \frac{2\varepsilon_2\rho_{02}^*\chi}{\varepsilon_1\rho_{01}^*} \gg 1.$$

The maximum value of this ratio occurs in cases of gases with high solubility, where θ_3 is greater than θ_4 by more then two orders of magnitude. In numerical calculations we can employ the approximation that $\theta_4 = 0$.

The examination of (1.28) - (1.30) shows that the non-linear effects are most dominant when the non-linear interfacial mass transfer is limited in the gas phase ($\chi/\varepsilon_0 \to 0$). In the cases of commensurable diffusive resistance ($\chi/\varepsilon_0 \approx 1$) the non-linear effects are sufficiently small and their manifestation in the liquid phase is a result of the hydrodynamic influence of the gas phase. Non-linear effects are not observed when the processes are limited by mass transfer in the liquid phase.

The influence of the direction of the mass transfer on the diffusion mass-transfer kinetics in gas-liquid systems is the same as that observed in the gas(liquid)–solid systems, i.e. the diffusion-mass-transfer rate, under conditions of absorption, is higher than that under conditions of desorption.

[4]Species diffusion resistance is defined as $R_{m,dif} = L/D_{AB}S_A$, where L is a characteristic length, D_{AB} is diffusion coefficient and S_A is surface area, assuming that the molar rate is given as $N_{A,x} = (C_{0A,s1} - C_{0A,s2})/R_{m,dif}$.

The numerical results of Vulchanov & Boyadjiev (1990) demonstrates that when (in the case of absorption and desorption) the concentration gradients are equal and only their directions change, there is a non-symmetric deviation from the linear theory ($\theta_3 = 0$). This apparent "contradiction" to the asymptotic theory (1.29) (where the deviations are symmetric) can be explained by noting that the quadratic terms are not present ($\approx \theta_3^2$). This suggests that the asymptotic theory should be corrected so that all quadratic terms are taken into account.

Under circumstances of non-linear interfacial mass transfer limited in the gas phase (acting only within the gas phase), the problem (1.25) is governed by the following system of equations:

$$
\begin{aligned}
&\Phi_1''' + \varepsilon_1^{-1}\Phi_1\Phi_1'' = 0,\\
&\Phi_2''' + 2\varepsilon_2^{-1}\Phi_2^{-1}\Phi_2\Phi_2'' = 0,\\
&\Psi_1'' + \varepsilon_1\Phi_1\Psi_1' = 0,\\
&\Phi_1(0) = \theta_3\Psi_1'(0),\ \Phi_2(0) = 0;\ \Phi_1'(\infty) = \frac{2}{\varepsilon_1},\ \Phi_2'(\infty) = \frac{1}{\varepsilon_2};\\
&\Phi_1'(0) = 2\theta_1\frac{\varepsilon_2}{\varepsilon_1}\Phi_2'(0),\ \ \Phi_2''(0) = -0.5\theta_2\left(\frac{\varepsilon_1}{\varepsilon_2}\right)^2\Phi_1''(0),\\
&\Psi_1'(0) = 1;\ \ \Psi_1(\infty) = 0.
\end{aligned}
\tag{1.31}
$$

The solution of system (1.31) as a series expansion in powers of the small parameters θ_j ($j = 1, \ldots 4$) up to and including quadratic terms gives

$$
\begin{aligned}
-\Psi_1'(0) \ = \ & \frac{2}{\varepsilon_1\varphi_{10}} + \theta_1\frac{2}{\alpha\varepsilon_1\varphi_{10}^2} + \theta_3\frac{\varphi_{13}}{\varphi_{10}^3}\\
&+\theta_1^2\left(-\frac{\varepsilon_1^3\varphi_{11}}{4\alpha^2\varphi_{10}^2} + \frac{\varepsilon_1\varphi_{12}}{\varphi_{10}^2} + \frac{2}{\alpha^2\varepsilon_1\varphi_{10}^3}\right)\\
&+\theta_3^2\left(\frac{2\varepsilon_1\varphi_{13}^2}{\varphi_{10}^5} - \frac{\varepsilon_1\varphi_{113}}{\varphi_{10}^4} - \frac{\varepsilon_1\bar{\varphi}_{113}}{\varepsilon_1\varphi_{10}^4}\right)\\
&+\theta_1\theta_3\left(\frac{\varepsilon_1\varphi_{13}}{\alpha\varphi_{10}^4} - \frac{2\varphi_{113}}{\alpha\varphi_{10}^3} - \frac{2\bar{\varphi}_{113}}{\alpha\varphi_{10}^3} + \frac{2\varphi_{13}}{\alpha\varphi_{10}^4}\right) + O(\theta_1^3, \ldots).
\end{aligned}
\tag{1.32}
$$

A succession of functions of the Schmidt number is included in the expressions (1.28) - (1.30) and (1.32) (see Vulchanov & Boyadjiev (1990))

$$
\begin{aligned}
&\varphi_{10} = \varphi_0(Sc_1),\ \ \varphi_{13} = \varphi_3(Sc_1),\ \ \bar{\varphi}_2 = \frac{1}{8}\sqrt{\frac{\pi}{Sc_2}},\ \ \alpha_0 = \frac{\chi\sqrt{\pi}}{\varepsilon_0\varepsilon_1\varphi_{10}},\\
&\varphi_{11} = \varphi_1(Sc_1) = 3.01Sc^{-1.608},\ \ \varphi_{12} = \varphi_2(Sc_1) = 3.05Sc^{-1.285},\\
&\varphi_{133} = \varphi_{33}(Sc_1),\ \ \bar{\varphi}_{133} = \bar{\varphi}_{33}(Sc_1),\ \ \varphi_{113} = \varphi_{33}(Sc_1) = Sc^{-1.3},\\
&\bar{\varphi}_{113} = \bar{\varphi}_{13}(Sc_1) = 4.18Sc^{-0.46}.
\end{aligned}
$$

The expansion (1.32) is a basic result of the asymptotic theory of non-linear interfacial mass transfer in gas–liquid systems and is in good agreement with the results obtained

through the numerical calculations $\Psi'_{1N}(0)$ of problem (1.31). The theoretical result (1.32) shows that the direction of the intense interfacial mass transfer in the gas–liquid systems influences its kinetics, that is different values of $\Psi'_1(0)$ arise for positive and negative values of θ_3 respectively. It is a hydrodynamic fact and it could well be expected that the same effect could appear in the cases of multi-component interfacial mass transfer in gas–liquid systems.

1.5 Multi-component interfacial mass transfer in gas–liquid systems

The kinetics of multi-component mass transfer in gas–liquid systems is of practical interest in cases of intense interfacial mass transfer of one of the components (the species with the largest concentration gradient), when this component induces a secondary flow in the boundary layer as a result of its large gradient of concentration. The gas and liquid flow dynamics are taken to depend upon the non-linear mass transfer of this dominant component in the gas phase.

Let us consider n components for which the interfacial mass transfer does not affect the hydrodynamics of the flow; this problem has been considered in Boyadjiev (1998). In this case the theory of multi-component interfacial mass transfer is studied under the approximation of independent diffusion. To that purpose convection-diffusion equations governing the mass transfer of each species (components) with small concentration gradients must be added to the system (1.22); as a result the mathematical model takes the following form:

$$\frac{\partial U_{0j}}{\partial x} + \frac{\partial V_{0j}}{\partial y} = 0, \tag{1.33a}$$

$$U_{0j}\frac{\partial U_{0j}}{\partial x} + V_{0j}\frac{\partial U_{0j}}{\partial y} = \nu_j \frac{\partial^2 U_{0j}}{\partial y^2}, \tag{1.33b}$$

$$U_{0j}\frac{\partial C_{0j}}{\partial x} + V_{0j}\frac{\partial C_{0j}}{\partial y} = D_j \frac{\partial^2 C_{0j}}{\partial y^2}, \tag{1.33c}$$

$$U_{0j}\frac{\partial C_{0ij}}{\partial x} + V_{0j}\frac{\partial C_{0ij}}{\partial y} = D_{ij} \frac{\partial^2 C_{0ij}}{\partial y^2}, \tag{1.33d}$$

$$i = 1, \ldots, n \quad j = 1, 2,$$

with the initial and boundary conditions

$$
\begin{aligned}
x=0: \quad & U_{0j}=U_{\infty j},\ C_{0j}=\bar{C}_{\infty j},\ C_{0ij}=\bar{C}_{\infty ij};\\
y=0: \quad & U_{01}=U_{02},\ \mu_1\frac{\partial U_{01}}{\partial y}=\mu_2\frac{\partial U_{02}}{\partial y},\ V_{0j}=-\frac{MD_j}{\rho^*_{0j}}\frac{\partial C_{0j}}{\partial y},\\
& C_{01}=\chi C_{02},\ C_{0i1}=\chi_i C_{0i2},\ \frac{D_1\rho^*_1\partial C_{01}}{\rho_{01}\partial y}=\frac{D_2\rho^*_2\partial C_{02}}{\rho_{02}\partial y};\\
& -D_{i1}\frac{\partial C_{0i1}}{\partial y}+C_{0i1}V_{01}=-D_{i2}\frac{\partial C_{0i2}}{\partial y}+C_{0i2}V_{02};\\
y\to\infty: \quad & U_{01}=U_{\infty 1},\ C_{01}=\bar{C}_{\infty 1},\ C_{0i1}=\bar{C}_{\infty i1};\\
y\to-\infty: \quad & U_{02}=U_{\infty 2},\ C_{02}=\bar{C}_{\infty 2},\ C_{0i2}=\bar{C}_{\infty i2}.
\end{aligned}
\tag{1.34}
$$

In dimensionless form and after introducing similarity variables, defined via (1.24) we obtain the following equations and boundary conditions that supplement (1.31):

$$
\begin{aligned}
&\Psi''_{ij}+j\varepsilon_j\alpha_{ij}\Phi_j\Psi'_{ij}=0,\ \ \Psi'_{i1}(0)+\Psi'_{i2}(0)=1,\\
&\Psi'_{i1}(0)=\frac{\varepsilon_{i0}}{\chi_i}\Psi'_{i2}(0)+\varepsilon_1\theta_3\alpha_{i1}\left[\Psi_{i1}(0)-\frac{\bar{C}_{\infty i1}}{\bar{C}_{\infty i1}-\chi_i\bar{C}_{\infty i2}}\right]\Psi'_1(0);\\
&\Psi_{ij}(\infty)=0,\quad i=1\ldots,n,\ \ j=1,2.
\end{aligned}
\tag{1.35}
$$

Here

$$
\Psi_{ij}=\Psi_{ij}(\eta_j)=(-\chi_i)^{j-1}\frac{C_{ij}-\bar{C}_{\infty i1}}{\bar{C}_{\infty i1}-\chi_i\bar{C}_{\infty i2}},
$$

$$
\varepsilon_{i0}=\frac{D_{i2}}{D_{i1}}\left(\frac{U_{20}D_1}{U_{10}D_2}\right)^{1/2},\quad \alpha_{ij}=\frac{D_j}{D_{ij}}
$$

and χ_i $(i=1,\ldots,n)$ are the Henry's constants for the n components. The solution of the system (1.31) together with (1.35) has been obtained by expanding Φ_j and Ψ_{ij} in series of the small parameters θ_k $(k=1,2,3)$ (see Boyadjiev (1998)).

The Sherwood numbers in the gas and liquid phases can be obtained from

$$
\begin{aligned}
&Sh_{i1}=-Pe_1^{1/2}\left\{\Psi'_{i1}(0)+\theta_3\varepsilon_{i1}\Psi'_1(0)\left[\frac{\bar{C}_{\infty i1}}{\bar{C}_{\infty i1}-\chi_i\bar{C}_{\infty i2}}\right]\right\},\\
&Sh_{i1}=-Pe_2^{1/2}\Psi'_{i2}(0),\ \ i=1,\ldots,n,
\end{aligned}
\tag{1.36}
$$

where $\Psi'_1(0)$ and $\Psi_{i1}(0)$ are zeroth-order approximations

$$
\Psi'_1(0)=-\frac{2}{\varepsilon_1\varphi_{10}},\quad \Psi_{i1}(0)=-\frac{1}{1+a_i},\quad i=1,\ldots,n,
$$

while $\Psi'_{i1}(0)$ and $\Psi'_{i2}(0)$ can be obtained by solving the system (1.31) together with (1.35):

$$
\begin{aligned}
-\Psi'_{i1}(0) &= \frac{2}{\varepsilon_1\varphi_{10i}}\frac{1}{1+a_i} + \frac{2\theta_1}{\alpha\varepsilon_1\varphi_{10i}^2}\frac{1}{(1+a_i)^2} + \frac{8\theta_2\alpha\varepsilon_{i1}\bar{\varphi}_{2i}}{\varepsilon_1\varphi_{10i}\sqrt{a_{i2}}} + \\
&\quad \theta_3\left[\frac{2\varphi_{13i}}{\varphi_{10}\varphi_{10i}^2}\frac{1}{(1+a_i)^2} + \frac{\varepsilon_{i1}a_i}{\varphi_{10}(1+a_i)}\left(\frac{2}{1+a_i} - \frac{\bar{C}_{\infty i1}}{\bar{C}_{\infty i1}-\chi_i\bar{C}_{\infty i2}}\right)\right], \\
-\Psi'_{i2}(0) &= \frac{2\sqrt{a_{i2}}}{\sqrt{\pi}}\frac{a_i}{1+a_i} + \frac{2\theta_1\sqrt{a_{i2}}}{\sqrt{\pi}\alpha\varphi_{10i}}\frac{a_i}{(1+a_i)^2} + \\
&\quad \frac{8\theta_2\alpha\varepsilon_{i2}\bar{\varphi}_{i2}}{\sqrt{\pi}}\frac{a_i^2}{(1+a_i)^2} + \theta_3\left[\frac{2\sqrt{a_{i2}}\varepsilon_{i1}\varphi_{13i}}{\sqrt{\pi}\varphi_{10}\varphi_{10i}^2}\frac{a_i}{(1+a_i)^2} - \right. \\
&\quad \left.\frac{\sqrt{a_{i2}}\varepsilon_i\varepsilon_{i1}\varphi_{10i}}{\sqrt{\pi}}\frac{a_i}{(1+a_i)^2}\left(\frac{1}{1+a_i} - \frac{\bar{C}_{\infty i1}}{\bar{C}_{\infty i1}-\chi_i\bar{C}_{\infty i2}}\right)\right], i = 1,\dots,n.
\end{aligned}
\tag{1.37}
$$

The expressions (1.37) include functions of the Schmidt number through their dependence upon ε_j

$$
\varphi_{10i} = \varphi_0(\bar{\varepsilon}_{i1}^2),\quad \varphi_{13i} = \varphi_3(\bar{\varepsilon}_{i1}^2),\quad \bar{\varphi}_{2i} = \frac{\sqrt{\pi}}{8\varepsilon_2\sqrt{a_{i2}}},
$$

$$
a_i = \frac{\sqrt{\pi}\chi_i}{\varphi_{10i}\varepsilon_1\varepsilon_{i0}\sqrt{a_{i2}}},\quad \bar{\varepsilon}_{ij} = \sqrt{\varepsilon_j\varepsilon_{ij}},\quad \varepsilon_{ij} = \varepsilon_j a_{ij},\quad i = 1,\dots,n,\quad j = 1,2.
$$

In the cases where the interfacial mass transfer is limited by the mass transfer in the gas phase, $\chi_i \to 0$, we can substitute in (1.37) $\chi_i/\varepsilon_{i0} = 0$ and $a_i = 0$ $(i = 1,\dots,n)$ and the expression (1.36) for Sh_{i1} becomes

$$
Sh_{i1} = Pe_1^{1/2}\left(\frac{2}{\varepsilon_1\varphi_{10i}} + \frac{2\theta_1}{\alpha\varepsilon_1\varphi_{10i}^2} + \frac{2\theta_3 a_{i1}\varphi_{13i}}{\varphi_{10}\varphi_{10i}^2}\right),\quad i = 1,\dots,n. \tag{1.38}
$$

If the interfacial mass transfer is limited by the mass transfer in the liquid phase, $\chi_i \to \infty$, substituting $\varepsilon_{i0}/\chi_i \to \infty$ and $a_i \to \infty$ $(i = 1,\dots,n)$ in (1.37) the expression (1.36) for Sh_{i2} reduces to

$$
Sh_{i2} = Pe_2^{1/2}\left(\frac{2\sqrt{a_{i2}}}{\sqrt{\pi}} + \frac{8\theta_2\alpha\varepsilon_{i2}\bar{\varphi}_{i2}}{\sqrt{\pi}}\right),\quad i = 1,\dots,n. \tag{1.39}
$$

It was shown in Boyadjiev (1998) that in the cases where the diffusive resistance of the two phases are commensurable ($\chi_i/\varepsilon_{i0} \approx 1$), according to the equations (1.37), one can expect that an increase in the large concentration gradient (θ_3) can lead to an increase of the diffusion-mass-transfer rate in the gas phase and to a decrease of the diffusion-mass-transfer rate in the liquid phase. It is evident from (1.39) that in the cases where the multi-component interfacial mass transfer is limited by the mass transfer in the liquid phase, the non-linear effects have no impact on the mass-transfer rate, that is Sh_{i2} does not depend on θ_3.

The theoretical investigations of the non-linear mass transfer in gas–liquid systems by Boyadjiev & Vulchanov (1988) and Vulchanov & Boyadjiev (1988) demonstrate that, in

practice, non-linear effects are essential in cases when the diffusive resistances in the gas phase limits the mass-transfer rate.

The mathematical description of interfacial mass-transfer kinetics in liquid–liquid systems is the basis for improvements in extraction processes and equipment design. The intensification of this process, by generating large concentration gradients, leads to the appearance of non-linear effects in the mass-transfer kinetics in both phases. In a number of cases these effects are connected with the induction of tangential flows along the interface (Marangoni effect) as a result of a surface (interfacial) tension gradient. It has already been shown that large mass fluxes can induce secondary flows, the velocities of which are directed normal to the interface. The theoretical analysis of the influence of these secondary flows on the kinetics of the interfacial mass transfer in liquid–liquid systems makes it possible to separate this non-linear effect from that of Marangoni and is a basis for the calculation of extraction processes with intense interfacial mass transfer. It is for this reason that the next section is dedicated to the problem of interfacial mass transfer in liquid–liquid systems.

1.6 Interfacial mass transfer in liquid–liquid systems

The industrial implementation of extraction processes is connected with the need for mass-transfer intensification between two liquid phases. This is most often gained by the generation of large concentration gradients. They usually take place in equipment where one of the liquids is dispersed in the form of drops. The small sizes of the drops implies that the changes in the velocity and concentration fields are localised in thin layers along the droplet surface (i.e. the interface). This allows the use of the boundary-layer approximation for the theoretical analysis of the extraction kinetics under conditions of intense interfacial mass transfer. The thickness of these layers is much smaller than the diameter of the drops, hence the effect of the curvature of the interface can be safely ignored. For this reason the kinetics of non-linear mass transfer is studied (see Sapundjiev & Boyadjiev (1993)) in the case of interfacial mass transfer between two insoluble liquid phases with flat mobile phase boundary under the approximation of the existence of a concentration boundary layer.

In practice both liquids are moving, one of them being a dispersed phase (drops) and the other a dispersion medium (continuous phase). As the interfacial mass-transfer kinetics depends primarily on the velocities of the drops, our discussion will focus on the interfacial mass transfer between two liquids, one of them being stationary.

The movement of a liquid in drops is a result of movement of the flow around them at velocity $U_{\infty 1}$. Let us denote this liquid as "phase 1" and the liquid in the drops as "phase 2" (the stationary phase). The hydrodynamic interaction between the two phases can be considered in an analogous fashion to that of gas–liquid systems, when one of the phases is motionless (see Figure 1.4).

Thus, the system of equations (1.22) with initial and boundary conditions (1.23) are

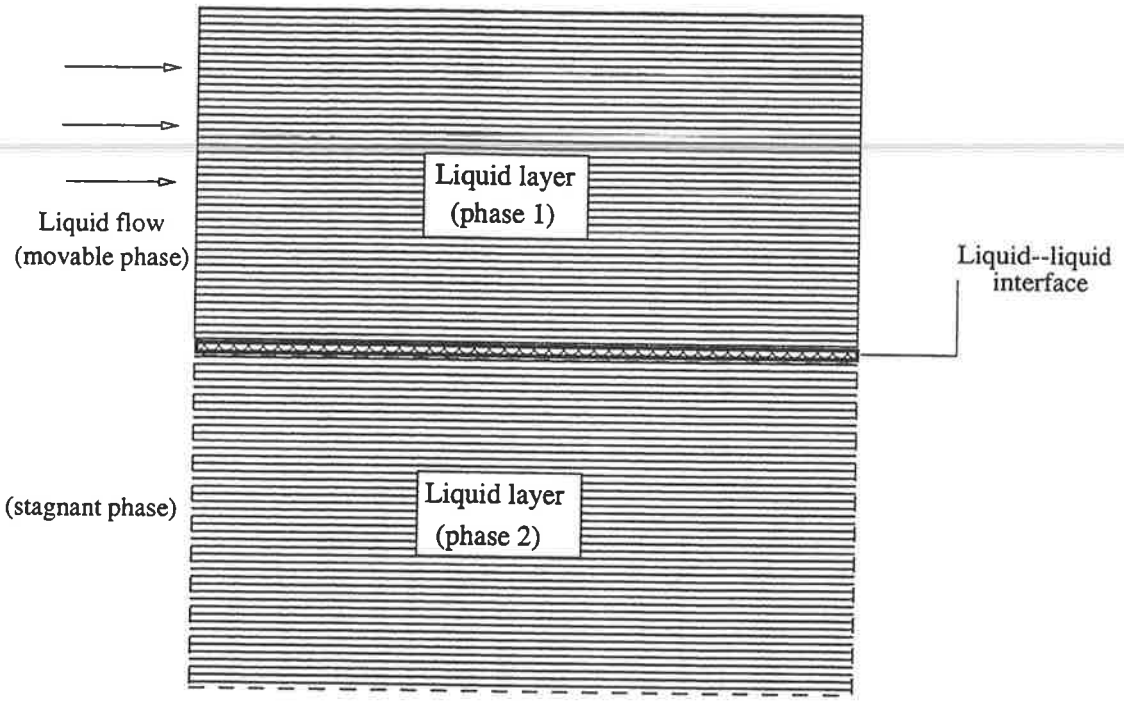

Figure 1.4: Schematic describing liquid–stagnant liquid two-phase system.

applicable to the interfacial mass transfer between movable ("phase 1") and stagnant ("phase 2") liquids, if we simply substitute in the boundary conditions on the interface $U_{02} = 0$ and $\chi = m$, where m is the coefficient of distribution of the extracted substance between phase 1 and phase 2.

In this case the interfacial mass-transfer rate and the Sherwood number are given by expressions

$$J = Mk_j(\bar{C}_{\infty 1} - m\bar{C}_{\infty 2}) = \frac{1}{L}\int_0^L I_j \,\mathrm{d}x, \tag{1.40a}$$

$$Sh_j = \frac{k_j L}{D_j} = \frac{\rho_j^*}{\rho_0^* j}\frac{m^{j-1}}{\bar{C}_{\infty 1} - m\bar{C}_{\infty 2}}\int_0^L \left(\frac{\partial C_{0j}}{\partial y}\right)_{y=0} \mathrm{d}x, \quad j = 1, 2. \tag{1.40b}$$

We shall introduce slightly modified similarity variables than those used earlier as follows:

$$U_{0j} = \frac{1}{2}U_{\infty j}\Phi_j', \quad V_{0j} = (-1)^{j-1}\left(\frac{U_{\infty j}D_j}{4x}\right)^{1/2}(\zeta_j\Phi_j' - \Phi_j), \quad \zeta_j = \frac{2}{\varepsilon_j}\eta_j, \tag{1.41}$$

$$C_{0j} = \bar{C}_{\infty j} + \frac{\bar{C}_{\infty 1} - m\bar{C}_{\infty 2}}{m^{j-1}}\Psi_j, \quad \eta_j = (-1)^{j-1}y\left(\frac{U_{\infty j}}{4D_j x}\right)^{1/2}, \quad j = 1, 2,$$

where $\varepsilon_j = Sc_j^{1/2}$ and $Sc = \nu_j/D_j$ $(j = 1, 2)$.

In the boundary-layer approximation after non-dimensionalising and introducing the sim-

ilarity variables (1.41), our problem reduces to

$$\begin{aligned}
&\Phi_j''' + \varepsilon_j^{-2}\Phi_j\Phi_j'' = 0,\\
&\Psi_j'' + \Phi_j\Psi_j' = 0,\\
&\Phi_j(0) = (-1)^{j-1}\theta_j\Psi_j'(0),\ \ \Phi_1'(0) = \Phi_2'(0),\\
&\Phi_1''(0) = -a\Phi_2''(0),\ \ \Psi_1(0) = 1 - \Psi_2(0),\ \ \Psi_1'(0) = \frac{b}{m}\Psi_2'(0);\\
&\Phi_1'(\infty) = 2,\ \ \Phi_2(\infty) = 0,\ \ \Psi_j(\infty) = 0,\ \ i = 1,2,
\end{aligned} \tag{1.42}$$

where

$$\varepsilon_j = Sc_j^{1/2},\ \ Sc_j = \frac{\nu_j}{D_j},\ \ \theta_j = \frac{M(m\bar{C}_{\infty 2} - \bar{C}_{\infty 1})}{\rho_j^* m^{j-1}},$$

$$a = \frac{\varepsilon_2\rho_{02}}{\varepsilon_1\rho_{01}}\sqrt{\frac{\nu_2}{\nu_1}},\ \ \nu_j = \frac{\mu_j}{\rho_{0j}},\ \ b = \frac{\rho_{01}^*\rho_2^*}{\rho_{02}^*\rho_1^*}\sqrt{\frac{D_2}{D_1}},\ \ j = 1,2.$$

In the new variables the Sherwood number (1.40b) can be written as

$$\begin{aligned}
Sh_j &= -\frac{\rho_j^*}{\rho_{0j}^*}Pe_j^{1/2}\Psi_1'(0),\\
Pe_j &= \frac{U_{\infty j}L}{D_j}\ \ j = 1,2,
\end{aligned} \tag{1.43}$$

where $\Psi_j'(0)$ $(j = 1,2)$ is given by the solution of the system of equations (1.42).

In the case of liquids, for which $\varepsilon_j^{-2} \ll 1$ $(j = 1,2)$, the equations for Φ_j can be integrated to give

$$\Phi_j \ = \ \alpha_j\zeta_j^2 + \beta_j\zeta_j + \gamma_j, \tag{1.44}$$

where α_j, β_j and γ_j are constant of integration. Introducing (1.44) into (1.42) gives us

$$\Psi_j \ = \ \frac{(2-j)b\varphi_1 + (j-1)m\varphi_2}{b\varphi_1 + m\varphi_2}\left[1 - \varphi_j^{-1}\int_0^{\xi_j} E(p_j)\mathrm{d}p_j\right],$$

where

$$\begin{aligned}
E(p_j) &= \exp\left(-\frac{\alpha_j}{3}p_j^3 - \frac{\beta_j}{2}p_j^2 - \gamma_j p_j\right),\\
\varphi_j &= \int_0^{\infty} E(p_j)\mathrm{d}p_j,\ \ i = 1,2.
\end{aligned}$$

Thus the dimensionless diffusion flux is

$$\Psi_j'(0) = \frac{(2-j)b\varphi_1 + (j-1)m\varphi_2}{b\varphi_1 + m\varphi_2}\frac{1}{\varphi_j},\ \ j = 1,2,$$

Now we can calculate the Sherwood number in (1.43)

On this basis an iterative numerical procedure to solve (1.42) has been used (see Sapundjiev & Boyadjiev (1993)). This iterative approach has been applied for the solution of the problem (1.42) at $\varepsilon_1 = \varepsilon_2 = 10$, $\theta_1 = \theta_2 = \pm 0.1, \pm 0.3, \pm 0.5$, $a = b = m = 1$, as well as in cases when the interfacial mass transfer is limited by the mass transfer either in the first ($m/b = 0$) or the second ($b/m = 0$) phase.

The results for the dimensionless diffusion flux for three cases are shown in Table 1.5 and these results are used to determine the Sherwood number Sh_j ($j = 1, 2$). The cases considered were (a) the case of commensurable diffusive resistance ($b/m = 1$) which represents mass transfer in both phases, (b) the case where the interfacial mass transfer is limited by mass transfer in the liquid ($b/m = 0$, $\Phi_2 = 0$) and (c) for the case of droplets for which $m/b = 0$.

$a = 1, \varepsilon_1 = \varepsilon_2 = 10$			
$\theta_1 = \theta_2$	$b/m = 1$, $\Psi_1'(0) = \Psi_2'(0)$	$m/b = 0, \Psi_2'(0) = 0$	$b/m = 0, \Psi_1'(0) = 0$
	$-\Psi_1'(0)$	$-\Psi_1'(0)$	$-\Psi_2'(0)$
0.0	0.4319	0.8786	0.8497
0.1	0.4316	0.8261	0.9073
-0.1	0.4316	0.9400	0.8003
0.3	0.4289	0.7398	1.0562
-0.3	0.4289	1.0996	0.7189
0.5	0.4237	0.6689	1.2703
-0.5	0.4237	1.3305	0.6519

Table 1.5: Dimensionless diffusion fluxes under conditions of intense interfacial mass transfer between two liquids.

From Table 1.5 (see Boyadjiev & Babak (2000)) we observe that, in the case of commensurable diffusion resistances ($b/m \approx 1$), the increase in the diffusion mass-transfer rate, as evidenced by the increase in $\Psi'(0)$, in the one phase is coupled with a decrease in the diffusion mass-transfer rate in the other phase. In the particular case ($b/m = 1$, $\theta_1 = \theta_2$) both effects compensate each other completely and the results from the non-linear theory ($\theta_1 = \theta_2 \neq 0$) coincide with those from the linear theory ($\theta_1 = \theta_2 = 0$).

1.7 Comparative analysis of the linear and non-linear theories of the interfacial heat and mass transfer

It has been demonstrated that the average mass-transfer rate for fluid–solid permeable surface systems can be determined from (1.7) for a given concentration distribution on the surface obtained solving the governing equations for a specific problem. Thus the following expression is readily obtained from (1.7) and (1.11):

$$J = -M \frac{D\rho^*}{L\rho_0^*} Pe^{1/2} \Psi'(0)(\bar{C}^* - \bar{C}_\infty), \tag{1.45}$$

where $(\bar{C}^* - \bar{C}_\infty)$ is the value of the concentration difference in the concentration boundary layer (see Boyadjiev (1984)). It can be directly seen (see equation 1 on p.xv) that the ratio ρ^*/ρ_0^* in (1.45) takes into account the convective transfer of the flow through the interfacial boundary, which is induced by a large concentration gradient.

The dimensionless diffusion flux $\Psi'(0)$ in the expression for average mass-transfer rate (1.45) depends on the Schmidt number ($\varepsilon = \sqrt{Sc}$) and on the maximum concentration difference ($\Theta = M(\bar{C}^* - \bar{C}_\infty)/\varepsilon\rho_0^*$):

$$\Psi'(0) = F(\varepsilon, \Theta).$$

A dimensionless concentration difference can be introduced in (1.45)

$$\Delta C = \frac{M(\bar{C}^* - \bar{C}_\infty)}{\rho_0^*} = \varepsilon\Theta,$$

and the mass-transfer rate is then

$$J = -\frac{D\rho_0^*}{L} Pe^{1/2} F(\varepsilon, \Theta)\Delta C. \tag{1.46}$$

In the approximation of the linear theory of mass transfer $\Theta = 0$, and $\rho^*/\rho_0^* = 1$, and the mass-transfer rate is denoted as J_0. The dimensionless diffusion flux depends on the direction of the interfacial mass transfer, i.e. it depends on the sign of Θ. For interfacial mass transfer from permeable surface toward the volume $\Theta > 0$, and in this case the mass-transfer rate is denoted as J_1. In the case of interfacial mass transfer toward the permeable surface ($\Theta < 0$) and $\bar{C}^* = 0$ and $\rho^*/\rho_0^* = 1$, the mass-transfer rate is denoted as J_2.

In the case of $\Theta > 0$, the rise of ΔC leads to an increase of Θ and the ratio ρ^*/ρ_0^*, and this also leads to a decrease of $F(\varepsilon, \Theta)$. When $\Theta < 0$ and $\bar{C}^* = 0$ ($\rho^*/\rho_0^* = 1$), the increase in ΔC results in an increase of $F(\varepsilon, \Theta)$. This multiple influence of the magnitude and the direction of the concentration gradient on the mass-transfer rate can be made clear through a comparative analysis of J_0, J_1 and J_2. In the case of diffusion of water vapour in air, when $U_\infty = 1m/s$, $L = 0.1m$, $D = 2.19 \times 10^{-5} m^2/s$ and $\varepsilon = 1$ the dependencies J_0, J_1 and J_2 on ΔC are shown at Figure 1.5 (see Boyadjiev & Babak (2000)).

The effects due to an increase in the concentration difference are shown in Table 1.6. It can be clearly seen that when $\Theta > 0$ the influence of the concentration difference ΔC on the convective (ρ^*/ρ_0^*) and diffusion ($F(\varepsilon, \Theta)$) effects is different, while the change of ρ_0^* also leads to a change in Θ. Regardless of the rise of ρ^*/ρ_0^*, the Sherwood number at $\Theta > 0$ is always smaller than the Sherwood number at $\Theta < 0$ (for equal concentration differences). This is analogous to the result for the mass-transfer rate (Figure 1.5), where non-linear effects due to large concentration differences increase the mass-transfer rate, in comparison to data from the linear theory.

The results shown in Table 1.6 and Figure 1.5 are valid in the case of mass transfer in a gas phase. In the case of liquids, the maximal possible concentration gradients observed

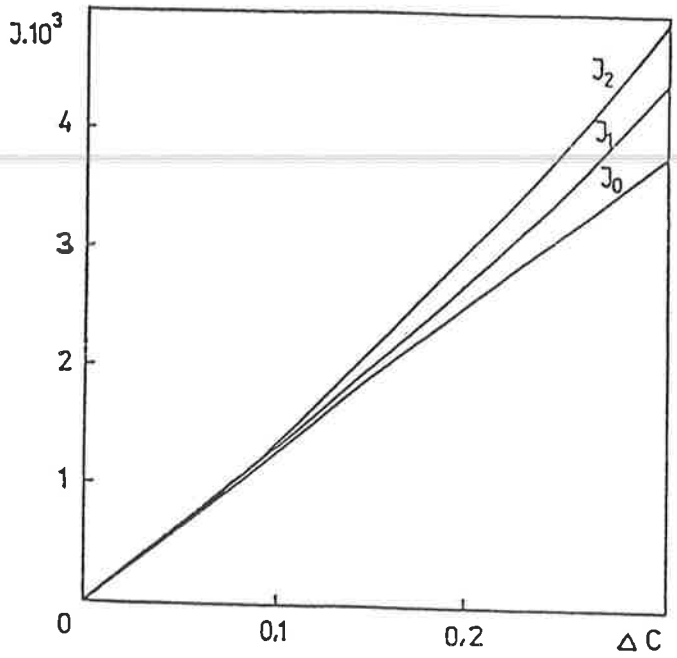

Figure 1.5: The influence of the direction of the mass transfer on the mass-transfer rate.

occur at small Θ and the above effects are not observed, except in the case of unlimited solubility of the diffused substance.

The heat-transfer rate (1.19) is determined from the coefficient of heat transfer (k_T), where the dimensionless flow $T'(0)$ depends on the Schmidt number (ε) and on the concentration difference

$$T'(0) = F_T(\varepsilon, \bar{\alpha}_T, \Theta). \tag{1.47}$$

In this manner the Nusselt number is

$$Nu = -Pe^{1/2}\left[F_T(\varepsilon, \bar{\alpha}_T, \Theta) + \Theta\bar{\varepsilon}_T\frac{\bar{T}^*}{\bar{T}^* - \bar{T}_0}F(\varepsilon, \Theta)\right]. \tag{1.48}$$

The level of heat transfer measured by the Nusselt number in (1.48) depends on the dimensionless temperature difference

$$\Delta T = \frac{\bar{T}^* - \bar{T}_0}{\bar{T}^*} \tag{1.49}$$

and upon the concentration difference ΔC. In particular it depends upon the sign of these quantities, i.e. whether the mass and heat transfer are co-directional or not.

In the approximation of the linear theory of the mass transfer ($\Theta = 0$) the following is obtained directly from (1.48)

$$Nu_0 = -Pe^{1/2}F_T(\varepsilon, \bar{\alpha}_T, 0). \tag{1.50}$$

Under the conditions of the non-linear mass transfer it follows from (1.48) that:

$$Nu_{mn} = -Pe^{1/2}\left[F_T(\varepsilon, \bar{\alpha}_T, \Theta_m) + \frac{\Theta_m\bar{\varepsilon}_T}{\Delta T_n}F(\varepsilon, \Theta_m)\right], \tag{1.51}$$
$$m = 1, 2, \quad n = 1, 2,$$

$\Delta C \times 10^2$	Θ	ρ^*/ρ_0^*	$F(1,\Theta)$	Sh
0.000	0.0000	1.00	0.644	44.9
0.215	0.0315	1.03	0.649	45.3
0.359	0.0544	1.05	0.639	45.5
0.718	0.1190	1.12	0.612	46.3
1.440	0.2950	1.29	0.550	48.1
2.150	0.5800	1.58	0.486	51.9
0.215	-0.030	1.00	0.679	45.9
0.359	-0.050	1.00	0.689	46.5
0.718	-0.010	1.00	0.716	48.4
1.440	-0.200	1.00	0.779	52.6
2.150	-0.300	1.00	0.855	57.8

Table 1.6: Comparison of the non-linear effects under conditions of intense interfacial mass transfer in gas-solid surface systems.

where $\Theta_1 > 0$, $\Theta_2 < 0$, $\Delta T_1 > 0$ and $\Delta T_2 < 0$, i.e. the mass and the heat transfer are co-directional at $m = n$, while at $m \neq n$ they are not co-directional. Under these conditions we obtain from (1.46)

$$\Theta_m = (-1)^{m-1} \frac{\rho_0^*}{\varepsilon \rho_0} \Delta C, \quad m = 1, 2. \tag{1.52}$$

Introducing (1.51) and (1.52) allows us to obtain the relationship describing the dependency of the Nusselt number on the concentration difference, i.e. a relation for the heat-transfer kinetics as well as the non-linear mass-transfer kinetics. These results are displayed in Figure 1.6 (see Boyadjiev & Babak (2000)); they are obtained at $Pe = 10^4$, $\varepsilon = 1$, $\bar{\alpha}_T = 2$, $\Delta T_n = (-1)^{n-1}$ $(n = 1, 2)$ and are compared to the results obtained from the linear theory (Nu_0).

It is seen from Figure 1.6 that the non-linear effects (as a result of an intense interfacial mass transfer under the conditions of large concentration differences) compared to the linear theory (Nu_0) lead to a rise in the heat-transfer rate (Nu_{mn}), when the mass transfer and the heat transfer are co-directional $(m = n)$, and to a decrease in the heat-transfer rate, when these two processes are not co-directional $(m \neq n)$.

The multi-component mass-transfer rate (1.16) is determined from the mass-transfer coefficient, i.e. from Sh_i $(i = 1, \ldots, n)$, where the following can be obtained for the dimensionless concentration gradient

$$\Psi_i'(0) = F_i(\varepsilon, \alpha_i, \Theta), \quad i = 1, \ldots, p. \tag{1.53}$$

Thus it is seen that the multi-component mass-transfer rate depends on the concentration difference of the separate components

$$\Delta C_i = \frac{\bar{C}_i^* - \bar{C}_{i0}}{\bar{C}_i^*}, \quad i = 1, \ldots, p, \tag{1.54}$$

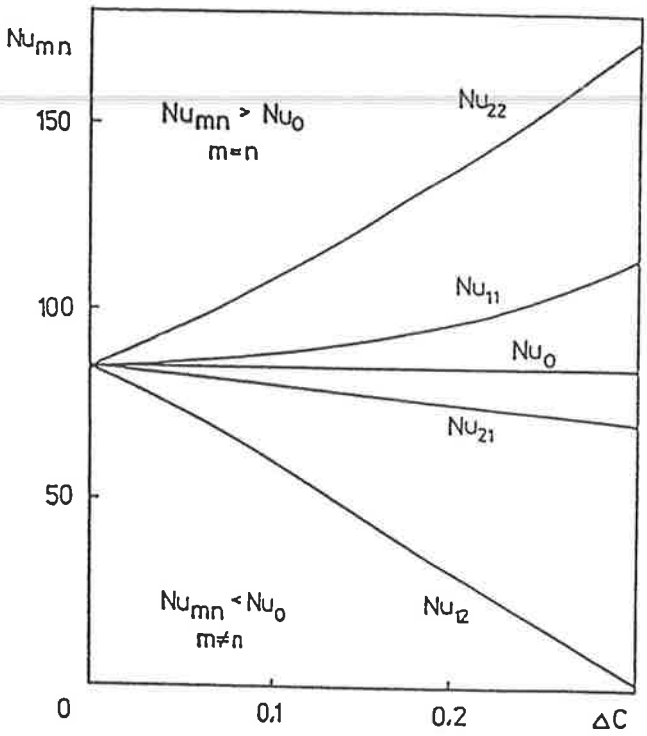

Figure 1.6: The influence of the direction of the mass transfer on the heat-transfer rate.

as well as upon the large concentration difference ΔC. In a similar way as in the case of heat transfer, it is important whether the non-linear mass transfer and the mass transfer of the other components are co-directional or not.

In the approximations of the linear theory ($\Theta = 0$) we obtain

$$Sh_{0i} = -Pe^{1/2} F_i(\varepsilon, \alpha_i, \Theta), \quad i = 1, \ldots, p. \tag{1.55}$$

Under conditions of non-linear mass transfer the Sherwood number is

$$Sh_{0i} = -Pe^{1/2} \left[F_i(\varepsilon, \alpha_i, \Theta) + \frac{\Theta_m \bar{\varepsilon}_i}{\Delta C_{in}} F(\varepsilon, \Theta_m) \right], \tag{1.56}$$
$$i = 1, \ldots, p, \quad i = 1, 2,$$

where $\Delta C_{i1} > 0$, $\Delta C_{i2} < 0$ $(i = 1, \ldots, n)$, i.e. the non-linear mass transfer and the mass transfer of the different components are co-directional when $m = n$, and they are not co-directional when $m \neq n$.

The relation (1.56) is shown on Figure 1.7 under the following conditions; $Pe = 4566$, $\varepsilon = 1$, $\bar{\alpha}_T = 2$, $\Delta C_i = (-1)^{i-1}$ $(i = 1, \ldots, n)$ and a comparison to linear theory (1.55) is done.

The data presented in Figure 1.7 (see Boyadjiev & Babak (2000)) shows that in comparison to linear theory (Sh_{i0}), the multi-component mass-transfer rate (Nu_{mn}) increases

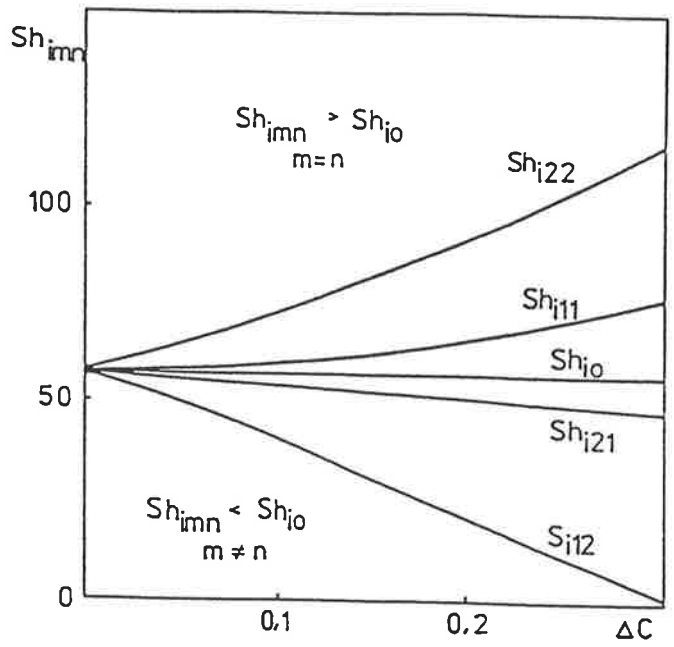

Figure 1.7: The influence of the direction of the mass transfer on the multi-component mass-transfer rate.

with the rise in the large concentration gradient (ΔC), when the non-linear mass transfer and the multi-component mass transfer are co-directional ($m = n$). In the cases of $m \neq n$, the multi-component mass transfer decreases with the rise of ΔC.

The theoretical analysis of the intense interfacial mass transfer in gas–liquid systems as a result of large concentration gradients shows that the non-linear effects are significant in the cases when the interfacial mass-transfer rate is limited by the mass transfer in the gas phase. In the dimensionless concentration gradient $F(\varepsilon, \Theta)$ the influence of the motion of the liquid on the velocity distribution in a gas diffusion boundary layer is considered. Results show that there is a difference between the absorption rates ($\Theta < 0$) and the desorption rates ($\Theta > 0$). The various effects under conditions of $Pe = 10^4$ and $Sc = 1$, in the cases of absorption and desorption of ammonia in water (or a water solution of acid) are displayed in Figure 1.8 and Table 1.7. These results are the same as the ones under the conditions of the interfacial mass transfer in gas–solid permeable systems (Figure 1.5 and Table 1.6).

The theoretical analysis above shows that the non-linear mass transfer due to large concentration gradients leads to an increase in the mass-transfer rate. This rise is higher when the interfacial mass transfer is from the volume toward the interfacial surface.

The influence of the non-linear mass transfer on the simultaneous processes of heat transfer and multi-component mass transfer depends on the direction of these processes. In the case when the non-linear mass transfer and the parallel transfer processes are co-directional, a rise in the concentration gradient leads to a rise in the parallel transfer process rate. In the case when these two processes are not co-directional, the parallel transfer process rate decreases.

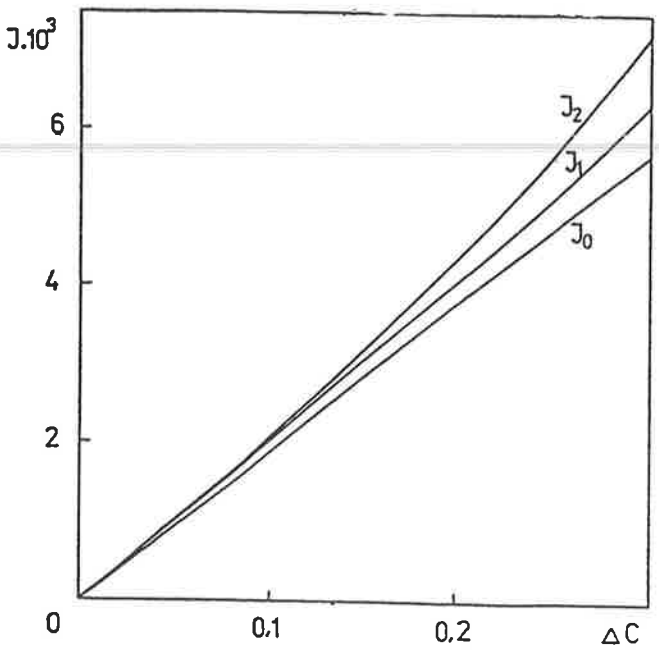

Figure 1.8: The influence of the direction of the mass transfer on the mass-transfer rate in gas-liquid systems.

$\Delta C \times 10^2$	Θ	ρ^*/ρ_0^*	$F(1,\Theta)$	Sh
0.00	0.000	1.00	0.730	73.2
0.65	0.113	1.11	0.676	75.0
1.30	0.274	1.27	0.614	78.0
1.95	0.517	1.52	0.535	81.3
0.65	-0.10	1.00	0.785	78.5
1.30	-0.20	1.00	0.851	85.1
1.95	-0.30	1.00	0.932	93.2

Table 1.7: Comparison of the non-linear effects under conditions of intense interfacial mass transfer in gas-liquid systems.

There are some additional effects. The work by Boyadjiev & Halatchev (1998a) studied non-linear mass transfer and Marangoni effect in gas–liquid systems; these were subsequently extended in Boyadjiev & Halatchev (1998b) to consider mass-transfer kinetics of systems with large concentration gradients. The large concentration gradients, which induce secondary flows, can be created not only by large concentration differences, as has been shown so far, but also from a decrease in the thickness of the boundary layer. This can arise through a chemical reaction together with the mass transfer. In the case of absorption in a falling film (see Boyadjiev & Babak (2000)) the chemical reaction in the liquid leads to a decrease in the boundary-layer thickness and the increase in the mass-transfer rate is proportional to the change in ρ^*/ρ_0^*. The same result has been obtained in the work by Boyadjiev (1992) when the effect of large concentrations is considered. The influence of the non-linear mass transfer on the flow in a laminar boundary layer (see Boyadjiev (1982)) is considerably more complex; when these layers start interacting, for example the flow of a gas or a liquid into a channel (see Boyadjiev (1992)). As a result

the Sherwood number depends on the length of the channel.

Chapter 2

Linear Stability Analysis of Two-phase Systems (uncoupled problem)

Most industrial scale processes depend, in one way or another, on the fluid flow stability. The equations describing such fluid (gas or liquid) flows are evolution equations which describe the change of both the velocity and the pressure with time and in space. As noted by Joseph (1976) this allows us to use existing techniques for the stability analysis of the evolution of hydrodynamics.

As demonstrated in Chapter 1 systems with interfacial mass transfer are characterised by a number of non-linear effects which can significantly change both the kinetics and the mass-transfer mechanism as a result of the effect of induced secondary flows on the velocity and concentration fields. The change may have a significantly greater effect if the system loses its stability and reaches a new stable state, what is termed a self-organising dissipative structure. The mathematical description of these systems can be carried out on the basis of stability theory. In the present chapter the stability of boundary-layer flows in fluid–solid permeable systems will be studied. An attempt to examine some aspects of the boundary-layer flow instabilities in the cases of gas–liquid and liquid–liquid systems will be briefly discussed.

2.1 Fluid–solid permeable surface systems

A linear stability analysis of the flow in the laminar boundary layer is considered under conditions, where high mass fluxes at the interface induce secondary flows. These secondary flows have the effect of "suction" or "blowing" from/into the boundary layer, depending upon the direction of the intense interfacial mass transfer. The induced secondary flow is a result of concentration differences and has a nonuniform velocity v_n (see equation (2) on p.xv) along the length of the surface. This velocity is proportional to the

local mass flux on the interface (see Figure 1.1).

Let us consider the steady laminar flow of a viscous incompressible fluid over a flat, semi-infinite permeable plate, across which a concentration difference exists. The mathematical model for this flow consists of the Navier-Stokes equations coupled to the convection-diffusion equation

$$\begin{aligned}
\frac{\partial U_0^*}{\partial x^*} + \frac{\partial V_0^*}{\partial y^*} &= 0, \\
\frac{\partial U_0^*}{\partial t^*} + U_0^* \frac{\partial U_0^*}{\partial x^*} + V_0^* \frac{\partial U_0^*}{\partial y^*} &= -\frac{1}{\rho_0^*}\frac{\partial P_0^*}{\partial x^*} + \nu\left(\frac{\partial^2}{\partial x^{*2}} + \frac{\partial^2}{\partial y^{*2}}\right) U_0^*, \\
\frac{\partial V_0^*}{\partial t^*} + U_0^* \frac{\partial V_0^*}{\partial x^*} + V_0^* \frac{\partial V_0^*}{\partial y^*} &= -\frac{1}{\rho_0^*}\frac{\partial P_0^*}{\partial y^*} + \nu\left(\frac{\partial^2}{\partial x^{*2}} + \frac{\partial^2}{\partial y^{*2}}\right) V_0^*, \\
\frac{\partial C_0^*}{\partial t^*} + U_0^* \frac{\partial C_0^*}{\partial x^*} + V_0^* \frac{\partial C_0^*}{\partial y^*} &= D\left(\frac{\partial^2}{\partial x^{*2}} + \frac{\partial^2}{\partial y^{*2}}\right) C_0^*,
\end{aligned} \tag{2.1}$$

with the initial and boundary conditions

$$(U_0^*, V_0^*) = (U_\infty, 0),\ C_0^* = \bar{C}_\infty^*,\ P_0^* = 0 \ \text{ at } x^* = 0; \tag{2.2a}$$

$$U_0^* = 0,\ V_0^* = -\frac{MD}{\rho_0^*}\frac{\partial C_0^*}{\partial y^*},\ C_0^* = \bar{C}_0^* \ \text{ at } y^* = 0; \tag{2.2b}$$

$$U_0^* \to U_\infty,\ C_0^* = \bar{C}_\infty^* \ \text{ as } y^* \to \infty. \tag{2.2c}$$

Here x^* and y^* denote Cartesian coordinates aligned along and normal to the plate surface, respectively, U_0^* and V_0^* are the velocity components in the x^* and y^* directions, P_0^* is the pressure, ν the kinematic viscosity, $\bar{C}_0^*$ the concentration at the permeable surface, $\bar{C}_\infty^*$ the free-stream concentration (as $y^* \to \infty$), ρ_0^* is the gas(liquid) density and an asterisk denotes a dimensional quantity. The coupling between the Navier-Stokes and convection-diffusion equations occurs in the boundary condition for the vertical velocity component (2.2b), where M is the molecular mass and D is the diffusion coefficient. This condition corresponds to existence of species flux at the surface. For the special case of impermeable surface it simply reduces to $\partial C_0^*/\partial y^* = 0$. In order to allow comparison with the classical triple-deck theory for the Blasius boundary layer we now employ a slightly different notation to that introduced in Chapter 1.

The above system is non-dimensionalised with respect to a typical length scale L (for example, the distance from the leading edge of the plate), the free-stream speed U_∞ and the concentrations $\bar{C}_0^*$ and $\bar{C}_\infty^*$ as follows:

$$\begin{aligned}
&(x^*, y^*) = L(x, y),\ \ t^* = \frac{Lt}{U_\infty},\ \ (U_0^*, V_0^*) = U_\infty(U_0, V_0), \\
&C_0^* = \bar{C}_\infty^* + (\bar{C}_0^* - \bar{C}_\infty^*)C_0 \ \ P_0^* = \rho_0^* U_\infty^2 P.
\end{aligned} \tag{2.3}$$

The resulting non-dimensional equations are then

$$\begin{aligned}
\frac{\partial U_0}{\partial x}+\frac{\partial V_0}{\partial y} &= 0,\\
\frac{\partial U_0}{\partial t}+U_0\frac{\partial U_0}{\partial x}+V_0\frac{\partial U_0}{\partial y} &= -\frac{\partial P_0}{\partial x}+\frac{1}{Re}\left(\frac{\partial^2}{\partial x^2}+\frac{\partial^2}{\partial y^2}\right)U_0,\\
\frac{\partial V_0}{\partial t}+U_0\frac{\partial V_0}{\partial x}+V_0\frac{\partial V_0}{\partial y} &= -\frac{\partial P_0}{\partial y}+\frac{1}{Re}\left(\frac{\partial^2}{\partial x^2}+\frac{\partial^2}{\partial y^2}\right)V_0,\\
\frac{\partial C_0}{\partial t}+U_0\frac{\partial C_0}{\partial x}+V_0\frac{\partial C_0}{\partial y} &= \frac{1}{ScRe}\left(\frac{\partial^2}{\partial x^2}+\frac{\partial^2}{\partial y^2}\right)C_0,
\end{aligned} \tag{2.4}$$

which must be solved subject to the initial and boundary conditions

$$\begin{aligned}
&(U_0,V_0)=(1,0),\ C_0=1 \ \text{ at } \ x=0;\\
&U_0=0,\ V_0=-\frac{\theta}{Sc\,Re}\frac{\partial C_0}{\partial y},\ C_0=1 \ \text{ on } \ y=0;\\
&U_0\to 1,\ C_0=0 \ \text{ as } \ y\to\infty.
\end{aligned} \tag{2.5}$$

Here $Re = U_\infty L/\nu$ is the Reynolds number, $Sc = \nu/D$ is the Schmidt number and $\theta = M(\bar{C}_0^* - \bar{C}_\infty^*)/\rho_0^*$ is a parameter which characterises the intensity of the mass transfer across the flat plate.

The influence of the intense mass transfer on the hydrodynamic stability of the flows in the laminar boundary layer will be investigated by applying linear stability theory (see Schlichting (1979), Drazin & Reid (1981)). This theory will be applied for an almost parallel flow in the boundary layer (see Boyadjiev, Halatchev & Tchavdarov (1996a)), i.e. under the boundary-layer approximation. The basic boundary-layer flow and concentration field for fluid–solid permeable surface systems are governed by the systems of equations (1.4) and boundary conditions (1.5). After introducing similarity variables, as was demonstrated in Chapter 1 (section 1.1), we obtain the system (1.9).

2.1.1 Disturbance equations

The linear stability analysis considers the total flow field (U, V, P) as a superposition of a small amplitude, two-dimensional disturbance (u, v, p) upon the basic flow (U_0, V_0, P_0):

$$\begin{aligned}
U(x,y,t) &= U_0(x,y)+\epsilon u(x,y,t),\\
V(x,y,t) &= V_0(x,y)+\epsilon v(x,y,t),\\
P(x,y,t) &= P_0(x,y)+\epsilon p(x,y,t),\\
C(x,y,t) &= C_0(x,y)+\epsilon c(x,y,t),
\end{aligned} \tag{2.6}$$

where ϵ $(0 < \epsilon \ll 1)$ is a small perturbation parameter.

The governing equations for two-dimensional disturbances follow from the Navier-Stokes equations and the convection-diffusion equation by linearisation about the basic steady

flow and concentration state. This yields the equations

$$
\begin{aligned}
u_x + v_y &= 0, && \text{(2.7a)}\\
u_t + U_0 u_x + u U_{0x} + v U_{0y} + V_0 u_y &= -p_x + Re^{-1}\left(u_{xx} + u_{yy}\right), && \text{(2.7b)}\\
v_t + U_0 v_x + u V_{0x} + V_0 v_y + v V_{0y} &= -p_y + Re^{-1}\left(v_{xx} + v_{yy}\right), && \text{(2.7c)}\\
c_t + U_0 c_x + u C_{0x} + V_0 c_y + v C_{0y} &= Re^{-1} Sc^{-1}\left(c_{xx} + c_{yy}\right). && \text{(2.7d)}
\end{aligned}
$$

2.1.2 Boundary conditions at the interface

In order to simplify the problem and study the dominant mass-transfer effect we shall make the first engineering approximation, that is linearisation of the vertical disturbance velocity inhomogeneous boundary condition. The system of equations (2.7) has the following initial and boundary conditions:

$$
\begin{aligned}
&(u, v) = (0, 0),\ c = 0 \ \text{ at } \ x = 0; && \text{(2.8a)}\\
&u = 0,\ v = -\frac{\theta}{Sc\,Re}\frac{\partial c}{\partial y},\ c = 0 \ \text{ on } \ y = 0; && \text{(2.8b)}\\
&u \to 0,\ c = 0 \ \text{ as } \ y \to \infty. && \text{(2.8c)}
\end{aligned}
$$

It was argued in Boyadjiev *et. al.* (1996a) that since in the first-order approximation the mass-transfer parameter θ is small ($|\theta| < 1$), a linearisation in the boundary condition for the disturbances equations can be made, resulting further in a decoupling of the disturbance equations thus leading to a classical eigenvalue problem of Orr-Sommerfeld type. This assumption was based upon the fact that the inhomogeneous boundary condition (2.8b) for the vertical velocity component contains a term proportional to the mass-transfer parameter θ and reciprocal of the Reynolds number. Thus, even for moderate values of the Reynolds number, this term would be small, and hence the inhomogeneity could be ignored. Considering this simplification in the first-order approximation of the small parameters ϵ^2, ϵ and θ the boundary condition for v at the surface (2.8b) reduces simply to $v = 0$. Hence, the only way the mass transfer can affect the boundary-layer flow stability is through its influence on the basic flow, changing the shape of its velocity profile and hence its hydrodynamic stability properties.

2.1.3 Orr-Sommerfeld equation for almost parallel boundary-layer flows

Under the above assumption, the boundary conditions at the interface decouple. Equations (2.7a), (2.7b) and (2.7c) are therefore decoupled from the convection-diffusion equation for the concentration disturbance (2.7d). Differentiating the first two equations with respect to y and x gives us the opportunity to eliminate the pressure p from the governing equations.

We shall employ a parallel flow like approximation. The stability of the basic flow will be examined by considering periodic disturbances of the form:

$$\begin{aligned} u(x,y) &= F'(y)\exp i\alpha(x-\hat{c}t), \\ v(x,y) &= -i\alpha F(y)\exp i\alpha(x-\hat{c}t), \end{aligned} \tag{2.9}$$

where $F(y)$ is the amplitude of the disturbances; α and $\hat{c}$ are respectively the wavenumber and wave-velocity:

$$\alpha = \frac{2\pi}{\lambda}, \quad \hat{c} = \hat{c}_r + i\hat{c}_i. \tag{2.10}$$

In the expression (2.10) λ is the length-wave, $\alpha\hat{c}_r$ is the frequency and $\alpha\hat{c}_i$ the growth rate. The condition for stability of the flow is $\hat{c}_i < 0$. In the case of $\hat{c}_i > 0$ the basic flow is unstable (the amplitude grows with time).

Introducing (2.9) into (2.7), eliminating the pressure, leads to an Orr-Sommerfeld type of equation for the amplitude of the disturbances

$$\begin{aligned} &(U_0-\hat{c})\,(F''-\alpha^2F) - \frac{\partial^2 U_0}{\partial y^2}F = \\ &-\frac{i}{\alpha Re}(F^{iv}-2\alpha^2F''+\alpha^4F) + \frac{i}{\alpha Re}\left[V_0F''' + \left(\frac{\partial^2 U_0}{\partial x\partial y}-\alpha^2\right)F'\right], \end{aligned} \tag{2.11}$$

which must be solved subject to the boundary conditions

$$\begin{aligned} y=0: &\quad F=0, \;\; F'=0; \\ y\to\infty: &\quad F=0, \;\; F'=0. \end{aligned}$$

The additional terms to the classical Orr-Sommerfeld equation which appear in (2.11) take into account the boundary-layer growth (see Van Stijn (1982, 1983)). In this sense the boundary-layer flow is termed "almost" parallel.

2.1.4 The basic flow field and disturbance amplitude governing equation

The basic velocity profiles were obtained through solving the two-point boundary-value problem (1.9) asymptotically and numerically and the results tabulated. As was noted in Chapter 1 (section 1.1.) the comparison of the results obtained using the two approaches shows good agreement (see Table 1.1). Having the exact boundary values for certain values of the parameter θ and Schmidt number Sc, found in the studies Vulchanov & Boyadjiev (1988) and Vulchanov & Boyadjiev (1990), and reported in Chapter 1 the basic flow profiles were generated by using the last step in the usual numerical procedure for solving two-point boundary-value problem, i.e. the problem (1.9) was reduced to an initial-value problem. In order to do this it is suitable to introduce the boundary-layer variables

$$y = Re^{-1/2}Y, \; U_0 = U_B, \; V_0 = Re^{-1/2}V_B, \tag{2.12}$$

where y is physical coordinate and Y is boundary-layer coordinate. The boundary-layer equations are such that a similarity solution exists and we therefore define a new similarity variable

$$\zeta = \frac{Y}{\sqrt{x}}.$$

From (1.8) it follows that the new similarity variable ζ can be related to the old similarity variable η via the Schmidt number ($\varepsilon = \sqrt{Sc}$, $Sc = \nu/D$) as

$$\zeta = \frac{2}{\varepsilon}\eta. \tag{2.13}$$

Hence all functions in the equation (2.11) can be expressed in terms of the new variable ζ

$$\begin{aligned} &U_B = f'(\zeta), \;\; V_B = \frac{1}{2\sqrt{x}}(\zeta f' - f), \\ &F(y) = \varphi(\zeta), \;\; F^{(j)} = \delta^{-j}\varphi^{(j)}, \;\; \delta = \sqrt{\frac{\nu x}{U_\infty}} \\ &j = 1, \ldots, 4. \end{aligned} \tag{2.14}$$

Now from (1.9), (2.13) and (2.14) f can be determined from

$$\begin{aligned} &2f''' + ff'' = 0, \\ &f(0) = a, \;\; f'(0) = 0, \;\; f''(0) = \frac{\varepsilon^2}{4}b, \end{aligned} \tag{2.15}$$

where a and b are tabulated in Table 2.1 and determined through solving the system of equations (1.9) ($\Phi(0) = a$, $\Phi'(0) = 0$, $\Phi''(0) = b$). The initial conditions a and b include the effect of the mass transfer on the velocity profiles in the boundary layer. They depend considerably on the direction and magnitude of the induced flow rate, i.e. on the direction and magnitude of the mass-transfer rate. The case of $\theta > 0$ corresponds to "blowing" while $\theta < 0$ corresponds to "suction" in/from the boundary layer and according to the theory of the hydrodynamic stability (see Schlichting (1979)) stabilisation or destabilisation of the boundary-layer flow should be expected.

Introducing (2.14) into equation (2.11) and its boundary conditions leads to the following Orr-Sommerfeld type of equation:

$$\begin{aligned} (f' - C)\left(\varphi'' - A^2\varphi\right) - f'''\varphi = -\frac{i}{ARe}\Big\{ &\left(\varphi^{iv} - 2A^2\varphi'' + \varphi\right) - \\ &\frac{1}{2}\left(\zeta f' - f\right)\varphi''' + \frac{1}{2}\left[\left(\zeta f''' + f''\right) + A^2\left(\zeta f' - f\right)\right]\varphi'\Big\}, \end{aligned} \tag{2.16}$$

with appropriate boundary conditions

$$\varphi(0) = 0, \;\; \varphi'(0) = 0; \;\; \varphi(\infty) = 0, \;\; \varphi'(\infty) = 0.$$

ε	θ	a	b
1	-0.30	0.2546	1.710
	-0.20	0.1557	1.557
	-0.10	0.0716	1.432
	0.0	0.0	1.329
	0.10	-0.0619	1.239
	0.20	-0.1162	1.162
	0.30	-0.1643	1.095
10	-0.05	0.0229	0.0136
	0.0	0.0	0.0133
	0.05	-0.0124	0.0131
	0.10	-0.0207	0.0129
	0.20	-0.0319	0.0128
20	-0.05	0.0239	0.0034
	-0.03	0.0122	0.0033
	0.0	0.0	0.0032
	0.03	-0.0057	0.0032

Table 2.1: Initial values a and b for several values of the parameter θ and Schmidt number Sc ($\varepsilon = \sqrt{Sc}$).

Here $A = \alpha\delta$ is the wavenumber, $C = \beta/\alpha U_\infty = C_r + iC_i$ the wave-speed and $Re = U_\infty\delta/\nu$ the Reynolds number.

The linear stability analysis of a laminar boundary layer under conditions of intense interfacial mass transfer is reduced to determining C_r and $\varphi(\zeta)$ at $C_i = 0$, when the Reynolds number Re and the wavenumber A are given. The critical Reynolds number Re_{cr} is defined as the point on the neutral curve of stability at which $\mathrm{d}\,Re/\mathrm{d}\,A = 0$, i.e. the turning point.

The eigenvalue problem (2.16) can be solved numerically[1]. Since the problem is a linear eigenvalue problem, in theory it is possible to solve for $C = C(Re, A)$. Solutions for this problem are usually presented in two ways: for specific values of the parameters A and Re, the corresponding value of C is tabulated or the locus in (Re, A)-plane on which $C_i = 0$ (the curve of neutral stability) is plotted. The critical Reynolds number is the minimum Reynolds number above which an infinitesimally small disturbance will grow. We consider only the temporal stability problem in which the Reynolds number Re and the wavenumber A are given real values, while the complex wave-speed C is determined as the eigenvalue.

[1]This work has been reported in Boyadjiev *et. al.* (1996a). The chasing method for solving two-point boundary-value problems has been used (see Na (1979), Berzin & Zhidkov (1965)).

2.1.5 Curves of neutral stability

The curves of neutral stability presented in the (Re, A)-plane as well as in (Re, C_r)-plane are given in Figures 2.1 to 2.6. They are obtained for gas–solid permeable surface systems ($\varepsilon = 1$) and for liquid–solid permeable surface systems ($\varepsilon = 10,\ 20$).

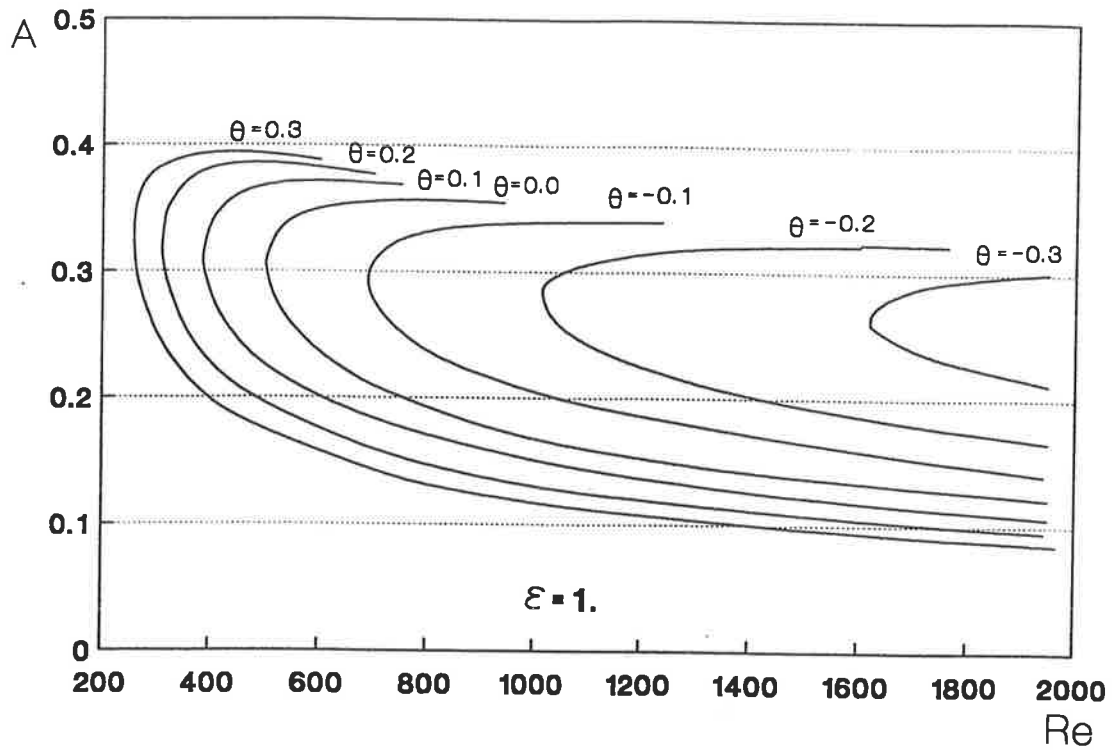

Figure 2.1: The curves of neutral stability in (Re, A)-plane in the case of gas-solid permeable surface systems ($\varepsilon = \sqrt{Sc} = 1$).

The critical Reynolds number Re_{cr}, the corresponding wave-speed C_r, and wavenumber A are obtained. $C_{r\,max}$ and A_{max} are also obtained from these results. We denote by A_{max} the maximal value for wavenumber and $C_{r\,max}$ the maximal value of the wave-speed at which the flow is stable at any Reynolds number. They are shown in Table 2.2 for different values of mass-transfer level (θ) in the case of "blowing" and "suction".

It is seen from Figures 2.1 - 2.6 and from Table 2.2, that interfacial mass transfer directed toward the phase boundary ($\theta < 0$) (the effect of "suction") stabilises the flow, i.e. an increase in the concentration difference $\left|\bar{C}_0^* - \bar{C}_\infty^*\right|$ (that is, θ) leads to an increase in Re_{cr} and to an increase in $C_{r\,max}$ and A_{max}. In the case of mass transfer directed from the phase boundary toward the volume ($\theta > 0$) (the effect of "blowing") a destabilisation of the flow is observed, i.e. an increase in the concentration difference $\left|\bar{C}_0^* - \bar{C}_\infty^*\right|$ leads to a decrease in Re_{cr} and to an increase in $C_{r\,max}$ and A_{max}.

Thus, high concentration gradients have a stabilising effect at $\theta < 0$, and this is significantly higher then the destabilising effect that occurs in the case of a change in the direction of mass transfer ($\theta > 0$).

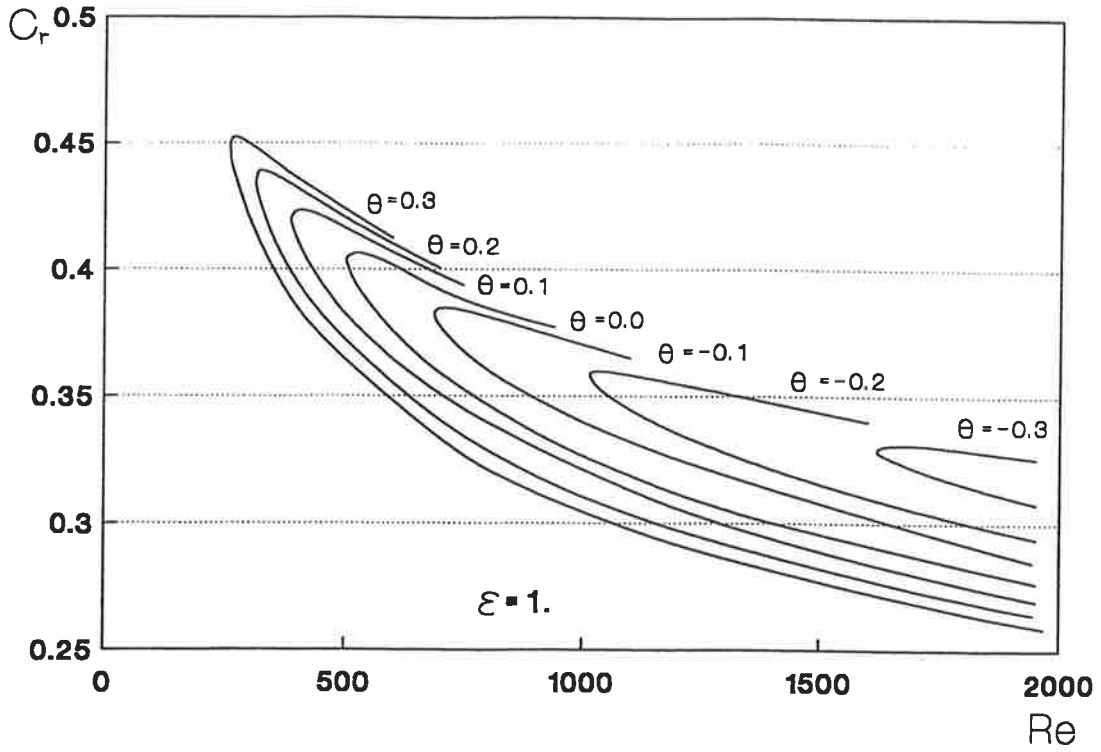

Figure 2.2: The curves of neutral stability in (Re, C_r)-plane in the case of gas-solid permeable surface systems ($\varepsilon = \sqrt{Sc} = 1$).

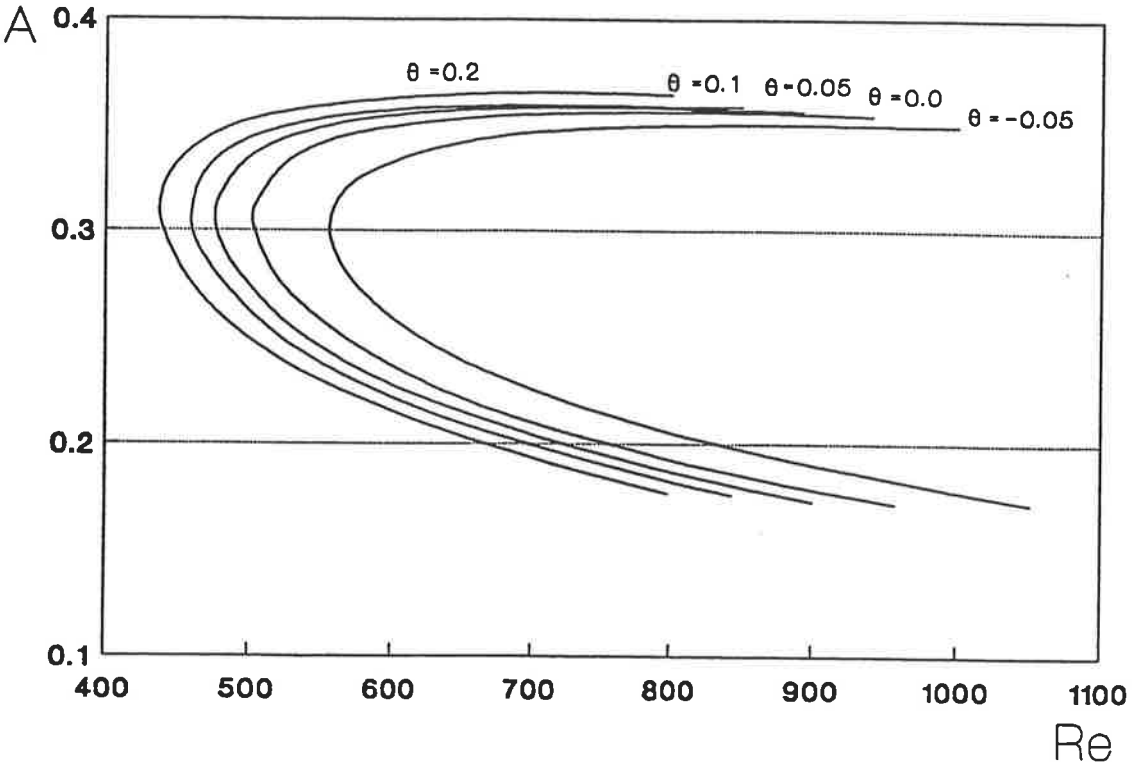

Figure 2.3: The curves of neutral stability in (Re, A)-plane in the case of liquid-solid permeable surface systems ($\varepsilon = \sqrt{Sc} = 10$).

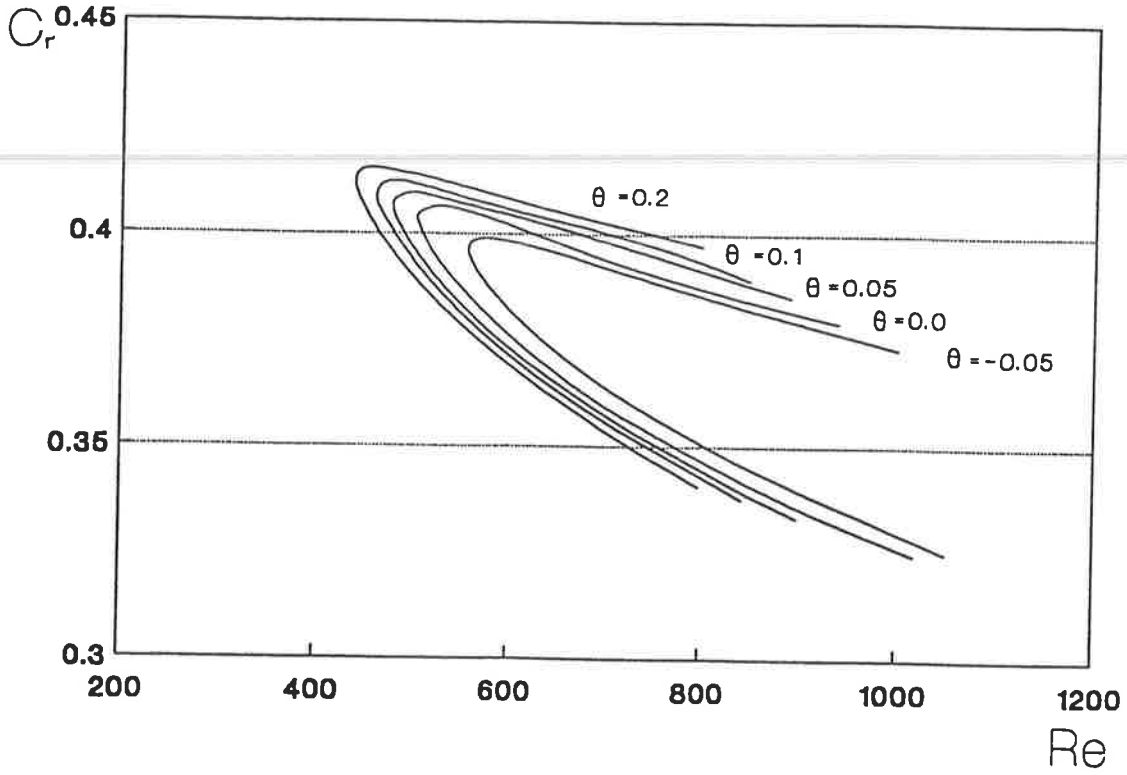

Figure 2.4: The curves of neutral stability in (Re, C_r)-plane in the case of liquid-solid permeable surface systems ($\varepsilon = \sqrt{Sc} = 10$).

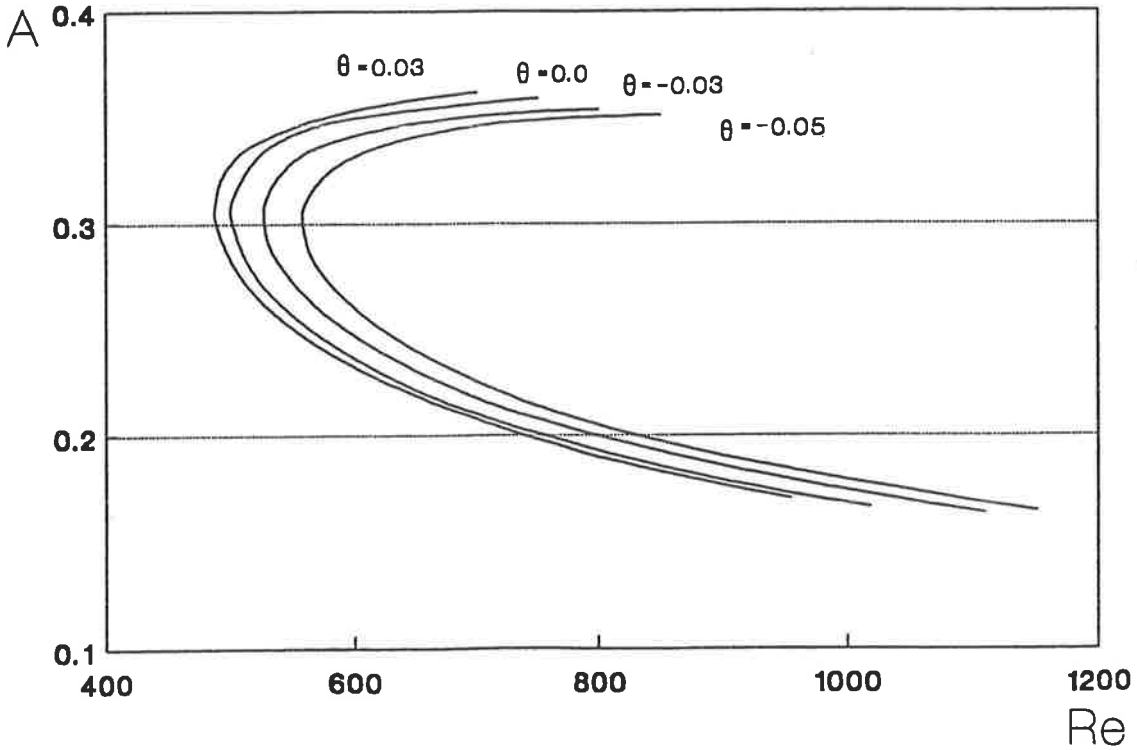

Figure 2.5: The curves of neutral stability in (Re, A)-plane in the case of liquid-solid surface systems ($\varepsilon = \sqrt{Sc} = 20$).

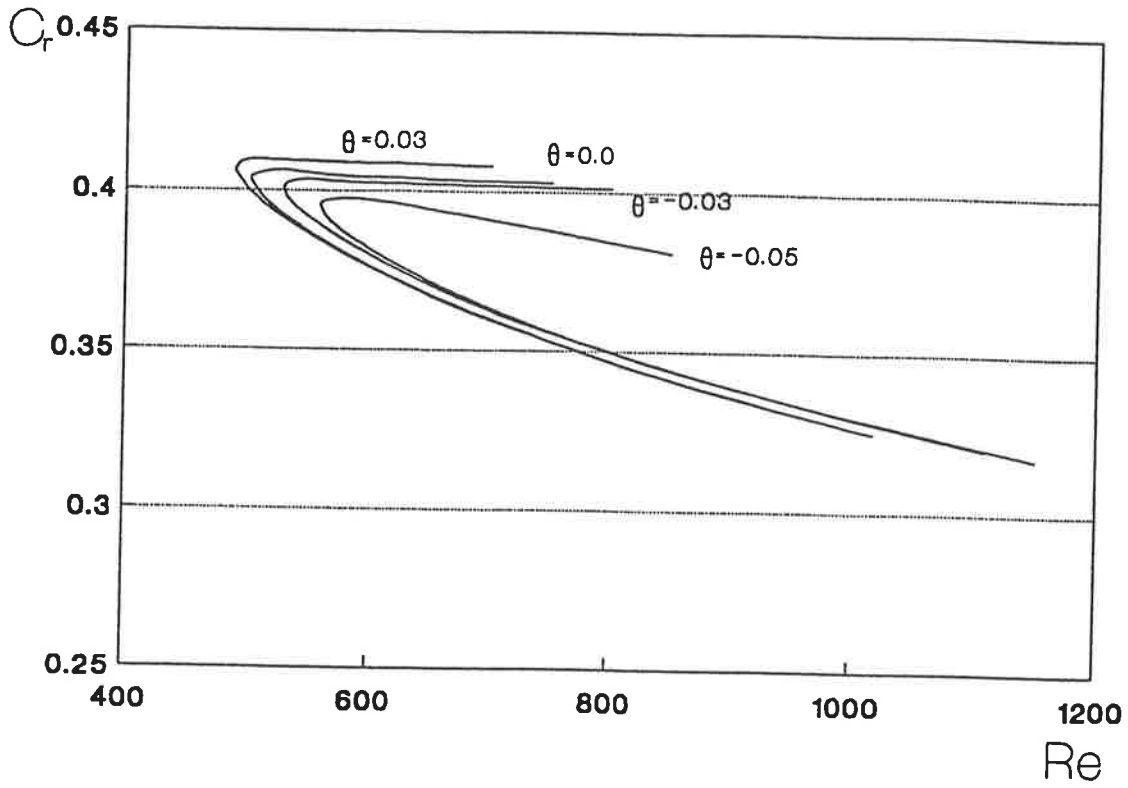

Figure 2.6: The curves of neutral stability in (Re, C_r)-plane in the case of liquid-solid permeable surface systems ($\varepsilon = \sqrt{Sc} = 20$).

ε	θ	Re_{cr}	A	C_r	A_{max}	$C_{r\,max}$
1	-0.30	1619	0.259	0.3281	0.301	0.3310
	-0.20	1014	0.285	0.3587	0.322	0.3599
	-0.10	689	0.290	0.3816	0.340	0.3848
	0.0	501	0.305	0.4035	0.359	0.4067
	0.10	386	0.309	0.4196	0.373	0.4243
	0.20	310	0.320	0.4351	0.387	0.4396
	0.30	258	0.331	0.4488	0.398	0.4526
10	-0.05	555	0.300	0.3960	0.351	0.3990
	0.0	501	0.305	0.4035	0.359	0.4067
	0.05	476	0.305	0.4062	0.360	0.4097
	0.10	459	0.305	0.4085	0.361	0.4124
	0.20	437	0.310	0.4123	0.367	0.4155
20	-0.05	558	0.305	0.3959	0.351	0.3978
	-0.03	528	0.305	0.4010	0.354	0.4037
	0.0	501	0.305	0.4035	0.359	0.4067
	0.03	488	0.305	0.4064	0.362	0.4099

Table 2.2: Values of the critical Reynolds numbers Re_{cr}, corresponding wave-speed C_r and $C_{r\,max}$ and A_{max} obtained.

The observed influence of the intense interfacial mass transfer on the hydrodynamic stability in the fluid–solid permeable systems is much more interesting for systems with

interfacial boundaries, such as gas–liquid and liquid–liquid systems.

2.2 Gas–liquid systems

In the previous section we considered the case of fluid–solid permeable surface systems. We now turn our attention to the problem of the stability of a laminar boundary-layer flow, under conditions of intense interfacial mass transfer, when high mass fluxes through the gas–liquid interface induce secondary flows. The results of this study have been reported in Boyadjiev & Halatchev (1996b). The interaction between the flow in the gas and liquid phase is considered in the case of movable liquid surface (see Figure 2.7). The flow stability under these conditions is not only of theoretical, but also of practical, interest in view of the fact that it defines the rate of a number of industrial absorption and desorption processes.

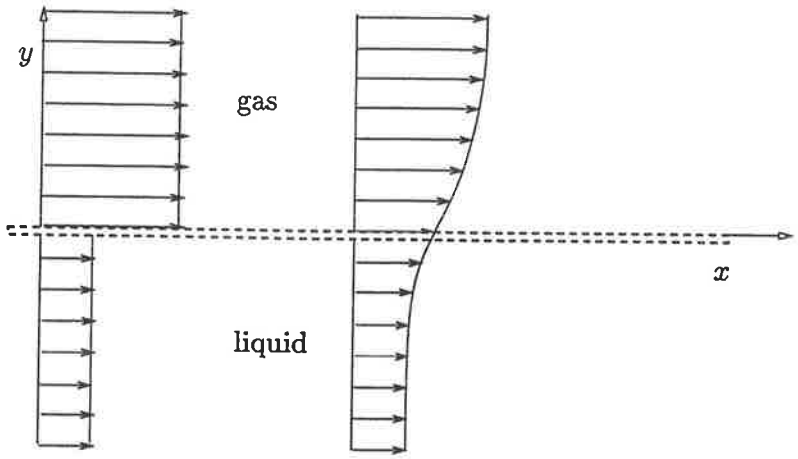

Figure 2.7: Schematic representation of the velocity profiles of the flows in the gas–liquid system.

The governing equations of the non-linear mass transfer in gas–liquid systems (1.25) will be considered under the approximation of mixing-layer theory (see Ting (1959)), assuming that the diffusive resistance is concentrated in the gas phase (see Vulchanov & Boyadjiev (1990)) where it was shown that the non-linear effects in the liquid phase can be neglected. Hence, attention will be focused on the problem when the mass transfer is limited (located) only in the gas phase. The basic boundary-layer velocity and concentration fields will be taken to be self-similar and governed by the system of equations (1.31). This two-point boundary-value problem has been solved asymptotically as well as numerically and the solutions tabulated (see Chapter 1, section 1.4). We will generate the velocity profiles in a similar manner, as in the last section, by reducing (1.31) to an initial value problem for the functions f_j $(j = 1, 2)$, which are solutions of

$$2f_j''' + f_j f_j'' = 0,$$
$$f_j(0) = a_j, \quad f_j'(0) = b_j, \quad f_j''(0) = c_j, \quad j = 1, 2,$$

where $a_1 = a_{10}$, $b_1 = \varepsilon_1 b_{10}/2$, $c_1 = \varepsilon_1^2 c_{10}/4$, $a_2 = 0$, $b_1 = \varepsilon_2 b_{20}$ and $c_2 = -\varepsilon_2^2 c_{20}/2$. The values of a_{10}, b_{10}, c_{10}, b_{20} and c_{20} (these are the exact boundary conditions of (1.31)) are tabulated in Table 2.3 for $\varepsilon_1 = 1$ and in Table 2.4 for $\varepsilon_2 = 20$ and different values

θ_3	a_{10}	b_{10}	c_{10}
-0.30	0.2797	0.2185	1.662
-0.20	0.1703	0.2166	1.520
-0.10	0.0785	0.2152	1.402
0.0	0.0	0.2138	1.304
0.10	-0.0682	0.2129	1.220
0.20	-0.1283	0.2118	1.084
0.30	-0.1816	0.2107	1.084

Table 2.3: Initial values f and its derivatives in the gas phase at $\theta_1 = 0.1$, $\theta_2 = 0.152$, several values of the parameter θ_3 and Schmidt number Sc ($\varepsilon_1 = \sqrt{Sc_1} = 1$).

θ_3	b_{20}	c_{20}
-0.30	0.0546	0.00033
0.0	0.0536	0.00026
0.30	0.0527	0.00022

Table 2.4: Initial values f and its derivatives in the liquid phase at $\theta_1 = 0.1$, $\theta_2 = 0.152$, several values of the parameter θ_3 and Schmidt number Sc ($\varepsilon_2 = \sqrt{Sc_2} = 20$).

of the parameters θ_1, θ_2 and θ_3 (1.26). Note the parameters θ_1 and θ_2 account for the kinematic and dynamic interactions between the gas and liquid phases respectively, while θ_3 characterise the mass-transfer level in the gas phase.

The effects of the intense interfacial mass transfer in the gas–liquid systems appear as a difference in the rates of absorption and desorption. In the cases where the process is limited by the diffusion resistance in the gas phase this difference can be explained by the Marangoni effect in the liquid phase. The higher rate of absorption (compared with the rate of desorption) can be explained by the effect of non-linear mass transfer, i.e. the influence of the induced secondary flow on the kinetics of the mass transfer. Those cases, where the desorption rate is higher then the absorption rate can be explained with the flow destabilisation and transition to turbulence, since it is possible for the flow in the gas phase to be turbulent for desorption and laminar for absorption at equal Reynolds numbers.

As has already been mentioned, the flow instability analysis will be carried out under the assumption that the interaction between the gas and liquid phases in the disturbances equations can be ignored in the first-order approximation; that is the effect of interfacial mass transfer is dominant. Furthermore, it was argued in Boyadjiev & Halatchev (1996b) that the disturbances are in the flow volume but not on the interface. In this sense the stability of the profiles f_j ($j = 1, 2$) will be studied by solving the Orr-Sommerfeld (2.16) equation separately in the two phases with the boundary conditions for a rigid

surface, excluding the effect of interfacial instabilities and considering the effect of mass transfer only through its influence on the basic boundary-layer flow. The Orr-Sommerfeld equation for the gas and liquid phases have the same form and can be written as:

$$(f_j' - C)\,(\varphi_j'' - A^2\varphi_j) - f_j'''\varphi_j = -\frac{i}{ARe}\left\{(\varphi_j^{iv} - 2A^2\varphi_j'' + \varphi_j) - \right. \tag{2.17}$$

$$\left. \frac{1}{2}\,(\zeta_j f_j' - f_j)\,\varphi_j''' + \frac{1}{2}\left[(\zeta_j f_j''' + f_j'') + A^2\,(\zeta_j f_j' - f_j)\right]\varphi_j' \right\},\quad j = 1, 2$$

and the boundary conditions

$$\varphi_j(0) = 0,\ \ \varphi_j'(0) = 0;\ \ \varphi_j(\infty) = 0,\ \ \varphi_j'(\infty) = 0,\ \ j = 1, 2. \tag{2.18}$$

The curves of neutral stability (Re, A) and (Re, C_r) for the gas phase are shown in Figures 2.8 and 2.9. The critical Reynolds number, the corresponding wavenumber and phase velocities are presented in Table 2.5.

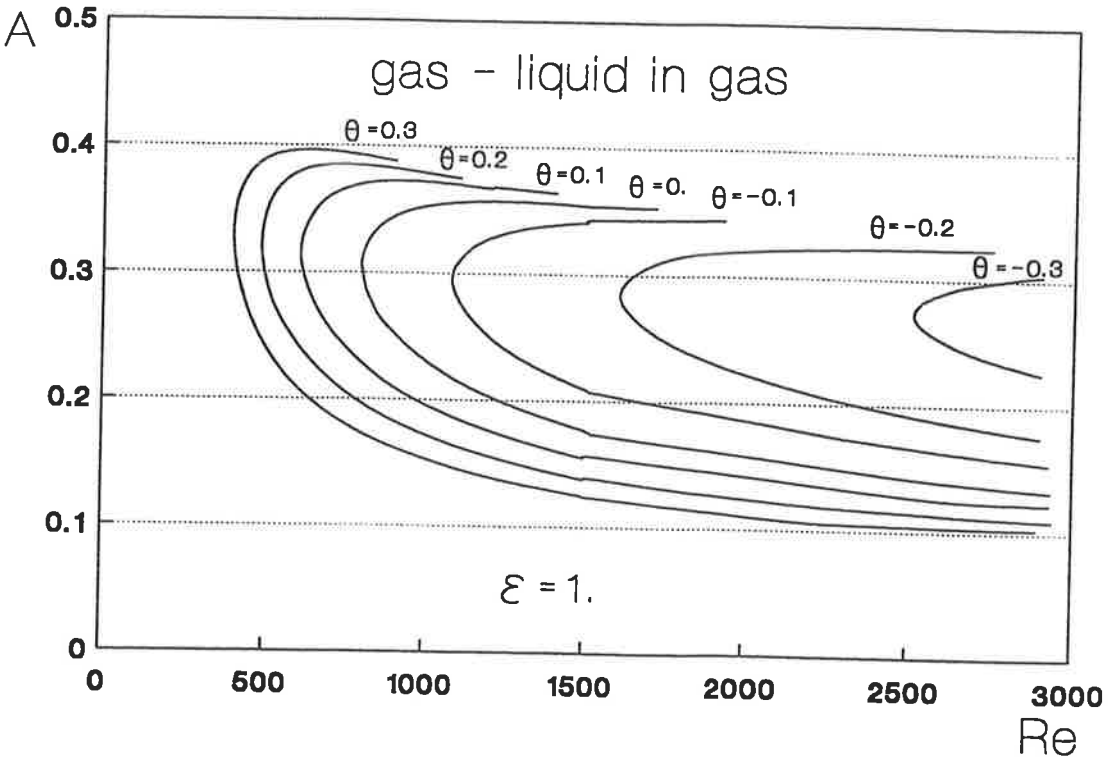

Figure 2.8: The curves of neutral stability in (Re, A)-plane in the case of gas–liquid systems (in gas phase $\theta = \theta_3$).

It is seen from the results that the direction of the intense interfacial mass transfer influences the hydrodynamic stability of the boundary-layer flow in the gas phase in a manner analogous to the case of the solid interface. Hence, in the case of absorption $\theta_3 > 0$ an increase in stability is observed. In the opposite case, of desorption $\theta_3 < 0$, the stability decreases.

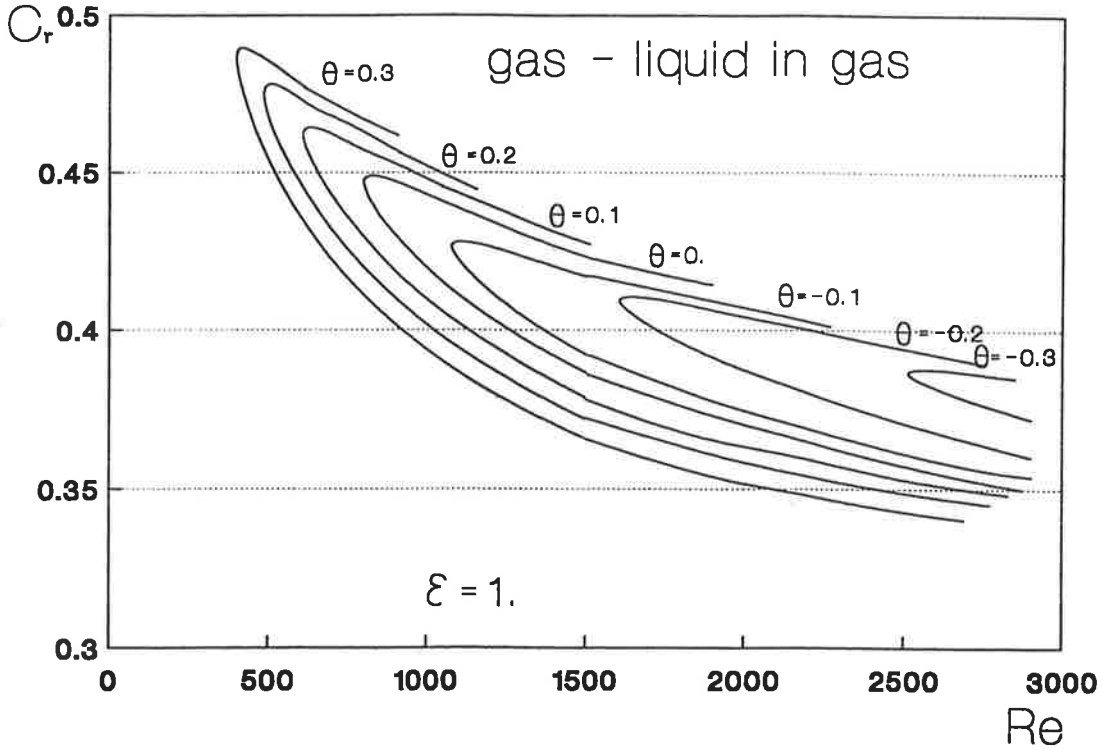

Figure 2.9: The curves of neutral stability in (Re, C_r)-plane in the case of gas–liquid systems (in gas phase $\theta = \theta_3$).

θ_3	Re_{cr}	A	C_r	A_{max}	$C_{r\,max}$
-0.30	2511	0.270	0.3863	0.304	0.3878
-0.20	1605	0.285	0.4095	0.325	0.4108
-0.10	1078	0.295	0.4264	0.341	0.4281
0.0	795	0.305	0.4469	0.356	0.4493
0.10	605	0.315	0.4620	0.373	0.4645
0.20	483	0.320	0.4749	0.386	0.4786
0.30	397	0.330	0.4866	0.398	0.4902

Table 2.5: Values of the critical Reynolds numbers Re_{cr}, corresponding wave-speed C_r and $C_{r\,max}$ and A_{max} obtained (in gas phase).

The solution of (2.17) for the liquid phase (f_2) shows that the flow is stable at large Reynolds numbers ($Re \approx 25,000$), which is readily explained by the fact that the velocity gradient in the liquid boundary layer is low and the profile has a shape similar to that of the plane flow (see Boyadjiev & Halatchev (1996b)).

2.3 Liquid–liquid systems

We now turn our attention to the case of a liquid–liquid system. In the previous section it was demonstrated that the motion of the interface significantly influences the hydrodynamic stability of a flow in the gas boundary layer, when the phase boundary

was considered to be a flat liquid surface. In addition, this motion and the effect of the intense interfacial mass transfer were superposed. We should emphasise again that these two effects are studied here only through their influence on the basic velocity and concentration fields, thus excluding from the problem the possibility of Kelvin-Helmholtz instabilities. The effect of a movable interface is expected to be considerably more pronounced under conditions of intense interfacial mass transfer between two liquids, where the hydrodynamic interaction between them is stronger and the surface velocity is higher.

Non-linear effects in the case of intense interfacial mass transfer between two liquids can manifest themselves with the same intensity in both phases. In a number of extraction processes, where the motion of one of the phases (the dispersion medium) induces motion in the other (the dispersed phase), these effects are of great interest. Further we consider the hydrodynamic stability of the flow under conditions of intense interfacial mass transfer between two liquid phases, where the velocity in the volume of one of them is zero. A linear analysis of the stability of a laminar boundary-layer flow under conditions of interfacial mass transfer between two liquids, when high mass fluxes through the liquid–liquid phase boundary induce secondary flows has been reported in Halatchev & Boyadjiev (1996). The first liquid (phase I) is in motion over the second one (phase II in rest) (see Figure 2.10)

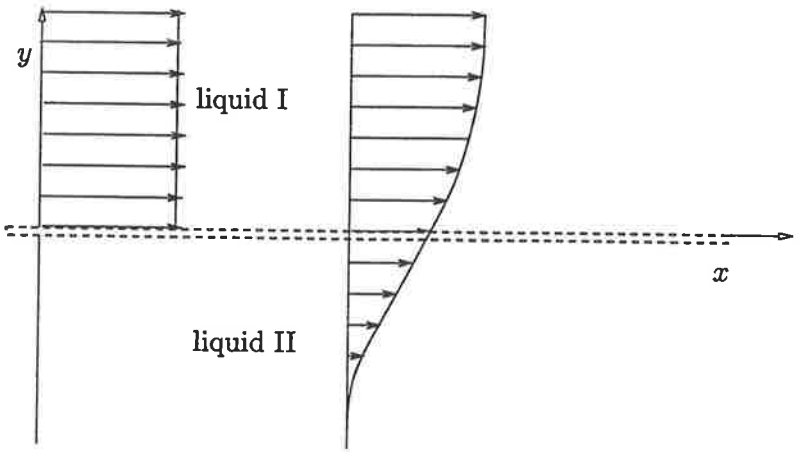

Figure 2.10: Schematic representation of the velocity profiles of the flows in the liquid-liquid system

The basic velocity and concentration fields for this problem are given by (1.42). This system has been solved asymptotically as well as numerically and the solutions tabulated. The velocity and concentration profiles are generated again by reducing this two-point boundary-value problem to an initial value problem for the functions f_j $(j = 1, 2)$, which are solutions of

$$
\begin{aligned}
&2f_j''' + f_j f_j'' = 0, \\
&f_j(0) = A_j, \quad f_j'(0) = B_j, \quad f_j''(0) = C_j, \quad j = 1, 2, \\
&(f_1'(\infty) = 1, \quad f_2'(\infty) = 0),
\end{aligned}
$$

where A_j, B_j, and C_j are a result of numerical solution of (1.42) and these values are tabulated for the velocity profile in the liquid I in Tables 2.6 at $\varepsilon = 10$ in the case when the diffusion resistance is limited by the mass transfer in the phase I ($m/b = 0$, $\theta_2 = 0$) and in the case of commensurable diffusion resistances in two liquids ($b/m = 1$, $\theta_1 = \theta_2$). Note the parameters θ_j ($j = 1, 2$) characterise the mass-transfer level in the two phases respectively.

$\varepsilon = 10$	θ_1	A_1	B_1	C_1
$m/b = 0$	-0.5	0.66525	0.439	0.38722
	-0.3	0.03299	0.420	0.29754
	-0.1	0.0094	0.405	0.27142
	0.0	0.0	0.4	0.26565
	0.1	-0.00826	0.394	0.25142
	0.3	-0.02219	0.384	0.23011
	0.5	-0.03345	0.376	0.21074
$b/m = 1$	-0.5	0.02117	0.413	0.36788
	-0.3	0.01287	0.408	0.29076
	-0.1	0.00432	0.402	0.27031
	0.0	0.0	0.4	0.26565
	0.1	-0.00432	0.397	0.24321
	0.3	-0.01287	0.39	0.22114
	0.5	-0.02117	0.385	0.20987

Table 2.6: Initial values f and its derivatives in the phase I ($m/b = 0$, $\theta_2 = 0$) and in the case of commensurable diffusion resistances in two liquids ($b/m = 1$, $\theta_1 = \theta_2$).

The linear stability analysis in the liquid–liquid systems is carried out in a similar fashion to that in the case of gas–liquid systems. The results obtained show that the stability of the flow depends considerably on the non-linear effects of the mass transfer θ_j ($j = 1, 2$), as well as on the interface velocity (B_j).

The effect of the non-linear mass transfer in the liquid I ($m/b = 0$) and the effects of the increase of the interface velocity are superposed and their total influence on the stability of the flow in phase I is shown in Figure 2.11 and the critical Reynolds number, and corresponding wavenumber and wave-speed are tabulated in Table 2.7. Under conditions of commensurable diffusive resistances in the two liquids ($b/m = 1$) the non-linear effects are lower (Table 2.7). The influence of the non-linear effects (θ_j) on the flow stability decreases.

A linear stability analysis of the liquid II (phase II) show analogous results as those in gas–liquid systems. The flow is stable to large Reynolds numbers ($Re \approx 25,000$), which can be explained by the profile shape (again, similar to that for plane flow).

The studies on the hydrodynamic stability in systems with intense interfacial mass transfer show that the stability increases with a rise in the interface velocity and the rise of concentration gradients in the cases when the mass transfer is directed from the vol-

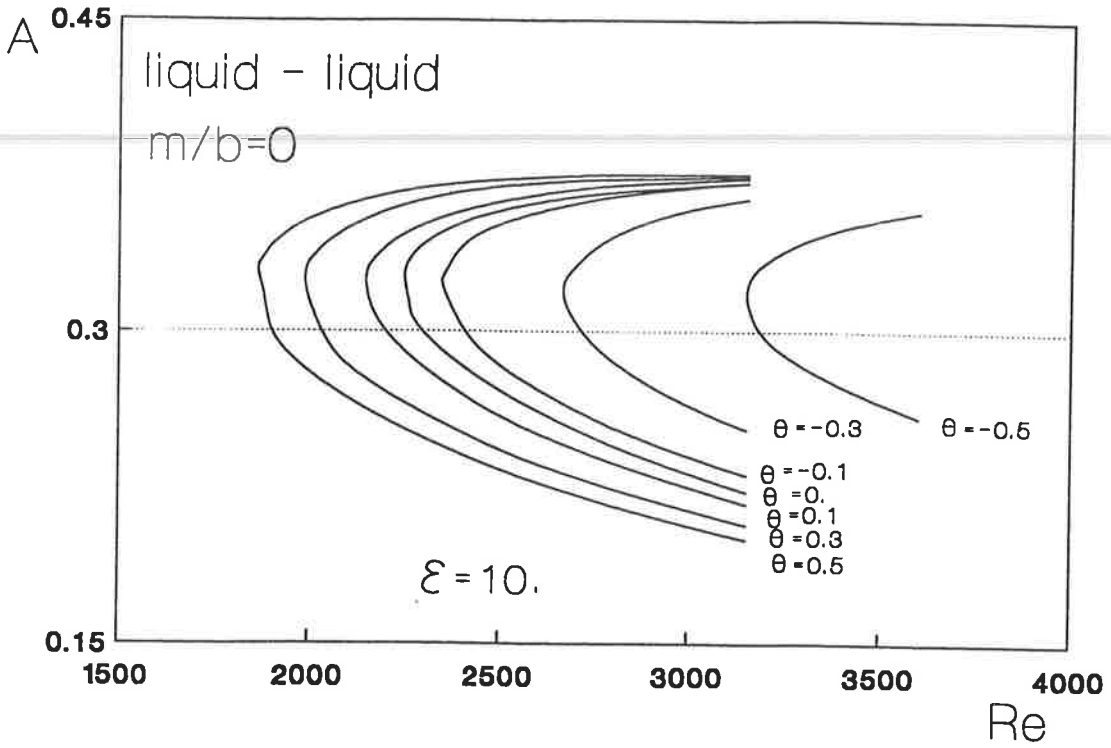

Figure 2.11: The curves of neutral stability in (Re, A)-plane in the case of liquid–liquid systems in the liquid I (phase I) ($\varepsilon = 10, m/b = 0$, $\theta_2 = 0$) at several values of $\theta = \theta_1$.

$\varepsilon = 10$	θ_1	Re_{cr}	A	C_r	A_{max}	$C_{r\,max}$
$m/b = 0$	-0.5	3145	0.315	0.6235	0.358	0.6246
	-0.3	2663	0.320	0.6155	0.364	0.6163
	-0.1	2343	0.325	0.6092	0.372	0.6101
	0.0	2243	0.330	0.6081	0.372	0.6085
	0.1	2145	0.320	0.6042	0.374	0.6053
	0.3	1983	0.320	0.5997	0.375	0.6009
	0.5	1859	0.330	0.5969	0.377	0.5974
$b/m = 1$	-0.5	2503	0.325	0.6130	0.367	0.6135
	-0.3	2398	0.325	0.6099	0.370	0.6111
	-0.1	2288	0.325	0.6079	0.371	0.6086
	0.0	2243	0.330	0.6081	0.372	0.6085
	0.1	2170	0.330	0.6064	0.374	0.6066
	0.3	2079	0.320	0.6020	0.375	0.6036
	0.5	1999	0.325	0.6008	0.375	0.6015

Table 2.7: Values of the critical Reynolds numbers Re_{cr}, corresponding wave-speed C_r and $C_{r\,max}$ and A_{max} obtained in cases $m/b = 0$, $\theta_2 = 0$ and $b/m = 1$, $\theta_1 = \theta_2$ for different values of θ_1.

ume toward the interface. The decrease in the interface velocity, and the change of the direction of interface mass transfer, serves to destabilise the flow in the boundary layer.

In a number of cases experimental studies of mass transfer in systems with intense in-

terfacial mass transfer between two liquids show a higher mass-transfer rate compared with that predicted by the linear theory of mass transfer (see Hennenberg, Bisch, Vignes-Adler & Sanfeld (1979) and Linde, Schwartz & Wilke (1979)). To date this has been explained as being a result of the Marangoni effect, i.e. the creation of interfacial tension gradients as a result of temperature or concentration heterogeneity on the phase boundary. The interfacial tension gradient induces secondary flows directed tangentially to the phase boundary. They change the velocity profiles in the boundary layer. Thus, the mass-transfer rate is directly affected. The results show that under conditions of intense interfacial mass transfer high mass fluxes induce secondary flows directed normally to the phase boundary. These secondary flows change the velocity profiles, consequentially they change the kinetics of mass transfer (non-linear mass transfer) and the hydrodynamic stability of the flow. In the case of hydrodynamic instability, there is a possible transition to turbulence and the mass-transfer rate drastically increases. This is a radically different mechanism of the intense interfacial mass transfer influence on the kinetics of the mass transfer and the hydrodynamic stability in liquid–liquid systems.

Only with a full solution of the problem, allowing for the possibility of interfacial instabilities, will a comparative analysis of the influence of the Marangoni effect and the effect of the non-linear mass transfer on the mass-transfer rate and the hydrodynamic stability of systems with intense interfacial mass transfer be possible.

Chapter 3

Effects of Concentration and Temperature on the Mass-Transfer Kinetics and Hydrodynamic Stability

In Chapter 1 we demonstrated that the large concentration gradients in systems with intense interfacial mass transfer induce secondary flows on the phase boundary. The induced velocities depend upon both the concentration and its gradient. In this chapter the influence of the concentration and its gradient on the velocity distribution in the laminar boundary layer and flow stability will be studied (this work has been reported in Boyadjiev & Halatchev (1998b) and Halatchev & Boyadjiev (1998)).

3.1 Concentration effects

The theoretical analysis of the non-linear mass transfer and flow instability in systems with intense interfacial mass transfer which has been presented so far considers only the effect of large concentration gradients. Under these conditions, however, the concentrations themselves are high and their influence manifests itself in a dependency of density, viscosity and diffusivity upon the concentration. In order to consider these effects we use the basic model of non-linear mass transfer.

We shall first consider the question of the dependency of the induced secondary flow velocity upon the density, viscosity and diffusivity for the case of a laminar gas flow over a solid permeable surface. Let us consider a binary gas mixture, in which gas phase II has partial density[1] ρ_2 and flows over a permeable surface with mass-transfer rate w_2,

[1] In a multicomponent mixture the density $\rho = \sum_{i=1}^{n} \rho_i$, $[kg/m^3]$ is a sum of the partial densities of its components, defined as $\rho_i = M_i c_i$. Here, M_i, $[kg/mol]$ is the molecular mass of the i-th component and c_i, $[mol/m^3]$ is its concentration.

while gas phase I, whose partial density is ρ_1, is blown through the porous surface with mass-transfer rate $\boldsymbol{w}_1$. Thus, we have the following expressions for the density of the binary mixture and the average mass-transfer rate:

$$\rho = \sum_{i=1}^{2} \rho_i, \quad \boldsymbol{w} = \frac{1}{\rho} \sum_{i=1}^{2} \rho_i \boldsymbol{w}_i. \tag{3.1}$$

The diffusion velocity $\boldsymbol{W}_i$ is the deviation of the velocity $\boldsymbol{w}_i$ from the gas mixture velocity $\boldsymbol{w}$:

$$\boldsymbol{W}_i = \boldsymbol{w}_i - \boldsymbol{w}, \quad i = 1, 2. \tag{3.2}$$

From (3.2) it follows directly that

$$\sum_{i=1}^{2} \rho_i \boldsymbol{w}_i = \boldsymbol{w} \sum_{i=1}^{2} \rho_i + \sum_{i=1}^{2} \rho_i \boldsymbol{W}_i = \boldsymbol{w}\rho + \sum_{i=1}^{2} \rho_i \boldsymbol{W}_i.$$

Thus, from (3.1) and (3.2) we obtain

$$\sum_{i=1}^{2} \rho_i \boldsymbol{W}_i = 0. \tag{3.3}$$

The law of conservation of mass holds for each component

$$\nabla \cdot (\rho \boldsymbol{w}_i) = \nabla \cdot [\rho_i (\boldsymbol{w} + \boldsymbol{W}_i)] = 0, \quad i = 1, 2, \tag{3.4}$$

where summation over the repeated index is assumed. For the mixture, we therefore have

$$\nabla \cdot (\rho \boldsymbol{w}) = 0.$$

We shall focus our attention on the case of isothermal diffusion of gas phase I into gas phase II. The mass flux of gas phase I, as a result of diffusion, is defined via the mass-fraction gradient as follows:

$$J_1 = C_{01}^* \boldsymbol{W}_1 = -D_{12} \nabla C_{01}^*, \quad C_{01}^* = \frac{\rho_1}{\rho}, \tag{3.5}$$

where D_1 is the diffusion coefficient and C_{01}^* is the mass fraction of gas phase I. From (3.2), (3.4), and (3.5) we obtain

$$\nabla \cdot (\rho \boldsymbol{w}) = \nabla \cdot (\rho D_{12} \nabla C_{01}^*),$$

and making use of the identity

$$\nabla \cdot (C_{01}^* \rho \boldsymbol{w}) = \rho \boldsymbol{w} \cdot \nabla C_{01}^* + C_{01}^* \nabla \cdot (\rho \boldsymbol{w}), \tag{3.6}$$

gives

$$\rho \boldsymbol{w} \cdot \nabla C_{01}^* = \nabla \cdot (\rho D_{12} \nabla C_{01}^*). \tag{3.7}$$

Denoting the components of the velocity $\boldsymbol{w}$ by U_0^* and V_0^* and applying the concentration boundary-layer approximation:

$$\frac{\partial C_{01}^*}{\partial y^*} \gg \frac{\partial C_{01}^*}{\partial x^*},$$

we obtain from (3.7) the convection-diffusion equation

$$\rho \left(U_0^* \frac{\partial C_{01}^*}{\partial x^*} + V_0^* \frac{\partial C_{01}^*}{\partial y^*} \right) = \frac{\partial}{\partial y^*} \left(\rho D_{12} \frac{\partial C_{01}^*}{\partial y^*} \right), \tag{3.8}$$

where U_0^* and V_0^* satisfy the boundary-layer equations of the gas mixture.

For definiteness, we shall consider the basic gas flow over a semi-infinite flat plate, with uniform free-stream velocity U_∞. Thus, the equations of motion of the gas mixture take the following form:

$$\begin{aligned}
&\nabla.(\rho \boldsymbol{w}) = 0, \\
&\rho \left(U_0^* \frac{\partial U_0^*}{\partial x^*} + V_0^* \frac{\partial U_0^*}{\partial y^*} \right) = \frac{\partial}{\partial y^*} \left(\mu \frac{\partial U_0^*}{\partial y^*} \right), \\
&U_0^* = U_\infty, \quad \rho = \text{constant} \quad \text{at} \quad x^* = 0; \\
&U_0^* = U_\infty, \quad V_0^* = V_n \quad \text{at} \quad y^* = 0; \\
&U_0^* = U_\infty \quad \text{as} \quad y^* \to \infty,
\end{aligned} \tag{3.9}$$

where V_n is the velocity of the flow induced from the intense interfacial mass transfer. If we assume that the second component of the gas does not penetrate down through the permeable surface, for example in the case when the mass transfer through the permeable surface is restricted by its porosity, we have from (3.2)

$$\boldsymbol{w} = -\boldsymbol{W}_2 \quad \text{at} \quad y^* = 0. \tag{3.10}$$

From (3.3) and (3.5) we find

$$-C_{01}^* \boldsymbol{W}_1 = C_{02}^* \boldsymbol{W}_2 = (1 - C_{01}^*) \boldsymbol{W}_2 = D_{12} \nabla C_{01}^*,$$

in which case (3.10) can be written as

$$\boldsymbol{w} = -\left(\frac{D_{12}}{1 - C_{01}^*} \nabla C_{01}^* \right)_{y=0} = -\left(\frac{D_{12} \rho}{\rho_2} \nabla C_{01}^* \right)_{y=0}. \tag{3.11}$$

Let us express the concentration of the gas phase I in (3.11) as moles per unit volume, and denote the values of diffusivity and density D_{12}, ρ and ρ_2 on the solid surface ($y^* = 0$) by D, ρ^* and ρ_0^*, respectively

$$C_{01}^* = \frac{\rho_1}{M \rho^*}, \quad D = D_{12}, \quad \rho^* = \rho, \quad \rho_0^* = \rho_2 \quad \text{at} \quad y^* = 0. \tag{3.12}$$

Then, from (3.11), we obtain the normal component of the velocity on the interfacial boundary as

$$V_n = -\frac{MD\rho^*}{\rho_0^*}\left[\frac{\partial}{\partial y^*}\left(\frac{C_{01}^*}{\rho}\right)\right]_{y=0}. \tag{3.13}$$

Note that $\partial C_{01}^*/\partial x = 0$ on the plate, thus implying $U_0^* = 0$.

Equations (3.8) - (3.13) allow us to formulate, in general, the mass transfer of a gas or a liquid flow over a semi-infinite flat permeable plate under the boundary-layer approximations. The governing equations are

$$\begin{aligned}
&\rho\left(U_0^*\frac{\partial U_0^*}{\partial x^*} + V_0^*\frac{\partial U_0^*}{\partial y^*}\right) = \frac{\partial}{\partial y^*}\left(\mu\frac{\partial U_0^*}{\partial y^*}\right),\\
&U_0^*\frac{\partial \rho}{\partial x^*} + V_0^*\frac{\partial \rho}{\partial y^*} + \rho\left(\frac{\partial U_0^*}{\partial x^*} + \frac{\partial U_0^*}{\partial y^*}\right) = 0,\\
&\rho\left(U_0^*\frac{\partial C_0^*}{\partial x^*} + V_0^*\frac{\partial}{\partial y^*}\right) = \frac{\partial}{\partial y^*}\left(\rho D\frac{\partial C_0^*}{\partial y^*}\right),
\end{aligned} \tag{3.14}$$

with the following set of initial and boundary conditions:

$$\begin{aligned}
&U_0^* = U_\infty,\ C_0^* = \bar{C}_0^* \ \text{ at } \ x^* = 0;\\
&U_0^* = 0,\ V_0^* = -\frac{MD}{\rho_0^*}\left(\frac{\partial C_0^*}{\partial y^*}\right) - \frac{D(\rho^* - \rho_0^*)}{\rho^*\rho_0^*}\left(\frac{\partial \rho}{\partial y^*}\right),\ C_0^* = \bar{C}_0^* \ \text{ at } \ y^* = 0;\\
&U_0^* = U_\infty,\ C_0^* = \bar{C}_\infty^* \ \text{ as } \ y^* \to \infty,
\end{aligned} \tag{3.15}$$

where

$$\rho^* = \rho_0^* + M\bar{C}_0^*;$$

in the above system (3.14) and its initial and boundary conditions (3.15) we have omitted the subscript 1 in the concentration. In what follows $C_0^* = C_{01}^*$, the concentration of the fluid phase.

In order to close this system an equation prescribing the density ρ should be added into (3.14) - (3.15). Under conditions of constant pressure and temperature ρ cannot be obtained from the equation of state ($\rho = \rho(T, P)$ at T = constant, P = constant and ρ = constant, i.e. it depends only on the substance of the mixture). The density ρ depends only on the concentration of the components

$$\rho = \rho_2 + MC_0^*.$$

Comparing (3.14) - (3.15) with the mathematical model (1.4) shows that the asymptotic theory of the non-linear mass transfer in systems with intense interfacial mass transfer has been derived by employing the following approximations:

$$\rho = \text{constant}, \quad \mu = \text{constant}, \quad D = \text{constant}. \tag{3.16}$$

Previous analysis has shown that, in a number of cases (see Table 3.1 and Figures 3.1 - 3.3), the effect of the diffused substance concentration on the density, viscosity and diffusion coefficient can be modelled in a first-order approximation as linear functions (see Boyadjiev (1984))

$$\rho = \rho_0(1 + \bar{\rho}\bar{C}), \quad \mu = \mu_0(1 + \bar{\mu}\bar{C}), \tag{3.17}$$
$$D = D_0(1 + \bar{D}\bar{C}), \quad \bar{C} = \frac{C_0^* - \bar{C}_\infty^*}{\bar{C}_0^* - \bar{C}_\infty^*}.$$

Here $\bar{\rho}$, $\bar{\mu}$ and $\bar{D}$ are small parameters which can be obtained from experimental data for the dependence of ρ, μ and D on the concentration.

Substituting (3.17) into the system (3.18) and its initial and boundary conditions (3.15) leads to a complete mathematical description of the hydrodynamics and the mass transfer in systems with intense interfacial mass transfer. These are a reduced form of the Oberbeck-Boussinesq equations (see Kundu (1990)). In our case the effect of gravity is neglected (it is insignificant) in the boundary-layer approximations in the case of a horizontal flat plate if the following condition holds

$$\frac{g}{U_\infty^2}\sqrt{\frac{\nu_0 L}{U_\infty}} < 10^{-2}, \quad \nu_0 = \frac{\mu_0}{\rho_0}.$$

In this case the vertical momentum equation reduces to the usual form under the boundary-layer approximations

$$\frac{\partial p}{\partial y^*} = 0.$$

The concentration effects were studied experimentally and reported in Boyadjiev (1996) (the experimental data was taken from Sherwood, Pigford & Wilke (1975)) within the concentration region $[0, C_{max}]$ where a significant effect of non-linear mass transfer ($\theta = 0.3$) is present. The concentration difference $\Delta C = M(\bar{C}_0^* - \bar{C}_\infty^*)/\rho_0^*$ is used to normalise the concentrations ($C_{max} = C_{max}/\Delta C$). These results are summarised in Table 3.1 for a variety of different chemical species.

From Table 3.1 it is clear that for the diffusion of ammonia into air, the influence of the ammonia concentration on the density ($\bar{\rho}C_{max}$) is 13% and viscosity ($\bar{\mu}C_{max}$) is of approximately 16%. These changes are significant and suggest that an analysis of these effects is required. For gas mixtures (such as ammonia/air) the concentration effect on the diffusion constant is negligible.

For liquid mixtures the influence of the concentration on the density (see Table 3.1) is of the order of a few percent (under 5%), which is valid for a large number of miscible two-liquid systems. The effect on the viscosity cannot be so easily classified, the results here showing variations from 2% (acetic acid/water) to 72% (acetone/water).

The influence of the concentration on the diffusion coefficient for one liquid diffusing to another is often significant (see Sherwood, Pigford & Wilke (1975)). For an acetone/water

system	ammonia air	acetic acid water	acetic acid toluene	acetone water	water acetone
$C_{max}[kmol/m^3]$	0.0134	3.80	3.40	3.68	10.60
θ	0.3	0.3	0.3	0.3	0.3
$\Delta C[kmol/m^3]$	0.0160	3.92	3.52	3.81	10.9
C_{max}	0.837	0.969	0.967	0.967	0.968
$\bar{\rho}$	-0.149	0.0134	0.0420	-0.518	0.0461
$\bar{\rho}C_{max}$	-0.125	0.0130	0.0420	-0.050	0.0450
$\bar{\mu}$	-0.190	0.0208	0.263	-0.0854	0.746
$\bar{\mu}C_{max}$	-0.159	0.0200	0.254	-0.0830	0.722
$\bar{D}$	0	0	0	-0.336	-0.843
$\bar{D}C_{max}$	0	0	0	-0.325	-0.816

Table 3.1: Maximum concentration effect on the density, viscosity and diffusivity.

system (see Table 3.1) the dependency deviates from the linear as proposed in (3.17). In cases where the parameters $\bar{\rho}$, $\bar{\mu}$ and $\bar{D}$ exceed 0.3 the linear approximation (3.17) becomes inaccurate; neglecting the second-order approximations leads to an error above 10%. The accuracy of the approximation (3.17) is shown in Figures 3.1 - 3.3. The accuracy is satisfactory for a relatively high concentration.

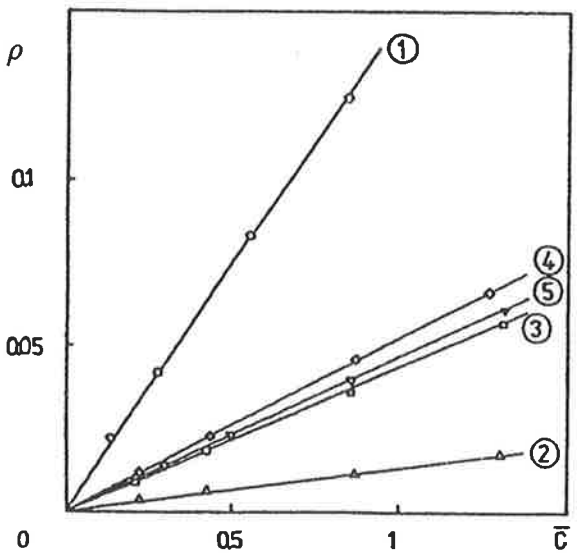

Figure 3.1: Linear approximation of the dependence of the density on the concentration for different systems. Shown are plots of ρ versus $\bar{C}$ for the cases: (1) ammonia/air ($\circ$); (2) acetic acid/water ($\triangle$); (3) acetic acid/thulium ($\square$); (4) acetone/water ($\diamond$); (5) water/acetone ($\triangledown$).

Boyadjiev (1996) provided an analysis of the approximations of non-linear mass-transfer theory, which was developed for cases $\bar{\rho} = \bar{\mu} = \bar{D} = 0$. It was shown that the results

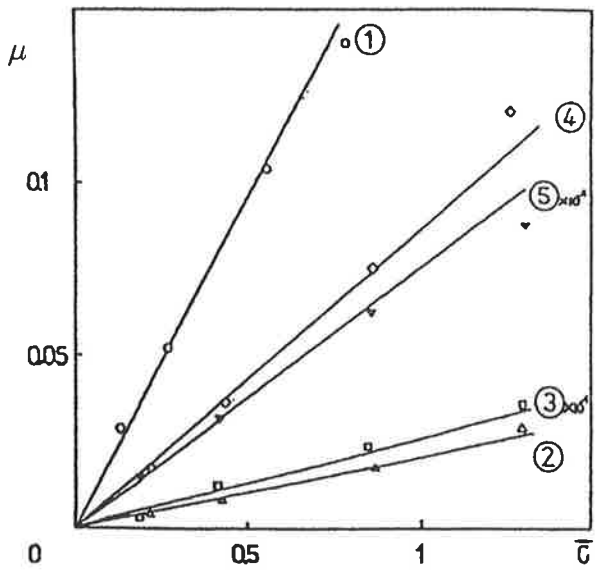

Figure 3.2: Linear approximation of the dependence of the viscosity on the concentration for different systems. Shown are plots of μ versus $\bar{C}$ for the cases: (1) ammonia/air ($\circ$); (2) acetic acid/water ($\triangle$); (3) acetic acid/thulium ($\square$); (4) acetone/water ($\diamond$); (5) water/acetone ($\triangledown$).

are valid in the cases where these parameters are small enough (for instance under 0.05). The linear approximations are also valid for different systems such as gas(liquid)–solid permeable surface, gas–liquid, liquid–liquid systems. In these cases, the hydrodynamics and the mass transfer depend on the concentration gradient (θ). When the parameters $\bar{\rho}$, $\bar{\mu}$ and $\bar{D}$ are within the interval $[0.1, 0.3]$ the concentration influences the mass transfer and this effect can be considered by introducing the linear approximation (3.17). In systems for which these parameters have higher values (above 0.3), quadratic terms should be included in (3.17).

3.2 Influence of the concentration on the mass-transfer rate

The mass-transfer rate can be expressed by the mass-transfer coefficient. We shall define this rate from the average diffusion flux, through a surface with the specific length L,

$$J = k(\bar{C}^*_\infty - \bar{C}^*_0) = \frac{1}{L}\int_0^L D\left(\frac{\partial C^*_0}{\partial y^*}\right)_{y=0} \mathrm{d}x.$$

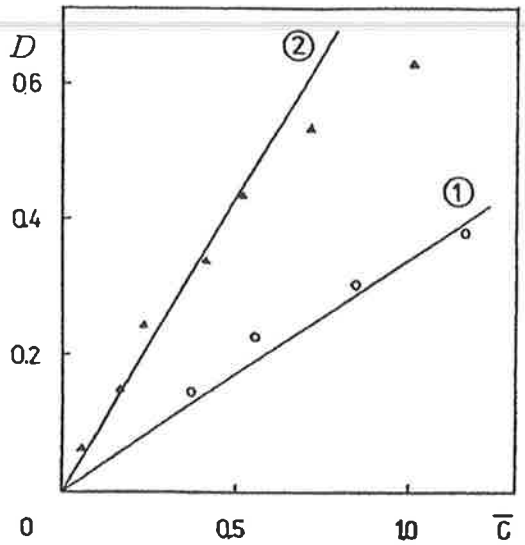

Figure 3.3: Linear approximation of the dependence of the diffusivity on the concentration for different systems. Shown are plots of D versus $\bar{C}$ for the cases: (1) acetone into water (○); (2) water into acetone (△).

3.2.1 Gas–solid permeable surface systems

The thickness of the momentum and the concentration boundary layers in gases are of the same order of magnitude, so one characteristic scale can be applied

$$\delta_0 = \sqrt{\frac{D_0 L}{U_\infty}}.$$

The problem (3.14) can be non-dimensionalised with respect to a typical length scale L, the concentration boundary-layer thickness δ_0, the free stream velocity U_∞ and the concentrations $\bar{C}_0^*$ and $\bar{C}_\infty^*$, at $y^* = 0$ and as $y^* \to \infty$, respectively as follows:

$$\begin{aligned} &x^* = Lx, \quad y^* = \delta_0 y, \quad U_0^* = U_\infty U_0, \\ &V_0^* = U_\infty \frac{\delta_0}{L} V_0, \quad C_0^* = \bar{C}_\infty^* + (\bar{C}_0^* - \bar{C}_\infty^*) C_0. \end{aligned} \tag{3.18}$$

Introducing (3.18) into the system (3.14) - (3.15) and transforming the variables using the standard boundary-layer variables (2.12) leads to the following system of boundary-layer

and concentration equations and their associated boundary conditions:

$$
\begin{aligned}
&\frac{\partial}{\partial x}(\varphi U_B)+\frac{\partial}{\partial Y}(\varphi V_B)=0,\\
&\varphi\left(U_B\frac{\partial U_B}{\partial x}+V_B\frac{\partial U_B}{\partial Y}\right)=Sc\frac{\partial}{\partial Y}\left(\psi\frac{\partial U_B}{\partial Y}\right),\\
&\varphi\left(U_B\frac{\partial C_B}{\partial x}+V_B\frac{\partial C_B}{\partial Y}\right)=\frac{\partial}{\partial Y}\left(\varphi\omega\frac{\partial C_B}{\partial Y}\right),\\
&x=0:\quad U_B=1,\ C_B=1;\\
&Y=0:\quad U_B=0,\ V_B=-\theta_0\frac{\partial}{\partial Y}\left(\frac{\tilde{C}+C_B}{\varphi}\right),\ C_B=1;\\
&Y\to\infty:\quad U_B=1,\ C_B=0,
\end{aligned}
\tag{3.19}
$$

where

$$
\begin{aligned}
&\theta_0=\frac{M\Delta C_0}{\rho_0^*}\varphi(1)\omega(1),\ \ \rho^*=\rho_0\varphi(1),\ \ \rho_0^*=\rho_0\varphi(1)-M\bar{C}_0^*\\
&\tilde{C}=\frac{\bar{C}_\infty^*}{\Delta C_0},\ \ \Delta C_0=\bar{C}_\infty^*-\bar{C}_0^*,\ \ Sc=\frac{\mu_0}{\rho_0 D_0},\\
&\varphi=\varphi(C_B)=\frac{\rho}{\rho_0},\ \ \psi=\psi(C_B)=\frac{\mu}{\mu_0},\ \ \omega=\omega(C_B)=\frac{D}{D_0},\\
&\varphi(0)=1,\ \ \psi(0)=1,\ \ \omega(0)=1.
\end{aligned}
\tag{3.20}
$$

We shall introduce the following similarity variables into (3.19):

$$
\begin{aligned}
&\varphi U_B=\Phi',\ \ \varphi V_B=\frac{1}{2\sqrt{x}}\left(\Phi'\eta-\Phi\right),\ \ C_B=F,\\
&\Phi=\Phi(\eta),\ \ F=F(\eta),\ \ \eta=\frac{Y}{\sqrt{x}}.
\end{aligned}
$$

System (3.19) reduces to

$$
\begin{aligned}
&2Sc\varphi^2\psi\Phi'''+\varphi^2\Phi\Phi''-\varphi\varphi'\Phi\Phi'F'\\
&\quad+2Sc\varphi(\varphi\psi'-\varphi'\psi)\Phi''F'-2Sc\varphi'(\varphi\psi'-2\varphi'\psi)\Phi'F'^2=0,\\
&2\varphi\omega F''+2(\varphi'\omega+\varphi'\psi)F'^2+\Phi F'=0,
\end{aligned}
\tag{3.21}
$$

with boundary conditions

$$
\begin{aligned}
&\Phi(0)=-\theta F'(0),\ \ \Phi'(0)=0,\ \ F(0)=1;\\
&\Phi'(\infty)=1,\ \ F(\infty)=0,\ \ \theta=2\theta_0\frac{\Delta C_0\varphi(1)-\bar{C}_0^*\varphi'(1)}{\Delta C_0\varphi(1)}.
\end{aligned}
\tag{3.22}
$$

The functions φ, ψ and ω in (3.21) can be determined by spline approximations of the experimentally measured dependencies of ρ, μ and D on the concentration. For a wide

range of gas mixtures these functions can be obtained, with suitable accuracy, through a linear approximation

$$\varphi - 1 + \bar{\rho}C_0, \quad \psi = 1 + \bar{\mu}C_0, \quad \omega = 1 + \bar{D}C_0. \tag{3.23}$$

Introducing (3.23) into (3.21) leads to following system of equations:

$$\begin{aligned} &2Sc(1+\bar{\rho}F)^2(1+\bar{\mu}F)\Phi''' + (1+\bar{\rho}F)^2\Phi\Phi'' \\ &\quad -\bar{\rho}(1+\bar{\rho}F)\Phi\Phi'F' + 2Sc(1+\bar{\rho}F)\left[\bar{\mu}(1+\bar{\rho}F) - \bar{\rho}(1+\bar{\mu}F)\right]\Phi''F' \\ &\quad -2Sc\bar{\rho}\left[\bar{\mu}(1+\bar{\rho}F) - 2\bar{\rho}(1+\bar{\mu}F)\right]\Phi'F'^2 = 0, \\ &2(1+\bar{\rho}F)(1+\bar{D}F)F'' + 2\left[\bar{\rho}(1+\bar{D}F) + \bar{D}(1+\bar{\rho}F)\right]F'^2 + \Phi F' = 0, \end{aligned} \tag{3.24}$$

where

$$\theta = 2\theta_0 \frac{\Delta C_0 - \bar{C}_0^*\bar{\rho}}{\Delta C_0(1+\bar{\rho})}.$$

The parameters $\bar{\rho}$ and $\bar{\mu}$ in (3.24) are to be considered as small, while $\bar{D} = 0$. Omitting the quadratic terms in the small parameters $\bar{\rho}$ and $\bar{\mu}$ leads to

$$\begin{aligned} &2Sc(1+2\bar{\rho}F+\bar{\mu}F)\Phi''' + (1+2\bar{\rho}F)\Phi\Phi'' \\ &\quad -\bar{\rho}\Phi\Phi'F' + 2Sc(\bar{\mu}-\bar{\rho})\Phi''F' = 0, \\ &2(1+\bar{\rho}F)F'' + 2\bar{\rho}F'^2 + \Phi F' = 0, \end{aligned} \tag{3.25}$$

with boundary conditions

$$\begin{aligned} &\Phi(0) = -\theta F'(0), \quad \Phi'(0) = 0, \quad F(0) = 1; \\ &\Phi'(\infty) = 1, \quad F(\infty) = 0. \end{aligned} \tag{3.26}$$

The system (3.25) subject to the boundary conditions (3.26) was solved using the following algorithm (see Boyadjiev & Halatchev (1998b)):

1. Determine the zeroth-order approximations to Φ and F by solving the boundary-value problem:

$$\begin{aligned} &2Sc\Phi'''^{(0)} + \Phi^{(0)}\Phi''^{(0)} = 0, \\ &\Phi^{(0)}(0) = 0, \quad \Phi'^{(0)}(0) = 0, \quad \Phi'^{(0)}(\infty) = 1; \\ &2F''^{(0)} + \Phi^{(0)}F'^{(0)} = 0, \\ &F^{(0)}(0) = 1, \quad F^{(0)}(\infty) = 0. \end{aligned} \tag{3.27}$$

2. Determine Φ at the k-th iteration by solving the boundary-value problem

$$\begin{aligned} &2Sc(1+2\bar{\rho}F^{(k-1)}+\bar{\mu}F^{(k-1)})\Phi'''^{(k)} + (1+2\bar{\rho}F^{(k-1)})\Phi^{(k)}\Phi''^{(k)} \\ &\quad -\bar{\rho}\Phi^{(k-1)}\Phi'^{(k-1)}F'^{(k-1)} + 2Sc(\bar{\mu}-\bar{\rho})\Phi''^{(k-1)}F'^{(k-1)} = 0, \\ &\Phi^{(k)}(0) = -\theta F'^{(k-1)}(0), \quad \Phi'^{(k)}(0) = 0; \quad \Phi'^{(k)}(\infty) = 1. \end{aligned} \tag{3.28}$$

3. Determine F at the k-th iteration by solving the boundary-value problem

$$2(1+\bar{\rho}F^{(k-1)})F'''^{(k)} + 2\bar{\rho}(F'^{(k-1)})^2 + \Phi^{(k)}F''^{(k)} = 0, \qquad (3.29)$$
$$F^{(k)}(0) = 1; \quad F^{(k)}(\infty) = 0.$$

The integration of (3.27) - (3.29) is done using finite difference schema with a step-size $h = 10^{-3}$ in the interval $0 \leq \eta \leq 6$.

4. The calculation procedure (from step 2 of the algorithm) is repeated until

$$\left|\Phi''^{(k)}(0) - \Phi''^{(k-1)}(0)\right| < \epsilon, \quad \left|F'^{(k)}(0) - F'^{(k-1)}(0)\right| < \epsilon. \qquad (3.30)$$

After some experimentation a tolerance of $\epsilon = 10^{-5}$ was found suitable to produce results converged to five significant figures.

The results for $\Phi''(0)$ and $F'(0)$ in the case of $Sc = 1$ are shown in Table 3.2 for different values of θ, $\bar{\rho}$ and $\bar{\mu}$. They were obtained in $3-4$ iterations.

No.	$Sc = 1$				
	θ	$\bar{\rho}$	$\bar{\mu}$	$\Phi''(0)$	$-F'(0)$
1	0	0	0	0.332	0.332
2	0.3	0	0	0.301	0.299
3	-0.3	0	0	0.373	0.372
4	0.3	0.15	0	0.356	0.187
5	0	0.15	0	0.379	0.198
6	-0.3	-0.15	0	0.329	0.531
7	0.3	0	0.2	0.264	0.292
8	0	0	0.2	0.290	0.322
9	-0.3	0	-0.2	0.447	0.386
10	0.3	0.15	0.2	0.320	0.187
11	0	0.15	0.2	0.340	0.198
12	-0.3	0.15	0.2	0.362	0.211
13	0	-0.15	0	0.280	0.446
14	0	0	-0.2	0.394	0.343
15	0	-0.15	-0.2	0.347	0.469
16	-0.3	-0.15	-0.2	0.417	0.558

Table 3.2: The results for $\Phi''(0)$ and $F'(0)$ in the case of gases ($Sc = 1$) for different values of θ, $\bar{\rho}$ and $\bar{\mu}$.

The Sherwood number and Reynolds number, respectively, are given as

$$Sh = \frac{kL}{D_0} = 2Pe^{1/2}F'(0), \quad Re = \frac{U_\infty L}{\nu_0}.$$

The mass-transfer rate in gases can be determined from data in Table 3.2. The results show that the dependence of $\Phi''(0)$ and $F'(0)$ on θ, $\bar{\rho}$ and $\bar{\mu}$ is monotone. The change

in viscosity $\bar{\mu}$ has little influence on the mass-transfer rate ($F'(0)$) as can be seen from results in rows 4 and 10 of Table 3.2, while the influence of the density $\bar{\rho}$ is six to seven times greater than the effect of the non-linear mass transfer (θ) (see Figure 3.4) .

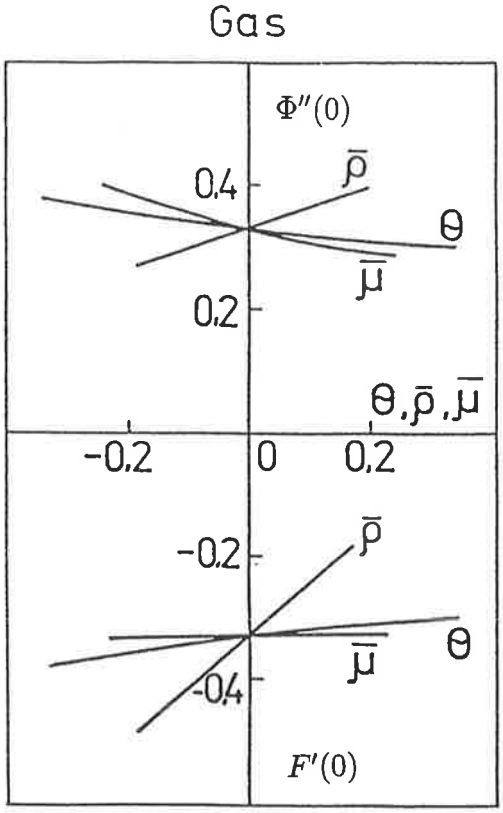

Figure 3.4: The dependence of $\Phi''(0)$ on θ, $\bar{\rho}$ and $\bar{\mu}$.

3.2.2 Liquid–solid permeable surface systems

The thickness of the hydrodynamic and concentration boundary layers in liquids are of different orders of magnitude. As such, two specific scales should be taken into account

$$\delta_1 = \sqrt{\frac{\mu_0 L}{\rho_0 U_\infty}}, \quad \delta_2 = \sqrt{\frac{D_0 L}{U_\infty}}, \quad \frac{\delta_1}{\delta_2} = \varepsilon = Sc^{1/2},$$

the hydrodynamic boundary-layer and concentration boundary-layer thickness respectively.

Considering these two scales the following dimensionless variables are introduced

$$\begin{aligned} &x^* = Lx, \quad y^* = \delta_1 y_1 = \delta_2 y_2, \\ &U_0^* = U_\infty U_1(x, y_1) = U_\infty U_2(x, y_2), \\ &V_0^* = U_\infty \frac{\delta_1}{L} V_1(x, y_1) = U_\infty \frac{\delta_2}{L} V_2(x, y_1), \\ &C_0^* = \bar{C}_\infty^* + \Delta C_0 C_1(x, y_1) = \bar{C}_\infty^* + \Delta C_0 C_2(x, y_1), \end{aligned} \tag{3.31}$$

where U_i, V_i, and C_i are the velocity and concentration fields in the liquid boundary layer, so that $y_2 = \varepsilon y_1$, $U_2(x, y_2) = U_1(x, \varepsilon^{-1} y_2)$, $U_1(x, y_1) = U_2(x, \varepsilon y_1)$, $V_2(x, y_2) = \varepsilon V_1(x, \varepsilon^{-1} y_2)$, $V_1(x, y_1) = \varepsilon^{-1} V_2(x, \varepsilon y_1)$, $C_2(x, y_2) = C_1(x, \varepsilon^{-1} y_2)$, $C_1(x, y_1) = C_2(x, \varepsilon y_1)$.

In these new variables the boundary-layer equations are

$$\begin{aligned} &\varphi_1 \left(U_1 \frac{\partial U_1}{\partial x} + V_1 \frac{\partial U_1}{\partial y_1} \right) = Sc \frac{\partial}{\partial y_1} \left(\psi_1 \frac{\partial U_1}{\partial y_1} \right), \\ &\frac{\partial}{\partial x}(\varphi_1 U_1) + \frac{\partial}{\partial y_1}(\varphi_1 V_1) = 0, \\ &\varphi_2 \left(U_2 \frac{\partial C_2}{\partial x} + V_2 \frac{\partial C_2}{\partial y_2} \right) = \frac{\partial}{\partial y_2} \left(\varphi_2 \omega_2 \frac{\partial C_2}{\partial y_2} \right), \end{aligned} \tag{3.32}$$

subject to the following initial and boundary conditions:

$$\begin{aligned} &x = 0: \quad U_1 = U_2 = 0, \quad C_1 = C_2 = 0; \\ &y_1 = 0: \quad U_1 = 0, \quad C_1 = 0, \\ &y_2 = 0: \quad U_2 = 0, \quad C_2 = 0, \\ &\qquad V_2 = -\theta_0 \frac{\partial}{\partial y_2} \left(\frac{\bar{C}_\infty^* + \Delta C_0 C_2}{\Delta C_0 \varphi_2} \right); \\ &y_1 \to \infty: \quad U_1 \to 1, \quad C_1 \to 0, \\ &y_2 \to \infty: \quad U_2 \to 1, \quad C_2 \to 0, \end{aligned} \tag{3.33}$$

where φ_j, ψ_j and ω_j $(j = 1, 2)$ are defined in a similar fashion to the previous subsection.

Introducing the new variables

$$\begin{aligned} &\varphi_1 U_1 = \Phi_1'(\eta_1), \quad \varphi_2 U_2 = \Phi_2'(\eta_2), \quad \eta_1 = \frac{y_1}{x}, \quad \eta_2 = \frac{y_2}{x}, \\ &\varphi_1 V_1 = \frac{1}{2\sqrt{x}}(\Phi_1' \eta_1 - \Phi_1), \quad \varphi_2 V_2 = \frac{1}{2\sqrt{x}}(\Phi_2' \eta_2 - \Phi_2), \\ &C_1 = F_1(\eta_1), \quad C_2 = F_2(\eta_2), \quad \eta_2 = \varepsilon \eta_1, \end{aligned}$$

the boundary-layer and concentration equations (3.32) and their boundary conditions (3.33) become

$$\begin{aligned} &2Sc(1 + 2\bar{\rho} F_1 + \bar{\mu} F_1)\Phi_1''' + (1 + 2\bar{\rho} F_1)\Phi_1 \Phi_1'' \\ &\quad - \bar{\rho} \Phi_1 \Phi_1' F_1' + 2Sc(\bar{\mu} - \bar{\rho})\Phi_1'' F_1' = 0, \\ &2(1 + \bar{\rho} F_2 + \bar{D} F_2) F_2''' + 2(\bar{\rho} + \bar{D}) F_2''^2 + \Phi_2 F_2' = 0, \\ &\Phi_2(0) = -\theta F_2'(0), \quad \Phi_1'(0) = 0, \quad F_2(0) = 1; \\ &\Phi_1'(\infty) = 1, \quad F_2(\infty) = 0. \end{aligned} \tag{3.34}$$

where

$$F_1(\eta_1) = F_2(\eta_2) = F_2(\varepsilon\eta_1), \quad F_1'(\eta_1) = \varepsilon F_2'(\varepsilon\eta_1),$$
$$\Phi_2(\eta_2) = \varepsilon\Phi_1(\eta_1) = \varepsilon\Phi_1(\varepsilon^{-1}\eta_2), \quad \Phi_2(0) = \varepsilon\Phi_1(0) = -\theta F_2'(0),$$

and we have employed the linear approximations

$$\varphi_i = 1 + \bar{\rho}F_i, \quad \psi_i = 1 + \bar{\mu}F_i, \quad \omega_i = 1 + \bar{D}F_i \quad (i = 1, 2).$$

In deriving (3.34) we have ignored all quadratic terms in the small parameters $\bar{\rho}$, $\bar{\mu}$ and $\bar{D}$.

The system (3.34) is solved by using modification of the algorithm employed in the solution of (3.25) - (3.26):

1. Determine the zeroth-order approximation of $\Phi_1(\eta_1)$ by solving the two-point boundary-value problem

$$\begin{aligned} &2\Phi_1^{'''(0)} + \Phi_1^{(0)}\Phi_1^{''(0)} = 0, \\ &\Phi_1^{(0)}(0) = 0, \quad \Phi_1^{'(0)}(0) = 0; \quad \Phi_1^{'(0)}(\infty) = 1. \end{aligned} \tag{3.35}$$

   A step-size of 0.001 was found to be suitable and the interval of integration was $0 \leq \eta_1 \leq 6$.

2. Determine the zeroth-order approximation of $\Phi_2(\eta_2)$ by solving

$$\Phi_2^{(0)}(\eta_2) = \varepsilon\Phi_1^{(0)}(\eta_1), \quad \eta_2 = \varepsilon\eta_1, \quad 0 \leq \eta_1 \leq 6. \tag{3.36}$$

3. Determine the zeroth-order approximation of $F_2(\eta_2)$ by solving

$$\begin{aligned} &F_2^{''(0)} + \Phi_2^{(0)}F_2^{'(0)} = 0, \\ &F_2^{(0)}(0) = 1; \quad F_2^{(0)}(\infty) = 0, \end{aligned} \tag{3.37}$$

   with a step-size $h_2 = 0.01$ in the interval $0 \leq \eta_2 \leq 6\varepsilon$. In order to do this $F_2^{'(0)}(0)$ is varied until the condition $F_2^{(0)}(\infty) < 10^{-5}$ is satisfied.

4. Determine the zeroth-order approximations of $F_1(\eta_1)$ and $F_1'(\eta_1)$

$$F_1^{(0)}(\eta_1) = F_2^{(0)}(\eta_2) = F_2^{(0)}(\varepsilon\eta_1), \quad F_1^{'(0)}(\eta_1) = \varepsilon F_2^{'(0)}(\eta_2) = \varepsilon F_2^{'(0)}(\varepsilon\eta_1). \tag{3.38}$$

5. Determine $\Phi_1(\eta_1)$ at the k-th iteration:

$$\begin{aligned} &2Sc(1 + 2\bar{\rho}F_1^{(k-1)} + \bar{\mu}F_1^{(k-1)})\Phi_1^{'''(k)} + (1 + 2\bar{\rho}F_1^{(k-1)})\Phi_1^{(k)}\Phi_1^{''(k)} \\ &\quad -\bar{\rho}\Phi_1^{(k-1)}\Phi_1^{'(k-1)}F_1^{'(k-1)} + 2Sc(\bar{\mu} - \bar{\rho})\Phi_1^{''(k-1)}F_1^{'(k-1)} = 0, \\ &\Phi^{(k)}(0)_1 = -\frac{\theta}{\varepsilon}F^{'(k-1)}(0)_2, \quad \Phi_1^{'(k)}(0) = 0; \quad \Phi_1^{'(k)}(\infty) = 1, \end{aligned} \tag{3.39}$$

   while the value of $\Phi_1^{''(0)}(0)$ is varied till the condition $|\Phi_1^{'(0)}(\infty) - 1| < 10^{-5}$ is satisfied.

6. Determine $\Phi_2(\eta_2)$ at the k-th iteration:

$$\Phi_2^{(k)}(\eta_2) = \varepsilon\Phi_1^{(k)}(\eta_1) = \varepsilon\Phi_1^{(k)}(\varepsilon\eta_2), \quad 0 \le \eta_2 \le 6\varepsilon. \tag{3.40}$$

7. Determine $F_2(\eta_2)$ at the k-th iteration with a step-size h_2 in the interval $0 \le \eta_2 \le 6\varepsilon$

$$\begin{aligned} &2(1+\bar{\rho}F_2^{(k-1)} + \bar{D}F_2^{(k-1)})F_2^{\prime\prime(k)} + 2(\bar{\rho}+\bar{D})(F_2^{\prime(k-1)})^2 \\ &\quad +\Phi_2^{(k)}F_2^{\prime(k)} = 0, \\ &F_2^{(k)}(0) = 1; \quad F_2^{(k)}(\infty) = 0, \end{aligned} \tag{3.41}$$

while the value of $F_2^{\prime(k)}(0)$ is varied till the condition $F_2^{(k)}(\infty) < 10^{-5}$ is satisfied.

8. Determine $F_1(\eta_1)$ and $F_1'(\eta_1)$ at the k-th iteration

$$F_1^{(k)}(\eta_1) = F_2^{(k)}(\eta_2) = F_2^{(k)}(\varepsilon\eta_1), \quad F_1^{\prime(k)}(\eta_1) = \varepsilon F_2^{\prime(k)}(\eta_2) = \varepsilon F_2^{\prime(k)}(\varepsilon\eta_1), \quad 0 \le \eta_1 \le 6. \tag{3.42}$$

9. The calculation procedure (from step 5 of the algorithm) is repeated until

$$\left|\Phi_1^{\prime\prime(k)}(0) - \Phi_1^{\prime\prime(k-1)}(0)\right| < \epsilon, \quad \left|F_2^{\prime(k)}(0) - F_2^{\prime(k-1)}(0)\right| < \epsilon. \tag{3.43}$$

Here $\varepsilon = \sqrt{Sc}$ and $Sc = 100$ (liquid–solid permeable surface systems) and $\epsilon = 10^{-5}$.

The Sherwood number is given as

$$Sh = 2(1+\bar{D})Pe^{1/2}F_2'(0).$$

The results obtained for $\Phi_1''(0)$ and $F_2'(0)$ by solving (3.34) using the algorithm described above at $\varepsilon = 10$ and for different values of θ, $\bar{\rho}$, $\bar{\mu}$ and $\bar{D}$ are shown in Table 3.3. The mass-transfer rate in liquids can be determined from the data in Table 3.3. These results show that the influence of the density and viscosity ($\bar{\rho}$ and $\bar{\mu}$) on the velocity profiles (hydrodynamics) ($\Phi''(0)$) is similar to the case of gases, in that the dependency of $\Phi''(0)$ on $\bar{\rho}$ and $\bar{\mu}$ is monotone, while its effect on the mass-transfer rate ($F_2'(0)$) is practically negligible. The change in diffusivity ($\bar{D}$) does not affect $\Phi''(0)$ and $F_2'(0)$ (see Figure 3.5)

.

The analysis (see Boyadjiev & Halatchev (1998b)) of the influence of high concentration gradients of transferred substance on the hydrodynamics (measured by $\Phi''(0)$) and mass transfer (measured by $F'(0)$) through the concentration dependencies of density ($\bar{\rho}$), viscosity ($\bar{\mu}$) and diffusivity ($\bar{D}$) allow us to make some conclusions. First, a change in the density with concentration influences the hydrodynamics in gases and liquids but does not influence the mass transfer in gases. Second, a change in the viscosity with concentration influences the hydrodynamics in gases and liquids and the mass transfer, and finally, the change in the diffusivity with concentration has no influence on either the hydrodynamics or the mass transfer.

No.	$Sc = 100$				
	θ	$\bar{\rho}$	$\bar{\mu}$	$\Phi''(0)$	$-F'(0)$
1	0	0	0	0.332	0.332
2	0.3	0	0	0.330	0.176
3	-0.3	0.15	0	0.334	0.206
4	0	-0.15	0	0.397	0.194
5	0	0.15	0	0.201	0.181
6	0	0	0.2	0.272	0.186
7	0	0	-0.2	0.418	0.194
8	0	0	0	0.332	0.192
9	0	0	0	0.332	0.186
10	0.03	0.15	0.2	0.272	0.177
11	-0.03	0.15	0.2	0.275	0.200
12	0.03	-0.15	-0.2	0.243	0.164
13	-0.03	-0.15	-0.2	0.247	0.206
14	0.3	0	0	0.318	0.135
15	-0.1	0	0	0.342	0.268

Table 3.3: The results for $\Phi''(0)$ and $F'(0)$ in the case of liquids ($Sc = 100$) for different values of θ, $\bar{\rho}$ and $\bar{\mu}$.

These results show that the non-linear theory on mass transfer at constant values of density, viscosity and diffusivity (see Sherwood, Pigford & Wilke (1975), Zierp & Oertel (1981), Boyadjiev *et. al.* (1996a)) is sufficiently accurate for gases and liquids if the density of the transferred substance is not significantly different from the density of the gas mixture. This result then allows us to considerably simplified models describing mass transfer in systems with intense interfacial mass transfer whilst still capturing the dominant (or significant) features of the flow. We now turn our attention to the question of how these concentration dependencies affect the hydrodynamic stability of the flow.

3.3 Influence of the concentration on the hydrodynamic stability

The data for the basic velocity and concentration fields in the laminar boundary layer gives us the opportunity to analyse the hydrodynamic stability of the flow. This work was reported in Halatchev & Boyadjiev (1998).

3.3.1 Linear instability analysis of gas–solid permeable systems

The linear stability analysis considers a non-stationary flow, in the form of a superposition of a basic stationary flow and a small amplitude two-dimensional periodic disturbances in

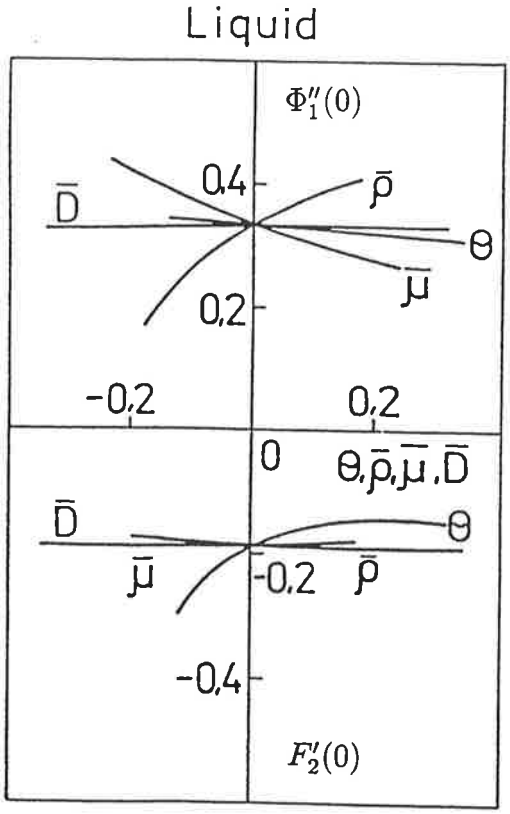

Figure 3.5: The dependence of $\Phi_1''(0)$ on θ, $\bar{\rho}$.

a similar fashion as has been done in Chapter 2. The non-stationary flow satisfies the full system of Navier-Stokes equations (2.7). Linear approximations (3.17) are introduced to account for the dependencies of the density, viscosity and diffusivity on the concentration, while the $\bar{\rho}$, $\bar{\mu}$ and $\bar{D}$ are considered to be small parameters. Again, the governing equations do not explicitly include the convection-diffusion equation for the concentration because at the linear approximation for the small perturbation parameter and mass-transfer parameter θ it was argued in Halatchev & Boyadjiev (1998) that the momentum and continuity disturbance equations may be decoupled in the boundary conditions. The periodic disturbances was considered as a travelling wave of the form

$$\begin{aligned} u(x,y) &= G'(y)\exp i\alpha(x-\hat{c}t), \\ v(x,y) &= -i\alpha G(y)\exp i\alpha(x-\hat{c}t), \end{aligned}$$

In the case of mass transfer in gases, for which the basic flow is governed by (3.21) with non-dimensionalisation (3.18), we introduce into (2.11) the similarity variables

$$U_0(x,y)=\frac{U_\infty}{\varphi}\Phi'(\eta),\quad V_0=\frac{U_\infty\delta}{2x\varphi}\left(\eta\Phi'(\eta)-\Phi(\eta)\right),\quad G(y)=\gamma(\eta)$$

$$\eta=\frac{y}{\delta},\quad \delta=\sqrt{\frac{D_0x}{U_\infty}},\quad \varphi=1+\bar{\rho}F(\eta),\quad F(\eta)=\frac{C_0-\bar{C}_\infty^*}{\bar{C}_0^*-\bar{C}_\infty^*}.$$

Linearising the full system of Navier-Stokes equations for the disturbances then yields, (after some minor manipulations) the modified Orr-Sommerfeld equation

$$\begin{aligned}\left(\frac{\Phi'}{\varphi}-C\right)(\gamma''-A^2\gamma)-\frac{1}{\varphi}\left(\Phi'''-2\bar{\rho}F'\frac{\Phi''}{\varphi}-\bar{\rho}F''\frac{\Phi'}{\varphi}\right)\gamma \\ =-\frac{i}{ARe}(\gamma^{iv}-2A_0^2+A^4\gamma)+\frac{i}{2\varepsilon^2ARe\varphi}(\eta\Phi'-\Phi)\gamma''' \\ -\frac{i}{2\varepsilon^2ARe\varphi}\left[\eta\Phi'''+\Phi''-\frac{\bar{\rho}}{\varphi}(2\eta F'\Phi''+\eta F''\Phi'+F'\Phi')+A^2(\eta\Phi'-\Phi)\right]\gamma',\end{aligned} \tag{3.44}$$

which must be solved subject to the boundary conditions

$$\begin{aligned}y=0: &\quad F=0,\ F'=0; \\ y\to\infty: &\quad F=0,\ F'=0,\end{aligned}$$

where, in (3.44), we have defined

$$A=\alpha\delta,\ C=\frac{\beta}{\alpha U_\infty}=C_r+iC_i,\ Re=\frac{U_\infty\delta}{\nu_0},\ \varepsilon=Sc^{1/2}.$$

The functions $\Phi(\eta)$, $F(\eta)$ and their derivatives are obtained by solving the two-point boundary-value problem (3.25). The solution of (3.44) was found using the same numerical approach as done in Chapter 2.

The neutral curves of stability are plotted in Figures 3.6, 3.7 and 3.8. The critical Reynolds number Re_{cr}, corresponding wave-speed C_r, and wave number A are obtained. $C_{r\,max}$ and A_{max} are also obtained from these results. We denote by $C_{r\,max}$ and A_{max} the minimal values for wave number and wave-speed at which the flow is stable at any Reynolds number (Re) respectively. These are presented in Table 3.4 together with their dependence on the concentration of transferred substance ($\bar{\rho}$ and $\bar{\mu}$) and its gradient (θ).

3.3.2 Linear instability analysis of liquid–solid permeable systems

In the case of liquids the basic flow velocity, as has been defined by Sherwood, Pigford & Wilke (1975), is introduced into (2.11)

$$\begin{aligned}U_0(x,y)=\frac{U_\infty}{\varphi}\Phi_1'(\eta_1),\ V_0=\frac{U_\infty\delta_1}{2x\varphi}\left(\eta_1\Phi_1'(\eta_1)-\Phi_1(\eta_1)\right), \\ \eta_1=y\sqrt{\frac{U_\infty}{\nu_0x}},\ \delta_1=\sqrt{\frac{\nu_0x}{U_\infty}},\ \varphi=1+\bar{\rho}F_1(\eta_1),\ G(y)=\gamma_1(\eta_1),\end{aligned} \tag{3.45}$$

where $\Phi_1(\eta_1)$, $F_1(\eta_1)$ and their derivatives are obtained by solving (3.34). The introduction of (3.45) into (2.11) leads to an equation for the disturbance amplitude of Orr-Sommerfeld type. The basic flow profiles are obtained directly from (3.34) using the

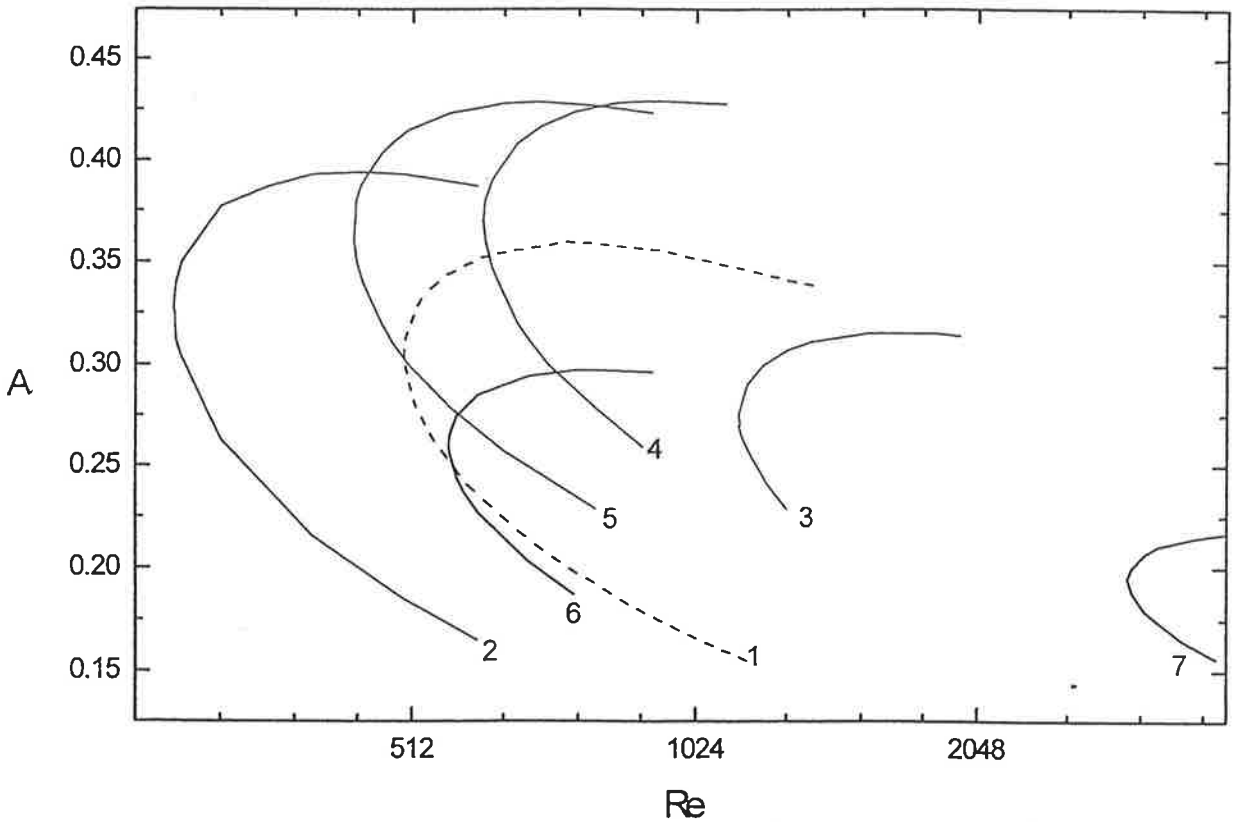

Figure 3.6: The curves of neutral stability in the (Re_{cr}, A)-plane in the case of gas flows in a laminar boundary layer under conditions of high concentrations. Shown are plots for the cases: 1) $\theta = 0$, $\bar{\rho} = 0$, $\bar{\mu} = 0$; 2) $\theta = 0$, $\bar{\rho} = 0$, $\bar{\mu} = 0.2$; 3) $\theta = 0$, $\bar{\rho} = 0$, $\bar{\mu} = -0.2$; 4) $\theta = 0$, $\bar{\rho} = 0.15$, $\bar{\mu} = 0$; 5) $\theta = 0$, $\bar{\rho} = 0.15$, $\bar{\mu} = 0.2$; 6) $\theta = 0$, $\bar{\rho} = -0.15$, $\bar{\mu} = 0$; 7) $\theta = 0$, $\bar{\rho} = -0.15$, $\bar{\mu} = -0.2$.

following substitutions:

$$\Phi(\eta) = \Phi_1(\eta_1), \quad F(\eta) = F_1(\eta_1), \quad \gamma(\eta) = \gamma_1(\eta_1),$$
$$\eta = \eta_1, \quad A = A_1 = \alpha\delta_1, \quad Re = Re_1 = \frac{U_\infty \delta_1}{\nu_0}, \quad \varepsilon = 10.$$

The eigenvalue problem has been solved in a similar fashion to (3.44). The critical Reynolds number Re_{cr}, corresponding wave-speed C_r, and wave number A are obtained. $C_{r\,max}$ and A_{max} are also obtained from these results. The curves of neutral stability in the case of liquid–solid permeable surface systems are shown in Figure 3.9, and the corresponding values of the critical parameters are presented in Table 3.5. These results show a dependence on the concentration of transferred substance ($\bar{\rho}$, $\bar{\mu}$ and $\bar{D}$) and its gradient (θ). The plots in Figure 3.8 presented with triangles and squares, having the same locus as the doted line (1), are obtained in the case where the diffusivity depends on the concentration.

The results give us opportunity to determine (see Figures 3.10 and 3.11) the dependence of Re_{cr} on the parameters characterising the concentration dependencies of density ($\bar{\rho}$), viscosity ($\bar{\mu}$), diffusivity ($\bar{D}$) and large concentration gradients (θ).

The data presented in Tables 3.4, 3.5 and Figures 3.10 and 3.11 show that in gases and liq-

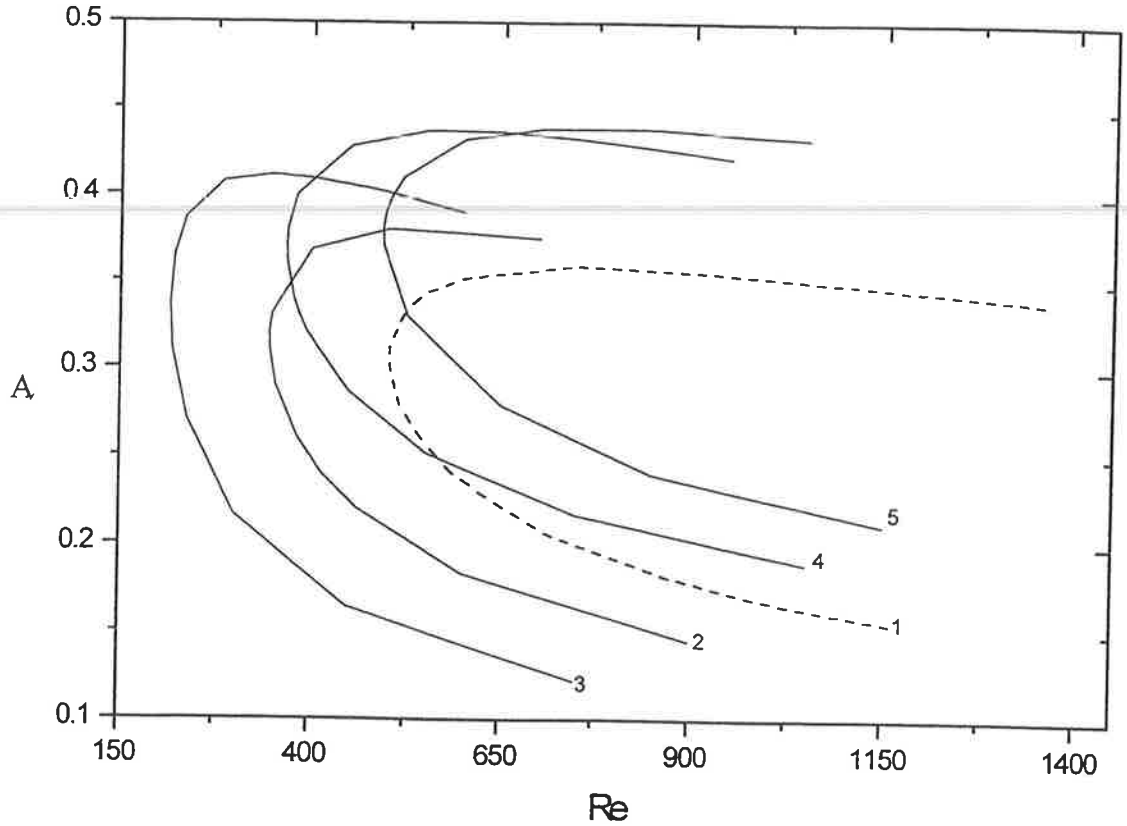

Figure 3.7: The curves of neutral stability in the (Re_{cr}, A)-plane in the case of gas flow in a laminar boundary layer under conditions of high concentrations and large concentration gradients. Shown are plots for the cases: 1) $\theta = 0$, $\bar{\rho} = 0$, $\bar{\mu} = 0$; 2) $\theta = 0.3$, $\bar{\rho} = 0$, $\bar{\mu} = 0.2$; 3) $\theta = 0.3$, $\bar{\rho} = 0$, $\bar{\mu} = 0.2$; 4) $\theta = 0.3$, $\bar{\rho} = 0.15$, $\bar{\mu} = 0$; 5) $\theta = 0.3$, $\bar{\rho} = 0.15$, $\bar{\mu} = 0.2$.

uids the stability of the flow as governed by the critical Reynolds number, Re_{cr}, increases when the density depends on concentration ($\bar{\rho} \neq 0$); a decrease of the concentration gradient (θ) leads to a decrease in stability (Re_{cr} decreases) and that in the cases when the increase of concentration leads to an increase of viscosity, we can observe stabilisation of the boundary-layer flow, i.e. high concentrations lead to high mass-transfer rates in gases. The change in the diffusivity ($\bar{D}$) does not influence the boundary-layer flow stability (see the data presented with triangles and squares in Figure 3.8). The results (see Figures 3.10 and 3.11) show that the effect of the viscosity ($\bar{\mu}$) on the concentration is analogous to that one of the large concentration gradient, that is a decrease in the critical Reynolds number (destabilising the boundary-layer flow) when density increases, while the change in the density ($\bar{\rho}$) has little effect and this dependence is not monotone.

3.4 Non-linear mass transfer and the Marangoni effect

Intensification of the mass transfer in industrial gas–liquid systems is quite often obtained through the creation of large concentration gradients. This can be realised in a number

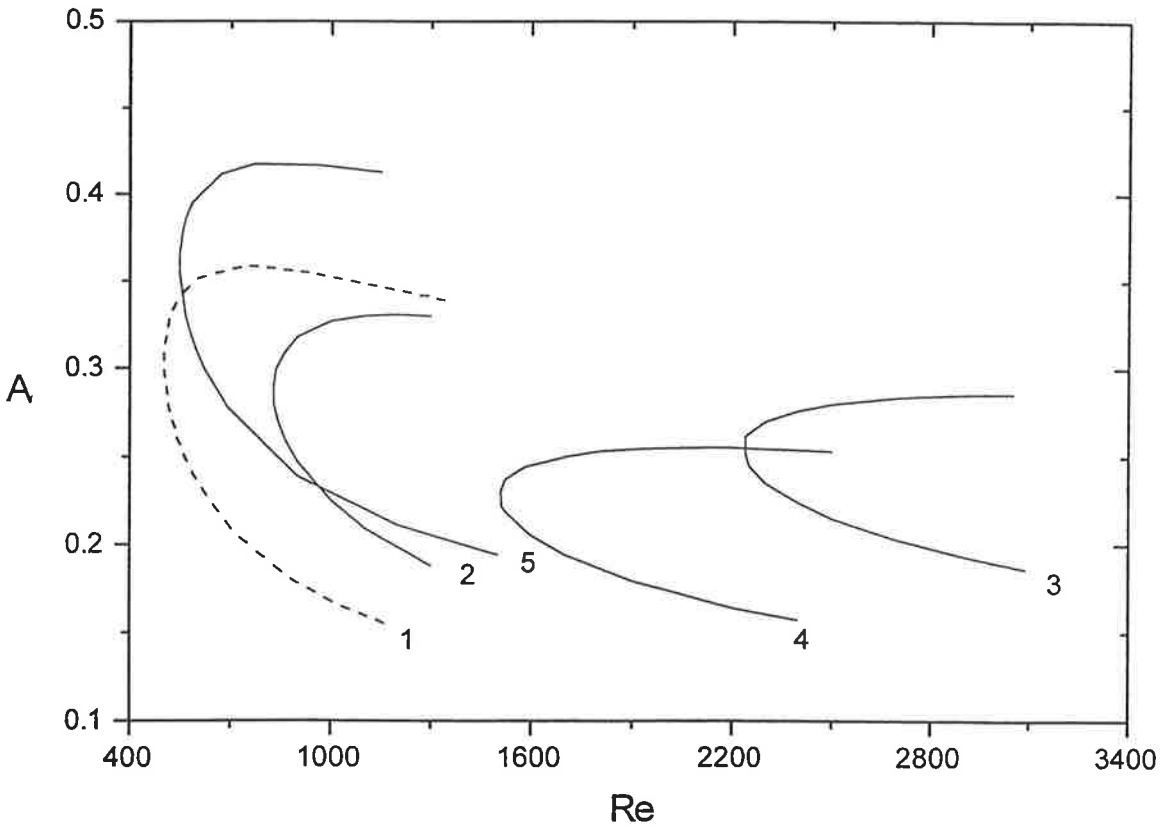

Figure 3.8: The curves of neutral stability in the (Re_{cr}, A)-plane in the case of gas flow in a laminar boundary layer under conditions of high concentrations. Shown are plots for the cases: 1) $\theta = 0$, $\bar{\rho} = 0$, $\bar{\mu} = 0$; 2) $\theta = -0.3$, $\bar{\rho} = 0$, $\bar{\mu} = 0.2$; 3) $\theta = -0.3$, $\bar{\rho} = 0$, $\bar{\mu} = -0.2$; 4) $\theta = -0.3$, $\bar{\rho} = -0.15$, $\bar{\mu} = 0$; 5) $\theta = -0.3$, $\bar{\rho} = 0.15$, $\bar{\mu} = 0.2$.

No.	θ	$\bar{\rho}$	$\bar{\mu}$	Re_{cr}	A_{max}	$C_{r\,max}$
1	0	0	0	501	0.356	0.407
2		0	0.2	285	0.394	0.445
3		0	-0.2	1135	0.315	0.352
4		0.15	0	608	0.429	0.356
5		0.15	0.2	443	0.428	0.373
6		-0.15	0	559	0.296	0.403
7		-0.15	-0.2	2972	0.217	0.289
8	-0.3	0	0	1619	0.301	0.331
9		0	-0.2	2238	0.286	0.312
10		-0.15	0	1508	0.255	0.332
11		0.15	0.2	547	0.418	0.361
12	0.3	0	0	345	0.380	0.431
13		0	0.2	215	0.411	0.467
14		0.15	0	491	0.439	0.369
15		0.15	0.2	367	0.437	0.384

Table 3.4: Values of the critical parameters Re_{cr}, $C_{r\,max}$ and A_{max} obtained under conditions of high concentrations (demonstrating the effects due to density, viscosity concentration dependences) and large concentration gradients in gases.

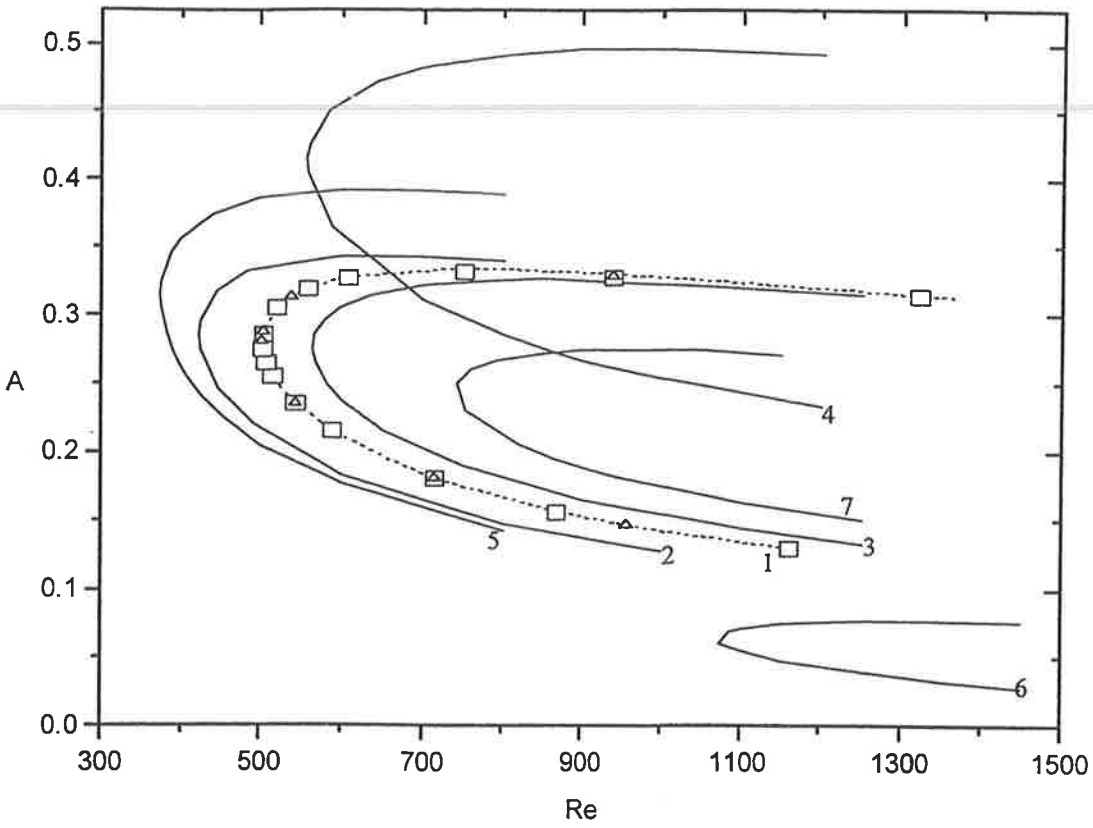

Figure 3.9: The curves of neutral stability in the (Re_{cr}, A)-plane in the case of liquid flow in a laminar boundary layer under conditions of high concentrations and large concentration gradients. Shown are plots for the cases: 1) $\theta = 0$, $\bar{\rho} = 0$, $\bar{\mu} = 0$, $\bar{D} = 0$; 2) $\theta = 0.3$, $\bar{\rho} = 0$, $\bar{\mu} = 0$, $\bar{D} = 0$; 3) $\theta = -0.1$, $\bar{\rho} = 0$, $\bar{\mu} = 0$, $\bar{D} = 0$; 4) $\theta = 0$, $\bar{\rho} = -0.15$, $\bar{\mu} = 0$, $\bar{D} = 0$; 5) $\theta = 0$, $\bar{\rho} = 0$, $\bar{\mu} = 0.2$, $\bar{D} = 0$; 6) $\theta = 0$, $\bar{\rho} = -0.15$, $\bar{\mu} = 0$, $\bar{D} = 0$; 7) $\theta = 0$, $\bar{\rho} = 0$, $\bar{\mu} = -0.2$, $\bar{D} = 0$; ($\square$) $\theta = 0$, $\bar{\rho} = 0$, $\bar{\mu} = 0$, $\bar{D} = 0.3$; ($\triangle$) $\theta = 0$, $\bar{\rho} = 0$, $\bar{\mu} = 0$, $\bar{D} = -0.3$.

of cases as a result of a chemical reaction of the transferred substance in the liquid phase. The thermal effect of such chemical reactions can create significant large temperature gradients. The temperature and concentration gradients so generated can then affect the mass-transfer kinetics in gas–liquid systems. Hence, experimentally obtained mass-transfer coefficients are found to differ significantly from those predicted by the linear theory of mass transfer.

It was shown in a number of papers (see Sterling & Scriven (1959), Linde, Schwartz & Groeger (1967), Porter, Cantwell & McDermott (1971), Hennenberg, Bisch, Vignes-Adler & Sanfeld (1979), Linde, Schwartz & Wilke (1979), Sanfeld, Steinchen, Hennenberg, Bisch, Van Lamswerde & Dall-Vedove (1979), Savistowski (1981) and Sorensen & Henennberg (1979)) that temperature and concentration gradients on the gas–liquid or liquid–liquid interface can create an interfacial tension gradient. As a result of this a secondary flow is induced. The velocity of the induced flow is directed tangentially to

No.	θ	$\bar{\rho}$	$\bar{\mu}$	$\bar{D}$	Re_{cr}	A_{max}	$C_{r\,max}$
1	0	0	0	0	501	0.356	0.407
2	0.3	0	0	0	422	0.367	0.418
3	-0.1	0	0	0	564	0.351	0.398
4	0	0.15	0	0	556	0.518	0.358
5	0	-0.15	0	0	1073	0.102	0.392
6	0	0	0.2	0	373	0.416	0.414
7	0	0	-0.2	0	742	0.300	0.395
8 (□)	0	0	0	0.3	502	0.357	0.406
9 (△)	0	0	0	-0.3	501	0.357	0.406

Table 3.5: Values of the parameters Re_{cr}, $C_{r\,max}$ and A_{max} obtained under conditions of high concentrations (demonstrating the effects due to density, viscosity concentration dependences) and large concentration gradients in liquids.

the interface and it leads to a change in the velocity distribution in the boundary layer and therefore to a change in the mass-transfer kinetics. These effects are thought to be of the Marangoni type and to provide an explanation to all experimental deviations from the prediction of the linear theory of the mass transfer, where the hydrodynamics of the flow does not depend on the mass transfer.

Studies of gas–liquid and liquid–liquid systems with intense interfacial mass transfer as a result of large concentration gradients show (see Chapter 1) that under these conditions the induced secondary flow is directed normal to the interface. It leads to "injection" or "suction" of a substance into the boundary layer, therefore to a change in the velocity distribution of the boundary-layer flow and a change in the mass-transfer kinetics. This effect of non-linear mass transfer can also explain a number of the experimental deviations from the linear theory of mass transfer which have, to date, been attributed to the Marangoni effect.

The Marangoni effect and that of non-linear mass transfer can manifest themselves separately as well as both being active. Thus their influence on the mass-transfer kinetics and the hydrodynamic stability of the flow should be considered. We turn our attention to this problem.

3.4.1 Mass-transfer kinetics

Co-current gas and liquid flows in the laminar boundary layer along a flat interface are considered. One of the components of the gas phase is absorbed by the liquid phase and reacts with a liquid component (see Boyadjiev & Halatchev (1998a)). The chemical reaction rate is taken to be of first-order. Under these conditions, the thermal effect from the chemical reaction creates a temperature gradient, so that mass transfer along with an accompanying heat transfer is observed. Under these conditions the mathematical model

for the boundary-layer flow takes the following form:

$$
\begin{aligned}
&\frac{\partial U_{0j}^*}{\partial x^*} + \frac{\partial V_{0j}^*}{\partial y^*} = 0,\\
&U_{0j}^*\frac{\partial U_{0j}^*}{\partial x^*} + V_{0j}^*\frac{\partial U_{0j}^*}{\partial y^*} = \nu_j\frac{\partial^2 U_{0j}^*}{\partial y^{*2}},\\
&U_{0j}^*\frac{\partial C_{0j}^*}{\partial x^*} + V_{0j}^*\frac{\partial C_{0j}^*}{\partial y^*} = D_j\frac{\partial^2 C_{0j}^*}{\partial y^{*2}} - (j-1)kC_{0j}^*,\\
&U_{0j}^*\frac{\partial T_{0j}^*}{\partial x^*} + V_{0j}^*\frac{\partial T_{0j}^*}{\partial y^*} = \alpha_j\frac{\partial T_{0j}^*}{\partial y^{*2}} + (j-1)\frac{q}{\rho_j c_{pj}}kC_{0j}^*;\\
&j = 1 \text{ - gas phase}, \quad j = 2 \text{ - liquid phase},
\end{aligned}
\tag{3.46}
$$

where α_j is the thermal diffusivity, q is a constant which parametrises the heat production of the chemical reaction, c_{pj} is the specific heat and k is the chemical reaction rate. The influence of the temperature on the chemical reaction rate is not considered in (3.46) as it has only a minor impact on the comparative analysis of the Marangoni effect and the non-linear interfacial mass transfer, which are the subject of the present section.

The boundary conditions applicable to (3.46) are derived to take account of thermodynamic equilibrium and the continuity of velocity, flux of momentum, mass and heat fluxes on the interface. It has been shown in Vulchanov & Boyadjiev (1990) that in the gas–liquid systems the effect of non-linear mass transfer is located within the gas phase. Taking into account these considerations the initial and boundary conditions have the following form:

$$
\begin{aligned}
&x^* = 0: \quad U_{0j}^* = U_{\infty j}^*, \;\; C_{01}^* = \bar{C}_{01}^*, \;\; C_{02}^* = 0 \;\; T_{0j}^* = \bar{T}_0^*, \;\; j = 1,2;\\
&y^* = 0: \quad U_{01}^* = U_{02}^*, \;\; \mu_1\frac{\partial U_{01}^*}{\partial y^*} = \mu_2\frac{\partial U_{02}^*}{\partial y^*} - \frac{\partial \sigma}{\partial x^*},\\
&\qquad V_{01}^* = -\frac{MD_1}{\rho_{01}^*}\frac{\partial C_{01}^*}{\partial y^*}, \;\; V_{02}^* = 0,\\
&\qquad C_{01}^* = \chi C_{02}^*, \;\; D_1\frac{\rho_1^*}{\rho_{01}^*}\frac{\partial C_{01}^*}{\partial y^*} = D_2\frac{\partial C_{02}^*}{\partial y^*}, \;\; (\rho_1^* = \rho_{10}^* + M\bar{C}_0^*),\\
&\qquad T_{01}^* = T_{02}^*, \;\; \lambda_1\frac{\partial T_{01}^*}{\partial y^*} + \rho_1^* c_{p1}\nu_1 T_{01}^* = \lambda_2\frac{\partial T_{02}^*}{\partial y^*};\\
&y^* \to \infty: \quad U_{01}^* = U_{\infty 1}, \;\; C_{01}^* = \bar{C}_{01}^*, \;\; T_{01}^* = \bar{T}_0^*;\\
&y^* \to -\infty: \quad U_{02}^* = U_{\infty 2}, \;\; C_{02}^* = 0, \;\; T_{02}^* = \bar{T}_0^*,
\end{aligned}
\tag{3.47}
$$

where the subscript j denotes different phases (1 for the gas phase and 2 for the liquid phase), asterisk is used for dimensional variables, U_{0j}^* and V_{0j}^* are velocities of the two phases in x^* and y^* directions respectively, C_{0j}^* denotes concentration, σ is the surface tension coefficient, T_{0j}^* are temperatures, D_j the diffusivity coefficients and λ_j the heat-conductivity coefficients. At the free-stream the temperatures of the two phases equal the temperature of the ambient $\bar{T}_0^*$, the free-stream velocities and concentration are denoted by $U_{\infty j}$ and $\bar{C}_{01}^*$.

At large values of the concentration on the wall one observes large concentration gradients directed normal to interface $(\partial C_{01}/\partial y^*)_{y^*=0}$, which induce a secondary flow with rate

$V_{01}(x^*,0)$. The tangential concentration and temperature gradients on the interfacial boundary create a surface tension gradient

$$\frac{\partial\sigma}{\partial x^*}=\frac{\partial\sigma}{\partial C^*_{02}}\frac{\partial C^*_{02}}{\partial x^*}+\frac{\partial\sigma}{\partial T^*_{02}}\frac{\partial T^*_{02}}{\partial x^*},$$

which in turn induces a secondary tangential flow, whose rate is proportional to $\partial\sigma/\partial x^*$. We shall restrict our attention to substances which are not surface active, i.e. $\partial\sigma/\partial C_{02}\approx 0$.

The mass-transfer rate (J_C) and the heat-transfer rate (J_T) can be determined from the local mass (I_C) and heat (I_T) fluxes after taking the mean value of these fluxes along a length (L) of interface. Thus,

$$\begin{aligned}
J_C &= k_C\bar{C}^*_0=\frac{1}{L}\int_0^L I_C\,\mathrm{d}x^*,\quad I_C=\frac{MD_1\rho^*_1}{\rho^*_{10}}\left(\frac{\partial C^*_{01}}{\partial y^*}\right)_{y^*=0},\\
J_T &= k_T\bar{T}^*_0=\frac{1}{L}\int_0^L I_T\,\mathrm{d}x^*,\quad I_T=-\lambda\left(\frac{\partial T^*_{01}}{\partial y^*}\right)_{y^*=0}+\rho_1c_{p1}(\nu_1T^*_{01})_{y^*=0},
\end{aligned}\tag{3.48}$$

where k_C is the mass-transfer coefficient, k_T is the heat-transfer coefficient, C^*_{01} and T^*_{01} are determined after solving the problems (3.46) - (3.47). In order to do this the following dimensionless variables are introduced:

$$\begin{aligned}
&x^*=Lx,\quad y^*=(-1)^{j+1}\delta_jy_j,\quad \delta_j=\sqrt{\frac{\nu_jL}{\bar{U}^*_{\infty j}}},\\
&U^*_{0j}=\bar{U}^*_{\infty j}U_j(x,y_j),\quad V^*_{0j}=\frac{1}{L}(-1)^{j+1}\bar{U}^*_{\infty j}\delta_jV_j(x,y_j),\\
&C^*_{0j}=(-\chi)^{1-j}\bar{C}^*_0C_j(x,y_j),\quad T^*_{0j}=\bar{T}^*_0+(-1)^{j+1}\bar{T}^*_0T_j(x,y_j),\quad j=1,2,
\end{aligned}\tag{3.49}$$

where χ is a Henry's constant as defined in Chapter 1.

Introducing (3.49) into (3.46) and (3.47) leads to the following non-dimensionalised system of boundary layer and concentration equations:

$$\begin{aligned}
&\frac{\partial U_j}{\partial x}+\frac{\partial V_j}{\partial y_j}=0,\\
&U_j\frac{\partial U_j}{\partial x}+V_j\frac{\partial U_j}{\partial y_j}=\frac{\partial^2U_j}{\partial y_j^2},\\
&U_j\frac{\partial C_j}{\partial x}+V_j\frac{\partial C_j}{\partial y_j}=\frac{1}{Sc_j}\frac{\partial^2C_j}{\partial y_j^2}-(j-1)DaC_j,\\
&U_j\frac{\partial T_j}{\partial x}+V_j\frac{\partial T_j}{\partial y_j}=\frac{1}{Pr_j}\frac{\partial^2T_j}{\partial y_j^2}+(j-1)QDaC_j,\\
&j=1\text{ - gas},\quad j=2\text{ - liquid},
\end{aligned}\tag{3.50}$$

where

$$Da=\frac{kL}{\bar{U}_{\infty 2}},\quad Q=\frac{q\bar{C}^*_0}{\chi\rho_2c_{p2}\bar{T}^*_0},\quad Sc_j=\frac{\nu_j}{D_j},\quad Pr_j=\frac{\nu_j}{\alpha_j},\quad j=1,2.$$

Here Da is the Damkhöler number[2] and Q is a scaled dimensional number, a ratio between the concentration of the species 1 at the free-stream, the constant taking into account the heat effect of the chemical reaction and the temperature at the free-stream, the specific heat.

The initial and boundary conditions of system (3.50) then become

$$\begin{aligned}
&x = 0: \quad U_j = 1, \ C_1 = 1, \ C_2 = 0, \ T_j = 0, \ j = 1, 2; \\
&y_1 = y_2 = 0: \quad U_1 = \theta U_2, \ \theta_2 \frac{\partial U_1}{\partial y_1} = -\frac{\partial U_2}{\partial y_2} + \theta_4 \frac{\partial T_2}{\partial x}, \\
&\qquad V_1 = -\theta_3 \frac{\partial C_1}{\partial y_1}, \ V_2 = 0, \ C_1 + C_2 = 0, \ T_1 + T_2 = 0, \\
&\qquad \theta_5 \frac{\partial C_1}{\partial y_1} = \frac{\partial C_2}{\partial y_2}, \ \theta_6 \frac{\partial T_1}{\partial y_1} = \frac{\partial T_2}{\partial y_2}; \\
&y_1 \to \infty: \quad U_1 = 1, \ C_1 = 1, \ T_1 = 0; \\
&y_2 \to \infty: \quad U_2 = 1, \ C_2 = 1, \ T_2 = 0.
\end{aligned} \tag{3.51}$$

The effect of convective transfer in (3.51) is omitted as in practice, it is negligible, while parameters θ_i $(i = 1, \ldots, 6)$ have the following form:

$$\begin{aligned}
&\theta_1 = \frac{U^*_{\infty 2}}{U^*_{\infty 1}}, \ \theta_2 = \frac{\mu_1}{\mu_2}\sqrt{\frac{\nu_2}{\nu_1}}\left(\frac{U^*_{\infty 2}}{U^*_{\infty 1}}\right)^{3/2}, \\
&\theta_4 = \frac{\partial \sigma}{\partial T^*_{02}} \frac{\bar{T}^*_0}{U^*_{\infty 2}\mu_2}\sqrt{\frac{\nu_2}{U^*_{\infty 2} L}}, \ \theta_3 = \frac{M \bar{C}^*_0}{\rho^*_{10} Sc_1}, \\
&\theta_5 = \chi \frac{D_1 \rho^*_1}{D_2 \rho^*_{10}}\sqrt{\frac{U^*_{\infty 1}\nu_2}{U^*_{\infty 2}\nu_1}}, \ \theta_6 = \frac{\lambda_1}{\lambda_2}\sqrt{\frac{U^*_{\infty 1}\nu_2}{U^*_{\infty 2}\nu_1}}.
\end{aligned} \tag{3.52}$$

From (3.48) and (3.49) we obtain expressions for the Sherwood and Nusselt numbers

$$Sh = \frac{k_c L}{D_1} = M\sqrt{Re_1}\int_0^1 (1 + \theta_3 Sc_1 C^*_1)\left(\frac{\partial C_1}{\partial y_1}\right)_{y_1=0} \mathrm{d}x, \tag{3.53}$$

$$Nu = \frac{k_t L}{\lambda_1} = -Re_1\left[\int_0^1 \left(\frac{\partial T_1}{\partial y_1}\right)_{y_1=0} \mathrm{d}x + \theta_3 Pr_1 \int_0^1 (1 + T^*_1)\left(\frac{\partial C_1}{\partial y_1}\right)_{y_1=0} \mathrm{d}x\right],$$

$$C^*_1 = C_1(x, 0), \ T^*_1 = T_1(x, 0), \ Re_1 = \frac{U^*_{\infty 1} L}{\nu_1}, \ Pr_1 = \frac{U^*_{\infty 1} L}{D_1}.$$

The problem (3.50), with initial and boundary conditions (3.51), was solved using the following iterative algorithm:

1. Step I: Solve the two-point boundary-value problem, assuming that at the first

[2]Here $L/\bar{U}_{\infty 2}$ may be called the residence time, i.e. the time available for the chemical reaction, while $1/k$ is the time scale of the chemical reaction.

iteration $\theta_1 = \theta_3 = 0$, then setting $\theta_1 = 0.1$

$$
\begin{aligned}
&\frac{\partial U_1^{(k)}}{\partial x} + \frac{\partial V_1^{(k)}}{\partial y_1} = 0,\\
&U_1^{(k)}\frac{\partial U_1^{(k)}}{\partial x} + V_1^{(k)}\frac{\partial U_1^{(k)}}{\partial y_1} = \frac{\partial^2 U_1^{(k)}}{\partial y_1^2},\\
&x = 0: \quad U_1^{(k)} = 1;\\
&y_1 = 0: \quad U_1^{(k)} = \theta_1 U_2^{(k-1)}, \quad V_1^{(k)} = -\theta_3\frac{\partial C_1^{(k-1)}}{\partial y_1};\\
&y_1 \to \infty: \quad (y_1 \geq y_{1\infty}), \quad U_1^{(k)} = 1;\\
&0 \leq x \leq 1 \quad 0 \leq y_1 \leq y_{1\infty}, \quad y_{1\infty} = 6.
\end{aligned}
\tag{3.54}
$$

2. Step II: Solve the two-point boundary-value problem, where $\theta_2 = 0.145$, assuming that at the first iteration $\theta_4 = 0$

$$
\begin{aligned}
&\frac{\partial U_2^{(k)}}{\partial x} + \frac{\partial V_2^{(k)}}{\partial y_2} = 0,\\
&U_2^{(k)}\frac{\partial U_2^{(k)}}{\partial x} + V_2^{(k)}\frac{\partial U_2^{(k)}}{\partial y_2} = \frac{\partial^2 U_2^{(k)}}{\partial y_2^2},\\
&x = 0: \quad U_2^{(k)} = 1;\\
&y_2 = 0: \quad \frac{\partial U_2^{(k)}}{\partial y_2} = -\theta_2\left(\frac{\partial U_1^{(k)}}{\partial y_1}\right)_{y_1=0} + \theta_4\left(\frac{\partial T_1^{(k-1)}}{\partial x}\right)_{y_2=0}, \quad V_2^{(k)} = 0;\\
&y_2 \to \infty: \quad (y_2 \geq y_{2\infty}), \quad U_2^{(k)} = 1;\\
&0 \leq x \leq 1 \quad 0 \leq y_2 \leq y_{2\infty}, \quad y_{2\infty} = 6.\theta_4 = 0
\end{aligned}
\tag{3.55}
$$

3. Step III: Solve the two-point boundary-value problem at $Sc_1 = 0.735$, at the first iteration $C_2^{(k)}(x, 0) = 0$

$$
\begin{aligned}
&U_1^{(k)}\frac{\partial C_1^{(k)}}{\partial x} + V_1^{(k)}\frac{\partial C(k)_1}{\partial y_1} = \frac{1}{Sc_1}\frac{\partial^2 C_1^{(k)}}{\partial y_1^2},\\
&x = 0: \quad C_1^{(k)} = 1;\\
&y_1 = 0: \quad C_1^{(k)} = C_2^{(k-1)}(x, 0);\\
&y_1 \to \infty: \quad (y_1 \geq \bar{y_1}), \quad C_1^{(k)} = 1;\\
&0 \leq x \leq 1 \quad 0 \leq y_1 \leq \bar{y_1}, \quad \bar{y_1} = 7.
\end{aligned}
\tag{3.56}
$$

4. Step IV: Solve the two-point boundary-value problem at $Sc_2 = 564$, $\theta_5 = 18.3$ and

$Da = 10$

$$U_2^{(k)}\frac{\partial C_2^{(k)}}{\partial x} + V_2^{(k)}\frac{\partial C_2^{(k)}}{\partial y_2} = \frac{1}{Sc_2}\frac{\partial^2 C_2^{(k)}}{\partial y_2^2} - DaC_2^{(k)},$$

$$x = 0: \quad C_2^{(k)} = 0;$$

$$y_2 = 0: \quad \frac{\partial C_2^{(k)}}{\partial y_2} = \theta_5\left(\frac{\partial C_1^{(k)}}{\partial y_1}\right)_{y_1=0}; \tag{3.57}$$

$$y_2 \to \infty: \quad (y_2 \geq \bar{y_2}), \quad C_2^{(k)} = 0;$$

$$0 \leq x \leq 1 \quad 0 \leq y_2 \leq \bar{y_2}, \quad y_2 \leq \bar{y_2} = 0.26.;$$

5. Step V: Solve the two-point boundary-value problem at $Pr_1 = 0.666$, at the first iteration $T_2^{(k)}(x,0) = 0$

$$U_1^{(k)}\frac{\partial T_1^{(k)}}{\partial x} + V_1^{(k)}\frac{\partial T_1^{(k)}}{\partial y_1} = \frac{1}{Pr_1}\frac{\partial^2 T_1^{(k)}}{\partial y_1^2},$$

$$x = 0: \quad T_1^{(k)} = 0;$$

$$y_1 = 0: \quad T_1^{(k)} = T_2^{(k-1)}(x,0); \tag{3.58}$$

$$y_1 \to \infty: \quad (y_1 \geq \bar{\bar{y_1}}), \quad T_1^{(k)} = 0;$$

$$0 \leq x \leq 1 \quad 0 \leq y_1 \leq \bar{\bar{y_1}}, \quad \bar{\bar{y_1}} = 7.4.$$

6. Step VI: Solve the two-point boundary-value problem at $Pr_2 = 6.54$, $\theta_6 = 0.034$ and $QDa = 8.6$

$$U_2^{(k)}\frac{\partial T_2^{(k)}}{\partial x} + V_2^{(k)}\frac{\partial T_2^{(k)}}{\partial y_2} = \frac{1}{Pr_2}\frac{\partial^2 T_2^{(k)}}{\partial y_2^2} + QDaC_2^{(k)},$$

$$x = 0: \quad T_2^{(k)} = 0; \tag{3.59}$$

$$y_2 = 0: \quad \frac{\partial T_2^{(k)}}{\partial y_2} = \theta_6\left(\frac{\partial T_1^{(k)}}{\partial y_1}\right)_{y_1=0};$$

$$y_2 \to \infty: \quad (y_2 \geq \bar{\bar{y_2}}), \quad \bar{\bar{y_2}} = 2.4, \quad T_2^{(k)} = 0.$$

The values of the parameters in (3.54) - (3.59) are calculated for the process of absorption of NH_3 in water or water solutions of strong acids.

The solution of (3.54) - (3.59) allows us to determine

$$J_1 = \int_0^L \left(\frac{\partial C_1}{\partial y_1}\right)_{y_1=0} \mathrm{d}x, \quad J_2 = \int_0^L C_1(x,0)\left(\frac{\partial C_1}{\partial y_1}\right)_{y_1=0} \mathrm{d}x,$$

$$J_3 = \int_0^L \left(\frac{\partial T_1}{\partial y_1}\right)_{y_1=0} \mathrm{d}x, \quad J_2 = \int_0^L T_1(x,0)\left(\frac{\partial T_1}{\partial y_1}\right)_{y_1=0} \mathrm{d}x.$$

Introduction of (3.60) into (3.53) allows us to determine the Sherwood and Nusselt numbers

$$Sh = M\sqrt{Re_1}(J_1 + \theta_3 Sc_1 J_2), \quad Nu = -\sqrt{Re_1}\left[J_3 + \theta_3 Pr_1(J_1 + J_4)\right].$$

The results obtained by solution of these problems in the case of gas–liquid systems are shown in Table 3.6.

No.	θ_3	θ_4	J_1	J_2	J_3	J_4
1	0	0	0.5671	0.09721	0.01855	-0.01337
2	0.2	0	0.6129	0.11155	0.02143	-0.01554
3	-0.2	0	0.5274	0.08542	0.01623	-0.01162
4	0	10^{-4}	0.5671	0.09721	0.01855	-0.01338
5	0	10^{-3}	0.5671	0.09721	0.01855	-0.01337
6	0	10^{-2}	0.5670	0.09718	0.01857	-0.01339
7	0	10^{-1}	0.5658	0.09696	0.01879	-0.01364
8	0	1	0.5658	0.09696	0.01879	-0.01364
9	0	5	0.5660	0.09696	0.01854	-0.01345

Table 3.6: Values of the average mass and heat fluxes at $Da = 10$, $\theta_1 = 0.1$, $\theta_2 = 0.145$, $\theta_5 = 18.3$ and $\theta_6 = 0.034$.

The comparison of values of J_k $(k = 1, \ldots, 4)$ shows that the rate of mass and heat transfer depends upon the concentration gradient (θ_3) and in the cases of absorption $(\theta_3 = 0.2)$ and desorption $(\theta_3 = -0.2)$ the mass and heat-transfer coefficients differ by approximately 10% from predictions of linear theory $(\theta_3 = 0)$. The comparative analysis of the non-linear mass-transfer effect and the Marangoni effect in gas–liquid and liquid–liquid systems show (see Boyadjiev & Babak (2000)) that the Marangoni effect has little impact upon the heat and mass-transfer kinetics, since in real systems the parameter θ_4 is very small. This is clearly seen in rows 7, 8 and 9 of Table 3.6.

However, in cases where the velocity of the second phase is very low the occurrence of the Marangoni effect is to be expected because of the velocity dependence of θ_4 from $U_{\infty 2}$ $(U_{\infty 2}^{-3/2})$. In order to evaluate the above case, systems with a small velocity in the volume of the second phase $(U_{\infty 2} \ll 1)$ have also been investigated. Numerical results of Boyadjiev & Babak (2000) show that under these conditions the Marangoni effect remains negligible.

The results obtained show that the Marangoni effect is negligible in two-fluid systems with movable interfaces and absence of surface active agents. The deviations from the predictions of the linear theory of mass transfer are best explained by considering the non-linear mass-transfer effect under conditions of the large concentration gradients.

3.4.2 Boundary-layer flow instabilities

In the previous subsection the effect of non-linear mass transfer induced by high concentration gradients has been discussed. This effect can explain many deviations between experimental data and the predictions of the linear mass-transfer theory. To date, most of these effects were considered as Marangoni effects. However, in many cases the deviations from the linear theory are significantly greater than those predicted by the non-linear

mass-transfer theory. This may be attributed to the loss of hydrodynamic stability as a result of secondary flows induced by the large concentration gradients. These effects will be discussed to end of this chapter.

The analysis of the flow stability can be done directly by introducing the velocity profiles obtained by solving (3.54) - (3.59) into the Orr-Sommerfeld equation

$$(\bar{U}_j - C_j)(\gamma_j'' - A_j^2\gamma_j) - \frac{\partial^2 \bar{U}_j}{\partial y_j^2}\gamma_j = -\frac{i}{A_j Re_j}(\gamma_j^{iv} - 2A_j^2\gamma_j'' + A_j^4\gamma_j) \qquad (3.60)$$
$$+\frac{i}{A_j Re_j}\left(\bar{V}_j\gamma_j''' - \frac{\partial^2 \bar{V}_j}{\partial y_j^2}\gamma_j' - A_j^2\bar{V}_j\gamma'\right), \quad j = 1, 2,$$

where

$$C_j = \frac{\beta_j}{\alpha_j U_{\infty j}^*}, \quad A_j = \alpha_j\delta_j, \quad Re_j = \frac{U_{\infty j}^*\delta_j}{\nu_j} = \sqrt{\frac{U_{\infty j}^* L}{\nu_j}},$$
$$\bar{U}_j = U_j(1, y_j), \quad \bar{V}_j = V_j(1, y_j), \quad \frac{\partial^2 \bar{U}_j}{\partial y_j^2} = \left(\frac{\partial^2 U_j}{\partial y_j^2}\right)_{x=1},$$
$$\frac{\partial^2 \bar{V}_j}{\partial y_j^2} = \left(\frac{\partial^2 V_j}{\partial y_j^2}\right)_{x=1}, \quad \gamma_j(y_j) = G(y), \quad j = 1, 2.$$

Note that the problem was solved (see Boyadjiev & Halatchev (1998a)) only taking into account the diffusion through the interface between the two fluids and surface tension through their influence on the boundary-layer profiles, i.e. the interfacial instabilities are not accounted for. Hence the boundary conditions have the form (2.18).

The solution of (3.60) has been found using the same numerical approach as was employing in Chapter 2. As a result the curves of neutral stability have been obtained (Figure 3.12). The critical Reynolds number Re_{cr}, corresponding wave-speed C_r, and wave number A are obtained. $C_{r\,min}$ and A_{max} are also obtained from these results. They are shown in Table 3.7 for different values of the parameters θ_3 and θ_4, taking into account the intensity of the secondary flows, due to the concentration gradients and tangential temperature gradients.

No.	θ_3	θ_4	Re_{cr}	A_{max}	$C_{r\,max}$
1	0	0	800	0.357	0.4503
2	0.2	0	1411	0.329	0.4187
3	-0.2	0	512	0.382	0.4763
4	0	10^{-4}	800	0.357	0.4503
5	0	10^{-3}	800	0.357	0.4503
6	0	10^{-2}	800	0.357	0.4503
7	0	10^{-1}	799	0.356	0.4505
8	0	1	799	0.356	0.4505

Table 3.7: Values of the critical Reynolds numbers Re_{cr}, $C_{r\,max}$ and A_{max} obtained at $Da = 10$, $\theta_1 = 0.1$, $\theta_2 = 0.145$, $\theta_5 = 18.3$ and $\theta_6 = 0.034$.

The analysis of the influence of the effect on non-linear mass transfer and the Marangoni effect on the mass-transfer kinetics and the hydrodynamic stability in gas–liquid systems presented in this chapter leads us to some basic conclusions. First, in the case of absorption of the components of the gas phase into the liquid phase the increase in intensity of the mass transfer directed from the volume of the gas phase toward the phase boundary ($\theta_3 > 0$) leads to an increase in the mass-transfer rate (J_1) and an increase in the critical Reynolds number (Re_{cr}), i.e. it serves to stabilise the flow. Second, in the case of desorption of the components of the gas phase into the liquid phase the increase in intensity of the mass transfer directed from the phase boundary toward the volume of the gas phase ($\theta_3 < 0$) leads to a decrease in the mass-transfer rate (J_1) and a decrease in the critical Reynolds numbers (Re_{cr}), i.e. serves to destabilise the flow. The rise in the temperature gradient along the phase boundary length (θ_4) leads to a decrease in the mass-transfer rate (J_1) and a decrease in the critical Reynolds numbers (Re_{cr}), thus serving to destabilise the flow. The Marangoni effect, however, is negligible in gas–liquid systems with a movable interface and finally, the flow in the liquid phase is globally stable.

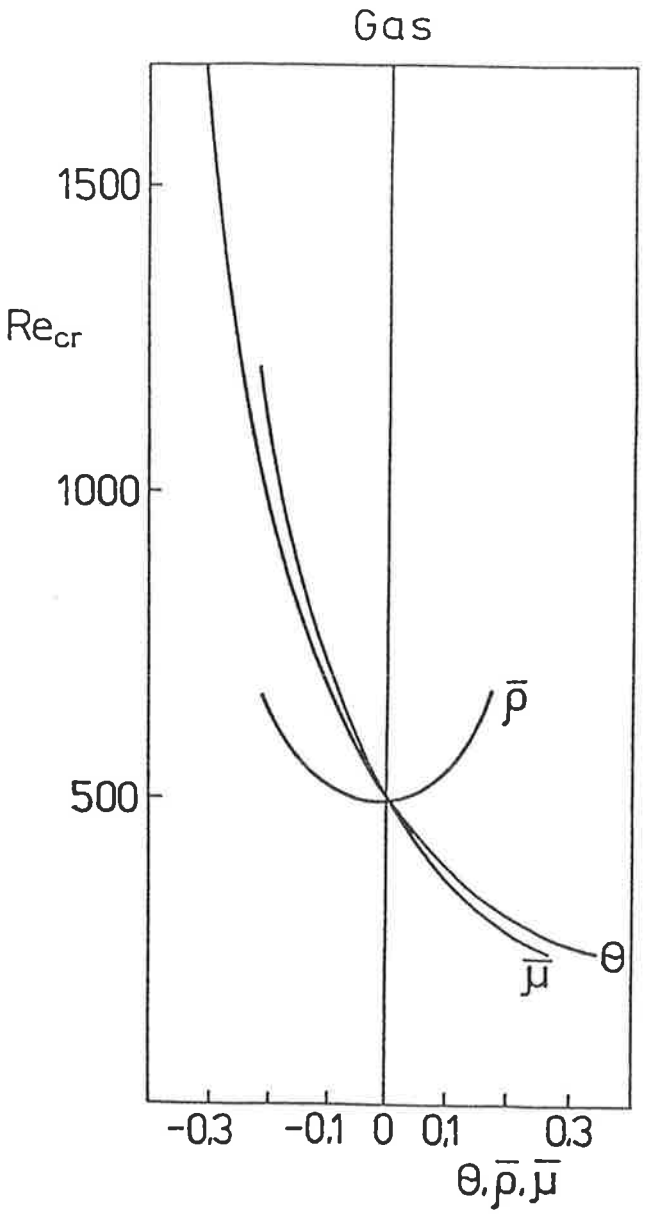

Figure 3.10: The dependence of the critical Reynolds number Re_{cr} from the concentration dependences of the viscosity ($\bar{\mu}$), the density $\bar{\rho}$ and the influence of the large concentration gradients (θ) in gases.

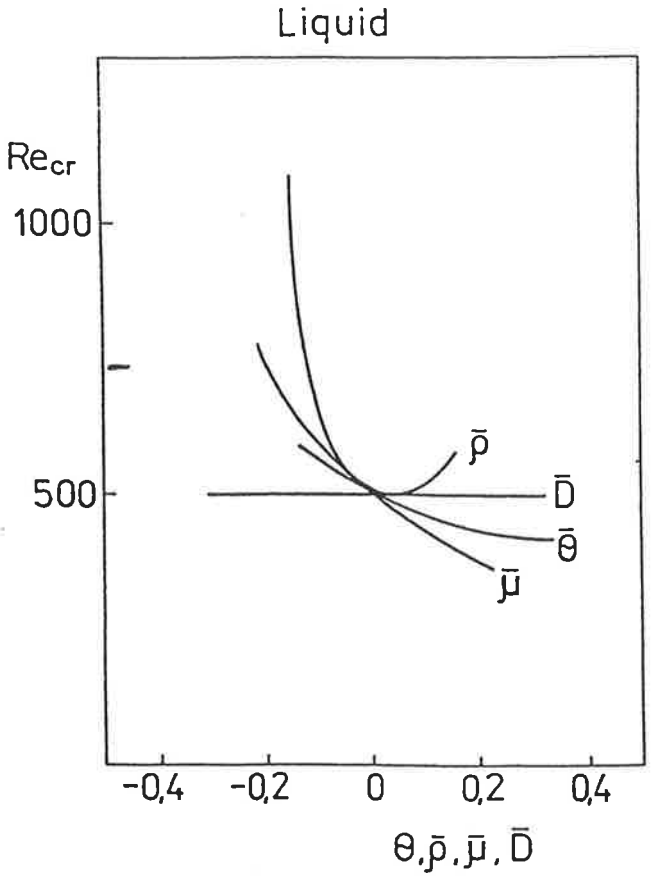

Figure 3.11: The dependence of the critical Reynolds number Re_{cr} from the concentration dependences of the viscosity ($\bar{\mu}$), the density $\bar{\rho}$, the diffusivity ($\bar{D}$) and the influence of the large concentration gradients (θ) in liquids.

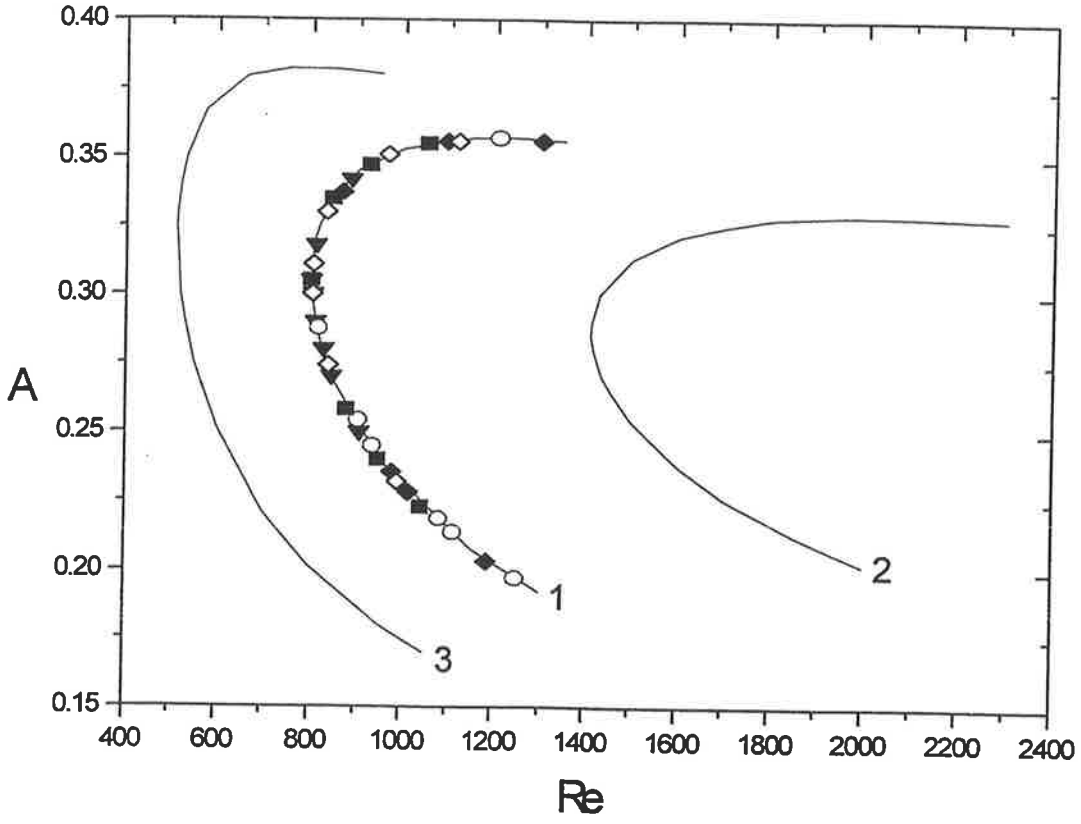

Figure 3.12: The curves of neutral stability in the (Re_{cr}, A)-plane for a gas flow in a laminar boundary layer at $Da = 10$, $\theta_1 = 0.1$, $\theta_2 = 0.145$, $\theta_5 = 18.3$ and $\theta_6 = 0.034$. Shown are plots for the cases: 1) $\theta_4 = 0$, $\theta_3 = 0$; 2) $\theta_4 = 0$, $\theta_3 = 0.2$; 3) $\theta_4 = 0$, $\theta_3 = -0.2$; ($\blacktriangledown$) $\theta_4 = 10^{-4}$, $\theta_3 = 0$; ($\diamond$) $\theta_4 = 10^{-3}$, $\theta_3 = 0.2$; ($\blacklozenge$) $\theta_4 = 10^{-2}$, $\theta_3 = 0.2$; ($\circ$) $\theta_4 = 10^{-1}$, $\theta_3 = 0$; ($\blacksquare$) $\theta_4 = -1$, $\theta_3 = 0$.

Conclusions

The results presented in this part give us the opportunity to make some basic conclusions. The flows in boundary layers of "Blasius type" are characterised by the hydrodynamic stability which increases with a rise in the tangential velocity component on the interface and a decrease of its normal component in going from "suction" ($\theta < 0$, $f(0) > 0$) to "injection" ($\theta > 0$, $f(0) < 0$) in the laminar boundary layer. The instability properties of this type of flows depend both upon the normal component of velocity on interface and interface velocity.

The flows in boundary layers with velocity which decreases with the depth of the fluid ("Couette flow" plane flow) are essentially globally stable, and they are not effected by changes in the normal and tangential component of the velocity on the interface.

Systems with intense interfacial mass transfer are characterised by the fact that the kinetics of mass transfer does not follow from the linear theory of the mass transfer and obvious changes in the hydrodynamic stability are observed. These effects have been previously explained by appealing to the Marangoni effect, i.e. the induction of tangential secondary flow on the phase boundary. The investigations of the kinetics and hydrodynamic instability of systems under conditions of interfacial mass transfer (see Boyadjiev *at. al* (1996a), Boyadjiev & Halatchev (1996b), Boyadjiev & Halatchev (1996c), Boyadjiev & Halatchev (1998a) and Boyadjiev & Halatchev (1998b)) show that the same effects can be explained as resulting from non-linear mass transfer, i.e. the induction of normal secondary flows on the phase boundary. Consequently, it is possible to compare the Marangoni effect with the effect of the non-linear mass transfer.

Part II

Stability and Separation

Chapter 4

The Stability of Boundary-Layer Flows under Conditions of Intense Interfacial Mass Transfer: the effect of interfacial coupling

Porous media surround us everywhere, in reactors of all kinds, almost every possible chemical engineering process, in aeronautics, in waste disposal, in aquifers, in fossil fuel deposits, and in the high intensity heat and interfacial mass-transfer processes. Developments in new technologies require both improvement and increased understanding of the fundamental processes involved. The former, with which our present chapter is concerned, includes an ability to create correct mathematical models and to improve their prediction capabilities. The later is connected with attempts to clarify the physical processes that underly the properties of transport phenomena. We shall study the mechanism of diffusion driven flows in terms of a permeable, two-phase system in which fluid flows over a solid porous surface. Our attention will focus on the question of effect of diffusion on the stability of the flow (see Halatchev & Denier (2000)).

The objectives of this research, as has been suggested in Gebhart *et. al* (1996), is a better understanding of the dynamics of controlled diffusion driven flows by concentration gradients; to devise a procedure which enables one to construct a two-dimensional mathematical model capable of providing, at least, a qualitatively correct description of the critical parameters of the phenomena so as to facilitate and study one possible control strategy and to correct the critical parameters obtained in previous investigations by Boyadjiev *et. al.* (1996a) (presented in Part I).

As mentioned in the Introduction the stability analysis of systems in the presence of mass transfer has been based on a fully decoupled theory. However, the interaction between the concentration and velocity disturbance fields is of great theoretical interest and requires a modification in the solution of the governing equations and boundary conditions. This modification involves the treatment of the problem as a fully coupled one numerically.

We shall discuss the numerical algorithm in detail in this chapter and point to the realm of validity of the earlier results for the decoupled problem, and to the range of critical parameters (namely the Schmidt number Sc) where the decoupled theory cannot be applied.

4.1 Fluid-permeable surface systems with active diffusion through the interface

Consider the laminar flow of a viscous incompressible fluid over a flat, semi-infinite, permeable plate across which a concentration gradient exists (see Figure 4.1). The mass

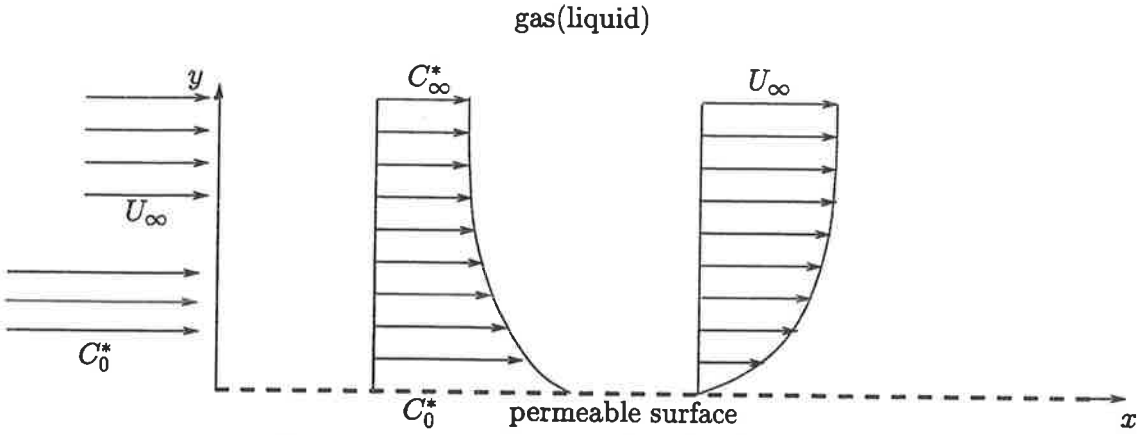

Figure 4.1: A schematic description of the flow.

transfer is simply a result of the concentration driving force. The rate v_n of the induced flow can be defined from the mass flux through the surface (see section 3.1).

The equations governing such a flow are the Navier-Stokes equations and the convection-diffusion equation for steady, incompressible two-dimensional flow with constant diffusivity (2.1) with the initial with initial and boundary conditions (2.2).

After being non-dimensionalised with respect to a typical length scale L (for example, the distance from the leading edge of the plate), the free-stream speed U_∞ and the concentrations $\bar{C}^*_0$ and $\bar{C}^*_\infty$ at the interface ($y^* = 0$) and at the free-stream ($y^* \to \infty$) the system of equations reduces to (2.4), which must be solved subject to the initial and boundary conditions (2.5).

We shall slightly reformulate the basic boundary-layer and concentration equations, by using the more usual similarity variables for Blasius boundary-layer flow. In the limit of large Reynolds number the flow develops a steady boundary layer of thickness $O(Re^{-1/2})$ attached to the leading edge of the plate. Thus we shall introduce boundary-layer vari-

ables (2.12). Substituting into (2.4) - (2.5) we obtain the steady boundary-layer equations

$$\begin{aligned} \frac{\partial U_B}{\partial x} + \frac{\partial V_B}{\partial Y} &= 0, \\ U_B \frac{\partial U_B}{\partial x} + V_B \frac{\partial U_B}{\partial Y} &= \frac{\partial^2 U_B}{\partial Y^2}, \\ \frac{\partial P_B}{\partial Y} &= 0, \\ U_B \frac{\partial C_B}{\partial x} + V_B \frac{\partial C_B}{\partial Y} &= \frac{1}{Sc} \frac{\partial^2 C_B}{\partial Y^2}, \end{aligned} \tag{4.1}$$

where we assume that the free-stream is uniform so that $\partial P_B/\partial x = 0$. The boundary conditions are as follows:

$$\begin{aligned} Y = 0: &\quad U_B = 0,\ V_B = -\frac{\theta}{Sc}\frac{\partial C_B}{\partial Y},\ C_B = 1; \\ Y \to \infty: &\quad U_B \to 1,\ C_B \to 0. \end{aligned} \tag{4.2}$$

Depending on the direction of the mass transfer, noting that $C_{BY}(0) < 0$, there will be "suction" ($\theta < 0$) from, or "blowing" ($\theta > 0$) into, the boundary layer (see Boyadjiev *et. al.* (1996a) and Chapter 1). Our concern is with the effect of this blowing or suction on the hydrodynamic stability of the flow.

In what follows we will employ a similarity solution to the boundary-layer equations as our "basic flow". Thus we set

$$\eta = \frac{Y}{x^{1/2}},\ U_B = f'(\eta),\ V_B = \frac{1}{2\sqrt{x}}(\eta f' - f),\ C_B = g(\eta), \tag{4.3}$$

where f and g are solutions of

$$f''' + \frac{1}{2} f f'' = 0, \qquad g'' + \frac{Sc}{2} g' f = 0 \tag{4.4}$$

subject to the boundary conditions

$$\begin{aligned} &f(0) = \frac{2\theta}{Sc} g'(0),\ f'(0) = 0,\ g(0) = 1; \\ &f'(\infty) = 1,\ g(\infty) = 0. \end{aligned} \tag{4.5}$$

The two-point boundary-value problem (4.4) and (4.5) can be solved numerically by employing a simple shooting technique, using a fourth-order Runge-Kutta quadrature routine coupled with Newton iteration to determine the values $f''(0)$ and $g'(0)$ for which the boundary conditions (4.5) are satisfied (see Halatchev & Denier (2000)). Some of the solutions of this system are presented in Figures 4.2, 4.3 and 4.4 at different values of the mass-transfer parameter θ, and the Schmidt number Sc (for instance the cases $Sc = 1,\ 50$).

It is seen in Figures 4.3 and 4.4 that "blowing" ($\theta > 0$) serves to increase the boundary-layer thickness, while in the case of "suction" ($\theta > 0$) boundary-layer thickness decreases.

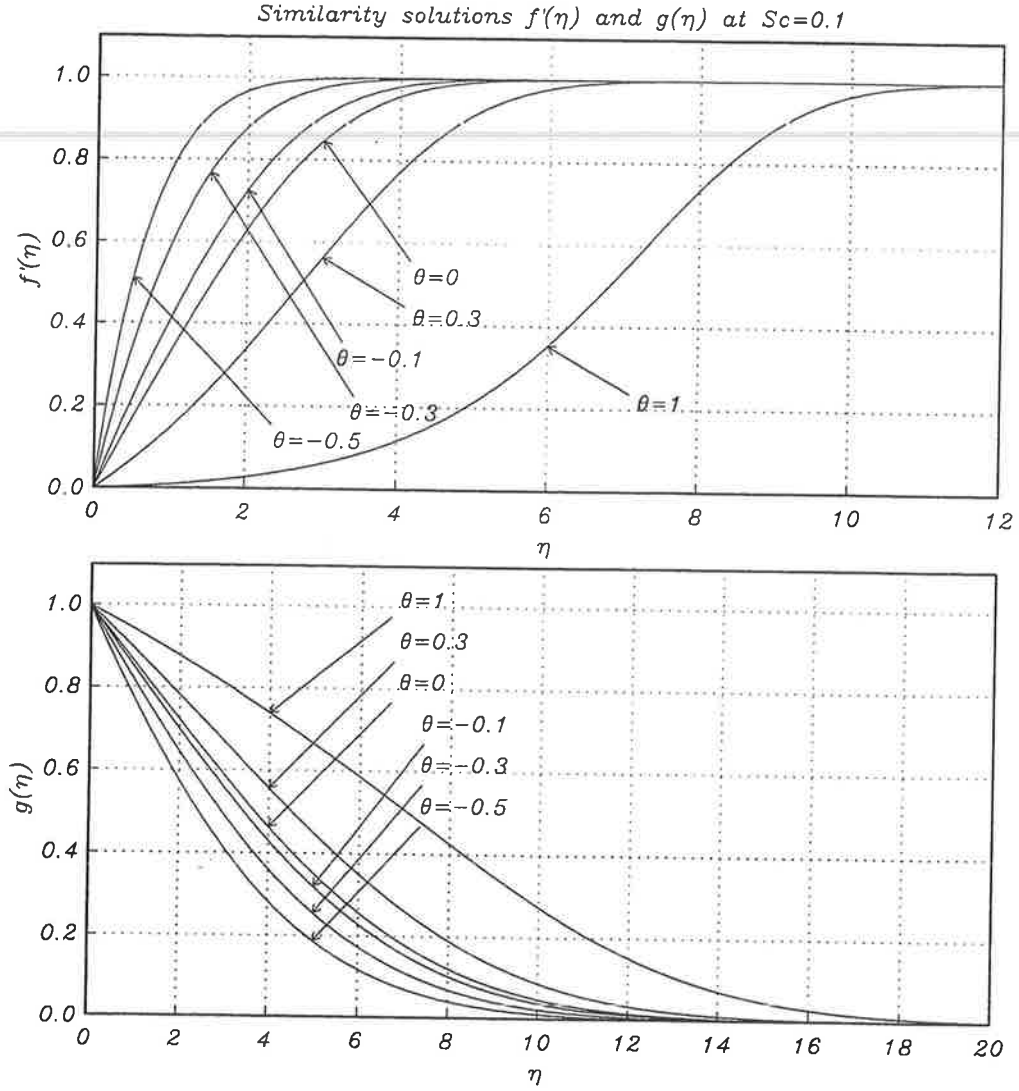

Figure 4.2: Graphs of the Blasius function $f'(\eta)$ and the basic concentration $g(\eta)$ versus η at different values of the mass-transfer parameter θ for Schmidt number $Sc = 0.1$.

This change in the boundary-layer thickness is significant at small Schmidt numbers Sc as in the case of gas flow. At large Schmidt numbers, i.e. in the case of liquid flow, the concentration boundary layer is thinner than the momentum boundary layer and the mass transfer has little impact on the velocity and concentration profiles. At $\theta = 0$, i.e. in the absence of mass transfer, we simply have the classical Blasius boundary-layer flow. A more complete description of the effect of the mass transfer on the boundary-layer flow can be found in Boyadjiev & Vulchanov (1990) where it was shown that the secondary flow, with flow rate $f(0)$, simply serves to modify the shape of the velocity profile $f'(\eta)$.

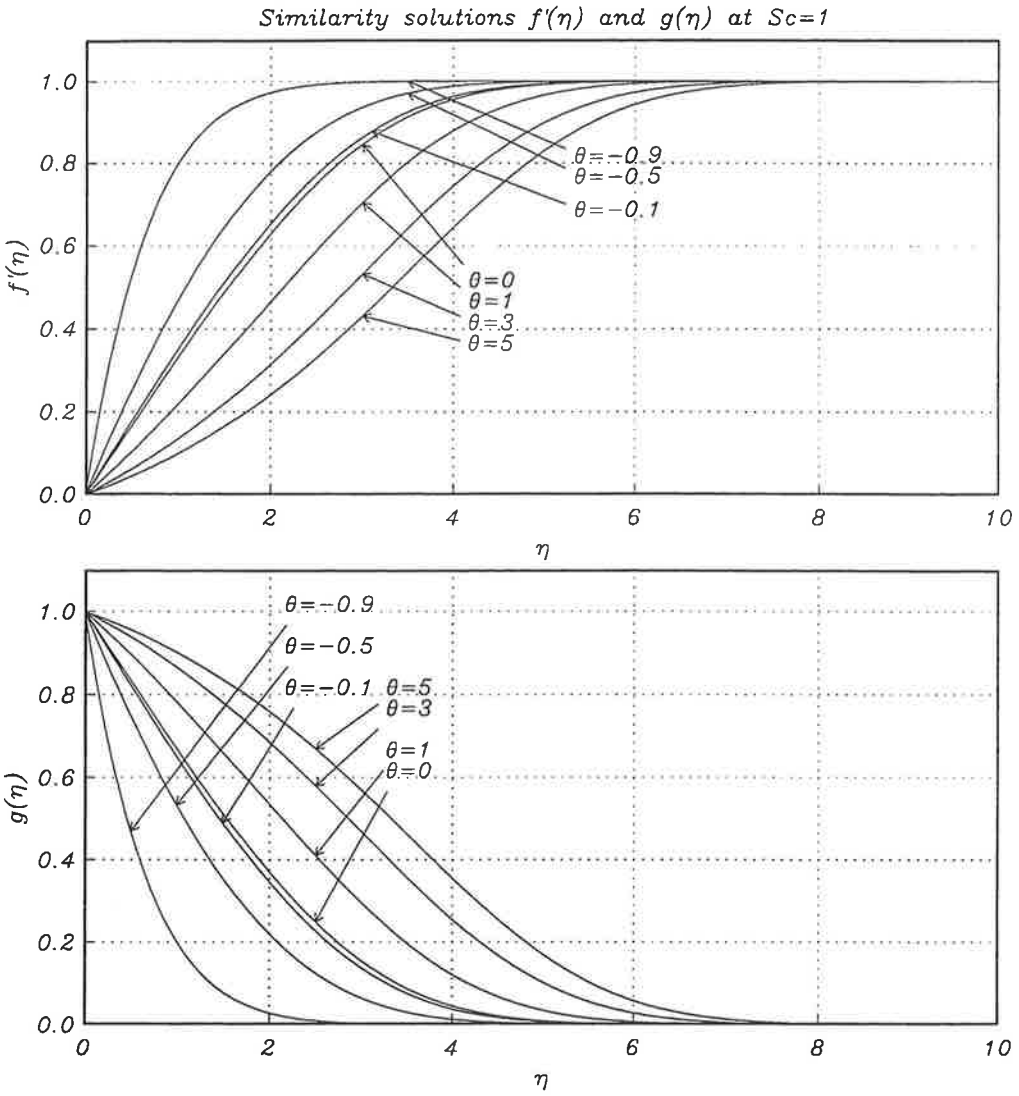

Figure 4.3: Graphs of the Blasius function $f'(\eta)$ and the basic concentration $g(\eta)$ versus η at different values of the mass-transfer parameter θ for Schmidt number $Sc = 1$.

4.2 Hydrodynamic stability analysis at finite Reynolds numbers

To investigate the stability of the flow we superimpose a two-dimensional, small amplitude, disturbance on the basic flow. The total flow field is then written as

$$(U, V, P, C) = (U_0, V_0, P_0, C_0) + \epsilon(u, v, p, c) + \cdots, \tag{4.6}$$

where ϵ is a small perturbation parameter.

The governing equations for two-dimensional disturbances follow from the Navier-Stokes equations and the convection-diffusion equation by linearisation about the basic steady

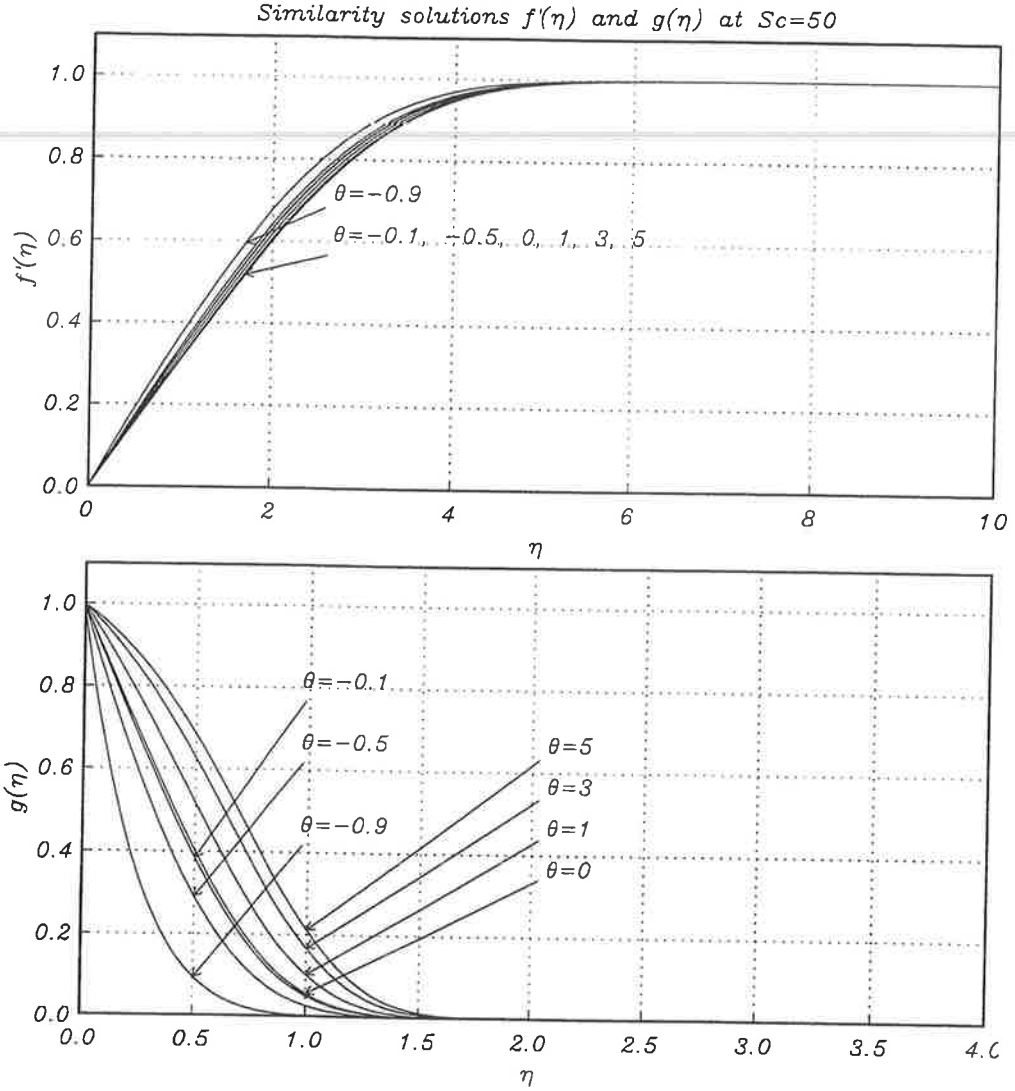

Figure 4.4: Graphs of the Blasius function $f'(\eta)$ and the basic concentration $g(\eta)$ versus η at different values of the mass-transfer parameter θ for Schmidt number $Sc = 50$.

flow and concentration state. This yields the equations

$$\begin{aligned} u_x + v_y &= 0, \\ u_t + U_0 u_x + u U_{0x} + v U_{0y} + V_0 u_y &= -p_x + Re^{-1}\left(u_{xx} + u_{yy}\right), \\ v_t + U_0 v_x + u V_{0x} + V_0 v_y + v V_{0y} &= -p_y + Re^{-1}\left(v_{xx} + v_{yy}\right), \\ c_t + U_0 c_x + u C_{0x} + V_0 c_y + v C_{0y} &= Re^{-1} Sc^{-1}\left(c_{xx} + c_{yy}\right), \end{aligned} \tag{4.7}$$

where (u, v) is the small unsteady perturbation to the steady basic flow (U_0, V_0), p is the pressure perturbation, c is the concentration perturbation, t denotes time, $Re = U_\infty L/\nu$ ($Re \gg 1$) is the Reynolds number based on the characteristic velocity, the typical length scale and the kinematic viscosity ν and $Sc = \nu/D$ is the Schmidt number. The position of flat plate is given by $y = 0$, $x > 0$ and the free-stream by $U_0 = 1$. This system has been non-dimensionalised using (2.3).

The mean flow in the x-direction is assumed to be influenced by a disturbance which is composed of a number of discrete partial fluctuations, each of which consists of a wave which is propagated in the x-direction (see Schlichting (1979)). It is therefore appropriate to represent a single oscillation in the following form

$$\begin{aligned} u(x,y) &= F'(y)\exp\left[i(\alpha x-\beta t)\right], \\ v(x,y) &= -i\alpha F(y)\exp\left[i(\alpha x-\beta t)\right], \\ c(x,y) &= i\alpha G(y)\exp\left[i(\alpha x-\beta t)\right], \end{aligned} \tag{4.8}$$

where $F(y)$ and $G(y)$ are the amplitudes of the disturbances, α is a real quantity and $\beta=\beta_r+i\beta_i$ is complex; they are the wavenumber, the frequency (β_r) and the amplification factor (β_i). If $\beta_i<0$ the disturbance is damped and the flow deemed to be stable, whereas if $\beta_i>0$ the flow is unstable and the disturbance grows exponentially with time. In (4.8), we have employed the classical parallel flow approximation, i.e. the disturbance amplitude is assumed to depend only on the normal coordinate y and the dependence on the longitudinal coordinate x enters the problem parametrically through the x-dependency of the mean flow quantities.

In order to reduce the disturbance equations to their standard form we will make use of the boundary-layer approximation and introduce the factor

$$\delta_*=1.720\frac{Re}{R_\delta},$$

where $R_\delta=1.72(xRe)^{1/2}$ is the Reynolds number based on the local boundary-layer thickness (see Halatchev & Denier (2000) for full details). After eliminating the pressure term from equations (4.7) by cross-differentiation, introducing the similarity variables (4.3) and taking into account the transformations

$$F^{(n)}(y)=\delta_*^n\varphi^{(n)}(\eta),\quad G^{(n)}(y)=\delta_*^n\sigma^{(n)}(\eta)$$

we obtain the following system, consisting of an Orr-Sommerfeld type equation for the disturbance amplitude φ and a second-order equation for the concentration disturbance amplitude σ:

$$\begin{aligned} \left(f'-\hat{C}\right)\left(\varphi''-\hat{A}^2\varphi\right)-f'''\varphi=-\frac{1.720i}{\hat{A}R_\delta}\Bigg\{&\left(\varphi^{iv}-2\hat{A}^2\varphi''+\hat{A}^4\varphi\right) \\ &-\frac{1}{2}\left(\eta f'-f\right)\varphi'''+\frac{1}{2}\left[\left(\eta f'''+f''\right)+\hat{A}^2\left(\eta f'-f\right)\right]\varphi'\Bigg\}, \end{aligned} \tag{4.9a}$$

$$\left(f'-\hat{C}\right)\sigma+ig'\varphi=-\frac{1.720i}{\hat{A}R_\delta}\left[\frac{1}{Sc}\left(\sigma''-\hat{A}^2\sigma\right)-\frac{1}{2}\left(\eta f'-f\right)\sigma'\right]. \tag{4.9b}$$

These must be solved subject to boundary conditions

$$\begin{aligned} &\varphi(0)=\frac{1.720\theta}{ScR_\delta}\sigma'(0),\quad \varphi'(0)=0,\quad \sigma(0)=0; \\ &\varphi(\infty)=0,\quad \varphi'(\infty)=0,\quad \sigma(\infty)=0. \end{aligned} \tag{4.10}$$

Here we have defined

$$\hat{A} = \frac{\alpha}{\delta_*}, \quad \hat{C} = \frac{\beta}{\alpha} = \hat{C}_r + i\hat{C}_i, \quad R_\delta = 1.720\,(xRe)^{1/2}.$$

The system (4.9) with boundary conditions (4.10) constitutes an eigenvalue problem for $\hat{C}_r$ as a function of $\hat{A}$ and R_δ. The relationship between R_δ and x can be interpreted in the following way; in determining a critical Reynolds number R_δ (beyond which the flow is unstable) we will, in effect, be determining a critical position x_{cr} at which the boundary layer becomes linearly unstable to wave-like disturbances.

The results presented in Part I on this problem were obtained by assuming that the parameter θ is small and subsequently the right-hand-side of the boundary condition for $\varphi(0)$ is negligible. This assumption allows the momentum and concentration fields to decouple and results in a classical Orr-Sommerfeld eigenvalue problem for the complex wave-speed. In this case the effect of the interfacial mass transfer on the flow occurs only through the coupling in the basic boundary-layer equations. This approximation, although capturing the effect of mass transfer on the boundary-layer flow, cannot correctly account for the forcing of the disturbance momentum transport due to the diffusion through the permeable surface. We therefore retain this coupling in both the basic boundary-layer equations and the disturbance equations. In order to determine the stability of the flow we must therefore solve system (4.9) subject to the full boundary conditions (4.10).

As the solution procedure has some important differences over that which could be employed if the boundary conditions were decoupled we will now present the details of the numerical method that have been used.

4.3 Numerical algorithm

Our solution strategy is based upon a finite difference discretisation of the system (4.9). It is convenient to write the system in the following generic form

$$\begin{aligned} &(D^4 + a_1 D^3 + a_2 D^2 + a_3 D + a_4)\varphi = 0, \\ &(D^2 + b_1 D + b_2)\sigma + b_3\varphi = 0, \end{aligned} \tag{4.11}$$

where $a_i = a_i(\eta)$ and $b_j = b_j(\eta)$ $(i = 1, \ldots, 4,\ j = 1, \ldots, 3)$ in the interval $0 \leq \eta < \infty$ and D denotes $\mathrm{d}/\mathrm{d}\eta$. For our specific problem the coefficients have the following form

$$\begin{aligned}
a_1 &= -\frac{1}{2}(\eta f' - f), \\
a_2 &= -2\hat{A}^2 - \frac{i\hat{A}R_\delta}{1.720}\left(f' - \hat{C}\right), \\
a_3 &= \frac{1}{2}\left[(\eta f''' + f'') + \hat{A}^2(\eta f' - f)\right], \\
a_4 &= \left\{\hat{A}^4 + \frac{i\hat{A}R_\delta}{1.720}\left[\hat{A}^2(f' - \hat{C}) + f'''\right]\right\}, \\
b_1 &= -\frac{1}{2}Sc\,(\eta f' - f) = a_1 Sc, \\
b_2 &= -\hat{A}^2 - \frac{i\hat{A}R_\delta Sc}{1.720}\left(f' - \hat{C}\right), \\
b_3 &= \frac{\hat{A}R_\delta Sc}{1.720}g'.
\end{aligned} \tag{4.12}$$

Special care must be taken dealing with the boundary conditions at infinity as has been done in Boyadjiev *et. al.* (1996a). For unbounded flows of this type we must necessarily truncate the semi-infinite domain at some $\eta_N \gg 1$, chosen to ensure that the variation in the basic flow is negligible at that point i.e.

$$\begin{aligned}
&f'(\eta_N) = 1, \quad f''(\eta_N) = f'''(\eta_N) = 0, \quad \eta_N f'(\eta_N) - f(\eta_N) = k, \\
&\eta_N f'''(\eta_N) = 0, \quad g(\eta_N) = g'(\eta_N) = 0.
\end{aligned} \tag{4.13}$$

We will employ Keller's method for eigenvalue problems on infinite domains to first derive the correct asymptotic form for the far-field ($\eta \to \infty$) boundary conditions (see Keller (1976)). First we rewrite the system of equations (4.9) in the following form:

$$\mathbf{y}'(\eta) = \mathbf{D}(\eta; \hat{A}, R_\delta, \hat{C})\mathbf{y}, \tag{4.14}$$

where

$$\mathbf{y}^T(\eta) = (\varphi'' - \hat{A}^2\varphi, \varphi''' - \hat{A}^2\varphi', \varphi, \varphi', \sigma, \sigma'),$$

and the matrix $\mathbf{D}(\eta; \hat{A}, R_\delta, \hat{C})$ is defined using (4.12); it is given in the Appendix A.2.

As noted by Keller (1976), to obtain the correct exponential decay of the eigensolutions as $\eta \to \infty$ we must ensure that the far field boundary conditions (applied at $\eta = \eta_N \gg 1$) have the correct asymptotic form. These are derived by considering the asymptotic form of (4.14) as $\eta \to \infty$. Thus,

$$\lim_{\eta\to\infty} \mathbf{D}(\eta; \hat{A}, R_\delta, \hat{C}) \tag{4.15}$$

$$= \mathbf{D}_\infty(\hat{A}, R_\delta, \hat{C}) \equiv \begin{pmatrix}
0 & 1 & 0 & 0 & 0 & 0 \\
\beta_0^2 & \frac{1}{2}k & 0 & 0 & 0 & 0 \\
0 & 0 & 0 & 1 & 0 & 0 \\
1 & 0 & \hat{A}^2 & 0 & 0 & 0 \\
0 & 0 & 0 & 0 & 0 & 1 \\
0 & 0 & 0 & 0 & \beta_1^2 & \frac{1}{2}kSc
\end{pmatrix},$$

where

$$\beta_0^2 = \hat{A}^2 + \frac{i\hat{A}R_\delta}{1.72}(1-\hat{C}), \qquad (4.16)$$
$$\beta_1^2 = \hat{A}^2 + \frac{i\hat{A}R_\delta Sc}{1.72}(1-\hat{C}).$$

The eigenvalues $(\lambda_i,\ i=1,\ldots,6)$ of $\mathbf{D}_\infty(\hat{A},R_\delta,\hat{C})$ are

$$\pm\hat{A},\ \ \frac{1}{4}k \pm \frac{1}{4}\sqrt{k^2+16\beta_0^2},\ \ \frac{1}{4}kSc \pm \frac{1}{4}\sqrt{k^2Sc^2+16\beta_1^2}, \qquad (4.17)$$

and in order to ensure exponential decay as $\eta \to \infty$ we choose those with negative real component:

$$\lambda_1 = -\hat{A},\ \ \lambda_2 = \frac{1}{4}k - \frac{1}{4}\sqrt{k^2+16\beta_0^2},\ \ \lambda_3 = \frac{1}{4}kSc - \frac{1}{4}\sqrt{k^2Sc^2+16\beta_1^2}. \qquad (4.18)$$

The requirement that our numerical solution captures only these exponentially decaying components can, in the notation of Keller (1976), be written as

$$\mathbf{G}_\infty^+\mathbf{y} = \mathbf{0},\ \ \text{as}\ \ \eta \to \infty, \qquad (4.19)$$

where the matrix $\mathbf{G}_\infty^+$ consists of the left eigenvectors of D_∞ corresponding to eigenvalues (4.18); $\mathbf{G}_\infty^+$ is given in Appendix A.2.

These far-field radiation boundary conditions can now be written as

$$\begin{aligned}
&\left(D^2-\hat{A}^2\right)\left(D+\frac{1}{4}\sqrt{k^2+16\beta_0^2}-\frac{1}{4}k\right)\varphi = 0,\\
&\left(D+\hat{A}\right)\left(D^2-\beta_0^2-\frac{1}{2}kD\right)\varphi = 0, \qquad (4.20)\\
&\left(D+\frac{1}{4}\sqrt{k^2Sc^2+16\beta_1^2}-\frac{1}{4}kSc\right)\sigma = 0,
\end{aligned}$$

in the limit $\eta \to \infty$. Note that in the far-field, the boundary conditions on φ and σ decouple. In the case $k=0$ (i.e. ignoring the non-parallel effects arising from the boundary-layer growth) the first two equations in (4.20) reduce to those obtained by Keller (1976) thus providing a useful consistency check.

We now turn our attention to the question of the coupling between the disturbance equations at $\eta = 0$. As noted above, our general approach to the solution of the eigenvalue problem governed by (4.9) - (4.10) will be to employ a second-order accurate, finite difference discretisation of the disturbance equations. In the absence of the coupling at $\eta = 0$ such a discretisation would lead to a simple penta-diagonal matrix equation for the velocity disturbance amplitude φ; an iteration procedure based upon the smallness of $\varphi(0)$, say, can then be used to solve for the eigenvalues. In the presence of the boundary coupling such a scheme is not suitable and an alternate scheme is necessary.

To proceed, let us introduce an unknown function $H = H(x)$ defined such that $\varphi''(0) = H$. We will normalise all dependent variables in (4.10) with respect to H; for instance $\varphi = H\tilde{\varphi}$ so that $\tilde{\varphi}''(0) = 1$. Due to the linearity of system (4.9), it remains unchanged under this rescaling except for the fact that φ and σ are replaced by $\tilde{\varphi}$ and $\tilde{\sigma}$. Further, let us suppose that the value of $\tilde{\sigma}'$ is known at the boundary and denote it by B; of course B must be found as part of the solution procedure (see below). The boundary conditions (4.10) can be written as

$$\begin{aligned} &\tilde{\varphi}(0) = \frac{1.720\theta}{ScR_\delta}B, \;\; \tilde{\varphi}''(0) = 1, \;\; \tilde{\sigma}'(0) = B; \\ &\tilde{\varphi}(\infty) = 0, \;\; \tilde{\varphi}'(\infty) = 0, \;\; \tilde{\sigma}(\infty) = 0. \end{aligned} \tag{4.21}$$

For fixed values of Sc, R_δ, θ and $\hat{A}$ the "eigenvalues" (or unknowns) will be deemed found if the remaining two boundary conditions $\tilde{\sigma}(0) = 0$ and $\tilde{\varphi}'(0) = 0$ are satisfied. This will form the basis of our iterative procedure for the eigenvalues of the generalised Orr-Sommerfeld system. For the sake of convenience, from herein we shall omit the tilde from our notation.

Based upon (4.21) we implemented the following algorithm to solve the problem:

- Step I: Set up initial guesses for $\hat{C}$ and B at given R_δ, $\hat{A}$, Sc and θ;
- Step II: Solve the Orr-Sommerfeld equation and the concentration equation, subject to the boundary conditions (4.21);
- Step III: Iterate on $\hat{C}$ and B until $\varphi'(0) = 0$ and $\sigma(0) = 0$ are satisfied to within some desired tolerance (the result is the eigenvalues for $\hat{C}$, B and the corresponding eigenfunctions φ and σ).

Letting φ_j and σ_j denote values of φ and σ at grid point $\eta_j = jh$, discretising the disturbance equations using second-order accurate centred differencing (see Abramowitz & Stegun (1972)) yields

$$\begin{aligned} &\mu_1\varphi_{j-2} + \mu_2\varphi_{j-1} + \mu_3\varphi_j + \mu_4\varphi_{j+1} + \mu_5\varphi_{j+2} = 0, \\ &\varphi_0 = \frac{1.72\theta}{ScR\delta}B, \;\; \varphi_{-1} = \frac{3.44\theta}{ScR\delta}B - \varphi_1 + h^2, \\ &-\frac{1}{2}\varphi_{N-2} + \zeta_1\varphi_{N-1} - \zeta_2\varphi_N - \zeta_3\varphi_{N+1} + \frac{1}{2}\varphi_{N+2} = 0, \\ &-\frac{1}{2}\varphi_{N-2} + \zeta_4\varphi_{N-1} - \zeta_5\varphi_N - \zeta_6\varphi_{N+1} + \frac{1}{2}\varphi_{N+2} = 0, \end{aligned} \tag{4.22}$$

and

$$\begin{aligned} &\mu_6\sigma_{j-1} + \mu_7\sigma_j + \mu_8\sigma_{j+1} = \mu_9\varphi_j, \\ &\sigma_{-1} = \sigma_1 - 2hB, \\ &\sigma_{N+1} = \sigma_{N-1} - \zeta_7\sigma_N, \end{aligned} \tag{4.23}$$

where the asymptotic boundary conditions η_N have been satisfied explicitly and we have introduced the false grid point η_{-1} in order to retain second-order accuracy in η. The

resulting matrix systems are given in Appendix A.1, together with their compact storage forms, and the full list of the coefficients is given in the Appendix A.3. We used a step-size of $h = \Delta\eta = 0.001$. There are no numerical instabilities in the method described above.

4.4 Curves of neutral stability and discussion

The system was solved using the algorithm described above to generate curves of neutral stability in $(R_\delta, \hat{A})$ and $(R_\delta, \hat{C}_r)$-plane. These are presented in Figures 4.5 - 4.10.

Let us consider firstly the results for a Schmidt number of 0.7 presented in Figure 4.5. Following the usual convention the curves of neutral stability delineate the boundary

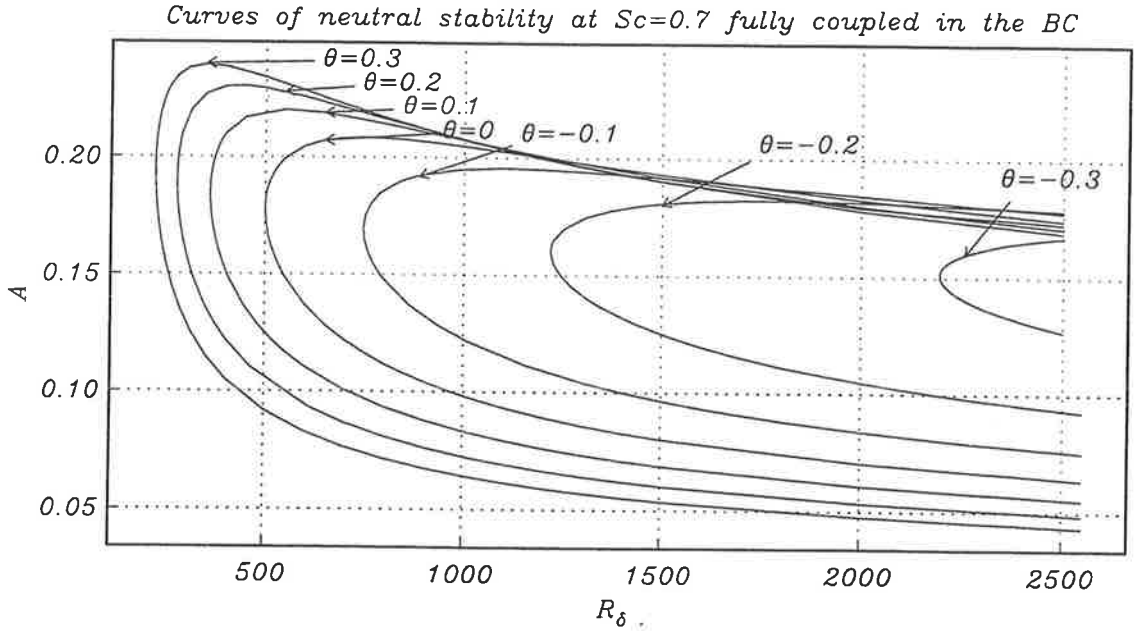

Figure 4.5: Curves of neutral stability in the $(R_\delta, \hat{A})$-plane at $Sc = 0.7$ for different values of θ.

in the parameter space between stable and unstable disturbances; the flow is unstable for values of the parameter that lay inside the neutral curve. From Figure 4.5 we see that the effect of positive mass transfer (i.e. blowing) is to reduce the critical Reynolds number and consequently destabilise the boundary layer; the point of neutral stability therefore moves towards the leading edge of the plate which suggests an earlier onset to turbulence within the flow. This conclusion is in agreement with that made in the previous works (see Boyadjiev *et. al.* (1996a), Boyadjiev & Halatchev (1996b,c) and Halatchev & Boyadjiev (1996) presented in Chapter 2) which was based upon the approximation of decoupling the disturbance fields. We note that, for the present case ($Sc = 0.7$), the critical Reynolds number, for a value of $\theta = -0.3$, is 2.19264×10^3 as compared to the value of 2.23226×10^3 predicted by the analysis of

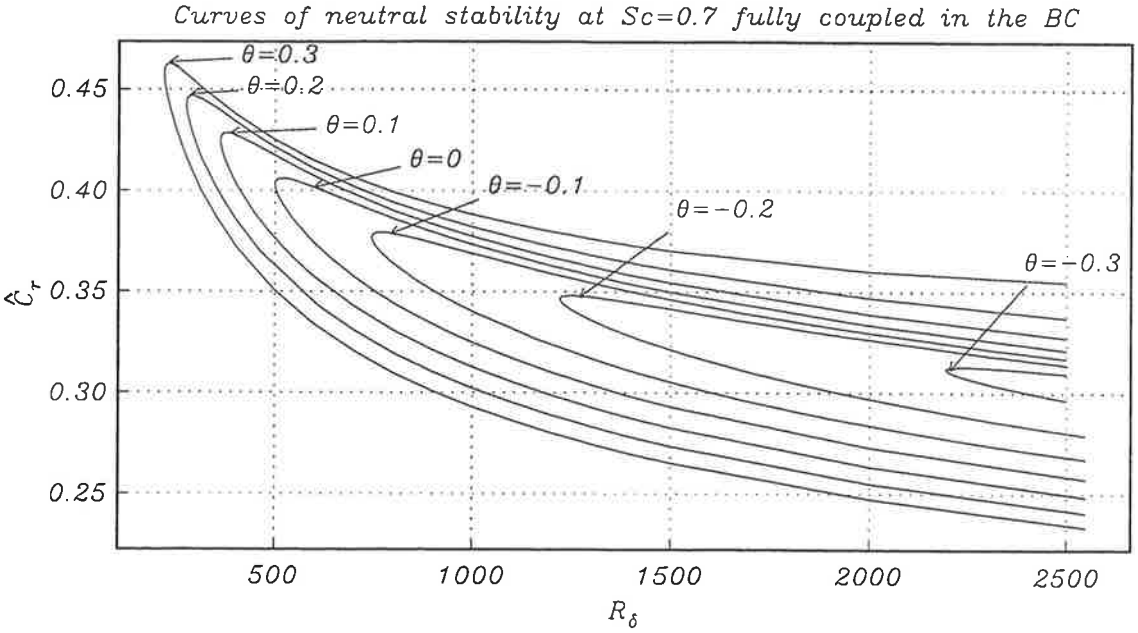

Figure 4.6: Curves of neutral stability in the $(R_\delta, \hat{C}_r)$-plane at $Sc = 0.7$ for different values of θ.

Boyadjiev *et. al.* (1996a) whereas for $\theta = 0.3$ the respective values are 2.210018×10^2 (current results) and 2.18419×10^2 (results of Boyadjiev *et. al.* (1996a)). These differences are summarised in Figure 4.11. Further from Figures 4.5 and 4.6 we observe that blowing serves to increase the critical wavenumber and wave-speed. These general conclusions also hold for higher values of the Schmidt number as presented in Figure 4.9 and 4.10. The changes in the critical Reynolds number, wavenumber and wave-speed as a function of θ are summarised in Tables 4.1 - 4.4.

$Sc = 0.7$					
θ	$R_\delta \times 10^3$	$\hat{A}$	$\hat{C}_r$	$\hat{A}_{max}$	$\hat{C}_{r\,max}$
-0.3	2.192640	0.1510000	0.3116931	0.1672360	0.3130090
-0.2	1.219656	0.1600000	0.3462902	0.1825266	0.3481817
-0.1	0.746276	0.1700000	0.3772822	0.1956240	0.3795264
0.0	0.500000	0.1773200	0.4028357	0.2083170	0.4061027
0.1	0.361021	0.1840000	0.4242387	0.2198905	0.4283788
0.2	0.276331	0.1880000	0.4414703	0.2300431	0.4470361
0.3	0.221001	0.1920000	0.4563870	0.2390913	0.4626900

Table 4.1: Values of critical Reynolds number R_δ, corresponding wave-speed $\hat{C}_r$, wave number $\hat{A}$ and $\hat{A}_{max}$ and $\hat{C}_{r\,max}$ at $Sc = 0.7$.

Finally, the eigenfunctions φ and σ at $Sc = 0.7$ and $\theta = -0.3$ for certain values from the neutral curve of stability on the $(R_\delta, \hat{A})$ locus are presented in Figures 4.12 and 4.13.

It is seen that in the range of these Reynolds numbers and mass-transfer rates, at

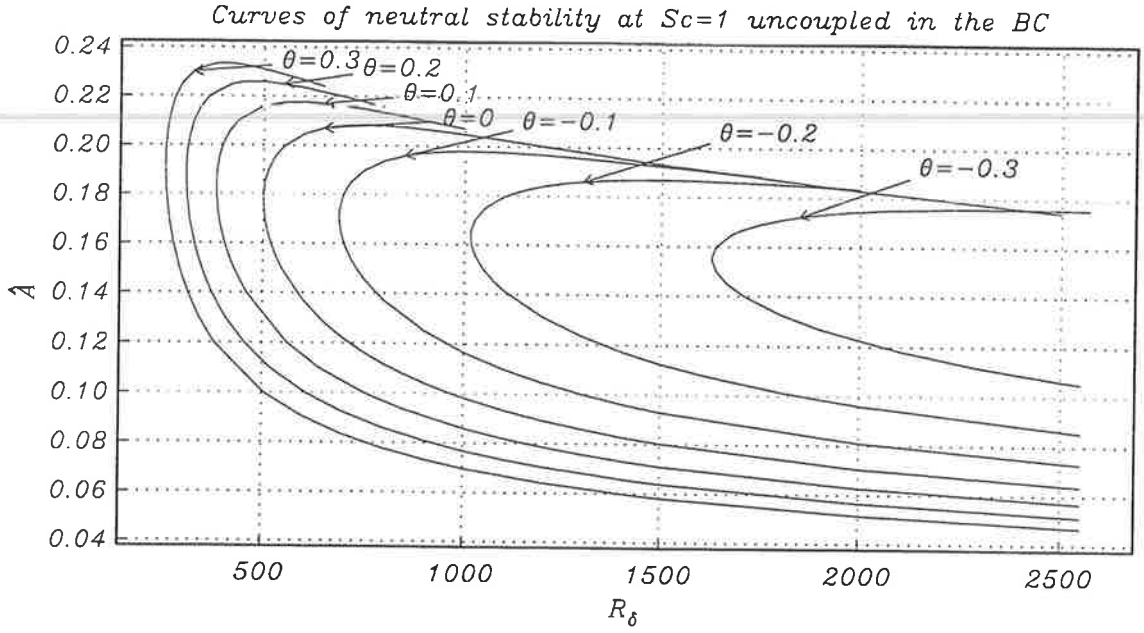

Figure 4.7: Curves of neutral stability in the $(R_\delta, \hat{A})$-plane at $Sc = 1$ for different values of θ.

high Schmidt numbers Sc, the coupling effect has a relatively minor role in the whole mechanism (Figures 4.9 and 4.10). This is a simple consequence of the factor Sc^{-1} appearing in the boundary condition which forces the vertical momentum transport. However, at low to "moderate" values of the Schmidt number, the effect of coupling is considerable and must be taken into account if a reasonable and accurate estimate of the critical parameter values is to be obtained.

In conclusion we have considered the problem of the instability of a boundary-layer flow over a permeable surface under conditions of interfacial mass transfer. The equations governing a small amplitude disturbance have been derived and numerical solutions to the fully coupled problem have been obtained. These improve upon the earlier results (see

$Sc = 1$					
θ	$R_\delta \times 10^3$	$\hat{A}$	$\hat{C}_r$	$\hat{A}_{max}$	$\hat{C}_{r\,max}$
-0.3	1.604998	0.15500	0.3295478	0.1763175	0.3312340
-0.2	1.007698	0.16500	0.3585616	0.1872046	0.3601031
-0.1	0.685857	0.17000	0.3820112	0.1981166	0.3850448
0.0	0.500000	0.17732	0.4028357	0.208317	0.4061027
0.1	0.385065	0.18300	0.4201429	0.2175227	0.4240635
0.2	0.309554	0.19000	0.4356791	0.2256855	0.4391204
0.3	0.257094	0.19000	0.4466740	0.2330865	0.4521988

Table 4.2: Values of the critical Reynolds number R_δ, corresponding wave-speed $\hat{C}_r$, wave number $\hat{A}$ and $\hat{A}_{max}$ and $\hat{C}_{r\,max}$ at $Sc = 1$.

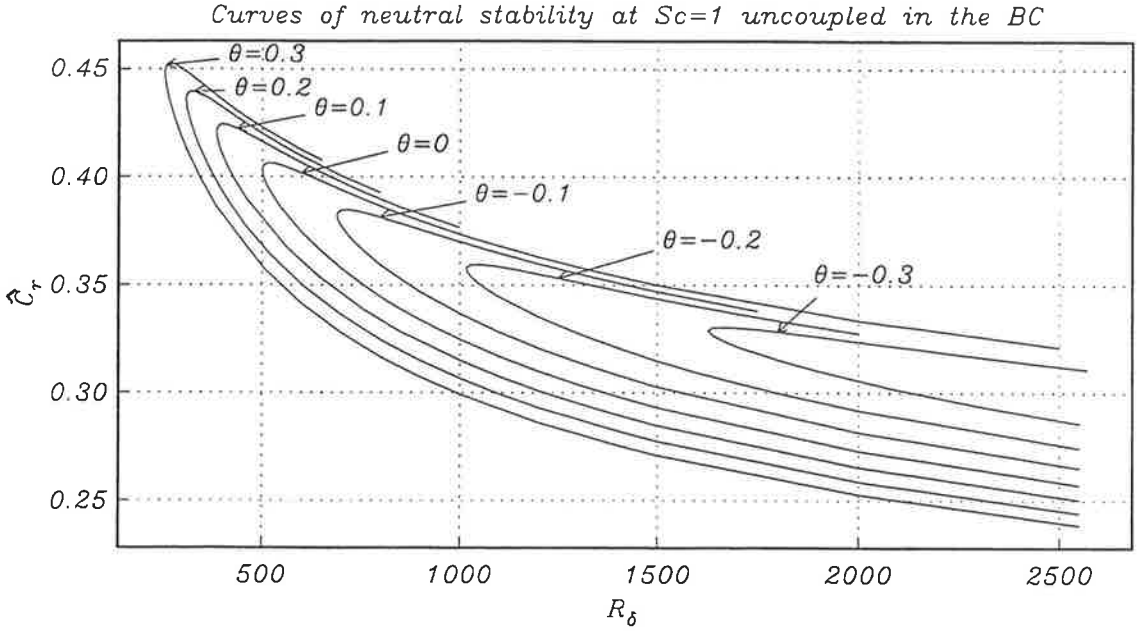

Figure 4.8: Curves of neutral stability in the $(R_\delta, \hat{C}_r)$-plane at $Sc = 1$ for different values of θ.

Chapter 2) of Boyadjiev *et. al.* (1996a) to consistently account for the effect of coupling between the momentum and concentration fields.

In this chapter the parallel-flow approximation has been used in order to reduce the partial differential equations describing an infinitesimally small disturbance of a basic non-parallel motion to a more analysable ordinary differential equation. The fully coupled problem was studied leading to a system consisting of an Orr-Sommerfeld type of equation and a concentration equation for the disturbance amplitudes. The results were restricted to relatively small Reynolds numbers; the focus being on the determination of the critical Reynolds number for different values of the mass-transfer parameter θ and Schmidt number Sc. A number of studies (see Jordinson (1970), Gaster (1974)) show

$Sc = 50$					
θ	$R_\delta \times 10^3$	$\hat{A}$	$\hat{C}_r$	$\hat{A}_{max}$	$\hat{C}_{r\,max}$
-0.3	0.5419671	0.17620	0.3977870	0.2056077	0.4007827
-0.2	0.5256418	0.17520	0.3991445	0.2066190	0.4028352
-0.1	0.5117888	0.17632	0.4011101	0.2075208	0.4045790
0.0	0.5000000	0.17732	0.4028357	0.208317	0.4061027
0.1	0.4899471	0.17932	0.4047787	0.2089932	0.4075515
0.2	0.4809837	0.17972	0.4059957	0.2095971	0.4088320
0.3	0.4731381	0.18072	0.4073290	0.2102122	0.4099835

Table 4.3: Values of the critical Reynolds number R_δ, corresponding wave-speed $\hat{C}_r$, wave number $\hat{A}$ and $\hat{A}_{max}$ and $\hat{C}_{r\,max}$ at $Sc = 50$.

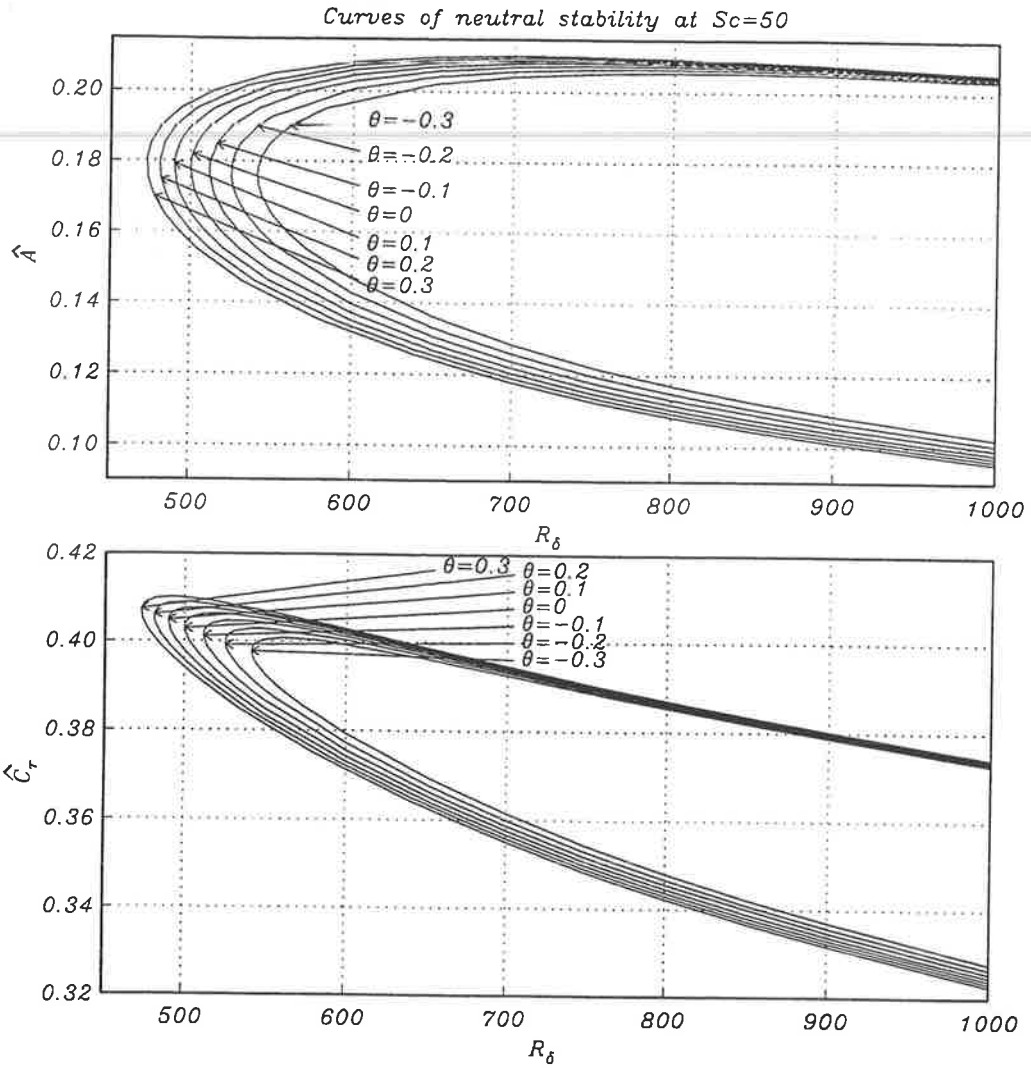

Figure 4.9: Curves of neutral stability at $Sc = 50$ for different values of θ.

the relevance of the parallel-flow approach in comparison with experiments. However, some discrepancies still remain between the Orr-Sommerfeld theoretical predictions and experimental results. The agreement between theory and experiment can be improved by considering the non-parallel flow effects. In the next chapter we shall consider the natural asymptotic limit of large Reynolds number $Re \gg 1$. It is the largeness of the Reynolds number that under-pins the boundary-layer assumption (see Smith (1979a)). Under this assumption the linearised disturbance equations are governed by the standard triple-deck structure of Smith (1979a). By solving a series of equations in each layer of the triple-deck, the eigenrelations, which determine the stability of the flow (or the position of neutral stability), will be derived.

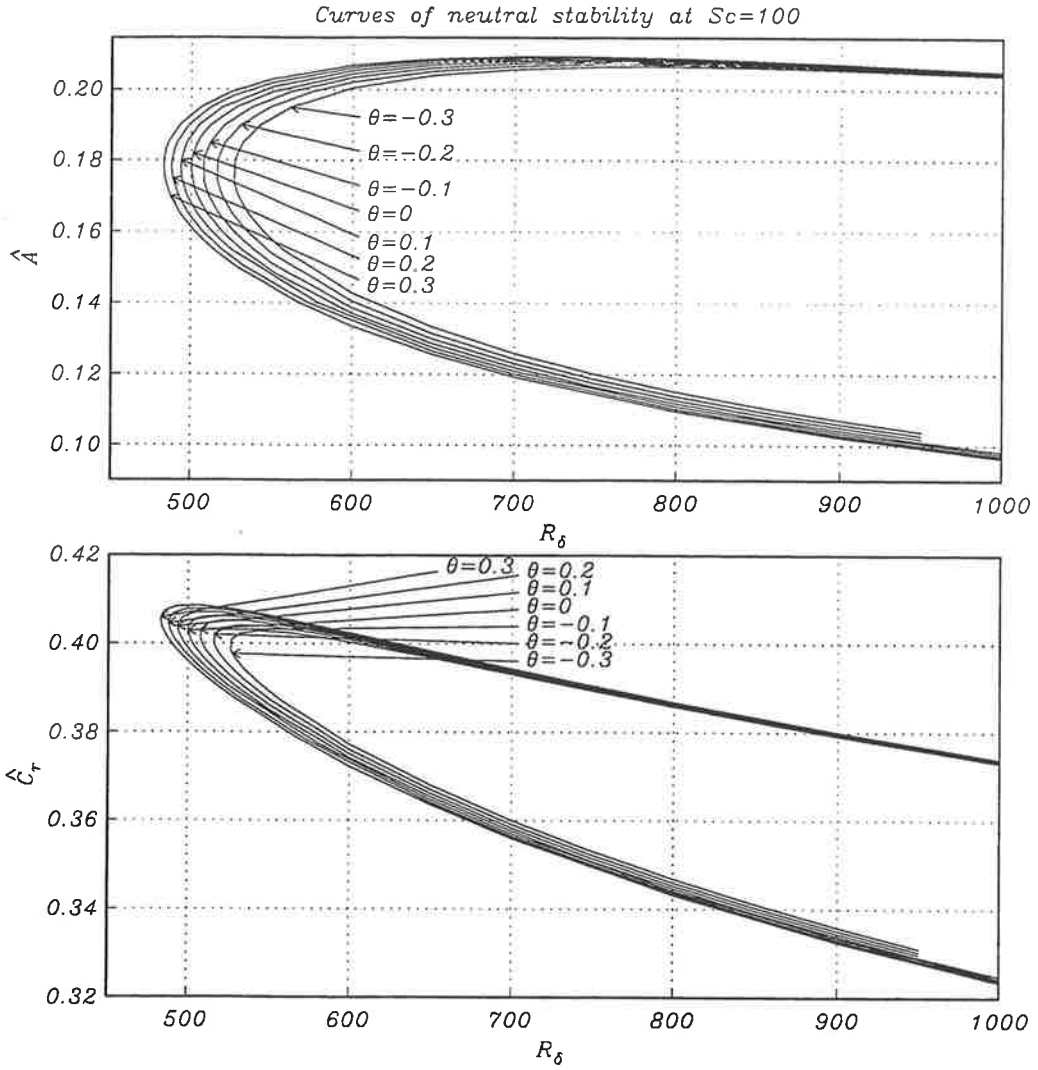

Figure 4.10: Curves of neutral stability at $Sc = 100$ for different values of θ.

$Sc = 100$					
θ	$R_\delta \times 10^3$	$\hat{A}$	$\hat{C}_r$	$\hat{A}_{max}$	$\hat{C}_{r\,max}$
-0.3	0.5264242	0.17400	0.3985858	0.2065904	0.4027809
-0.2	0.5161596	0.17500	0.4001046	0.2072468	0.4040509
-0.1	0.5078787	0.18000	0.4029710	0.2078189	0.4051436
0.0	0.5000000	0.17732	0.4028357	0.208317	0.4061027
0.1	0.4935537	0.17800	0.4038453	0.2087288	0.4070192
0.2	0.4878432	0.17800	0.4045131	0.2091419	0.4078304
0.3	0.4827328	0.17900	0.4055078	0.2094927	0.4085544

Table 4.4: Values of the critical Reynolds number R_δ, corresponding wave-speed $\hat{C}_r$, wave number $\hat{A}$ and $\hat{A}_{max}$ and $\hat{C}_{r\,max}$ at $Sc = 100$.

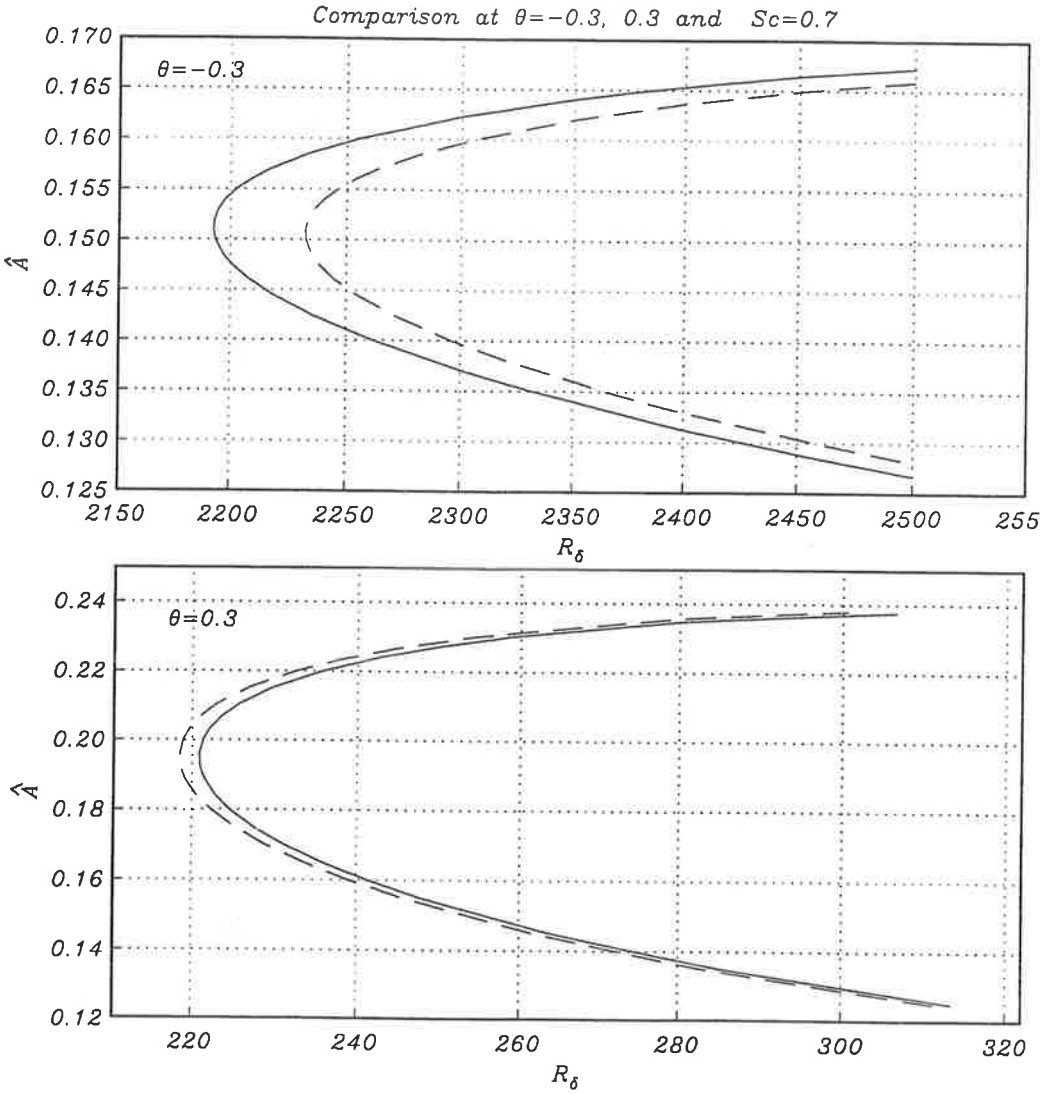

Figure 4.11: Comparison between the present results and those of Boyadjiev *et. al.* (1996a) (dashed curve).

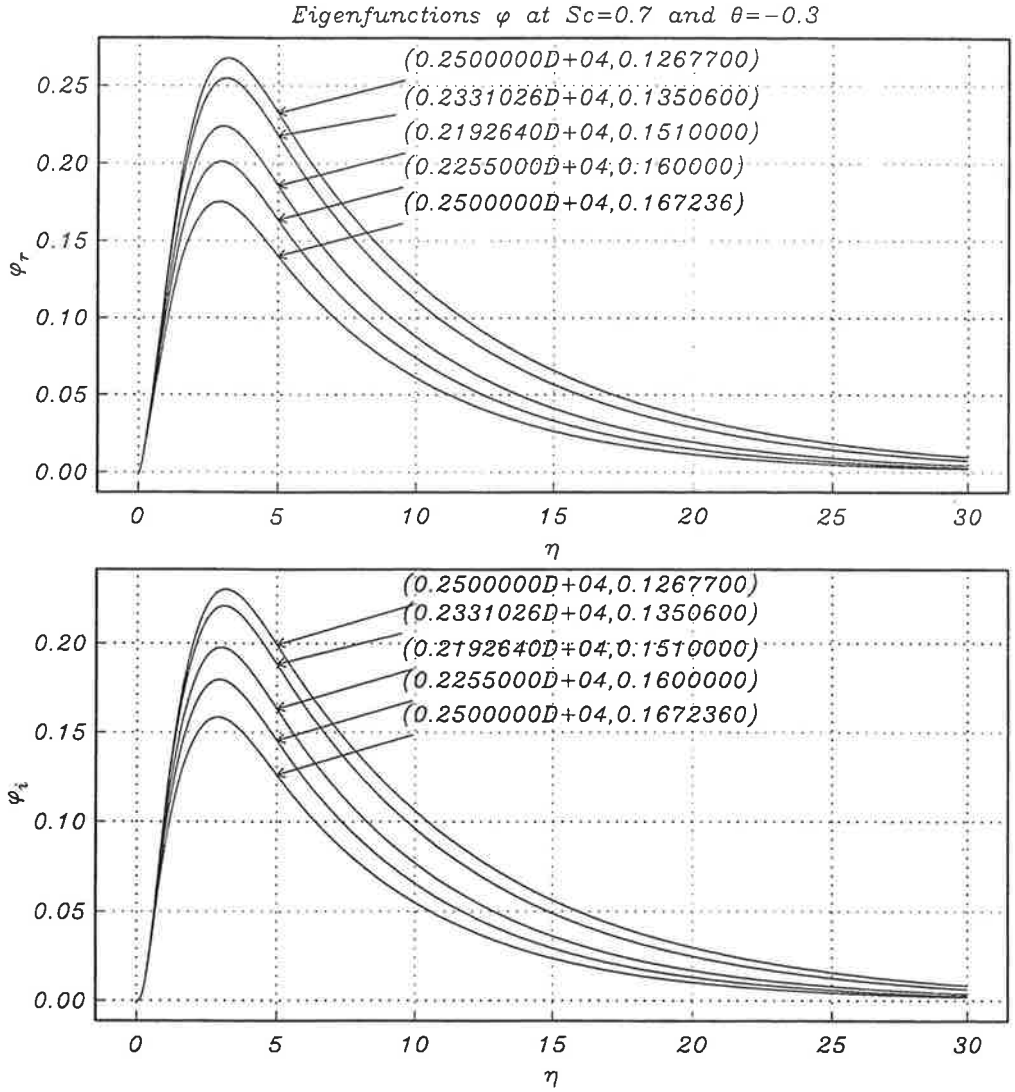

Figure 4.12: Eigenfunctions φ at $Sc = 0.7$ and $\theta = -0.3$ for certain values of $(R_\delta, \hat{\alpha})$ from the curve of neutral stability on the $(R_\delta, \hat{A})$ locus.

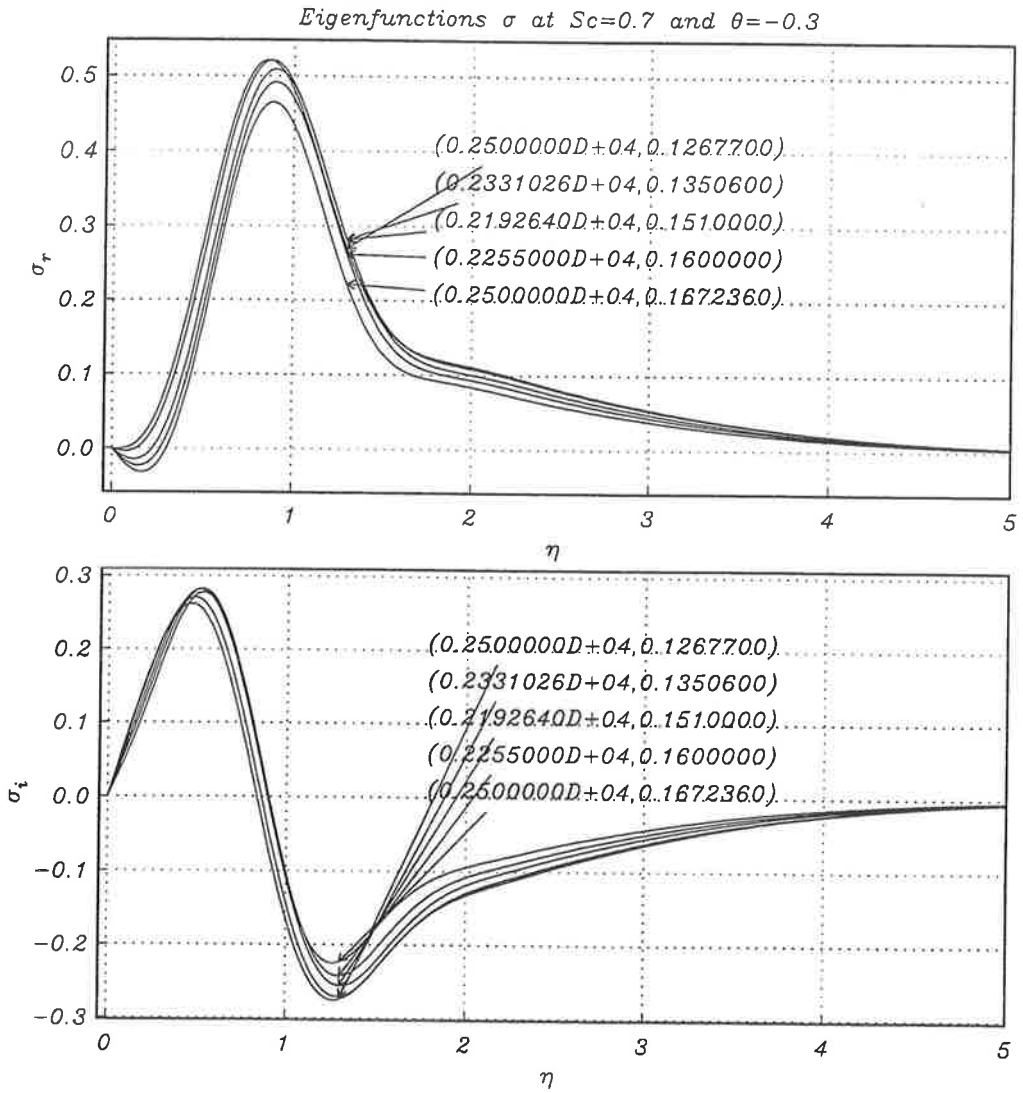

Figure 4.13: Eigenfunctions σ at $Sc = 0.7$ and $\theta = -0.3$ for certain values of $(R_\delta, \hat{\alpha})$ from the curve of neutral stability on the $(R_\delta, \hat{A})$ locus.

Chapter 5

Linear Lower-branch Stability of Blasius Boundary-Layer Flow under Conditions of Interfacial Mass Transfer - Asymptotic Approach

In this chapter we study the lower-branch of the curve of neutral stability (see Smith (1979a)) for a boundary-layer flow over a semi-infinite, permeable, flat plate under conditions of interfacial mass transfer.

The asymptotic structure of non-linear disturbances in a momentum boundary layer has been described by Smith (1979a); this structure has a three-tiered form, commonly referred as the triple-deck, in which the fluid adjusts from a thin layer (the "lower-deck") at the boundary, where viscous forces dominate, to a thick outer layer (the "upper-deck") where inertia dominates. In the presence of interfacial mass transfer, the momentum and concentration fields will be coupled in the lower deck, which suggests a fully numerical approach will be required to determine the non-linear response of the boundary layer. In this chapter these equations will be linearised and the asymptotic form of the lower-branch of the curve of neutral stability will be derived, at different values of the mass-transfer parameter θ and Schmidt number Sc (the parameter which provides a measure of the relative importance of diffusion as compared to viscosity).

5.1 Basic Blasius boundary-layer flow and concentration

Let us consider the flow conditions sketched in Figure 5.1. A fluid moving with velocity $\boldsymbol{u} = (U_\infty, 0)$ in the free-stream flows over a semi-infinite permeable flat plate. The fluid contains a species whose concentration is $C_0^*(x)$ on the surface and $C_\infty^*(x)$ in the free-stream. The governing equations describing the two-dimensional, steady flow of an

incompressible fluid and the development of the concentration field are the Navier-Stokes equations and the convection diffusion equation (2.1) with initial and boundary conditions (2.2).

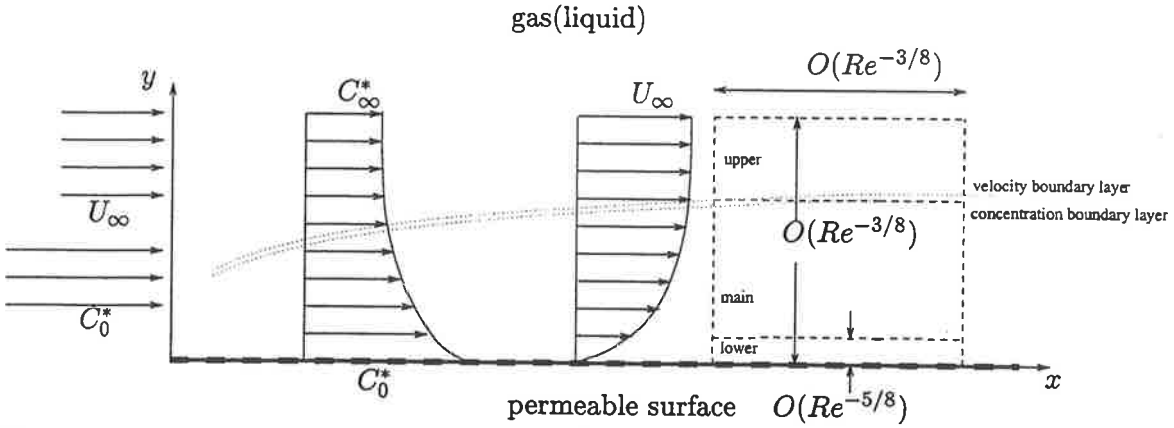

Figure 5.1: A schematic of the boundary-layer flow over a permeable surface when the velocity and the concentration boundary layers are commensurable.

The non-dimensionalisation of the above system of equations and boundary conditions has been done using (2.3). After applying the standard approach used in Chapter 4, the basic Blasius boundary-layer flow and concentration field are governed by the system of equations and boundary conditions (4.4) - (4.5).

The problem (4.4) - (4.5) has been solved numerically as in Chapter 4, using a fourth-order Runge-Kutta quadrature routine coupled with a Newton-Raphson iteration procedure. The skin friction $f''(0)$ and concentration gradient at the wall $g'(0)$ at different values of the mass-transfer parameter θ and Schmidt number Sc are shown in Figures 5.2 and 5.3 and 5.3, and tabulated in Tables 5.1 - 5.5. The calculations have been carried out for different values of the mass-transfer parameter θ within the interval $[-1, 1]$ and different values of the Schmidt number, $Sc = 0.01,\ 0.2,\ 0.5,\ 0.7$, and 1 in the case of gas flows, and $Sc = 2,\ 25,\ 50$, and 100 - liquid flows. It is clearly seen from Figures 5.2 and 5.3 that the skin friction $f''(0)$ depends on θ and Sc. At lower values of the Schmidt number (note $Sc = \nu/D$), corresponding to a thicker concentration boundary layer, one can expect rapid momentum boundary-layer thickening even at moderately low values of the mass-transfer parameter θ (the case of gas flows). As the concentration boundary-layer thickness decreases, for increasingly higher values of Schmidt number, the effect of the secondary flux through the interface (the "suction" or "blowing") becomes less significant and the diffusion will not have an impact on the boundary-layer growth as evidenced by the plots of skin friction $f''(0)$ in Figure 5.3. It is evident that the Blasius boundary-layer flow will separate in the case of lower Sc, while in the case of liquids the boundary-layer growth is similar to the classical Blasius one ($\approx x^{1/2}$) even at high values of the mass-transfer rate θ. The concentration gradient through the interface $g'(0)$ depends on θ and Sc as well. The figures show that the absolute value of the concentration gradient

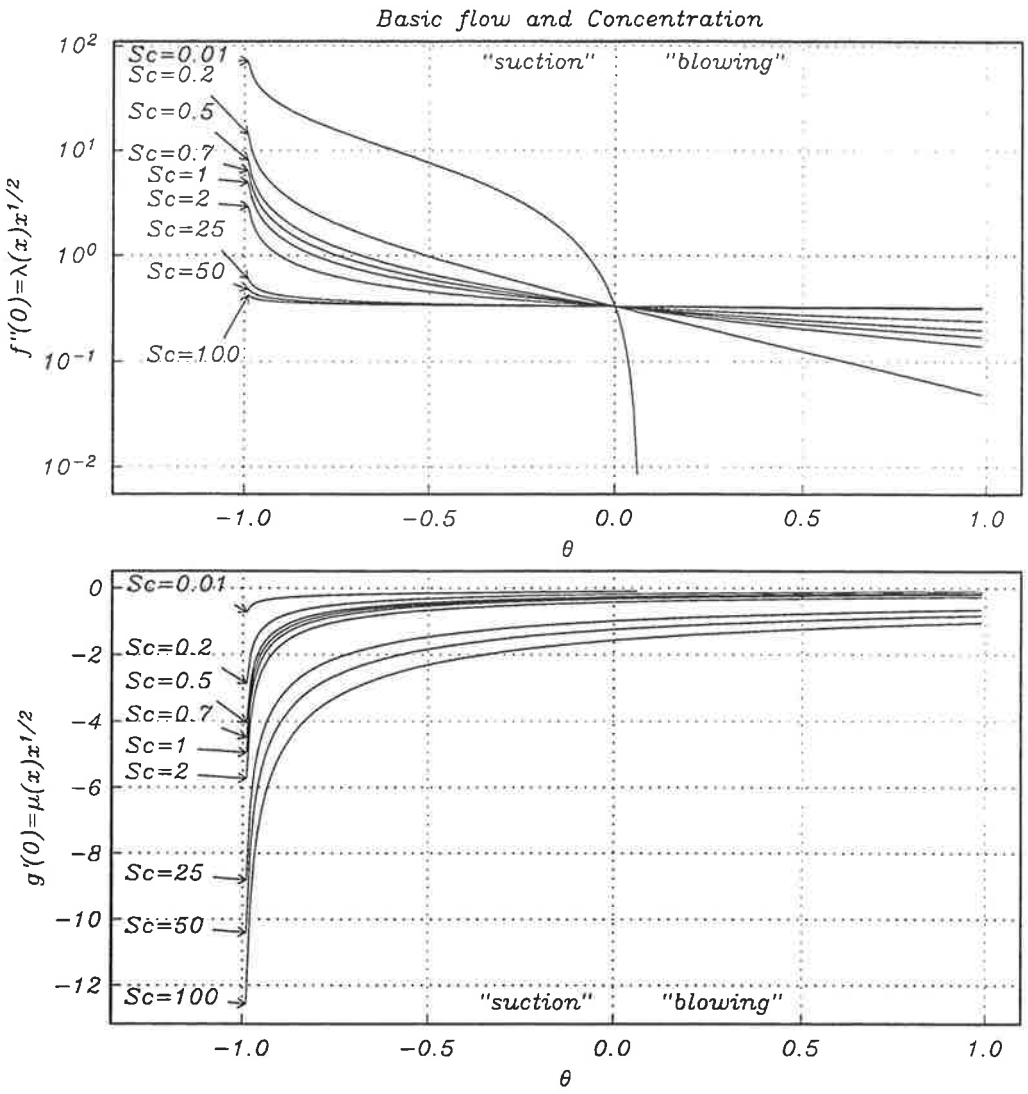

Figure 5.2: Graphs of $f''(0)$ and $g'(0)$ versus θ for different values of Sc.

increases when Schmidt number increases and this increase in the regime of "suction" is much more pronounced than in the regime of "blowing". At fixed values of the mass-transfer parameter θ the concentration gradient decreases with a decrease in Schmidt number Sc, nevertheless its impact on the boundary-layer growth is significant due to the greater thickness of the concentration boundary layer and its interaction with the hydrodynamic boundary layer.

5.2 Asymptotic expansions within the triple-deck structure and linear stability analysis

The influence of the intense interfacial mass transfer on the hydrodynamic stability of the boundary-layer flow will be investigated by applying linear stability theory. In the

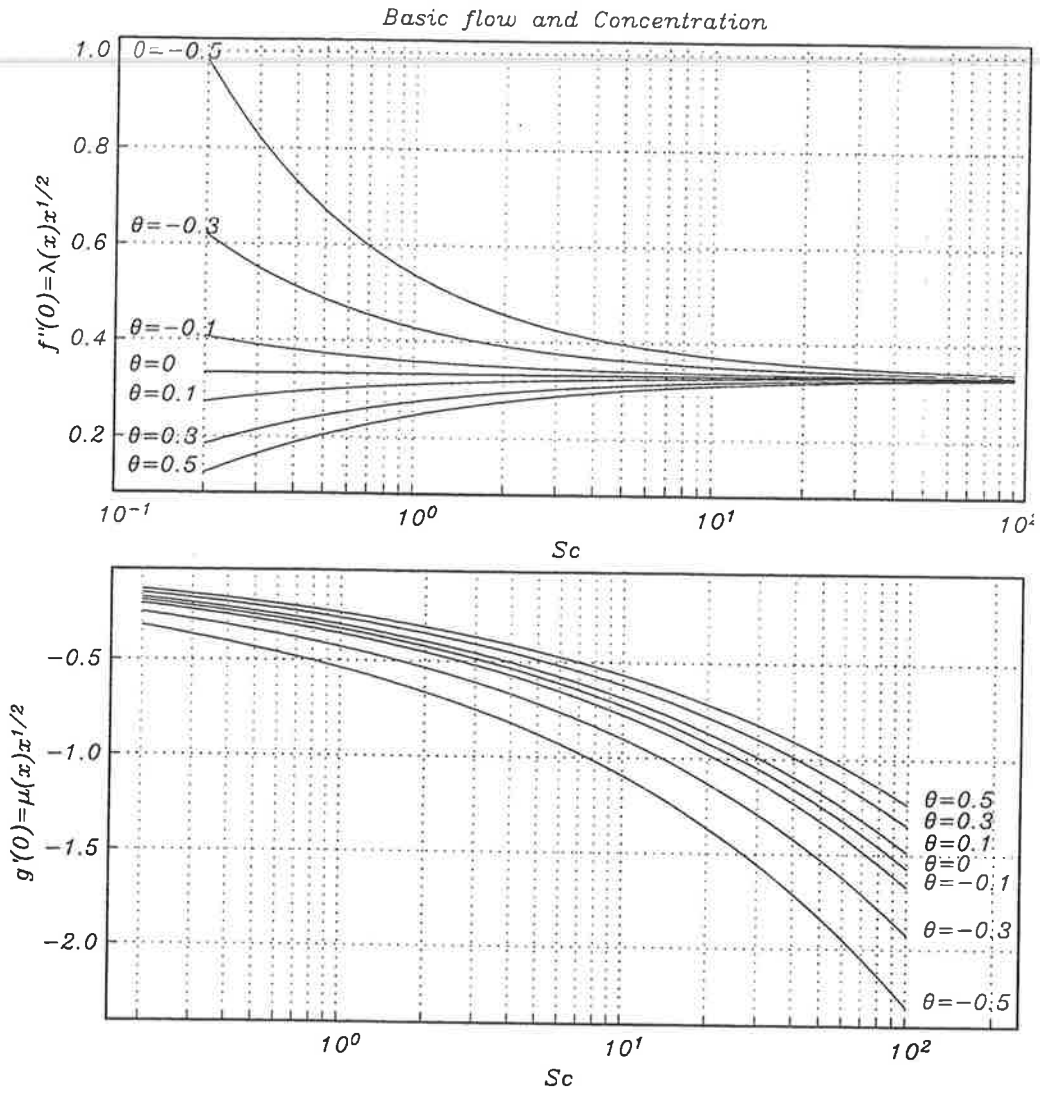

Figure 5.3: Graphs of $f''(0)$ and $g'(0)$ versus Sc for different values of θ.

work presented in Part I the flow was assumed to be parallel (but with the effect of the underlying boundary-layer growth accounted for via a parametric dependency on the streamwise variable) and the stability properties governed by the solution of an Orr-Sommerfeld type eigenvalue problem. In this linear approximation the influence of the concentration disturbances on the velocity disturbances, and vise versa, was neglected. These results were also limited to, large, but finite values of the Reynolds number. In practice however the Reynolds numbers encountered in such flows are significantly larger than can readily be dealt with by employing a numerical solution of the Orr-Sommerfeld equation. In the limit of large Reynolds numbers a self-consistent asymptotic solution of the governing equations is possible without recourse to any of the *ad hoc* assumptions employed in the Orr-Sommerfeld approach. Here, in considering the natural asymptotic limit of large Reynolds number $Re \gg 1$, the disturbances equation will be coupled in the

boundary conditions on the interface.

The governing equations for two-dimensional disturbances follow from the Navier-Stokes equations and the convection-diffusion equation by linearisation about the basic steady flow $\boldsymbol{u} = (U_0(x,y), V_0(x,y))$ and concentration $C_0(x,y)$, where $\boldsymbol{u}$ is the velocity vector in Cartesian coordinates x, y. This yields the system of equations (4.7), which for completeness we reproduce here

$$\begin{aligned} u_x + v_y &= 0, \\ u_t + U_0 u_x + u U_{0x} + v U_{0y} + V_0 u_y &= -p_x + Re^{-1}\left(u_{xx} + u_{yy}\right), \\ v_t + U_0 v_x + u V_{0x} + V_0 v_y + v V_{0y} &= -p_y + Re^{-1}\left(v_{xx} + v_{yy}\right), \\ c_t + U_0 c_x + u C_{0x} + V_0 c_y + v C_{0y} &= Re^{-1} Sc^{-1}\left(c_{xx} + c_{yy}\right). \end{aligned} \tag{5.1}$$

Equations (5.1) define a problem similar to that studied by Smith (1979a) but with the addition of a convection-diffusion equation coupled to the momentum field in the boundary condition for the vertical component of the disturbance velocity at the surface ($y = 0$). We shall focus on the lower-branch modes of instability since, in practice they are the first to become unstable.

5.3 The triple-deck

When $Re \gg 1$ the velocity (u, v) and the concentration disturbances fields c and the pressure p are governed by a triple-deck structure (see Figure 5.1) on the streamwise length scale $O(\epsilon^3)$, where $\epsilon = Re^{-1/8} \ll 1$. This follows from the fact that the typical wavelength of neutrally stable lower-branch modes are proportional to $Re^{-3/8}$ as $Re \to \infty$.

The stability of the basic flow will be examined by setting $x = \epsilon^3 X$ and considering fixed frequency disturbances proportional to

$$E = \exp\left[i\left(\hat{\theta}(X) - \beta\tau\right)\right], \tag{5.2}$$

where

$$\beta = \beta_1 + \epsilon\beta_2 + \epsilon^2\beta_3 + \epsilon^3 \ln\epsilon\beta_{4L} + \epsilon^3\beta_4 + O\left(\epsilon^3\right) \tag{5.3}$$

is the frequency (a constant), $\hat{\theta}$ the wavenumber, which is a slowly varying function of x in the form

$$\mathrm{d}\hat{\theta}/\mathrm{d}X = K_1(x) + \epsilon K_2(x) + \epsilon^2 K_3(x) + \epsilon^3 \ln\epsilon K_{4L}(x) + \epsilon^3 K_4 + O\left(\epsilon^3\right), \tag{5.4}$$

and $\tau = \epsilon^{-2}t$ is a scaled time variable. In this multiple-scales approach (see Smith (1979a)) $\partial/\partial x$ is replaced by $\epsilon^{-3}\partial/\partial X + \partial/\partial x$. Our concern is with how the presence of the concentration equation in the full set of equations modifies the triple-deck structure and the corresponding eigenrelations.

Generally, we shall use the standard triple-deck scaling set down by Stewartson (1974). The triple-deck structure has length $O(\epsilon^3)$ in the x-direction. Normal to the plate the upper deck is of thickness $O(\epsilon^3)$ and is governed by the inviscid irrotational flow equations. The upper deck, which relates the induced pressure to the local displacement, provides a pressure gradient which helps drive the lower deck, the lower deck provides a change in the displacement thickness of the boundary layer. The main deck, with thickness $O(\epsilon^4)$ plays a relatively passive role in the mechanism, the equations are inviscid, but there are small pressure variations across the deck. The lower deck has thickness $O(\epsilon^5)$ and is located on the wall; it is controlled by the conventional boundary-layer equations but with new boundary conditions. The effect of the concentration gradient, and hence the intense interfacial mass transfer, is shown to be limited to the lower and the main decks.

The scalings above and expansions for disturbances in all three decks can be obtained by inspection through *a priori* estimates. They can also be obtained deductively in the style of Mauss (1994). A comprehensive review of the triple-deck theory and its broad range of applications can be found in Smith (1982).

5.3.1 The main deck.

The main deck is an inviscid middle layer where the oncoming flow undergoes a downward displacement. It is characterised by the predominant small effect of displacement. Here the scales are $y = \epsilon^4 Y$, $x = \epsilon^3 X$, $\tau = \epsilon^{-2} t$, where $Y = O(1)$, $X = O(1)$, $\tau = O(1)$. The disturbances expand in the following form:

$$\begin{aligned} u &= \left[u_1 + \epsilon u_2 + \epsilon^2 u_3 + \epsilon^3 \ln \epsilon u_{4L} + \epsilon^3 u_4 + o\left(\epsilon^3\right)\right] E, \\ v &= \left[\epsilon v_1 + \epsilon^2 v_2 + \epsilon^3 v_3 + \epsilon^4 \ln \epsilon v_{4L} + \epsilon^4 v_4 + o\left(\epsilon^4\right)\right] E, \\ p &= \left[\epsilon p_1 + \epsilon^2 p_2 + \epsilon^3 p_3 + \epsilon^4 \ln \epsilon p_{4L} + \epsilon^4 p_4 + o\left(\epsilon^4\right)\right] E, \\ c &= \left[c_1 + \epsilon c_2 + \epsilon^2 c_3 + \epsilon^3 \ln \epsilon c_{4L} + \epsilon^3 c_4 + o\left(\epsilon^3\right)\right] E, \end{aligned} \tag{5.5}$$

where $u_1, \ldots, v_1, \ldots, p_1, \ldots, c_1, \ldots$ are functions of the normal coordinate Y and the slow streamwise coordinate x. The basic Blasius flow and the basic concentration take the following form:

$$\begin{aligned} U_0 &= U_B(x, Y) + O\left(\epsilon^8 \ln \epsilon\right) \\ V_0 &= \epsilon^4 V_B(x, Y) + O\left(\epsilon^{12} \ln \epsilon\right) \\ C_0 &= C_B(x, Y) + O\left(\epsilon^8 \ln \epsilon\right), \end{aligned} \tag{5.6}$$

where U_B, V_B and C_B have been defined in (4.3) - (4.5).

In what follows we will require the limiting forms of U_B, V_B and C_B as $Y \to 0$ and

$Y \to \infty$. Expanding these in a Taylor series about $Y = 0$ we obtain from (4.4) - (4.5)

$$\begin{aligned}
U_B(x,Y) &\approx \lambda Y - \frac{1}{2}\theta Sc^{-1}\lambda\mu Y^2 + \frac{1}{6}\theta^2 Sc^{-2}\lambda\mu^2 Y^3 - \frac{1}{24}\theta^3 Sc^{-3}\lambda\mu^3 Y^4 \\
&\quad -\frac{1}{48}\lambda x^{-1} Y^4 + O(Y^5), \\
V_B(x,Y) &\approx \theta Sc^{-1}\mu - \frac{1}{2}\lambda_x Y^2 + \frac{1}{6}\theta Sc^{-1}(\lambda\mu)_x Y^3 - \frac{1}{24}\theta^2 Sc^{-2}(\lambda\mu^2)_x Y^4 \\
&\quad +\frac{1}{120}\theta^3 Sc^{-3}(\lambda\mu^3)_x Y^5 + \frac{1}{240}(\lambda^2 x^{-1})_x Y^5 + O(Y^6), \\
C_B(x,Y) &\approx 1 + \mu Y - \frac{1}{2}\theta\mu^2 Y^2 + \frac{1}{6}\theta^2\mu^3 Y^3 - \frac{1}{24}\theta^3\mu^4 Y^4 \\
&\quad -\frac{1}{48}Sc\lambda\mu x^{-1} Y^4 + O(Y^5),
\end{aligned} \tag{5.7}$$

as $Y \to 0$. In the limit $Y \to \infty$ we have

$$\begin{aligned}
U_B(x,Y) &\to 1, \\
V_B(x,Y) &\to \frac{k}{2\sqrt{x}}, \\
C_B(x,Y) &\to 0,
\end{aligned} \tag{5.8}$$

where k is defined in (4.13). In (5.7) $\lambda(x) = f''(0)x^{-1/2}$ is the skin friction and $\mu(x) = g'(0)x^{-1/2}$ is the first derivative of the concentration in the Blasius variables. As noted earlier the values of $f''(0)$ and $g'(0)$ are tabulated for different values of Sc and θ in Tables 5.1 - 5.5.

Substitution of (5.5) and (5.6) into (5.1), introducing the operators $\mathcal{M}_1$, $\mathcal{M}_2$ and $\mathcal{M}_3$ (see Smith (1979a)) defined as

$$\begin{aligned}
\mathcal{M}_1(u,v) &= iK_1 u + v_Y, \\
\mathcal{M}_2(u,v) &= U_B iK_1 u + vU_{BY}, \\
\mathcal{M}_3(c,v) &= U_B iK_1 c + vC_{BY},
\end{aligned}$$

and equating coefficients of powers of ϵ to zero gives the following system of equations for the main deck:
continuity:

$$\begin{aligned}
\mathcal{M}_1(u_1,v_1) &= 0 \\
\mathcal{M}_1(u_2,v_2) &= -iK_2 u_1, \\
\mathcal{M}_1(u_3,v_3) &= -i(K_2 u_2 + K_3 u_1), \\
\mathcal{M}_1(u_{4L},v_{4L}) &= -iK_{4L} u_1, \\
\mathcal{M}_1(u_4,v_4) &= -i(K_2 u_3 + K_3 u_2 + K_4 u_1) + u_{1x};
\end{aligned} \tag{5.9}$$

***x*-momentum**:

$$\begin{aligned}
\mathcal{M}_2(u_1,v_1) &= 0,\\
\mathcal{M}_2(u_2,v_2) &= i\beta_1 u_1 - U_B i K_2 u_1 - iK_1 p_1,\\
\mathcal{M}_2(u_3,v_3) &= i(\beta_1 u_2+\beta_2 u_1) - U_B i(K_2 u_2 + K_3 u_1) - i(K_1 p_2 + K_2 p_1),\\
\mathcal{M}_2(u_{4L},v_{4L}) &= -U_B i K_{4L} u_1,\\
\mathcal{M}_2(u_4,v_4) &= i(\beta_1 u_3+\beta_2 u_2+\beta_3 u_1) - U_B i(K_2 u_3 + K_3 u_2 + K_4 u_1)\\
&\quad -(U_B u_1)_x - V_B u_{1Y} - i(K_1 p_3 + K_2 p_2 + K_3 p_1) + u_{1YY};
\end{aligned} \tag{5.10}$$

***y*-momentum**:

$$\begin{aligned}
0 &= -p_{1Y},\\
U_B i K_1 v_1 &= -p_{2Y},\\
U_B i(K_2 v_1 + K_1 v_2) &= i\beta_1 v_1 - p_{3Y},\\
0 &= -p_{4LY},\\
U_B i(K_3 v_1 + K_2 v_2 + K_1 v_3) &= i(\beta_1 v_2 + \beta_2 v_1) - p_{4Y};
\end{aligned} \tag{5.11}$$

and
concentration:

$$\begin{aligned}
\mathcal{M}_3(c_1,v_1) &= 0,\\
\mathcal{M}_3(c_2,v_2) &= i\beta_1 c_1 - U_B i K_2 c_1,\\
\mathcal{M}_3(c_3,v_3) &= i(\beta_1 c_2+\beta_2 c_1) - U_B i(K_2 c_2 + K_3 c_1),\\
\mathcal{M}_3(c_{4L},v_{4L}) &= -U_B i K_{4L} c_1,\\
\mathcal{M}_3(c_4,v_4) &= i(\beta_1 c_3+\beta_2 c_2+\beta_3 c_1) - U_B i(K_2 c_3 + K_3 c_2 + K_4 c_1)\\
&\quad -U_B c_{1x} - u_1 C_{Bx} - V_B c_{1Y} + Sc^{-1} c_{1YY}.
\end{aligned} \tag{5.12}$$

The boundary conditions to be imposed on the system of equations (5.9) - (5.12) are matching with the lower deck solutions as $Y \to 0$ and with the upper deck solutions as $Y \to \infty$.

5.3.2 The lower deck.

The lower deck, which together with the main deck comprises the boundary layer, is an inner viscous region driven by the induced pressure force. Hence, the scaling within the lower deck is as follows: $y = \epsilon^5 Z$, $x = \epsilon^3 X$, $\tau = \epsilon^{-2} t$, where $Z = O(1)$, $X = O(1)$, $\tau = O(1)$. The expansions of the disturbances, which come from the asymptotic form of the main deck solutions as $Y \to 0$, have the following form:

$$\begin{aligned}
u &= \left[U_1 + \epsilon U_2 + \epsilon^2 U_3 + \epsilon^3 \ln\epsilon U_{4L} + \epsilon^3 U_4 + o\left(\epsilon^3\right)\right] E,\\
v &= \left[\epsilon^2 V_1 + \epsilon^3 V_2 + \epsilon^4 V_3 + \epsilon^5 \ln\epsilon V_{4L} + \epsilon^5 V_4 + o\left(\epsilon^5\right)\right] E,\\
p &= \left[\epsilon P_1 + \epsilon^2 P_2 + \epsilon^3 P_3 + \epsilon^4 \ln\epsilon P_{4L} + \epsilon^4 P_4 + o\left(\epsilon^4\right)\right] E,\\
c &= \left[C_1 + \epsilon C_2 + \epsilon^2 C_3 + \epsilon^3 \ln\epsilon C_{4L} + \epsilon^3 C_4 + o\left(\epsilon^3\right)\right] E,
\end{aligned} \tag{5.13}$$

where $U_1, \ldots, V_1, \ldots, C_1, \ldots$ are dependent on Z and x, but $P_1, \ldots$ are functions only of x. The basic flow and the basic concentration here can be determined in the same fashion as for the main deck, they have the following forms:

$$\begin{aligned}
U_0(x,Z) &\approx \epsilon\lambda Z - \frac{1}{2}\epsilon^2\theta Sc^{-1}\lambda\mu Z^2 + \frac{1}{6}\epsilon^3\theta^2 Sc^{-2}\lambda\mu^2 Z^3 - \frac{1}{24}\epsilon^4\theta^3 Sc^{-3}\lambda\mu^3 Z^4 \\
&\quad -\frac{1}{48}\epsilon^4\lambda x^{-1} Z^4 + O(Z^5), \\
V_0(x,Z) &\approx \epsilon^4\theta Sc^{-1}\mu - \frac{1}{2}\epsilon^6\lambda_x Z^2 + \frac{1}{6}\epsilon^7\theta Sc^{-1}(\lambda\mu)_x Z^3 - \frac{1}{24}\epsilon^8\theta^2 Sc^{-2}(\lambda\mu^2)_x Z^4 \\
&\quad +\frac{1}{120}\epsilon^9\theta^3 Sc^{-3}(\lambda\mu^3)_x Z^5 + \frac{1}{240}\epsilon^9(\lambda^2 x^{-1})_x Z^5 + O(Z^6), \qquad (5.14) \\
C_0(x,Z) &\approx 1 + \epsilon\mu Z - \frac{1}{2}\epsilon^2\theta\mu^2 Z^2 + \frac{1}{6}\epsilon^3\theta^2\mu^3 Z^3 - \frac{1}{24}\epsilon^4\theta^3\mu^4 Z^4 \\
&\quad -\frac{1}{48}\epsilon^4 Sc\lambda\mu x^{-1} Z^4 + O(Z^5),
\end{aligned}$$

as $Z \to 0$. In an analogous way to the previous section we introduce the operators $\mathcal{L}_1$, $\mathcal{L}_2$ and $\mathcal{L}_3$, defined by

$$\begin{aligned}
\mathcal{L}_1(u,v) &= iK_1 u + v_Z, \\
\mathcal{L}_2(u,v,p) &= i(\lambda Z K_1 - \beta_1)u + \lambda v + iK_1 p - u_{ZZ}, \\
\mathcal{L}_3(c,v) &= i(\lambda Z K_1 - \beta_1)c + \mu v - Sc^{-1} c_{ZZ}.
\end{aligned}$$

Then substituting (5.13) and (5.14) into (5.1) we obtain the equations for the structure of the disturbance in the lower deck:
continuity:

$$\begin{aligned}
\mathcal{L}_1(U_1,V_1) &= 0, \\
\mathcal{L}_1(U_2,V_2) &= -iK_2 U_1, \\
\mathcal{L}_1(U_3,V_3) &= -i(K_2 U_2 + K_3 U_1), \qquad (5.15) \\
\mathcal{L}_1(U_{4L},V_{4L}) &= -iK_{4L} U_1, \\
\mathcal{L}_1(U_4,V_4) &= -i(K_2 U_3 + K_3 U_2 + K_4 U_1) + U_{1x};
\end{aligned}$$

***x*-momentum**:

$$
\begin{aligned}
\mathcal{L}_2(U_1,V_1,P_1) &= 0,\\
\mathcal{L}_2(U_2,V_2,P_2) &= i\beta_2U_1-\lambda ZiK_2U_1-iK_2P_1+\theta Sc^{-1}\lambda\mu Z\left(\frac{1}{2}ZiK_1U_1+V_1\right)\\
&\quad -\theta Sc^{-1}\mu U_{1Z},\\
\mathcal{L}_2(U_3,V_3,P_3) &= i(\beta_2U_2+\beta_3U_1)-\lambda Zi(K_2U_2+K_3U_1)-i(K_2P_2+K_3P_1)\\
&\quad +\frac{1}{2}\theta Sc^{-1}\lambda\mu Z^2i(K_1U_2+K_2U_1)-\frac{1}{2}\theta^2Sc^{-2}\lambda\mu^2Z^2\Big(\frac{1}{3}ZiK_1U_1\\
&\quad +V_1\Big)-\theta Sc^{-1}\mu U_{2Z}+\theta Sc^{-1}\lambda\mu ZV_2,\\
\mathcal{L}_2(U_{4L},V_{4L}) &= i\beta_{4L}U_1-\lambda ZiK_{4L}U_1-iK_{4L}P_1,\\
\mathcal{L}_2(U_4,V_4,P_4) &= i(\beta_2U_3+\beta_3U_2+\beta_4U_1)-\lambda Zi(K_2U_3+K_3U_2+K_4U_1)\\
&\quad -i(K_2P_3+K_3P_2+K_4P_1)+\frac{1}{2}\theta Sc^{-1}\lambda\mu Z^2\big(K_1U_3+K_2U_2\\
&\quad +K_3U_1\big)-\frac{1}{6}\theta^2Sc^{-2}\lambda\mu^2Z^3i(K_1U_2+K_2U_1)+\frac{1}{48}\lambda x^{-1}Z^4iK_1U_1\\
&\quad +\frac{1}{24}\theta^3Sc^{-3}\lambda\mu^3Z^4iK_1U_1-Z(\lambda U_1)_x-P_{1x}+\frac{1}{6}\theta^3Sc^{-3}\lambda\mu^3Z^3V_1\\
&\quad +\frac{1}{12}\lambda x^{-1}Z^3V_1-\frac{1}{2}\theta^2Sc^{-2}\lambda\mu^2Z^2V_2+\theta Sc^{-1}\lambda\mu ZV_3\\
&\quad +\frac{1}{2}\lambda_xZ^2U_{1Z}-\theta Sc^{-1}\mu U_{3Z};
\end{aligned}
\tag{5.16}
$$

and

concentration:

$$
\begin{aligned}
\mathcal{L}_3(C_1,V_1) &= 0,\\
\mathcal{L}_3(C_2,V_2) &= i\beta_2C_1-\lambda ZiK_2C_1+\frac{1}{2}\theta Sc^{-1}\lambda\mu Z^2iK_1C_1-\theta Sc^{-1}\mu C_{1Z}+\theta\mu^2ZV_1,\\
\mathcal{L}_3(C_3,V_3) &= i(\beta_2C_2+\beta_3C_1)-\lambda Zi(K_2C_2+K_3C_1)+\frac{1}{2}\theta Sc^{-1}\lambda\mu Z^2i\big(K_1C_2\\
&\quad +K_2C_1\big)-\frac{1}{6}\theta^2Sc^{-2}\lambda\mu^2Z^3iK_1C_1-\theta Sc^{-1}\mu C_{2Z}-\frac{1}{2}\theta^2\mu^3Z^2V_1\\
&\quad +\theta\mu^2ZV_2,\\
\mathcal{L}_3(C_{4L},V_{4L}) &= i\beta_{4L}C_1-\lambda ZiK_{4L}C_1,\\
\mathcal{L}_3(C_4,V_4) &= i(\beta_2C_3+\beta_3C_2+\beta_4C_1)-\lambda Zi(K_2C_3+K_3C_2+K_4C_1)\\
&\quad +\frac{1}{2}\theta Sc^{-1}\lambda\mu Z^2i(K_1C_3+K_2C_2+K_3C_1)+\frac{1}{12}Sc\lambda\mu x^{-1}Z^4iK_1C_1\\
&\quad -\frac{1}{6}\theta^2Sc^{-2}\lambda\mu^2Z^3i(K_1C_2+K_2C_1)+\frac{1}{24}\theta^3Sc^{-3}\lambda\mu^2Z^4iK_1C_1\\
&\quad -Z\lambda C_{1x}-\mu_xZU_1+\frac{1}{2}\lambda_xZ^2C_{1Z}-\theta Sc^{-1}\mu C_{3Z}+\frac{1}{6}\theta^3\mu^4Z^3V_1\\
&\quad +\frac{1}{12}Sc\lambda\mu x^{-1}Z^3V_1-\frac{1}{2}\theta^2\mu^3Z^2V_2+\theta\mu^2ZV_3.
\end{aligned}
\tag{5.17}
$$

The appropriate set of boundary conditions for the above equations (5.15) - (5.17) are matching with the main deck solutions as $Z\to\infty$. In order to define the wall boundary

conditions special attention needs to be given to the effect of the concentration gradient, due to the mass transfer, on the lower deck. The development of the velocity boundary layer is generally characterised by the no-slip condition (the no-slip condition pertains to $u = 0$ on $Z = 0$, the mass transfer modifies $v = 0$, i.e. no normal flow) for the disturbance velocities as well as for the basic velocity along the surface. However, if there is simultaneous mass transfer to/or from the surface it is clear that the no normal flow condition does not pertain to the transversal components of the disturbance V_i $(i = 1, \dots)$ and basic flow velocity V_0 (4.5). They are no longer forced to be zero along the surface (as $Z \to 0$). Using the lower deck scaling and the boundary conditions (2.5) we obtain the following form of the boundary conditions for the disturbance equations in the lower deck:

$$u = 0, \; v = -\epsilon^3 b \left[\frac{\partial c}{\partial Z}\right]_{Z=0}, \; c = 0 \tag{5.18}$$

where we denote $b = \theta Sc^{-1}$ and in addition the boundary conditions (4.2) for the basic flow and concentration held.

A close examination of the equations, and the corresponding boundary conditions (5.18), within the lower deck of the triple-deck structure, demonstrates that the vertical momentum and concentration field are coupled, the magnitude of this coupling being dependent upon the magnitude of the concentration gradient across the permeable boundary. The triple-deck structure itself is not modified, however the first-order correction to the neutral position will be modified.

We shall see that at low levels of mass transfer (corresponding to a relatively small concentration gradient) and under the conditions of mass transfer with the rate of order unity the eigenrelation for lower-branch Tollmien-Schlichting waves is unaltered (at leading order). As the level of mass transfer is increased so the standard triple-deck structure must be modified. The disturbance velocity and concentration fields now becomes fully coupled and the resulting eigenvalue problem must be tackled numerically.

Our analysis of the expansions give us an estimate of the order of magnitude of the compound parameter b for which the problem can be treated as decoupled in the leading order lower deck equations, in this case, characterised by $b = \theta Sc^{-1} = O(1)$. The boundary conditions have the following form:

$$\begin{aligned} &U_i = 0, \quad (i = 1, \dots) \\ &V_1 = 0, \\ &V_{i+1} = -b \left[\frac{\partial C_i}{\partial Z}\right]_{Z=0}, \\ &V_{4L} = 0, \\ &C_i = 0, \end{aligned} \tag{5.19}$$

as $Z \to 0$. Note that the study presented here has been carried out for the case of gas–permeable surface systems with $Sc = 0.01$, 0.2, 0.5, 0.7 and 1, and liquid–permeable surface systems with $Sc = 2$, 25 and 100 and the mass-transfer parameter θ within the interval $[-0.9, 0.9]$.

5.3.3 The upper deck.

Finally, the third layer is necessary in the potential flow outside the boundary layer in order to relate the pressure induced by streamwise changes in the boundary layer to the local displacement (streamlines in the boundary layer have been displaced by an effective change in the position of the wall). In this layer the wave motion is described by classical inviscid irrotational theory. Given that the disturbance to the concentration field are small and the assumption that the effect of concentration is limited to the region in the vicinity of the wall, the scaling within the upper deck is: $y = \epsilon^3 \bar{y}$, $x = \epsilon^3 X$, $\tau = \epsilon^{-2} t$, where $\bar{y} = O(1)$, $X = O(1)$, $\tau = O(1)$. The main deck scaling suggests the following expansions of the disturbances:

$$\begin{aligned} u &= \left[\epsilon \bar{u}_1 + \epsilon^2 \bar{u}_2 + \epsilon^3 \bar{u}_3 + \epsilon^4 \ln \epsilon \bar{u}_{4L} + \epsilon^4 \bar{u}_4 + o\left(\epsilon^4\right)\right] E, \\ v &= \left[\epsilon \bar{v}_1 + \epsilon^2 \bar{v}_2 + \epsilon^3 \bar{v}_3 + \epsilon^4 \ln \epsilon \bar{v}_{4L} + \epsilon^4 \bar{v}_4 + o\left(\epsilon^4\right)\right] E, \\ p &= \left[\epsilon \bar{p}_1 + \epsilon^2 \bar{p}_2 + \epsilon^3 \bar{p}_3 + \epsilon^4 \ln \epsilon \bar{p}_{4L} + \epsilon^4 \bar{p}_4 + o\left(\epsilon^4\right)\right] E, \end{aligned} \tag{5.20}$$

where $\bar{u}_1, \ldots, \bar{v}_1, \ldots, \bar{p}_1, \ldots$ are functions of $\bar{y}$ and x. In the upper deck the basic flow approximates the uniform stream and has the following form:

$$U_0 = 1 + O\left(\epsilon^4\right), \quad V_0 = O\left(\epsilon^4\right). \tag{5.21}$$

We introduce the operator $\mathcal{D}$ defined by

$$\mathcal{D} = p_{\bar{y}\bar{y}} - K_1^2 p.$$

Substituting (5.20) and (5.21) into (5.1), equating like powers of ϵ and eliminating the velocity components we obtain

$$\begin{aligned} \mathcal{D}(\bar{p}_1) &= 0, \\ \mathcal{D}(\bar{p}_2) &= 2K_1 K_2 \bar{p}_1, \\ \mathcal{D}(\bar{p}_3) &= 2K_1(K_3 \bar{p}_1 + K_2 \bar{p}_2) + K_2^2 \bar{p}_1, \\ \mathcal{D}(\bar{p}_{4L}) &= 2K_1 K_{4L} \bar{p}_1, \\ \mathcal{D}(\bar{p}_4) &= 2K_1(K_4 \bar{p}_1 + K_3 \bar{p}_2 + K_2 \bar{p}_3) \\ &\quad + K_2^2 \bar{p}_2 - iK_1\left(2\bar{p}_{1x} + (K_{1x}/K_1)\bar{p}_1\right). \end{aligned} \tag{5.22}$$

The boundary conditions for equations (5.22) are those of matching with the main deck solutions as $\bar{y} \to 0$ (as $Y \to \infty$ there) and decay as $\bar{y} \to \infty$.

5.4 The disturbance equations solutions

We shall first derive the main deck solutions, which will enable us to match them with the lower deck and the upper deck solutions.

5.4.1 The main deck solutions

Having the controlling equations and the boundary conditions we can solve the main deck equations to give

$$u_1 = A_1 U_{BY}, \tag{5.23a}$$
$$v_1 = -iK_1 A_1 U_B, \tag{5.23b}$$
$$p_1 = P_1, \tag{5.23c}$$
$$c_1 = A_1 C_{BY}; \tag{5.23d}$$

$$\begin{aligned} u_2 &= (A_2 - K_2 K_1^{-1} A_1) U_{BY} - P_1 (U_{BY} H_2 + U_B^{-1}), && (5.24a)\\ v_2 &= iK_1 P_1 U_B H_2 + i\beta_1 A_1 - iK_1 A_2 U_B, && (5.24b)\\ p_2 &= P_2 - A_1 K_1^2 H_1, && (5.24c)\\ c_2 &= (A_2 - K_2 K_1^{-1} A_1 - P_1 H_2) C_{BY}; && (5.24d) \end{aligned}$$

$$\begin{aligned} u_3 &= \left(A_3 - K_2 K_1^{-1} A_2 + K_2^2 K_2^{-2} A_1\right) U_{BY} - P_2 (U_{BY} H_2 + U_B^{-1}) \\ &\quad + K_1^2 A_1 U_B^{-1} (U_{BY} H_5 + H_1) - K_3 K_1^{-1} A_1 U_{BY} \\ &\quad - \beta_1 A_1 (U_{BY} H_6 + U_B^{-1} U_{BY} H_2 + U_B^{-2}), && (5.25a)\\ v_3 &= i(K_2 P_1 + K_1 P_2) U_B H_2 - i A_1 K_1^3 H_5 + i\beta_1 P_1 U_B H_6 \\ &\quad + i\beta_1 (A_2 - K_2 K_1^{-1} A_1) + i\beta_2 A_1 - iK_1 A_3 U_B, && (5.25b)\\ p_3 &= P_3 - K_1^2 P_1 H_3 - K_1 (K_2 A_1 + K_1 A_2) H_1 + 2\beta_1 K_1 A_1 H_4, && (5.25c)\\ c_3 &= \left(A_3 - K_3 K_1^{-1} A_1 - P_2 H_2 - K_2 K_1^{-1} A_2 + K_2^2 K_1^{-2} A_1\right. \\ &\quad \left. + K_1^2 A_1 U_B^{-1} H_5 - \beta_1 A_1 U_B^{-1} H_2\right) C_{BY}; && (5.25d) \end{aligned}$$

$$\begin{aligned} u_{4L} &= \left(A_{4L} - \frac{K_{4L}}{K_1} A_1\right) U_{BY}, && (5.26a)\\ v_{4L} &= -iK_1 A_{4L} U_B, && (5.26b)\\ p_{4L} &= P_{4L}, && (5.26c)\\ c_{4L} &= \left(A_{4L} - \frac{K_{4L}}{K_1} A_1\right) C_{BY}; && (5.26d) \end{aligned}$$

$$
\begin{aligned}
u_4 &= \big(A_4 - K_2K_1^{-1}A_3 - K_3K_1^{-1}A_2 + K_2K_1^{-1}A_1 - K_4K_1^{-1}A_1 \\
&\quad -K_2^2K_1^{-2}A_1 + K_2^2K_1^{-2}A_2 + K_3K_2K_1^{-2}A_1\big)U_{BY} - P_3(U_{BY}H_2 + U_B^{-1}) \\
&\quad -K_1^{-1}(\beta_1P_2 + \beta_2P_1)(U_{BY}H_6 + U_B^{-1}H_2 + U_B^{-2}) \\
&\quad +\beta_1K_2K_1^{-1}A_1(U_{BY}H_6 + U_B^{-1}H_2 + U_B^{-2}) + K_1^2A_2(U_{BY}H_5 + H_1)U_B^{-1} \\
&\quad +K_1^3A_1(U_BU_{BY}H_7 + H_3)U_B^{-1} + K_2K_1A_1(U_{BY}H_5 + H_1)U_B^{-1} \\
&\quad +\beta_1K_1A_1(U_B^{-2}U_{BY}H_5 + U_B^{-2}H_1 - U_{BY}H_8 - 2U_B^{-1}H_4) \\
&\quad +\beta_1^2K_1^{-1}A_1(U_B^{-1}U_{BY}H_6 + U_B^{-2}U_{BY}H_2 + U_{BY}H_9 + U_B^{-3}) \\
&\quad +iK_1^{-1}A_{1x}U_{BY} \qquad (5.27a) \\
v_4 &= i(K_3P_1 + K_2P_2 + K_1P_3)U_BH_2 - i(2A_1K_2K_1^2 + K_1^3A_2)H_5 \\
&\quad +i(\beta_2P_1 + \beta_1P_2)U_BH_6 + i\beta_1(A_3 - K_2K_1^{-1}A_2 + K_2^2K_1^{-2}A_1 \\
&\quad -K_3K_1^{-1}A_1) + i\beta_2(A_2 - K_2K_1A_1) + i\beta_3A_1 - iK_1A_4U_B \\
&\quad +iK_1^3P_1U_BH_7 + i\beta_1K_1^2A_1U_BH_8 + i\beta_1^2K_1^{-1}P_1U_BH_9 - A_1U_{Bx}, \qquad (5.27b) \\
p_4 &= P_4 + (K_1^2P_2 + 2K_1K_2P_1)H_3 - K_1(K_1A_3 + K_2A_2 + K_3A_1)H_1 \\
&\quad +2(\beta_2K_1A_1 + \beta_1K_1A_2)H_4 - \beta_1^2A_1Y - K_1^4A_1H_{11} \\
&\quad +\beta_1K_1P_1(H_{12} - H_{10}), \qquad (5.27c) \\
c_4 &= -iK_1^{-1}U_B^{-1}\Big[i(c_1\beta_3 + c_2\beta_2 + c_3\beta_1) - i(K_4c_1 + K_3c_2 + K_2c_3)U_B \\
&\quad -u_1C_{Bx} - c_{1Y}V_B - v_4C_{BY} + Sc^{-1}c_{1YY}\Big]. \qquad (5.27d)
\end{aligned}
$$

Here $P_i = P_i(x)$ and $A_i = A_i(x)$ $(i = 1, \dots)$ are unknown, slowly-varying amplitude, functions (the wall pressure and negative displacement perturbations respectively). The integrals $H_j = H_j(x, Y)$ $(j = 1, \dots, 12)$ are defined in Appendix A.4. The solutions for the pressure disturbances have been obtained by matching with the pressure in the lower deck.

5.4.2 The lower deck solutions

In order to obtain the solutions for U_i $(i = 1, \dots)$ we will apply the transformation

$$\xi = \Delta^{1/3}\left(Z - \beta_1/\lambda K_1\right), \ \Delta = i\lambda K_1, \qquad (5.28)$$

to eliminate Z from the x-momentum equations. We are interested only in the first modified eigenrelation.

The solution of the equations (5.15) - (5.17) for the disturbance velocity U_i $(i = 1, \dots, 4, 4L)$

in the lower deck yields

$$
\begin{aligned}
U_{1\xi} &= B_1 \mathrm{Ai}(\xi), && (5.29a)\\
U_{2\xi} &= B_2 \mathrm{Ai}(\xi) + \frac{1}{3}\big(K_2 K_1^{-1} - \theta Sc^{-1}\lambda^{-1}\mu\beta_1 K_1^{-1} \\
&\quad -i\theta Sc^{-1}\lambda^{-1}\mu K_1^{-1}\Delta^{2/3}\big) B_1 \mathrm{Ai}'''(\xi) \\
&\quad +i(\beta_1 K_2 K_1^{-1} - \beta_2 - \frac{1}{2}\theta Sc^{-1}\lambda^{-1}\mu\beta_1^2 K_1^{-1}) B_1 \Delta^{-2/3}\mathrm{Ai}'(\xi) \\
&\quad -\theta Sc^{-1}\mu\left(\mathrm{Ai}''(\xi) - \frac{1}{10}\mathrm{Ai}^{\mathrm{V}}(\xi)\right) B_1\Delta^{-1/3}, && (5.29b)\\
U_{4L\xi} &= B_{4L}\mathrm{Ai}(\xi) + [\delta_1 \mathrm{Ai}'(\xi) + \delta_2 \mathrm{Ai}'''(\xi)]\Delta^{-2/3}, && (5.29c)
\end{aligned}
$$

where

$$
\begin{aligned}
\delta_1 &= -B_1[K_{4L}K_1^{-1}\Delta^{2/3}\xi_0 + i\beta_{4L}], \\
\delta_2 &= \frac{1}{3}B_1 K_{4L}\Delta^{2/3}/K_1,
\end{aligned}
$$

$\mathrm{Ai}(\xi)$ is the Airy function and $B_i(x)$ $(i = 1, \dots)$ are unknown functions. A similar process can be performed for the higher order equations, but as we are predominantly interested in the higher order concentration effect we will terminate our expansions here.

Due to the different scale factors multiplying the arguments of the Airy functions which arise in the solution of the concentration equations, the algebra becomes particularly cumbersome at this stage. It is then prudent to obtain the solutions C_i $(i = 1, \dots, 4, 4L)$ numerically. These will be described further in the next section.

5.4.3 The upper deck solutions

The solutions of the upper deck equations are

$$
\begin{aligned}
\bar{p}_1 &= \bar{P}_1 \exp(-K_1\bar{y}), && (5.30a)\\
\bar{p}_2 &= \left[\bar{P}_2 - K_2 P_1 \bar{y}\right] \exp(-K_1\bar{y}), && (5.30b)\\
\bar{p}_3 &= \left[\bar{P}_3 - (K_3 P_1 + K_2\bar{P}_2)\bar{y} + \frac{1}{2}K_2^2 P_1 \bar{y}^2\right] \exp(-K_1\bar{y}), && (5.30c)\\
\bar{p}_{4L} &= \left[\bar{P}_{4L} - K_{4L}P_1\bar{y}\right] \exp(-K_1\bar{y}), && (5.30d)\\
\bar{p}_4 &= \Bigg[\bar{P}_4 - (K_4 P_1 + K_3\bar{P}_2 + K_2\bar{P}_3 - iP_{1x})\bar{y} \\
&\quad + \left(\frac{1}{2}K_2^2\bar{P}_2 + K_2 K_3 P_1 - \frac{1}{2}K_{1x}P_1\right)\bar{y}^2 - \frac{1}{6}K_2^3 P_1\bar{y}^3\Bigg] \exp(-K_1\bar{y}), && (5.30e)
\end{aligned}
$$

where $\bar{P}_i = \bar{P}_i(x)$ $(i = 1, \dots)$ are unknown functions of x.

Matching the solutions in the upper deck with those in the main deck yields

$$\begin{aligned}
\bar{P}_1 &= P_1, && (5.31a)\\
v_{1\infty} &= [-iK_1A_1U_B]_{Y\to\infty} = -iK_1A_1, \quad K_1\bar{P}_1 = K_1^2A_1;\\
\bar{P}_2 &= P_2 - A_1K_1^2H_{1\infty}, && (5.31b)\\
v_{2\infty} &= iK_1P_1H_{2\infty} + 2i\beta_1A_1 - iK_1A_2 = iK_2A_1 - i\bar{P}_2 - iK_2P_1/K_1;\\
\bar{P}_3 &= P_3 + K_1^2P_1H_{3\infty} - K_1(K_1A_2 + K_2A_1)H_{1\infty} + 2\beta_1K_1A_1H_{4\infty}, && (5.31c)\\
v_{3\infty} &= i(K_2P_1 + K_1P_2)H_{2\infty} - iA_1K_1^3H_{5\infty} + i\beta_1P_1H_{6\infty}\\
&\quad +i\beta_1(A_2 - K_2K_1^{-1}A_1) + i\beta_2A_1 - iK_1A_3 =\\
&\quad [(\beta_1 - K_2)v_{2\infty} + (\beta_2 - K_3)v_{1\infty}]\,K_1^{-1} - i\bar{P}_3 - iK_3P_1/K_1\\
&\quad -iK_2\bar{P}_2/K_1;\\
\bar{P}_{4L} &= P_{4L}, && (5.31d)\\
v_{4L\infty} &= -iK_1A_{4L} = iK_{4L}A_1 - \bar{P}_{4L} - iK_{4L}P_1/K_1;\\
\bar{P}_4 &= P_4 + (K_1^2P_2 + 2K_1K_2P_1)H_{3\infty} - K_1\big(K_1A_3 + K_2A_2\\
&\quad +K_3A_1\big)H_{1\infty} + 2(\beta_2K_1A_1 + \beta_1K_1A_2)H_{4\infty} - K_1^4A_1H_{11\infty}\\
&\quad +\beta_1K_1P_1(H_{12\infty} - H_{10\infty}), && (5.31e)\\
v_{4\infty} &= i(K_3P_1 + K_2P_2 + K_1P_3)H_{2\infty} - i(2A_1K_2K_1^2 + K_1^3A_2)H_{5\infty}\\
&\quad +i(\beta_2P_1 + \beta_1P_2)H_{6\infty} + i\beta_1(A_3 - K_2K_1^{-1}A_2 + K_2^2K_1^{-2}A_1)\\
&\quad +i\beta_2(A_2 - K_2K_1^{-1}A_1A_1) + i\beta_3A_1 - iK_1A_4 + iK_1^3P_1H_{7\infty}\\
&\quad +i\beta_1K_1^2A_1H_{8\infty} + i\beta_1^2K_1^{-1}P_1H_{9\infty} = \Big[(\beta_1 - K_2)v_{3\infty} + (\beta_2 - K_3)v_{2\infty}\\
&\quad +(\beta_3 - K_4)v_{1\infty}\Big]K_1^{-1} + K_1^{-1}(K_1A_1)_x - i\bar{P}_4 - iK_4\bar{P}_1/K_1 - iK_3\bar{P}_2/K_1\\
&\quad -iK_2\bar{P}_3/K_1 - P_{1x}/K_1.
\end{aligned}$$

5.5 Semi-numerical treatment

We have already mentioned that the solutions for the concentration disturbance in the lower deck will be solved numerically. In order to determine the second-order disturbance V_2 along the surface we need to determine the first derivative of the leading order concentration disturbance at $Z = 0$. We found it appropriate to solve the full system of equations for the leading order disturbances U_1, V_1 and C_1 in the systems of equations (5.15) - (5.17) with the boundary conditions (5.19). To do this, we first solved the standard triple-deck equations

$$\begin{aligned}
U_{1ZZ} &= iK_1^2A_1 + \lambda V_1 + i(\lambda ZK_1 - \beta_1)U_1, && (5.32)\\
V_{1Z} &= -iK_1U_1,
\end{aligned}$$

subject to the boundary conditions

$$U_1 = V_1 = 0 \text{ at } Z = 0; \quad U_1 \to \lambda \text{ as } Z \to \infty. \qquad (5.33)$$

To solve this system numerically we first replace the non-homogeneous boundary condition $U_1 \to \lambda$ as $Z \to \infty$ with the homogeneous boundary condition $U_{1Z} = 0$ at $Z = Z_\infty$. We then iterate on β_1 and K_1 using the Newton-Raphson method until the remaining boundary condition $|U_1 - \lambda| < \epsilon$ at $Z = Z_\infty$ is satisfied. After some experimentation a tolerance of $\epsilon = 10^{-5}$ was found to yield results converged to five significant figures. The subroutine we developed for solving the system (5.32) - (5.33) is based on the *NAG* subroutine *D02RAF* which solves the two-point boundary-value problems with general boundary conditions, using a deferred correction technique and Newton iteration (see Pereyra (1979)).

Finally we will solve the concentration equation

$$C_{1ZZ} = Sc(i\lambda K_1 Z C_1 - i\beta_1 C_1 + \mu V_1), \tag{5.34}$$

with the following boundary conditions:

$$C_1 = 0 \text{ at } Z = 0; \quad C_1 \to \mu \text{ as } Z \to \infty. \tag{5.35}$$

All equations have been normalised as follows:

$$U_1 \equiv \frac{U_1}{A_1}, \quad V_1 \equiv \frac{V_1}{A_1}, \quad C_1 \equiv \frac{C_1}{A_1}.$$

The equations for the leading order terms in the systems of equations (5.32) - (5.35) have been solved with $Z_\infty = 50$ and 2000 grid points. The first-order concentration disturbance equation (5.34) with the boundary conditions (5.35) has been solved by using simple second-order central difference discrete scheme, employing the Thomas algorithm to invert the resulting tri-diagonal system and using the solutions from the equations (5.32) - (5.33). The solution is obtained and tabulated, for different values of Sc and θ (see Tables 5.1 - 5.5 and Figures 5.4 and 5.5, where $\delta_1 = \partial C_1/\partial Z|_{Z=0}$).

Since we are interested only in the dominant effect of the induced secondary flow on the disturbance structure (mass-transfer effect) the higher order corrections have not been determined. However in Appendix A.5 we present the full system of governing equations.

5.6 Solutions - eigenrelations

As mentioned in the last section we are only interested in the first correction to the leading order eigenrelation, i.e. we shall limit our attention to the second-order neutral term in the expansions, in so doing we shall obtain the first modified eigenrelation.

The form of the leading order eigenrelation is unchanged. For completeness we give a brief derivation of its analytic form here as we will make use of it as a check of our numerical scheme for solving the leading order lower deck equations. Applying the wall boundary condition on $Z = 0$ in (5.16) gives

$$B_1 \mathrm{Ai}_0' \Delta^{2/3} = iK_1 P_1, \tag{5.36}$$

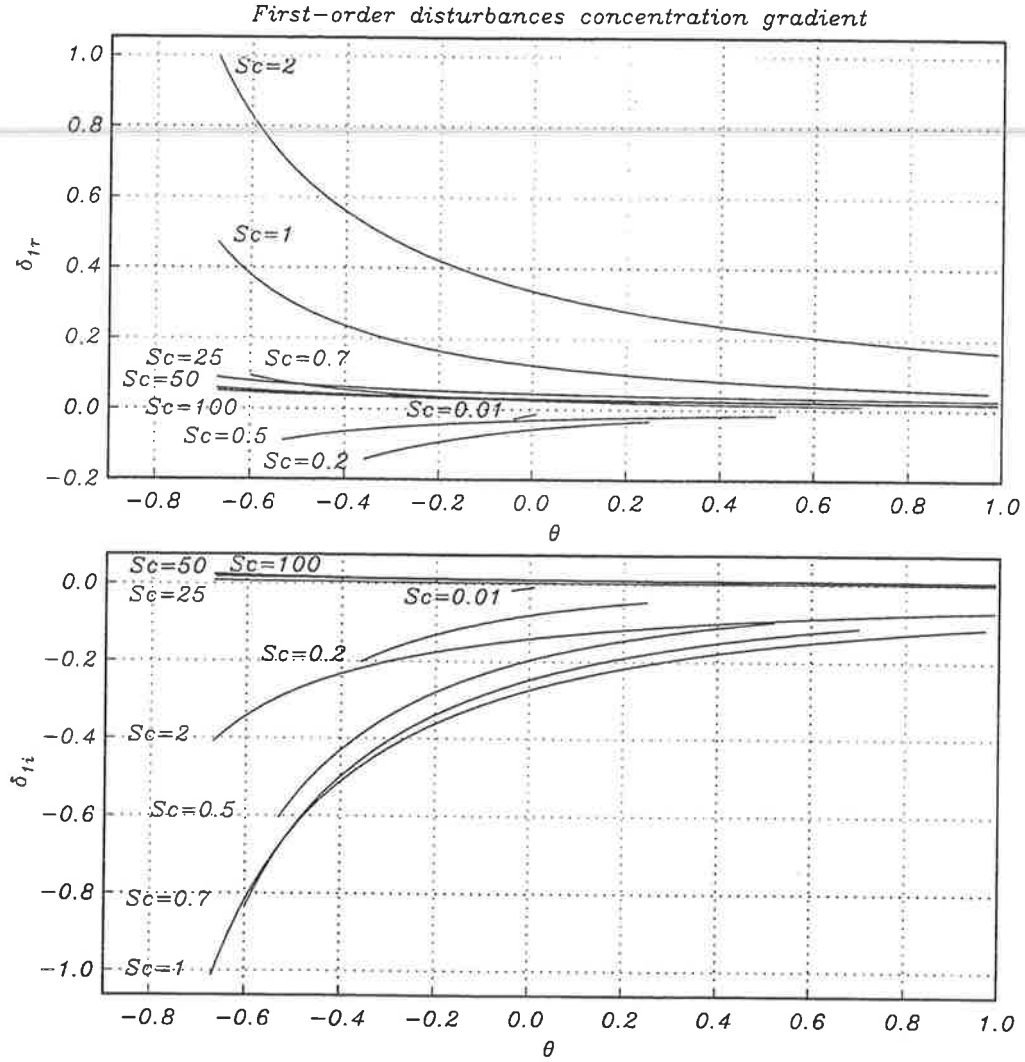

Figure 5.4: The first order disturbance concentration gradient along the surface versus the parameter θ for different values of the Schmidt number Sc.

where the subscript 0 refers to the function being evaluated at $\xi = \xi_0 = -i\beta_1\Delta^{-2/3}$.

Next the matching condition on U_1 as $\xi \to \infty$ is $U_1 \to \lambda A_1$, from (5.16) and (5.6) we obtain

$$B_1 k = \lambda A_1, \tag{5.37}$$

where

$$k = \int_{\xi_0}^{\infty} \mathrm{Ai}(q)\, \mathrm{d}q.$$

Eliminating B_1 between (5.36) and (5.37) we obtain a relation between the wall pressure (P_1) and the displacement $(-A_1)$. From (5.30) and continuity of pressure and normal

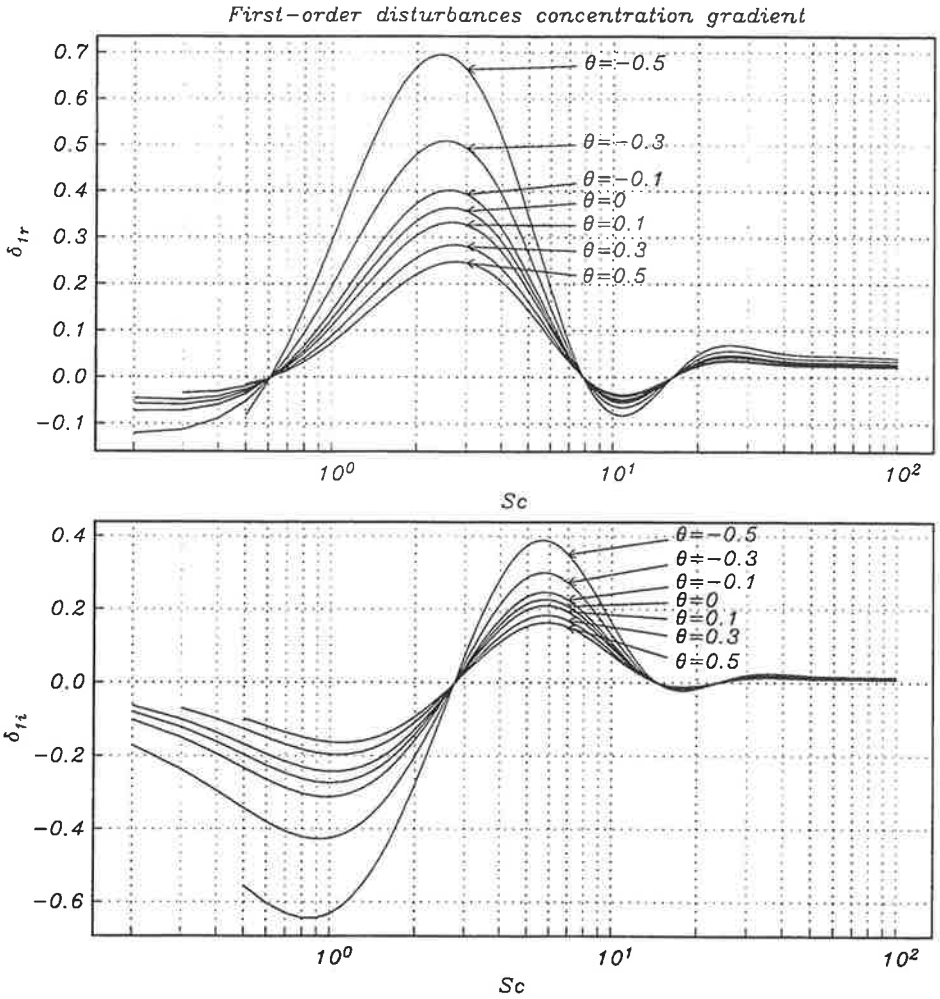

Figure 5.5: The first order disturbances concentration gradient along the surface versus the Schmidt number Sc for different values of the parameter θ.

velocity as $\bar{y} \to 0$ (5.31) and combining (5.36) with (5.37) we have the leading order eigenrelation

$$\frac{iK_1^2 k}{\lambda \mathrm{Ai}_0' \Delta^{2/3}} = 1, \tag{5.38}$$

which fixes the wavenumber $K_1(x)$ as a function of the frequency β_1 and the skin friction $\lambda(x)$.

For neutral stability (K_1 and β_1 real), it is found that (see Lin (1945), Reid (1965), Schlichting (1979), Stuart (1963), Tollmien (1929))

$$\frac{\beta_1}{(\lambda K_1)^{2/3}} = 2.297, \tag{5.39}$$

which implies the relation $\xi_0 \sim -2.297 i^{1/3}$, viz., ξ_0, Ai_0, Ai_0' and k are independent of λK_1. Their values have been obtained in the way similar to that in Bassom (1989) and are given in Appendix A.4. From (5.39) we can obtain that $\xi_0 k = -2.294 \mathrm{Ai}_0'$.

This is the first-order eigenrelation, which fixes the wavenumber $K_1(x)$ as a function of the frequency $\beta_1(x)$ and skin friction $\lambda(x)$. It is, of course, identical in form to that found in Smith (1979a). We have (see Smith (1979a) equation (4.1))

$$K_1 = 1.001\lambda^{5/4}x^{-5/8}, \tag{5.40a}$$

$$\beta_1 = 2.299\lambda^{3/2}x^{-3/4}, \tag{5.40b}$$

where, for the case of the Blasius boundary-layer flow $\lambda = 0.332$. The corresponding values of the wavenumber and frequency are found to be

$$K_1\lambda^{-5/4}x^{5/8} = 1.000489, \quad \beta_1\lambda^{-3/2}x^{-3/4} = 2.297967.$$

A similar process can be carried out to produce the successive eigenrelations for $K_2(x)$, $K_3(x)$, $K_{4L}(x)$, $K_4(x)$ as functions of $\lambda(x)$ and μ (and hence of θ and the Schmidt number Sc), and the constants $\beta_i(x)$ $(i = 1, \ldots, 4, 4L)$. Proceeding in this fashion the wall boundary conditions for the lower deck disturbance solutions at $Z = 0$ yield

$$\begin{aligned} &B_2\mathrm{Ai}_0' + \left(\frac{1}{2}\bar{a}_1 - a_1 - a_4\right)\mathrm{Ai}_0 + a_2\mathrm{Ai}_0'' + \frac{1}{2}\left(\frac{1}{2}\bar{a}_2 + 3a_4\right)\mathrm{Ai}_0''' + \frac{1}{3}a_3\mathrm{Ai}_0^{iv} \\ &-\frac{1}{5}a_4\mathrm{Ai}_0^{v\prime} - \theta Sc^{-1/2}x^{-1/2}\mu B_1\mathrm{Ai}_0\Delta^{-1/3} + \theta Sc^{-1/2}x^{-1/2}\lambda\delta_1\Delta^{-1/3} \\ &= i(K_1P + 2 + K_2P_1)\Delta^{-2/3}, \end{aligned} \tag{5.41}$$

where

$$\begin{aligned} \bar{a}_1 &= 2(K_2K_1^{-1} - \theta Sc^{-1/2}\lambda^{-1}\mu K_1^{-1}\beta_1)B_1, \\ \bar{a}_2 &= \theta Sc^{-1/2}\mu(x^{-1/2} - 2)B_1\Delta^{-1/3}, \end{aligned}$$

and

$$\begin{aligned} a_1 &= \theta Sc^{-1/2}\mu x^{-1/2}B_1\Delta^{-1/3}, \\ a_2 &= i\left(\beta_1K_2K_1^{-1} - \beta_2 - \frac{1}{2}\theta Sc^{-1/2}\lambda^{-1}\mu K_1^{-1}\beta_1^2\right)B_1, \\ a_3 &= 2\bar{a}_1, \\ a_4 &= \frac{1}{2}i\theta Sc^{-1/2}\lambda\mu K_1B_1\Delta^{-4/3}. \end{aligned}$$

The conditions of matching the second-order velocity disturbance solution of the main deck u_2 as $Y_2 \to 0$ with that of the lower deck U_2 as $\xi \to \infty$ imply

$$\begin{aligned} &B_2k + \left(\frac{1}{2}\bar{a}_1 - a_1 - a_4\right)\mathrm{Ai}_0 \int_{\xi_0}^{\infty}\int_{\xi_{01}}^{\xi_1} \mathrm{Ai}(q)\mathrm{d}q_1\mathrm{d}q_2 - a_2\mathrm{Ai}_0 \\ &-\frac{1}{2}\left(\frac{1}{2}\bar{a}_2 + 3a_4\right)\mathrm{Ai}_0' - \frac{1}{3}a_3\mathrm{Ai}_0'' + \frac{1}{5}a_4\mathrm{Ai}_0^{iv} = \lambda(A_2 - P_1\hat{I} - K_2K_1^{-1}A_1), \end{aligned} \tag{5.42}$$

where

$$\hat{I} = \int_{\bar{\lambda}}^{0} U_B^{-2}(Y_1)\,\mathrm{d}Y_1.$$

Now combining (5.41), (5.42) and (5.31a,b) we obtain the second-order eigenrelation, which is

$$\begin{aligned}\hat{D}K_2 &= iK_1^2\left(H_{2\infty}-H_{1\infty}-\hat{I}\right)-\frac{1}{2}\frac{\theta\mu}{\lambda Sc}\hat{D}\left(\beta_1-\frac{1}{\Delta^{2/3}}\right)\\ &\quad+2i\beta_1\left(1+i\frac{1}{20}\frac{\theta\mu}{\lambda Sc}\xi_0\frac{\mathrm{Ai}_0 D}{k}\right)+\left(\frac{1}{2}\frac{\theta\mu}{\lambda Sc}\beta_1^2+\beta_2 K_1\right)\frac{\mathrm{Ai}_0 D}{k\Delta^{2/3}}\\ &\quad+i\frac{2}{5}\frac{\theta\mu}{Sc\Delta^{1/3}}K_1\left(\xi_0+\frac{2}{k}\mathrm{Ai}_0'-\frac{1}{k}\frac{\mathrm{Ai}_0}{\mathrm{Ai}_0'}\right)+i\frac{\theta}{Sc}K_1\delta_1\frac{k}{\mathrm{Ai}_0'\Delta^{1/3}},\end{aligned}\tag{5.43}$$

where we have normalised δ_1 using A_1 and set

$$\begin{aligned}\delta_1 &= \left.\frac{\partial C_1}{\partial\xi}\right|_{\xi=\xi_0},\\ \hat{D} &= \frac{4}{3}i+\frac{2}{3}\left(\beta_1 Ai_0/k\Delta^{2/3}\right)D,\\ D &= 1+k\xi_0/\mathrm{Ai}_0'.\end{aligned}$$

Upon setting $\theta=0$ we have the first-order correction to the Tollmien-Schlichting eigenrelation, which again provides a useful check of our result.

The integral denoted by $\hat{I}$ is defined in the Hadamard sense. It has been obtained by matching the main deck solution u_2 with the lower deck U_2. With reference to Hadamard (1952)

$$\left.\frac{\partial U_B}{\partial Y}\right|_{Y\to 0}\int_{\tilde{\lambda}}^{0}U_B^{-2}(Y_1)\,\mathrm{d}Y_1=\lim_{Y\to 0}\left[\frac{\partial U_B}{\partial Y}\int_{\tilde{\lambda}}^{0}U_B^{-2}(Y_1)\,\mathrm{d}Y_1+\frac{1}{U_B}\right].\tag{5.44}$$

We term the limit on the right-hand-side of (5.44) by the "finite-part" of the integral on the left-hand-side. The value of the lower limit $\tilde{\lambda}$ is an arbitrary non-zero constant (modifying the constant of integration) which has no effect on the numerical value of the limit obtained.

The "finite-part" integral at the left-hand-side of (5.44) can be written as

$$J=-\int_0^{\tilde{\lambda}}\frac{f(Y)-f(0)-Yf'(0)}{Y^2}\,\mathrm{d}Y+\frac{1}{\tilde{\lambda}\lambda^2}-\frac{\theta Sc^{-1}\mu}{\lambda^2}\ln\tilde{\lambda},$$

where $f(Y)=Y^2/U_B^2$. We note also that the occurrence of the logarithmic terms in the asymptotic expansions, for instance (5.3), are due to the last two terms and is forced in the same manner as noted by Smith (1979a).

5.7 Curves of neutral stability

The calculation of δ_1 for different values of Sc and θ has been described in section 5.5. Some of the results for the first order-disturbance concentration gradient along the surface, for different values of the Schmidt number Sc and the parameter θ, are presented

in Figures 5.4 and 5.5, and Tables 5.1 - 5.5. In the special case $Sc = 1$ the first-order disturbances concentration equation (5.34) can be solved analytically as well.

The eigenrelations for K_1 and K_2 in (5.38) and (5.43) are results from parallel-flow stability. For neutral stability wavenumbers K_1 and K_2 must be real. In order for the wavenumber K_1 to be real the eigenrelation (5.38) requires that the frequency β_1 is given by (5.40b). Given that the frequency β_1 is a constant, the position of neutral stability, for a disturbance of constant frequency, is given by $x = x_n$, where

$$x_n = 0.334\beta_1^{-4/3} + O(Re^{-1/8}). \tag{5.45}$$

Beyond $x = x_n$ the disturbance will amplify spatially. Alternatively, we can express (5.40) in terms of Reynolds number R_δ based on the local boundary-layer thickness ($R_\delta = 1.720(xRe)^{1/2}$), for which the neutral stability frequency is given by

$$\beta_n = 5.1859R_\delta^{-3/2}\hat{\lambda}^{3/2} + O(Re^{-7/4}), \tag{5.46}$$

using (5.2), (5.3) and (5.40) and defining $\hat{\lambda} = f''(0)$.

For K_2 to be real the complex equation (5.43) yields

$$\beta_2^* = 2.5830R_\delta^{-7/4}\beta_2 \tag{5.47}$$

for neutral stability. There is no explicit dependence on θ and Sc in equation (5.47) because the variation of the parameters K_2 and β_2 is bound to the wall share λ, however, an explicit dependence upon these parameters occur at higher order in the solution expansion. We can continue this process indefinitely having all the eigenrelation but for the purposes of our present study we shall terminate this process here. Combining (5.40) and (5.47), the expression for the neutrally stable frequency β_n is

$$\beta_n = 0.995R_\delta^{-3/2}\left[5.2120\hat{\lambda}^{3/2} + 2.596\beta_2^*R_\delta^{-1/4} + O(R_\delta^{-1/2})\right]. \tag{5.48}$$

At $\theta = 0$ and $Sc = 1$, the case without mass transfer, the expression (5.48) reduces to that obtained by Smith (1979a), i.e. this is the result for the conventional, parallel-flow analysis (there is no presence of x-derivatives or small normal velocity components in the basic flow, because the boundary-layer growth terms are neglected).

The second-order neutral frequency β_2 and wavenumber K_2 as a function of the mass-transfer parameter θ, for different values of the Schmidt number Sc, are plotted in Figure 5.6 and tabulated in Tables 5.1 - 5.5. It is seen from Figure 5.6 that in the case of "blowing" into gas boundary-layer flows, i.e. when the mass transfer is directed towards the boundary layer, the contribution of the second-order frequency β_2 into (5.48) decreases the neutral stability frequency β_n. We also observe the same effect with the wavenumber K_2. As it is seen from the Figure 5.6 in the case of liquids, i.e. at moderately large Schmidt numbers Sc, the thinner the concentration boundary layer the less significant is this contribution. In the case of "suction", when the mass transfer is directed from the boundary layer towards the permeable surface, the contribution of the second-order frequency β_2 into (5.48) increases the neutral stability frequency β_n and again this contribution is much more significant at low Schmidt numbers (gas boundary-layer flow).

$Sc = 0.7$					
θ	$\lambda(x)x^{1/2}$	$\mu(x)x^{1/2}$	δ_{1r}	δ_{1i}	$\beta_2 x^{7/8}$
-0.99	0.6387	-4.4891	–	–	–
-0.5	0.5989	-0.4819	0.0695	-0.6309	6.9271
-0.3	0.4544	-0.3804	0.0434	-0.4058	5.2234
-0.1	0.3651	-0.3167	0.0301	-0.2872	2.5434
-0.05	0.3479	-0.3042	0.0278	-0.2661	1.6390
-0.03	0.3414	-0.2995	0.0269	-0.2583	1.2455
-0.01	0.3351	-0.2949	0.0262	-0.2509	0.8329
0	0.3321	-0.2927	0.0258	-0.2473	0.6219
0.01	0.3291	-0.2905	0.0254	-0.2438	0.4046
0.03	0.3232	-0.2862	0.0246	-0.2371	-0.0463
0.05	0.3176	-0.2821	0.0239	-0.2306	-0.5128
0.1	0.3042	-0.2723	0.0223	-0.2156	-1.7745
0.3	0.2598	-0.2394	0.0173	-0.1686	-8.1937
0.5	0.2261	-0.2140	0.0138	-0.1358	-17.0970
0.99	0.2261	-0.1704	–	–	–

Table 5.1: The values of the skin friction $f''(0) = \lambda(x)x^{1/2}$, the basic concentration gradient on the surface $g'(0) = \mu(x)x^{1/2}$, first order disturbance concentration gradient C_1' along the surface and the second order neutral frequency $\beta_2 x^{7/8}$ at $Sc = 0.7$ for different values of θ.

The curves of neutral stability for different values of the Schmidt number Sc and mass-transfer level θ are shown in Figures 5.7 - 5.11. It is seen that the results are in agreement with those made in the previous chapter. Increasing the absolute value of the mass-transfer parameter leads to an increase of the frequency of neutral stability. Depending on the direction of the mass transfer, i.e. the sign of the mass-transfer parameter θ, corresponding to "blowing" or "suction" we have a destabilising or stabilising effect on the stability of the boundary-layer flow. The high concentration gradients have a stabilising effect at $\theta < 0$; this is significantly higher then the destabilising one in the case of a change in the direction of mass transfer ($\theta > 0$).

The result obtained by Smith (1979a) is plotted in Figure 5.8 and differs slightly from ours at the mass-transfer level of $\theta = 0$ due to the non-parallel contributions taken into account in Smith's calculation. The boundary-layer growth has a stabilising effect on the boundary-layer flow if the wall pressure is taken to be the measure of the instability (see Smith (1979a)) but it is of less importance compared with the effect of mass transfer.

$Sc = 1$					
θ	$\lambda(x)x^{1/2}$	$\mu(x)x^{1/2}$	δ_{1r}	δ_{1i}	$\beta_2 x^{7/8}$
-0.99	4.9445	-4.9445	–	–	–
-0.5	0.5380	-0.5380	0.2922	-0.6329	6.7380
-0.3	0.4277	-0.4277	0.1947	-0.4251	4.8091
-0.1	0.3582	-0.3582	0.1424	-0.3124	2.2389
-0.05	0.3446	-0.3446	0.1329	-0.2921	1.4605
-0.03	0.3394	-0.3394	0.1295	-0.2846	1.1299
-0.01	0.3345	-0.3345	0.1262	-0.2774	0.7939
0	0.3321	-0.3321	0.1246	-0.2739	0.6219
0.01	0.3297	-0.3297	0.1229	-0.2705	0.4462
0.03	0.3250	-0.3250	0.1199	-0.2639	0.0868
0.05	0.3205	-0.3205	0.1170	-0.2575	-0.2807
0.1	0.3098	-0.3098	0.1102	-0.2428	-1.2451
0.3	0.2739	-0.2739	0.0887	-0.1959	-5.7540
0.5	0.2460	-0.2460	0.0734	-0.1626	-11.3519
0.99	0.1981	-0.1981	–	–	–

Table 5.2: The values of the skin friction $f''(0) = \lambda(x)x^{1/2}$, the basic concentration gradient on the surface $g'(0) = \mu(x)x^{1/2}$, first order disturbance concentration gradient C_1' along the surface and the second order neutral frequency $\beta_2 x^{7/8}$ at $Sc = 1$ for different values of θ.

$Sc = 25$					
θ	$\lambda(x)x^{1/2}$	$\mu(x)x^{1/2}$	δ_{1r}	δ_{1i}	$\beta_2 x^{7/8}$
-0.99	0.6029	-8.8122	0.5971	0.0704	6.3388
-0.5	0.3534	-1.4666	0.0688	0.0060	1.9158
-0.3	0.3427	-1.2165	0.0559	0.0049	1.3096
-0.1	0.3351	-1.0527	0.0476	0.0041	0.8282
-0.05	0.3335	-1.0199	0.0459	0.0039	0.7211
-0.03	0.3329	-1.0075	0.0454	0.0038	0.6799
-0.01	0.3323	-0.9954	0.0448	0.0038	0.6391
0	0.3321	-0.9895	0.0045	0.0038	0.6219
0.01	0.3318	-0.9837	0.0042	0.0038	0.6016
0.03	0.3312	-0.9723	0.0436	0.0037	0.5611
0.05	0.3307	-0.9613	0.0431	0.0037	0.5241
0.1	0.3294	-0.9350	0.0418	0.0036	0.4307
0.3	0.3247	-0.8453	0.0374	0.0032	0.0845
0.5	0.3209	-0.7741	0.0339	0.0029	-0.2162
0.99	0.3136	-0.6479	0.0279	0.0023	-0.8358

Table 5.3: The values of the skin friction $f''(0) = \lambda(x)x^{1/2}$, the basic concentration gradient on the surface $g'(0) = \mu(x)x^{1/2}$, first order disturbance concentration gradient C_1' along the surface and the second order neutral frequency $\beta_2 x^{7/8}$ at $Sc = 25$ for different values of θ.

$Sc = 50$					
θ	$\lambda(x)x^{1/2}$	$\mu(x)x^{1/2}$	δ_{1r}	δ_{1i}	$\beta_2 x^{7/8}$
-0.99	0.4880	-10.4084	0.3275	0.1459	5.4360
-0.5	0.3454	-1.8367	0.0462	0.0193	1.4700
-0.3	0.3387	-1.5284	0.0379	0.0152	1.0622
-0.1	0.3339	-1.3257	0.0326	0.0135	0.7497
-0.05	0.3329	-1.2849	0.0315	0.0131	0.6819
-0.03	0.3326	-1.2696	0.0311	0.0129	0.6584
-0.01	0.3322	-1.2546	0.0308	0.0127	0.6319
0	0.3321	-1.2473	0.0306	0.0127	0.6219
0.01	0.3319	-1.2401	0.0304	0.0126	0.6088
0.03	0.3315	-1.2259	0.0300	0.0124	0.5826
0.05	0.3312	-1.2122	0.0279	0.0123	0.5599
0.1	0.3304	-1.1796	0.0288	0.0119	0.5024
0.3	0.3274	-1.0679	0.0259	0.0107	0.2881
0.5	0.3249	-0.9792	0.0237	0.0098	0.1027
0.99	0.3203	-0.8215	0.0197	0.0081	-0.2621

Table 5.4: The values of the skin friction $f''(0) = \lambda(x)x^{1/2}$, the basic concentration gradient on the surface $g'(0) = \mu(x)x^{1/2}$, first order disturbance concentration gradient C_1' along the surface and the second order neutral frequency $\beta_2 x^{7/8}$ at $Sc = 50$ for different values of θ.

$Sc = 100$					
θ	$\lambda(x)x^{1/2}$	$\mu(x)x^{1/2}$	δ_{1r}	δ_{1i}	$\beta_2 x^{7/8}$
-0.99	0.4246	-12.5563	0.2559	0.1011	4.4029
-0.5	0.3404	-2.3048	0.0409	0.0152	1.1693
-0.3	0.3362	-1.9220	0.0339	0.0126	0.9015
-0.1	0.3333	-1.6696	0.0293	0.0108	0.7049
-0.05	0.3326	-1.6189	0.0284	0.0105	0.6596
-0.03	0.3324	-1.5996	0.0280	0.0104	0.6444
-0.01	0.3322	-1.5809	0.0277	0.0102	0.6294
0	0.3321	-1.5718	0.0275	0.0102	0.6219
0.01	0.3319	-1.5628	0.0273	0.0101	0.6112
0.03	0.3317	-1.5452	0.0270	0.0099	0.5965
0.05	0.3315	-1.5281	0.0267	0.0099	0.5819
0.1	0.3309	-1.4873	0.0259	0.0096	0.5426
0.3	0.3291	-1.3478	0.0235	0.0087	0.4125
0.5	0.3276	-1.2368	0.0215	0.0079	0.3014
0.99	0.3246	-1.0392	0.0179	0.0066	0.0776

Table 5.5: The values of the skin friction $f''(0) = \lambda(x)x^{1/2}$, the basic concentration gradient on the surface $g'(0) = \mu(x)x^{1/2}$, first order disturbance concentration gradient C_1' along the surface and the second order neutral frequency $\beta_2 x^{7/8}$ at $Sc = 100$ for different values of θ.

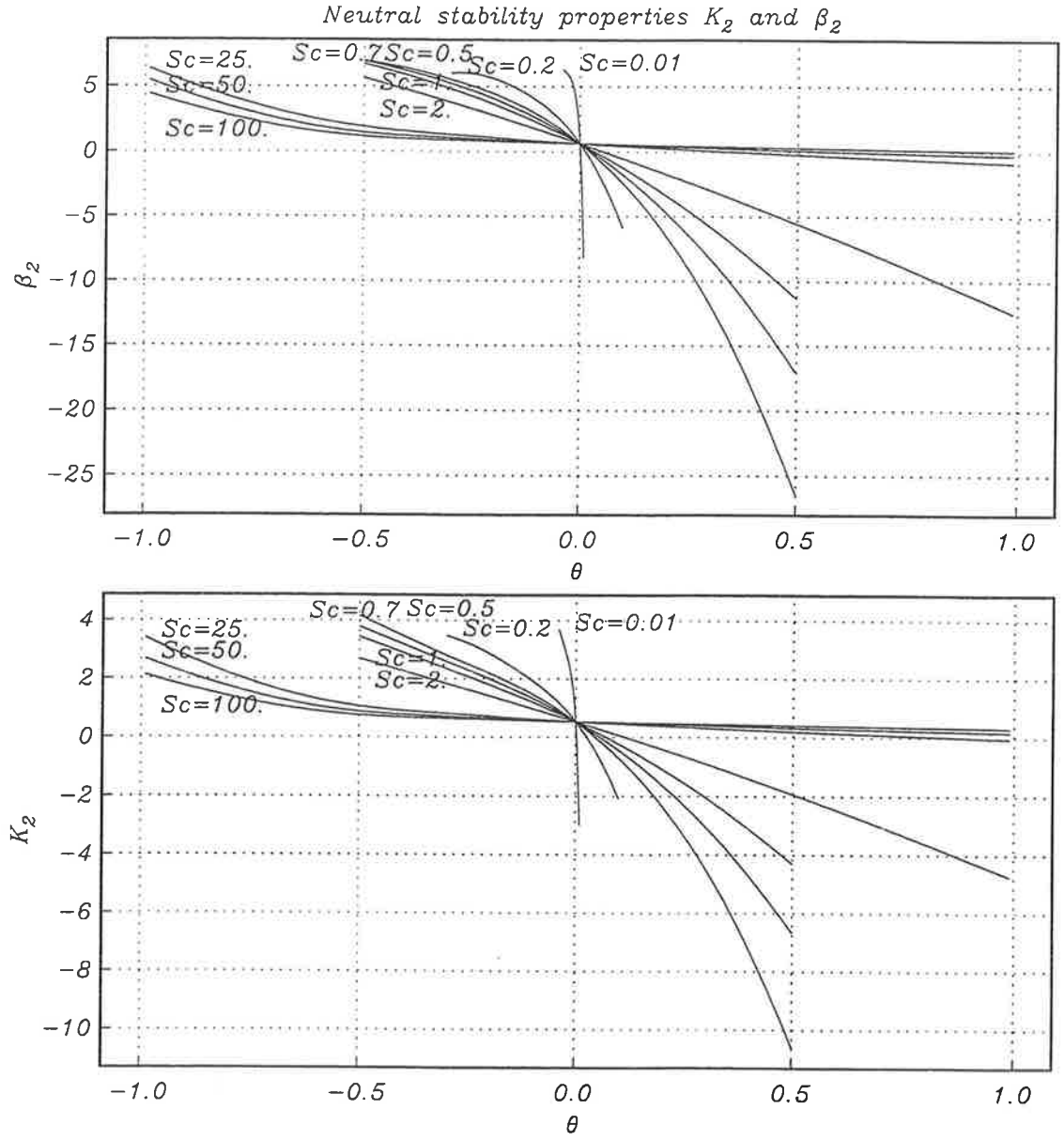

Figure 5.6: The second-order neutral frequency β_2 and wavenumber K_2 versus the mass-transfer parameter θ for different values of the Schmidt number Sc (fixed $x = 1$).

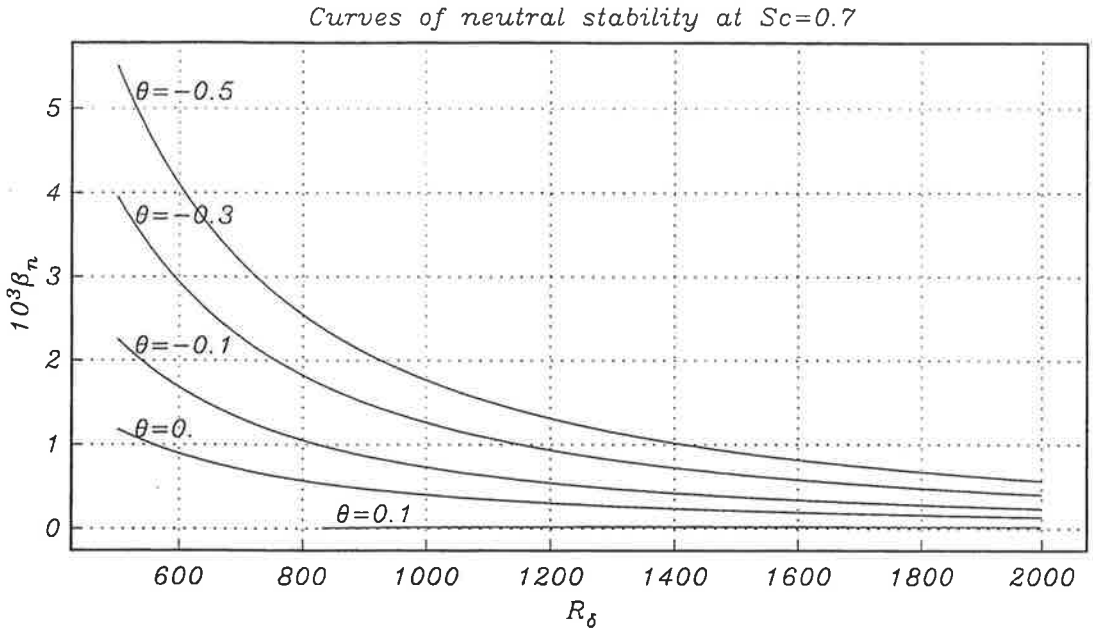

Figure 5.7: Lower-branch of the curve of neutral stability in the (R_δ, β_n)-plane at $Sc = 0.7$ for different values of θ.

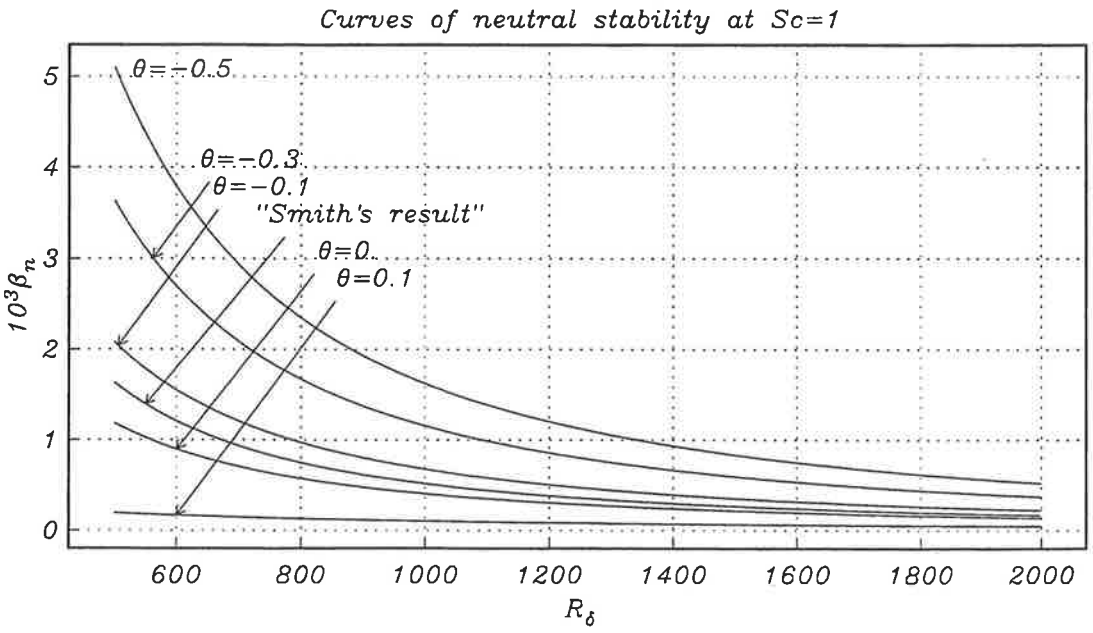

Figure 5.8: Lower-branch of the curves of neutral stability in the (R_δ, β_n)-plane at $Sc = 1$ for different values of θ.

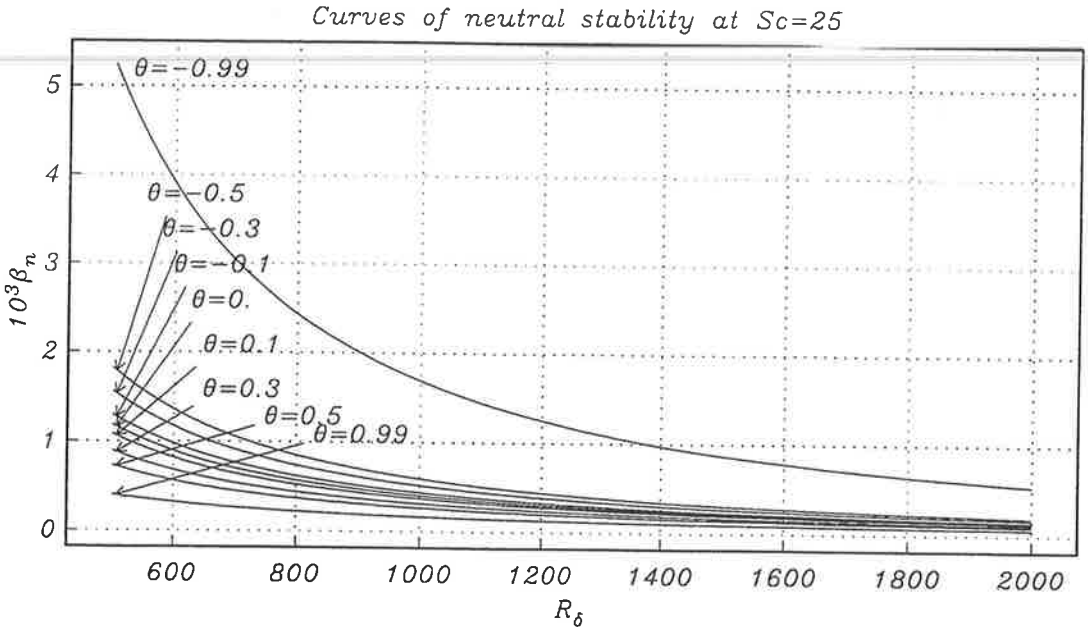

Figure 5.9: Lower-branch of the curves of neutral stability in the (R_δ, β_n)-plane at $Sc = 25$ for different values of θ.

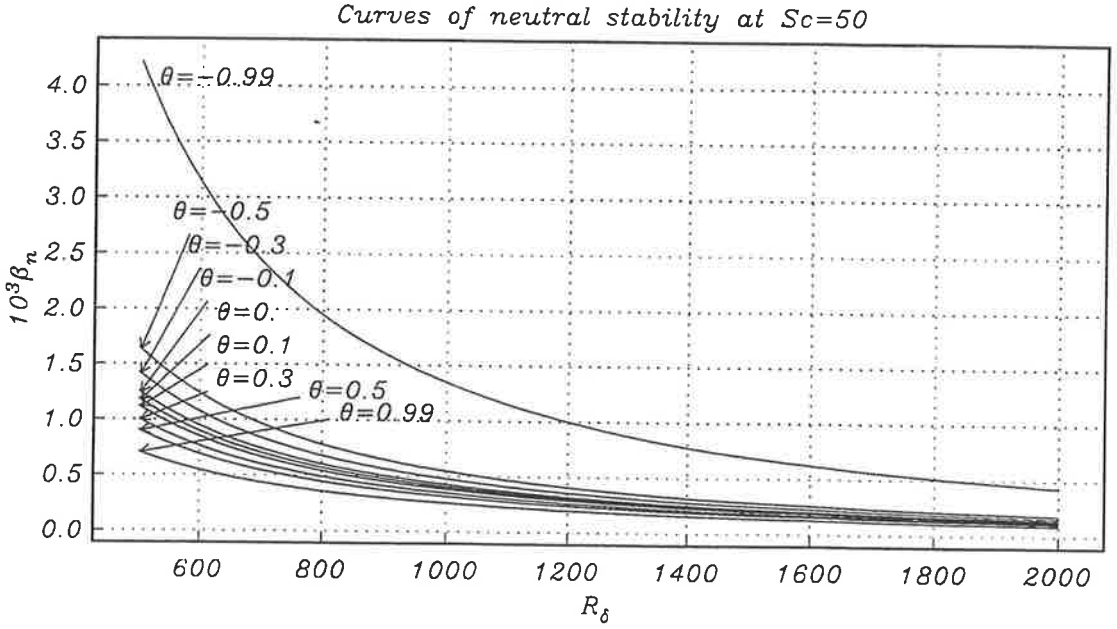

Figure 5.10: Lower-branch of the curves of neutral stability in the (R_δ, β_n)-plane at $Sc = 50$ for different values of θ.

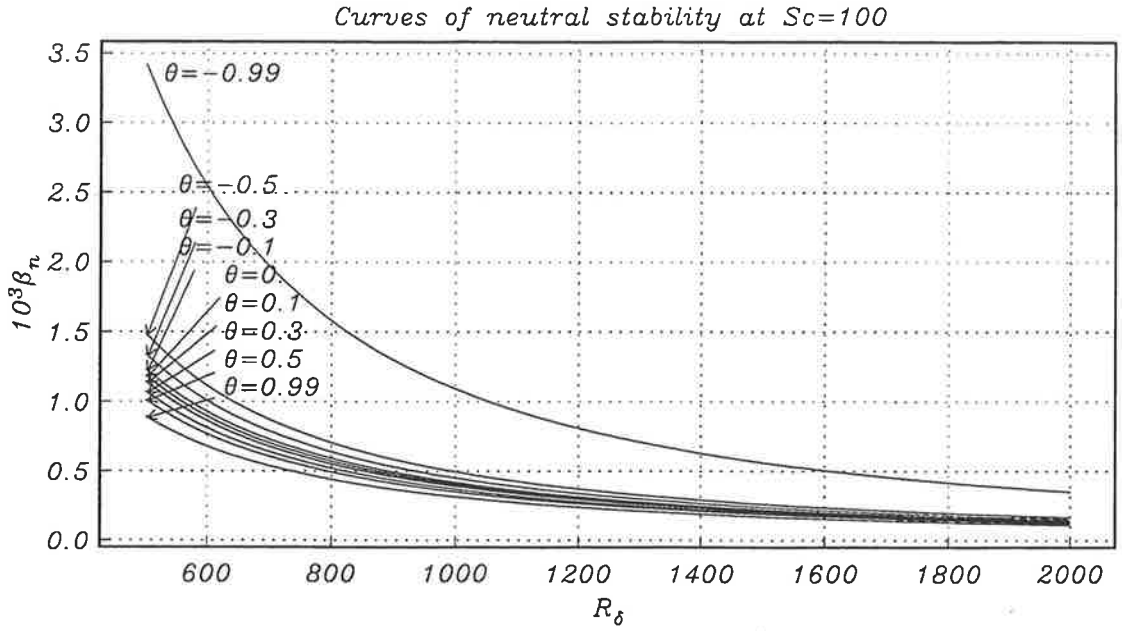

Figure 5.11: Lower-branch of the curves of neutral stability in the (R_δ, β_n)-plane at $Sc = 100$ for different values of θ.

Chapter 6

Diffusion Induced Separation and the Inviscid Instability of Boundary-Layer Flows Under Conditions of Interfacial Mass Transfer through a Finite "Slot"

There are numerous and varied investigations into the phenomenon of flow separation, either self-induced, by slot-injection or slot-blowing into boundary layers. Early work on this problem, summarised in Gadd, Jones & Watson (1963), was mainly concerned with similarity solutions in which the free-stream velocity is proportional to x^m, $m > 0$, while the blowing velocity is proportional to $x^{1/2(m-1)}$ and is $O(Re^{-1/2}U_\infty)$. In this case the governing equation is the classical Falkner-Skan equation

$$f''' + ff'' + \beta(1 - f'^2) = 0, \tag{6.1}$$

subject to boundary conditions

$$f'(0) = 0, \;\; f(0) = -C; \;\; f'(\infty) = 1. \tag{6.2}$$

Here $\beta = 2m/(m+1)$, $C = O(1)$ is a blowing parameter, f a stream-function and $\beta = O(1)$ (so-called "hard blowing"). Numerical solutions of the Falkner-Skan equation with $\beta = 0$ were obtained by Emmons & Leigh (1954) who found that as $C \to C_0 = 0.876$ the boundary-layer flow approaches a state of zero wall shear and is blown off the wall; no solution can be found if $C > C_0$. A uniform distribution of injection was considered in Catherall, Stewartson & Williams (1965). In this study the boundary-layer equations for an incompressible fluid over a flat plate, in the special case when the pressure gradient vanishes and there is a uniform injection of fluid from the plate, are examined numerically and analytically. In the numerical study the point of separation was computed with a high degree of accuracy and found to be $x_s = 0.7456$, while in the accompanying analytical study the structure of the singularity at separation was determined. An entirely

satisfactory agreement between the numerical and analytical studies was not possible, because the analytical study was only valid when $\ln(1/x^*) \gg 1$, here x^* is the non-dimensional distance from the point of separation ($x^* = x_s - x$). In work by Napolitano & Messick (1980) the problem of strong fluid injection into a steady, subsonic, laminar boundary-layer flow over a flat plate was studied. The problem was formulated within the triple-deck structure for asymptotic analysis of strong slot injection for large Reynolds numbers. It was found that in contrast to the supersonic case, separation occurs downstream of the slot, where a recirculating flow bubble is formed. Then in a related study by Klemp & Acrivos (1972) a rational expansion to describe the "blow-off" ("slot") region was developed. The structure of a supersonic laminar boundary layer near a flat plate under conditions of fluid injection velocity $O(\epsilon^{-3/8}U_\infty)$ over a distance of $O(L)$ was examined by Smith & Stewartson (1973) (here U_∞ is the undisturbed fluid velocity and L the length of the plate) and they found explicit expressions for the pressure variations and boundary-layer thickness using a modified form of the Cole-Aroesty model (see Cole & Aroesty (1968)). The relation between the strong injection, studied in this work, and massive injection, when the blowing velocity is of $O(U_\infty)$ was also discussed. A systematic account of more recent studies of flow separation phenomena can be found in surveys by Smith (1982) and Brown (1996).

The problem of the boundary-layer flow under conditions of interfacial mass transfer, governed by the classical Prandtl equations, the laminar boundary-layer convection-diffusion equation (1.4) and the steady heat transfer equation (1.18) was first treated by Hartnett & Eckert (1957). The system of governing equations was subject to boundary conditions taking account of foreign fluid injection (with blowing velocity $V(x,0) \neq 0$). It was shown that in the case when $V(x,0) \sim x^{-1/2}$ the system (1.4) and (1.18) admits a self-similar solution; they demonstrated that the velocity, concentration and temperature profiles are greatly influenced by either "suction" or "blowing".

We shall consider the problem of diffusion driven boundary-layer flow separation. As we wish to focus our attention upon the diffusion process we will exclude from our study one of the dominant causes for flow separation, namely the effect of an adverse pressure gradient. We therefore focus on a boundary-layer flow under conditions of interfacial mass transfer with zero pressure gradient. To overcome the inevitable difficulties connected with the presence of different scales, within which the relative importance of diffusivity to viscosity or vice versa is to be accounted for, we consider only the case of a gas–permeable surface for which $Sc = 1$; the concentration and momentum boundary layers are then of similar thickness. In contrast to the previous studies of a boundary-layer flow under conditions of intense interfacial mass transfer (see Boyadjiev *et. al.* (1996a), Halatchev & Denier (2000), Hartnett & Eckert (1957) and earlier chapters) we consider a finite mass-transfer region, this being a more realistic model of many mass-transfer (diffusion) dominated flows. The detachment of the boundary-layer flow is then a result of the shifting of fluid elements in the boundary layer far from the surface (membrane) due to the diffusion induced vertical velocity component on the surface.

We used arbitrary values for the vertical velocity component on the wall $V(x,0)$ (the rate

of "blowing") but within the weak or moderate injection description, where

$$V(x,0) = O(Re^{-1/2}/U_\infty),$$

in which case the classical boundary-layer equations hold. The blowing rates corresponding to so called strong injection, which can be loosely defined as

$$Re^{-1/2} \ll V(x,0)/U_\infty \ll 1,$$

are not considered in the present work, since the increase in the blowing rate moves the separation point upstream from the slot's leading edge, i.e. into a region where the boundary-layer equations certainly do not hold.

In this chapter we show that a concentration gradient acting within a finite region ("slot") can cause the boundary layer to separate. An appropriate discretisation scheme to deal with the discontinuities at the slot's edges and an unconditionally stable semi-implicit marching algorithm are constructed. The results from our numerical solutions will suggest that there is no Goldstein singularity at the point of separation. It is argued that for our boundary conditions the boundary layer can adjust so as to remove, or inhibit, the singularity.

We next turn our attention to the question of boundary-layer stability. An inflexion point appears in the streamwise velocity prior to the point of diffusion induced separation. Therefore the boundary-layer flow will become susceptible to the high frequency, short wavelength, instabilities known as Rayleigh waves. These waves are known to provide one route for the rapid onset of turbulence in boundary-layer flows. We will study the level of diffusion required to render the flow inviscidly unstable. The stability aspects of this flow will be considered by solving the Rayleigh pressure equation numerically, employing a global solver for complex eigenvalue problems, in order to determine the growth rate at selected streamwise locations over the slot region. This will allow us to determine the point at which the flow becomes unstable, in terms of the level of mass transfer through the slot. The ultimate aim of this study is the development of techniques which will allow for the prediction and active control of instability in the flow.

6.1 Governing equations

Let us consider the boundary-layer flow over a rigid, permeable, flat plate through which mass can diffuse due to a high concentration gradient. We pose the problem in terms of Prandtl's non-interacting boundary layer which develops when a uniform stream flows over the plate. We consider the case when the boundary-layer flow is affected by mass transfer due to a concentration gradient acting over a finite region of the plate. This concentration gradient induces a secondary flow normal to the plate and the resulting mass transfer has the effect of "blowing", or "suction", of the fluid into the flow depending upon the sign of the concentration gradient (positive for blowing, negative for suction).

Phenomenologically, we should formulate some terms relating to the geometry of our problem. By the word "slot" we shall understand the region of the plate where diffusion is active (the concentration driving force is active), x_{le} will denote the x-coordinate of the leading edge of the slot and x_{te} the x-coordinate of the trailing edge of the slot. A schematic of the geometry under consideration is shown in Figure 6.1.

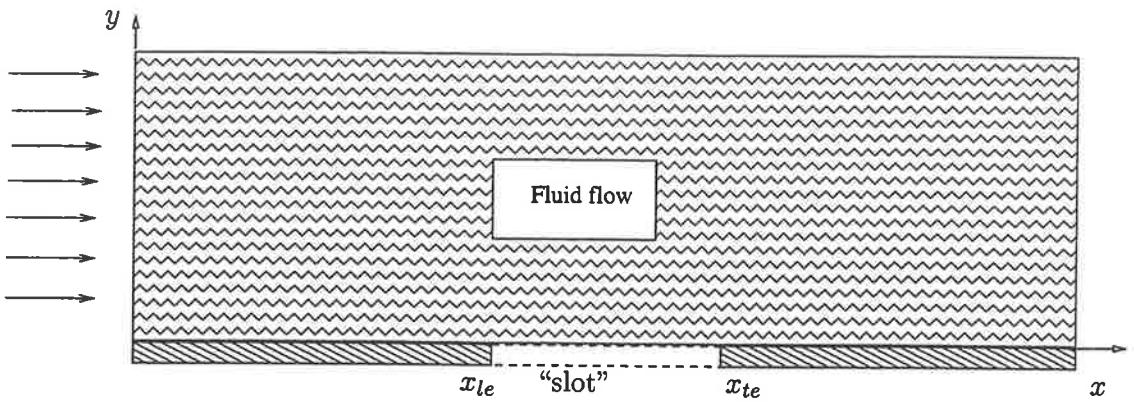

Figure 6.1: Schematic of the flow in a boundary layer over a finite region of permeable surface.

The basic flow and concentration fields are governed by the Navier-Stokes equations for a two-dimensional, incompressible, steady flow and the steady convection-diffusion equation which, in non-dimensional form, are

$$\nabla \cdot \mathbf{u} = 0, \tag{6.3a}$$

$$(\mathbf{u} \cdot \nabla)\mathbf{u} = -\nabla P_0 + \frac{1}{Re}\nabla^2 \mathbf{u}, \tag{6.3b}$$

$$(\mathbf{u} \cdot \nabla)C_0 = \frac{1}{ScRe}\nabla^2 C_0, \tag{6.3c}$$

where $\mathbf{u} = (U_0, V_0)$, $Re = U_\infty L/\nu$ is the Reynolds number, $Sc = \nu/D$ is the Schmidt number, ν the kinematic viscosity, C_0^* the concentration at the solid surface, C_∞^* the concentration of the species in the free-stream, ρ_0^* the density of the transfered substance and $\theta = M(C_0^* - C_\infty^*)/\rho_0^*$ is the mass-transfer parameter as defined in Chapter 2. Here we have non-dimensionalised all lengths with respect to a typical length scale L (a suitable choice being the distance from the leading edge of the plate to the slot), all velocities with respect to the free-stream speed U_∞ and the concentration with respect to the concentration difference $C_0^* - C_\infty^*$. The system (6.3) must be solved subject to the following initial and boundary conditions:

$$\begin{aligned}
&\mathbf{u} = (1,0),\ C_0 = 1 \ \text{ at } \ x = 0;\\
&U_0 = 0,\ C_0 = 1,\ V_0 = \begin{cases} 0 & \text{for } x \le x_{le} \\ \theta(Sc\,Re)^{-1} C_{0y} & \text{for } x_{le} < x < x_{te} \ \text{ on } \ y = 0; \\ 0 & \text{for } x \ge x_{te} \end{cases}\\
&U_0 \to 1,\ C_0 \to 0 \ \text{ as } \ y \to \infty.
\end{aligned} \tag{6.4}$$

Note that outside the slot the usual no-slip boundary condition is imposed.

6.1.1 The basic boundary-layer flow

In the limit $Re \to \infty$ the flow develops a boundary layer of thickness $O(Re^{-1/2})$ attached to the leading edge of the plate. We therefore introduce the boundary-layer variables

$$y = Re^{-1/2}Y,\ U_0 = U_B,\ V_0 = Re^{-1/2}V_B,\ C_0 = C_B, P_0 = P_B.$$

The full Navier-Stokes equations reduce to the classical boundary-layer equations coupled to a concentration equation which describes the change in the species concentration within the boundary layer:

$$\frac{\partial U_B}{\partial x} + \frac{\partial V_B}{\partial Y} = 0, \tag{6.5a}$$

$$U_B\frac{\partial U_B}{\partial x} + V_B\frac{\partial U_B}{\partial Y} = \frac{\partial^2 U_B}{\partial Y^2}, \tag{6.5b}$$

$$\frac{\partial P_B}{\partial Y} = 0, \tag{6.5c}$$

$$U_B\frac{\partial C_B}{\partial x} + V_B\frac{\partial C_B}{\partial Y} = \frac{1}{Sc}\frac{\partial^2 C_B}{\partial Y^2}, \tag{6.5d}$$

together with boundary conditions

$$U_B = 0,\ C_B = 1,\ V_B = \begin{cases} 0 & \text{for } x \le x_{le} \\ -\theta Sc^{-1}C_{BY} & \text{for } x_{le} < x < x_{te} \text{ on } Y = 0; \\ 0 & \text{for } x \ge x_{te} \end{cases} \tag{6.6}$$

$$U_B \to 1,\ C_B \to 0 \text{ as } Y \to \infty.$$

In order to focus upon the fundamental problem of diffusion induced separation, and not upon effects such as the relative importance of diffusivity compared to viscosity (as is measured by the Schmidt number Sc) we will take $Sc = 1$ in what follows.

6.1.2 The linear stability of the flow

When the effects of viscosity are negligible, that is the term consisting of the Reynolds number in the Orr-Sommerfeld equation is sufficiently large or the fluid is practically inviscid (this is the case in our study) the Orr-Sommerfeld type equation (4.9a) reduces to the Rayleigh equation (see Drazin & Reid (1981)).

To study the inviscid instability of the boundary-layer flow we let

$$(U, V, P, C) = (U_0, V_0, P_0, C_0) + \epsilon(u, v, p, c) + O(\epsilon^2),$$

where (U, V, P) is the total flow field, (U_0, V_0, P_0, C_0) the basic boundary-layer flow, (u, v, p, c) the disturbance velocity, pressure and concentration fields. On substituting

this into the full system of Navier-Stokes equations coupled to the convection-diffusion equation (2.1) and neglecting terms of $O(\epsilon^2)$, we then obtain the linearised equations (5.1).

We focus our attention on inviscid waves within the boundary layer, in which case the disturbances have the following form:

$$\begin{aligned} u(x,t) &= \hat{u}(Y)\exp[i\alpha Re^{1/2}(x-\omega t)], \\ v(x,t) &= \hat{v}(Y)\exp[i\alpha Re^{1/2}(x-\omega t)], \\ p(x,t) &= \hat{p}(Y)\exp[i\alpha Re^{1/2}(x-\omega t)], \\ c(x,t) &= \hat{c}(Y)\exp[i\alpha Re^{1/2}(x-\omega t)], \end{aligned} \tag{6.7}$$

where $\hat{u}$ and $\hat{v}$ are the amplitudes of the velocity of the disturbances, $\hat{p}$ the disturbance pressure amplitude and $\hat{c}$ the disturbance concentration amplitude; α and ω are respectively the wavenumber and wave-speed.

Substituting the expressions (6.7) into system (5.1), and transforming the boundary-layer coordinate $Y = Re^{-1/2}y$, we obtain the following system of differential equations:

$$i\alpha\hat{u} + \frac{\partial\hat{v}}{\partial Y} = 0, \tag{6.8a}$$

$$i\alpha(U_B-\omega)\hat{u} + \hat{v}\frac{\partial U_B}{\partial Y} = -i\alpha\hat{p}, \tag{6.8b}$$

$$i\alpha(U_B-\omega)\hat{v} = -\frac{\partial\hat{p}}{\partial Y}, \tag{6.8c}$$

$$-i\alpha(U_B-\omega)\hat{c} + \hat{v}\frac{\partial C_B}{\partial Y} = 0, \tag{6.8d}$$

subject to the boundary conditions

$$\hat{v}(0) = 0;\ \hat{v}\to 0 \ \text{ as } \ Y\to\infty. \tag{6.9}$$

We should note that the momentum and continuity equations are decoupled from the concentration equation and hence, we will omit it in our analysis. From (6.8d)

$$\hat{c} = \frac{i\hat{v}}{\alpha(U_B-\omega)}\frac{\partial C_B}{\partial Y} \tag{6.10}$$

which therefore satisfies

$$\hat{c}(0) = 0;\ \hat{c}\to 0 \ \text{ as } \ Y\to\infty.$$

Thus once $\hat{u}$ and $\hat{v}$ are determined the concentration disturbance field can simply be calculated from (6.10).

It is convenient to introduce a stream function $\varphi(x,Y,t)$ such that

$$\hat{u} = \frac{\partial\varphi}{\partial Y},\quad \hat{v} = -i\alpha\varphi.$$

Upon eliminating the disturbance pressure amplitude $\hat{p}$ in system (6.8) we obtain the classical Rayleigh equation

$$(U_B - \omega)(\varphi'' - \alpha^2\varphi) - U_B''\varphi = 0, \tag{6.11}$$

subject to the boundary conditions

$$\varphi(0) = 0; \;\; \varphi(\infty) = 0. \tag{6.12}$$

Here U_B is the basic velocity component, i.e. the solution of the system (6.5) with the boundary condition (6.6), α is a non-dimensionalised wavenumber, ω is the corresponding wave-speed and φ is the amplitude of the disturbance stream function.

Rayleigh equation (6.11) is the vorticity equation of the disturbance. Together with its boundary conditions (6.12) it defines the basic eigenvalue problem for our boundary-layer flow leading to an eigenvalue relation of the form

$$\mathcal{F}(\alpha, \omega) = 0.$$

6.2 Numerical analysis

In this section we shall discuss the numerical algorithms and finite difference scheme used to solve the problems described in the previous section.

6.2.1 Semi-implicit Crank-Nicholson scheme

The system of equations (6.5) with inhomogeneous boundary conditions (6.6) cannot be solved in self-similar form. We must therefore solve this system of parabolic partial differential equations using a numerical scheme that, given some suitable initial conditions, allows us to obtain the solution in the streamwise (x) direction. To facilitate this, and also to adequately account for boundary-layer growth, we employ the Levy-Lees transformation (see Blottner (1975))

$$\xi(x) = x, \;\; \eta(x, Y) = \frac{Y}{x^{1/2}}. \tag{6.13}$$

In this case system (6.5) is transformed to

$$\begin{aligned}
&2\xi\frac{\partial U_B}{\partial \xi} - \eta\frac{\partial U_B}{\partial \eta} + 2\xi^{1/2}\frac{\partial V_B}{\partial \eta} = 0, \\
&2\frac{\partial^2 U_B}{\partial \eta^2} - 2\xi U_B\frac{\partial U_B}{\partial \xi} + \eta U_B\frac{\partial U_B}{\partial \eta} - 2\xi^{1/2}V_B\frac{\partial U_B}{\partial \eta} = 0, \\
&\frac{2}{Sc}\frac{\partial^2 C_B}{\partial \eta^2} - 2\xi U_B\frac{\partial C_B}{\partial \xi} + \eta U_B\frac{\partial C_B}{\partial \eta} - 2\xi^{1/2}V_B\frac{\partial C_B}{\partial \eta} = 0.
\end{aligned} \tag{6.14}$$

This system can be further simplified by introducing new dependent variables

$$F = U_B,\ V = -\frac{1}{2}\eta F + \xi^{1/2} V_B,\ G = C_B, \tag{6.15}$$

to give

$$2\xi\frac{\partial F}{\partial \xi} + 2\frac{\partial V}{\partial \eta} + F = 0, \tag{6.16a}$$

$$\frac{\partial^2 F}{\partial \eta^2} - \xi F\frac{\partial F}{\partial \xi} - V\frac{\partial F}{\partial \eta} = 0, \tag{6.16b}$$

$$\frac{1}{Sc}\frac{\partial^2 G}{\partial \eta^2} - \xi F\frac{\partial G}{\partial \xi} - V\frac{\partial G}{\partial \eta} = 0. \tag{6.16c}$$

Under this transformation the boundary conditions (6.6) reduce to

$$F = 0,\ G = 1,\ V = \begin{cases} 0 & \text{for } \xi \le \xi_{le} \\ -\theta Sc^{-1} G_\eta & \text{for } \xi_{le} < \xi < \xi_{te} \text{ on } \eta = 0; \\ 0 & \text{for } \xi \ge \xi_{te} \end{cases} \tag{6.17}$$
$$F \to 1,\ G \to 0 \text{ as } \eta \to \infty.$$

As system (6.16) is parabolic in ξ we must supply appropriate initial conditions in order to start the numerical solution. Setting $\xi = 0$ in (6.16), and the boundary conditions (6.17), and defining

$$F(\eta) = f'(\eta),\ V(\eta) = -\frac{1}{2}f(\eta),\ G(\eta) = g(\eta), \tag{6.18}$$

we find that f and g are solutions of

$$f''' + \frac{1}{2}ff'' = 0,\ g'' + \frac{Sc}{2}g'f = 0 \tag{6.19}$$

subject to the boundary conditions:

$$f(0) = 0,\ f'(0) = 0,\ g(0) = 1; \tag{6.20}$$
$$f'(\infty) = 1,\ g(\infty) = 0.$$

Thus the initial condition is taken to be a solution of the Blasius equation for f, together with the solution of the concentration equation for g. This system was solved using a standard fourth-order Runge-Kutta quadrature routine coupled with Newton iteration to determine the values $f''(0)$ and $g'(0)$ for which the boundary conditions (6.20) are satisfied. We note at this point that there is no coupling between the concentration and momentum fields at the start of our numerical integration. This is due to the fact that, in applying the boundary condition $f(0) = 0$, we are implicitly assuming that the region of active diffusion (that is, the slot position) is within the region $\xi > 0$ (i.e. $\xi_{le} > 0$ in (6.17)). For completeness solutions of system (6.19) with boundary conditions (6.20) are presented in Figure 6.2.

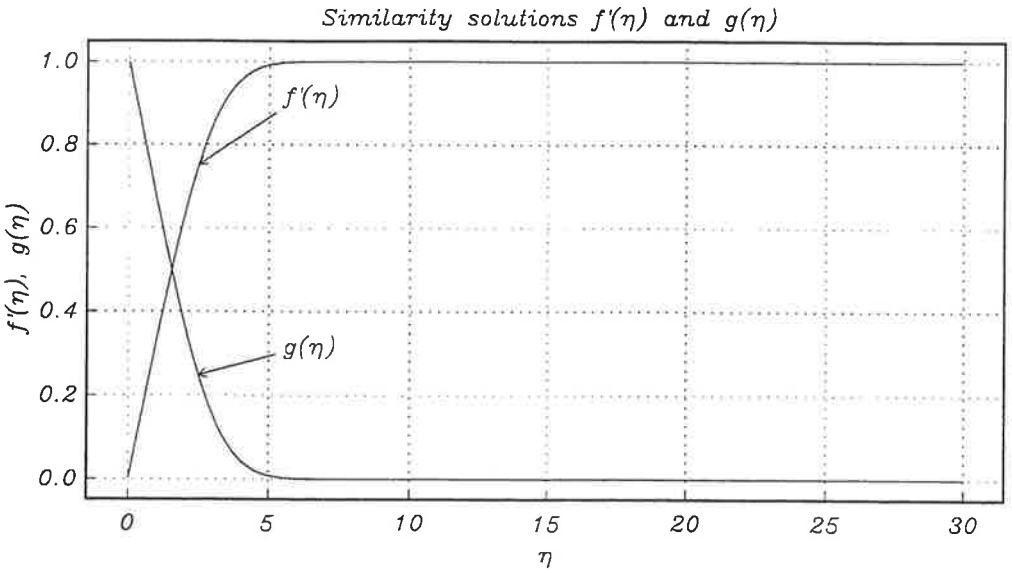

Figure 6.2: Graphs of $f'(\eta)$ and $g(\eta)$ versus η, for the case of no diffusion (i.e. $\theta = 0$ upstream of the "slot" region).

In order to solve (6.16) - (6.17) numerically we apply a semi-implicit Crank-Nicholson scheme which is unconditionally stable and second-order accurate in $\Delta\xi$ (see Fletcher (1988) for details). In order to achieve second-order accuracy in ξ, the Crank-Nicholson scheme requires a second-order treatment of the non-linear convection terms. This will be achieved by iteration at each downstream location.

We employ the following uniform-grid, finite-difference discretisation

$$\begin{aligned}
\frac{\partial F}{\partial \xi} &= \frac{1}{\Delta\xi}(F_j^{n+1} - F_j^n), \\
\frac{\partial F}{\partial \eta} &= \frac{1}{4\Delta\eta}\left[(F_{j+1}^n - F_{j-1}^n) - (F_{j+1}^{n+1} - F_{j-1}^{n+1})\right], \\
\frac{\partial^2 F}{\partial \eta^2} &= \frac{1}{2\Delta\eta^2}\left[(F_{j-1}^n - 2F_j^n + F_{j+1}^n) + (F_{j-1}^{n+1} - 2F_j^{n+1} + F_{j+1}^{n+1})\right],
\end{aligned} \tag{6.21}$$

where j denotes the jth grid point in the η-direction and n the nth grid point in the ξ-direction. Similar expressions hold for the derivatives of G.

To linearise the system for F^{n+1}, V^{n+1} and G^{n+1}, to reduce storage requirements, and to require only one level of initial data, the undifferentiated velocity components F and V are extrapolated using $F_j^{n+1} = F_j^n + O(\Delta\xi)$ and $V_j^{n+1} = V_j^n + O(\Delta\xi)$. In order to achieve second-order accuracy we must iterate at each downstream location; that is, the system of equations is solved repeatedly and the iteration is terminated when the solutions F_j^{k+1}, G_j^{k+1}, V_j^{k+1} do not differ from F_j^k, G_j^k, V_j^k in the sense of some initially prescribed tolerance, which in our case was set to be 10^{-7}. In order to start the iteration we set $F_j^k = F_j^n$. Convergence of the kth iteration yields the solution at the $(n+1)$th ξ-step whereupon we set $F^{n+1} = F^{k+1}$.

Applying this scheme to the system (6.16) and its boundary conditions (6.17) reduces the momentum and concentration equations and their boundary conditions to *momentum equation*:

$$a_j^k F_{j-1}^{k+1} + b_j^k F_j^{k+1} + c_j^k F_{j+1}^{k+1} = d_j^k, \tag{6.22}$$

subject to the boundary conditions

$$F_0^{k+1} = 0,\ F_{jmax+1}^{k+1} = 1,$$

where

$$\begin{aligned}
a_j^k &= \frac{1}{2}\left(1 + \frac{1}{2}\Delta\eta V_j^k\right), \\
b_j^k &= -1 - \frac{\xi^{n+1}}{\Delta\xi}\Delta\eta^2 F_j^k, \\
c_j^k &= \frac{1}{2}\left(1 - \frac{1}{2}\Delta\eta V_j^k\right), \\
d_j^k &= -\frac{1}{2}\left(F_{j-1}^k - 2F_j^k + F_{j+1}^k\right) + \frac{1}{4}\Delta\eta V_j^k\left(F_{j+1}^k - F_{j-1}^k\right) - \frac{\xi^{n+1}}{\Delta\xi}\Delta\eta^2 (F_j^n)^2,
\end{aligned}$$

and *concentration equation*:

$$p_j^k G_{j-1}^{k+1} + q_j^k G_j^{k+1} + r_j^k G_{j+1}^{k+1} = w_j^k, \tag{6.23}$$

with its boundary conditions

$$G_0^{k+1} = 1,\ G_{jmax+1}^{k+1} = 0,$$

where

$$\begin{aligned}
p_j^k &= \frac{1}{2}\left(\frac{1}{Sc} + \frac{1}{2}\Delta\eta V_j^k\right), \\
q_j^k &= -\frac{1}{Sc} - \frac{\xi^{n+1}}{\Delta\xi}\Delta\eta^2 F_j^{n+1}, \\
r_j^k &= \frac{1}{2}\left(\frac{1}{Sc} - \frac{1}{2}\Delta\eta V_j^k\right), \\
w_j^k &= -\frac{1}{2}\left(G_{j-1}^k - 2G_j^k + G_{j+1}^k\right) + \frac{1}{4}\Delta\eta V_j^n\left(G_{j+1}^k - G_{j-1}^k\right) - \frac{\xi^{n+1}}{\Delta\xi}\Delta\eta^2 F_j^{n+1} G_j^n.
\end{aligned}$$

The resulting tri-diagonal systems of equations can be solved by using a Thomas algorithm, repeatedly solving the equations by applying the iteration procedure described above. Once F_j^{n+1} and G_j^{n+1} are available, V_j^{n+1} is obtained by integrating the *equation of continuity* (6.16a) using

$$V_j^{k+1} = V_{j-1}^{k+1} - s_j(F_j^{k+1} + F_{j-1}^{k+1}) + t_j, \tag{6.24}$$

where

$$s_j = \Delta\xi\left(\frac{1}{4}+\frac{\xi^{n+1/2}}{\Delta\xi}\right),$$
$$t_j = -\Delta\eta\left(\frac{1}{4}-\frac{\xi^{n+1/2}}{\Delta\xi}\right)\left(F_j^k+F_{j-1}^k\right)-\left(V_j^k-V_{j-1}^k\right),$$

with $\xi^{n+1/2} = \xi^n + 1/2\Delta\xi$ and $V_0^{n+1} = -\theta_1 Sc^{-1}(-3+4G_1^{n+1}-G_2^{n+1})$. Here θ_1 denotes the value of the discretised mass-transfer parameter θ (see below) at the first grid point. The combination of (6.22), (6.23) and (6.24) is unconditionally stable (in the von Neumann sense), robust and efficient; it must be supplemented by a one-level initial condition to start the marching in the streamwise direction (full details can be found in Fletcher (1988)). When $n = 1$ we take F, G and V to be given by the solution of (4.4) and (4.5). Because of the anticipated boundary-layer separation we chose a relatively small step-size in the ξ-direction ($\Delta\xi = 10^{-6}$), the step-size in the wall normal direction being $\Delta\eta = 0.01$, with typically 3000 points in vertical direction. The criteria for convergence at each downstream iteration was set to be $||F_j^{k+1} - F_j^k|| < 10^{-7}$, where $||F_j^{k+1} - F_j^k|| = \sum_{j=1}^{N}(F_j^{k+1} - F_j^k)^2$.

We now turn our attention to the treatment of the mass-transfer parameter θ. In order to model a finite region of diffusion (that is, a "slot") and to avoid any discontinuities at the slots' edges we choose a form for θ that is piecewise continuous in ξ. Thus,

$$\theta(\xi) = \begin{cases} 0 & \text{for } \xi < 1 \\ \epsilon^{-1}\vartheta(\xi-\xi_{le}) & \text{for } 1 \le \xi \le 1+\epsilon \\ \vartheta & \text{for } 1+\epsilon < \xi < 1+\epsilon+l \\ -\epsilon^{-1}\vartheta(\xi-\xi_{le}-2\epsilon-l) & \text{for } 1+\epsilon+l \le \xi \le 1+2\epsilon+l \\ 0 & \text{for } \xi > 1+2\epsilon+l \end{cases}, \tag{6.25}$$

where ξ_{le} is the ξ-coordinate of the slots leading edge, ϵ is a smoothing parameter, l is the length of the slot, and ϑ is the actual magnitude of the mass-transfer parameter θ. A schematic of this slot configuration is given in Figure 6.3. Other forms for this finite region of diffusion were also used. However, the results obtained were qualitatively similar to those for the piecewise continuous profile (6.25); we therefore concentrate our discussion on "slot diffusion" as modelled by (6.25). This model avoids the ellipticity in the flow equations which is usually encountered at the leading edge as has been demonstrated in studies by Stewartson (1974), Smith (1982), Roy (2000) and presents a reasonable description for a real, finite extent permeable membrane.

In order to monitor the behaviour of the boundary-layer flow we calculate, at each streamwise location, the skin-friction coefficient given by

$$c_f = \frac{1}{\xi^{1/2}}\left(\frac{\partial F}{\partial \eta}\right)_{\eta=0}.$$

In discretised form this becomes, using a one-sided, second-order accurate difference formula

$$c_f = \frac{0.5}{\xi^{1/2}\Delta\eta}(4F_1^{n+1} - F_2^{n+1}).$$

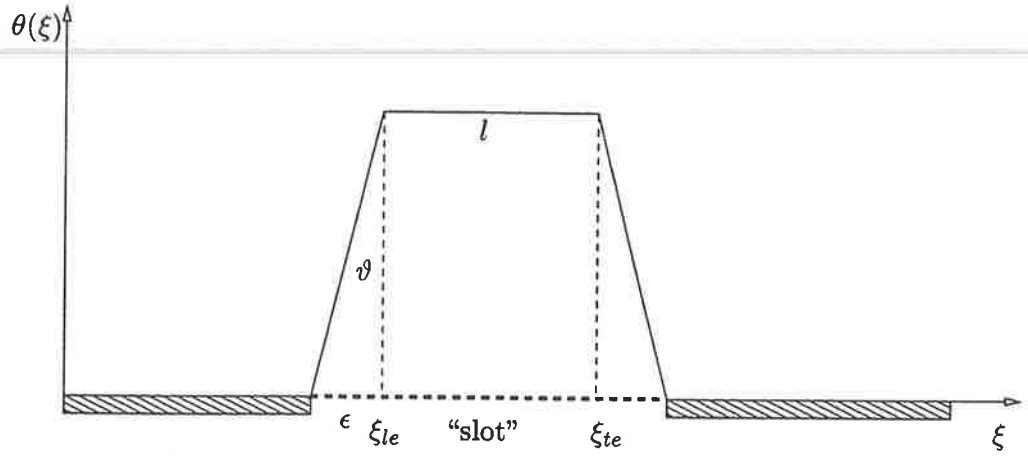

Figure 6.3: Schematic representation of a "slot" and the mass-transfer parameter $\theta(\xi)$.

The point of boundary-layer separation $\xi_s(x_s)$ is defined by the condition $c_f = 0$ at $\xi = \xi_s$.

6.2.2 Diffusion induced flow instability

We will solve the Rayleigh equation (6.11) numerically by employing a finite-difference approach. In order to do this we must introduce the new dependent variables (6.15) into the Rayleigh equation (6.11) with the result that, at each streamwise location, the stability of the flow is governed by

$$(F - \omega)(\varphi'' - \alpha^2\varphi) - F''\varphi = 0. \tag{6.26}$$

Focusing our attention on the temporal stability problem, where the wavenumber α is real and wave-speed ω is complex we can rewrite equation (6.26) in the form

$$F\varphi'' - (F\alpha^2 + F'')\varphi = \omega(\varphi'' - \alpha\varphi). \tag{6.27}$$

The appropriate set of boundary conditions is simply $\varphi(0) = 0$ and $\varphi(\infty) = 0$. On infinite domains, we note that $F'' \to 0$ (indeed, is asymptotically small as $\eta \to \infty$) so that (6.26) reduces to

$$\varphi''_\infty - \alpha^2\varphi_\infty = 0. \tag{6.28}$$

The boundary condition $\varphi \to 0$ as $\eta \to \infty$ can then be replaced by the more computationally convenient Robin type boundary condition $\varphi' = -\alpha\varphi$.

Approximating φ' and φ'' at the ith node using second-order centred finite differences allows us to replace the equation (6.27) and its boundary conditions with the finite-difference equation

$$\begin{aligned} F_i\varphi_{i-1} - [2U_i + \Delta\eta^2(F_i\alpha^2 + F_i'')]\varphi_i + F_i\varphi_{i+1} \\ = \omega[\varphi_{i-1} - (2 + \alpha^2\Delta\eta^2)\varphi_i + \varphi_{i+1}], \end{aligned} \tag{6.29}$$

where φ_i is the value of the complex function φ at η_i. We used a uniform grid with nodes at η_i, $i = 0, \ldots, N$. In order to satisfy $\varphi(0) = 0$ we set $\varphi_0 = 0$ and the boundary condition at infinity is satisfied by writing $(\varphi_N - \varphi_{N-2})/2\Delta\eta = -\alpha\varphi_{N-1}$ or $\varphi_N = -2\alpha\Delta\eta\varphi_{N-1} + \varphi_{N-2}$. Collecting the values of φ_i $(i = 1, \ldots, N-1)$ into the vector $\boldsymbol{\varphi} = (\varphi_1, \varphi_2, \ldots, \varphi_{N-2}, \varphi_{N-1})$ we can rewrite equation (6.29) in the following matrix form

$$\mathbf{A}\boldsymbol{\varphi} = \omega\mathbf{B}\boldsymbol{\varphi}, \tag{6.30}$$

where $\mathbf{A}$ and $\mathbf{B}$ are square tri-diagonal matrices of size $(N-1) \times (N-1)$ whose structure is readily seen from finite-difference equation (6.29). The structure of the matrices $\mathbf{A}$ and $\mathbf{B}$ is given in Appendix A.6.

Equation (6.30) presents a complex generalised eigenvalue problem for determining the eigenvalues ω and eigenvectors φ at a given wavenumber α. The solution provides a spectrum of $N-1$ eigenvalues. We are interested in the eigenvalues ω with the maximum growth rate $\mathrm{Im}(\sigma)$, where $\sigma = \alpha\omega$, i.e. the first, most unstable, modes.

The complex generalised eigenvalue problem (6.30), where $\mathbf{A}$ and $\mathbf{B}$ are real, square matrices and ω is complex was solved using the QZ algorithm (see Golub & van Loan (1982), Kerner (1989) for details).

6.3 Skin friction

In order to determine the significance of diffusion (that is mass transfer) in inducing separation we first consider the case of slot-injection. In this case we ignore the coupling between the momentum and concentration equations and simply impose a prescribed level of blowing through the finite slot. In the similar study by Roy (2000), a steady non-similar compressible laminar boundary-layer flow over a yawed infinite circular cylinder with nonuniform injection (suction) was studied, where mass injection (suction) occurs in a small porous section of the body surface. The discontinuities at the leading and trailing edges of the slot for the uniform injection (suction) were removed by choosing appropriate nonuniform mass-transfer distribution in the slot as has been done in our study. In Figures 6.4 - 6.5 the scaled skin-friction coefficient $\xi^{1/2}c_f$ is plotted as a function of the streamwise coordinate ξ, for different blowing rates ϑ, for two case studies: slot located upstream and downstream respectively ($\xi_{le} = 2$ and $\xi_{le} = 200$). It was found in our study that an increase in the blowing velocity of the nonuniform slot injection moves the point of separation upstream, which is in agreement with the results obtained by Roy (2000). It is seen from Figures 6.4 and 6.5 that in the case of passive slot-injection ("blowing") through a slot into the boundary layer, the flow separation is easily achieved, both upstream and far-downstream, at relatively "moderate" rates of "blowing", $V(\xi, 0) = 5$ and $V(\xi, 0) = 10$ upstream and downstream respectively.

The results from the problem above (passive blowing) now provide a benchmark against which the effect of diffusion on the separation process can be quantified (Figures 6.6 and 6.7). We studied two cases, the "slot" located upstream ($\xi_{le} = 2$) and far-downstream

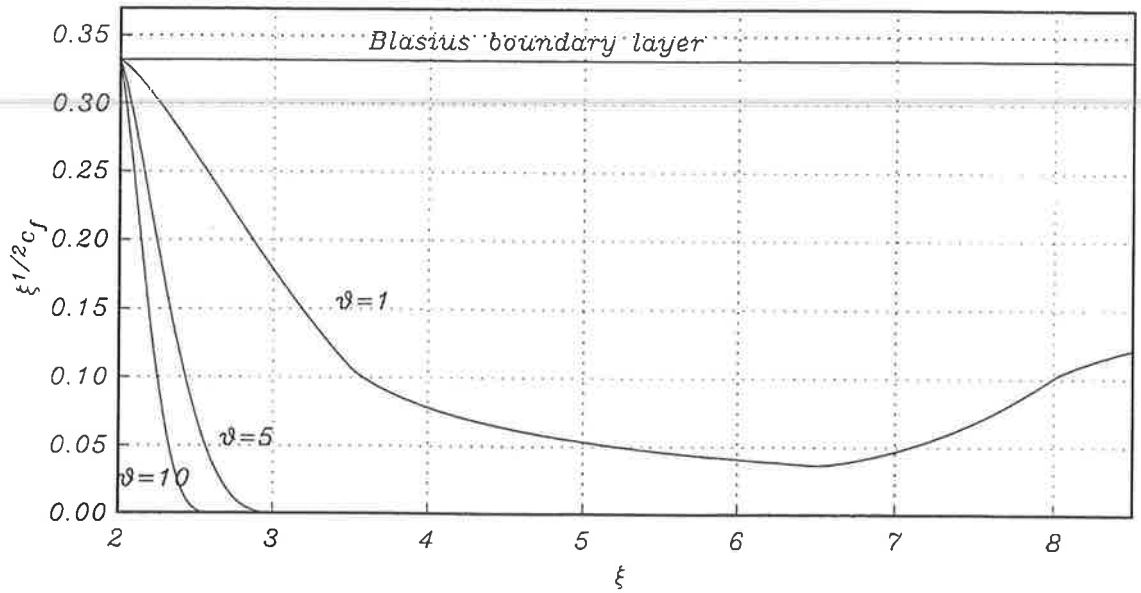

Figure 6.4: The scaled skin-friction coefficient as a function of ξ, for the case of slot-injection at $\xi_{le} = 2$, $l = 3$ and $\epsilon = 1.5$ for different values of the "blowing" velocity.

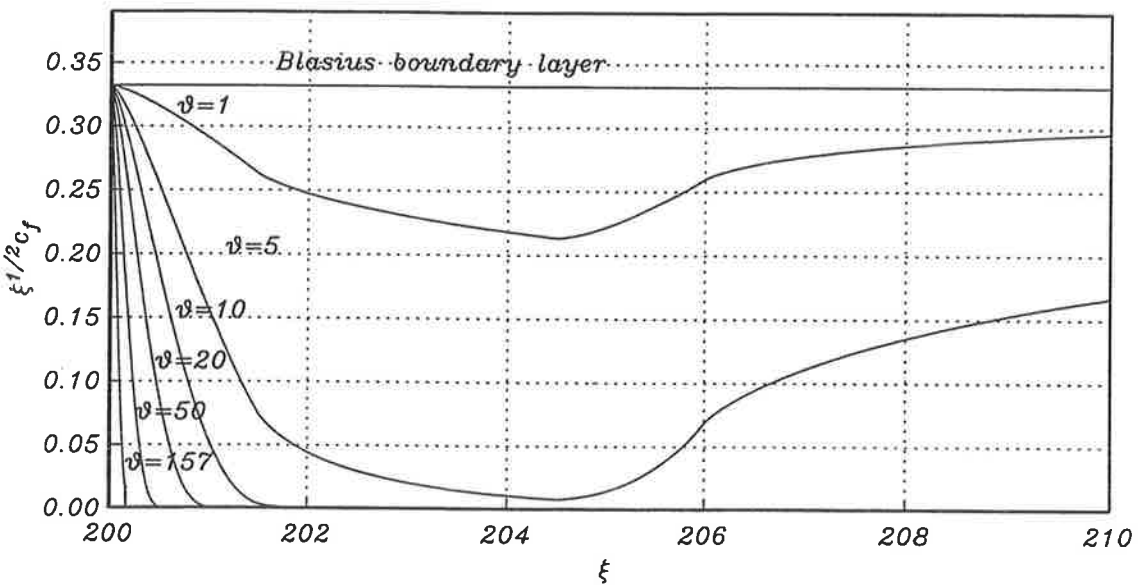

Figure 6.5: The scaled skin-friction coefficient as a function of ξ, for the case of slot-injection at $\xi_{le} = 200$, $l = 3$ and $\epsilon = 1.5$ for different values of the "blowing" velocity.

($\xi_{le} = 200$) for a slot with length $l = 3$ and a smoothing parameter $\epsilon = 1.5$. Using the point of vanishing skin friction as a criteria for separation the skin-friction coefficient graphs have been obtained for fixed Schmidt number $Sc = 1$ (corresponding to a gas–permeable surface system). The scaled skin-friction coefficient as a function of the streamwise coordinate ξ is plotted in Figures 6.6 and 6.7 for different values of the magnitude ϑ of the mass-transfer parameter θ.

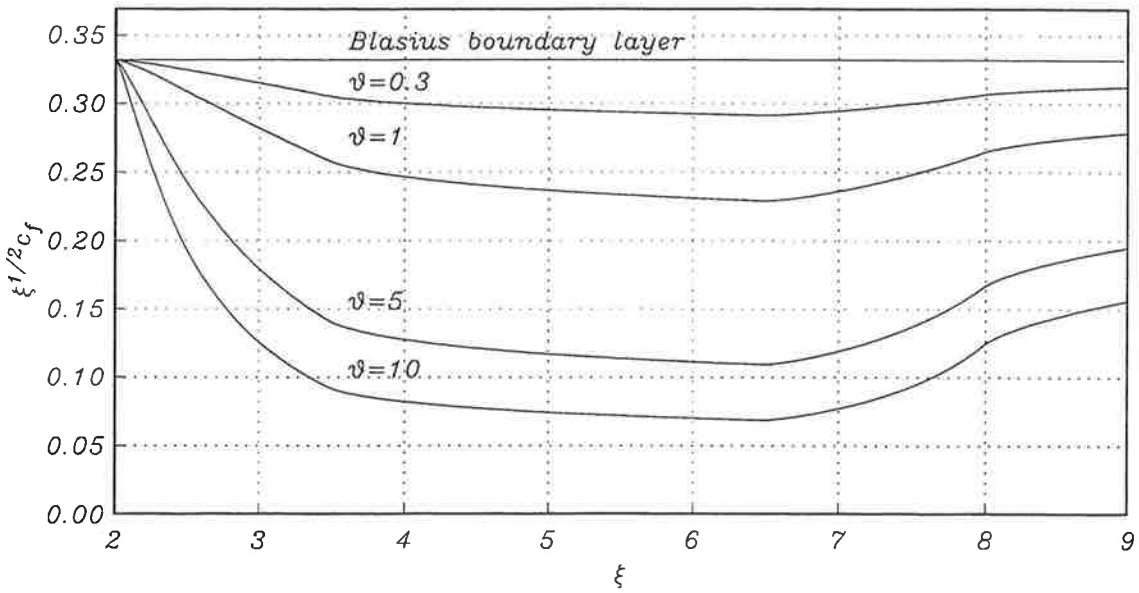

Figure 6.6: The scaled skin-friction coefficient as a function of ξ, for the case of diffusion driven flow at $\xi_{le} = 2$, $l = 3$ and $\epsilon = 1.5$ for different values of ϑ, the magnitude of the mass-transfer parameter θ.

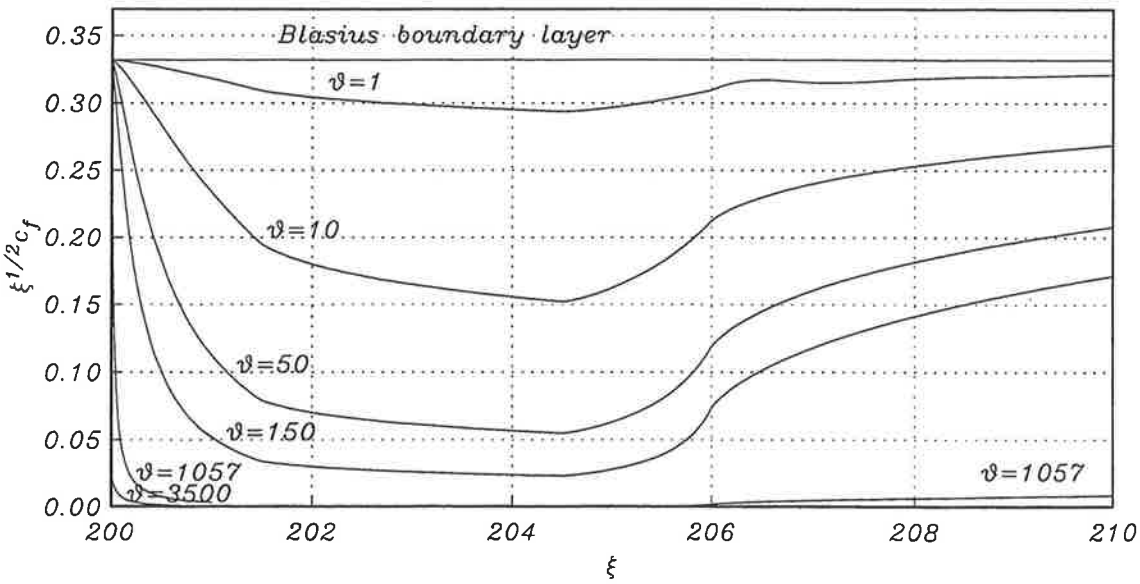

Figure 6.7: The scaled skin-friction coefficient as a function of ξ, for the case of diffusion driven flow at $\xi_{le} = 200$, $l = 3$ and $\epsilon = 1.5$ for different values of ϑ, the magnitude of the mass-transfer parameter θ.

When the diffusion region is located upstream, the results presented in Figure 6.6 show that boundary-layer flow separation is unachievable within the mass-transfer parameter interval we used in our calculations. The scaled skin friction coefficient decreases with an increase of the mass-transfer level over the region of active diffusion but once past

the trailing edge of the slot it starts recovering towards the Blasius value. In the case where the diffusion region is located far-downstream, it is seen from Figure 6.7 that flow separation can occur at high levels of mass transfer; in terms of its magnitude this occurs at $\vartheta = 3500$. However this value is a very large and unrealistic value for industrial diffusion processes.

Comparing the results from the passive blowing study with those from diffusion induced separation we notice that in the case of slot-injection an increase in the level of mass transfer (i.e. the mass-transfer parameter ϑ) moves the point of separation upstream. Although very large levels of mass transfer are necessary to achieve separation, in the case of diffusion driven boundary-layer flows an analogous effect is observed. It is clearly seen that in the case of simple slot-injection separation occurs at lower values of the vertical velocity $V(\xi, 0)$ ($V(\xi, 0) = \theta(\xi)$) than in the case of the diffusion induced separation. For instance, in the case where the slot's leading edge is at streamwise location $\xi = 2$ for slot injection boundary-layer flow, separation occurs at $\vartheta = 5$, while for diffusion driven separation at this value of the magnitude of the mass-transfer parameter the scaled skin friction is only mildly effected. This phenomena can be explained by noting the different mechanism of "blowing" in the case of non-linear mass transfer over a finite slot. Here the "blowing" velocity is not prescribed as in the case of slot-injection. In the diffusion problem the boundary-layer equations (6.16a,b) are coupled with the convection-diffusion equation (6.16c) through the boundary condition for the vertical velocity on $\eta = 0$ over the slot. In order to calculate the "blowing" velocity the convection-diffusion equation (6.16c) must be solved at each streamwise location, the concentration and the velocity fields affect each other and this interaction serves to allow the boundary-layer flow to adjust, so as to inhibit separation.

The "blowing" velocity $V(\xi, 0)$ as a function of the streamwise ξ-coordinate at different mass-transfer rates ϑ are shown in Figures 6.8 and 6.9, for the diffusion driven flow. Here we find large velocity gradients at the leading edge of the "slot", thereafter the vertical velocity at the wall rapidly relaxes to a moderate value at the trailing edge.

We can make some comments on trends which appear in our results. Generally speaking, increasing the mass-transfer parameter θ for a fixed slot length shifts the separation point from the vicinity of the trailing edge to that of the leading edge of the mass-transfer region. Different lengths of this region have also been explored. One such result is presented in Figure 6.10. Here it is evident that increasing the slot length (in this case $l = 30$) causes flow separation to occur at lower values of the mass-transfer parameter.

It is interesting to see from Figure 6.11 that the boundary layer far-downstream recovers the form of the classical Blasius flat plate flow (i.e. the skin friction recovers to that of the classical Blasius one $c_f \propto 1/\xi^{1/2}$).

The absence of a pressure gradient and the fact that the concentration is unknown suggests that the boundary-layer flow does not encounter the classical Goldstein singularity at the point of separation. This can be attributed to the boundary conditions which allow the flow to adjust so to remove, or inhibit, the singularity. This conclusion is in general agreement with Catherall & Mangler (1966) who demonstrated that if the pres-

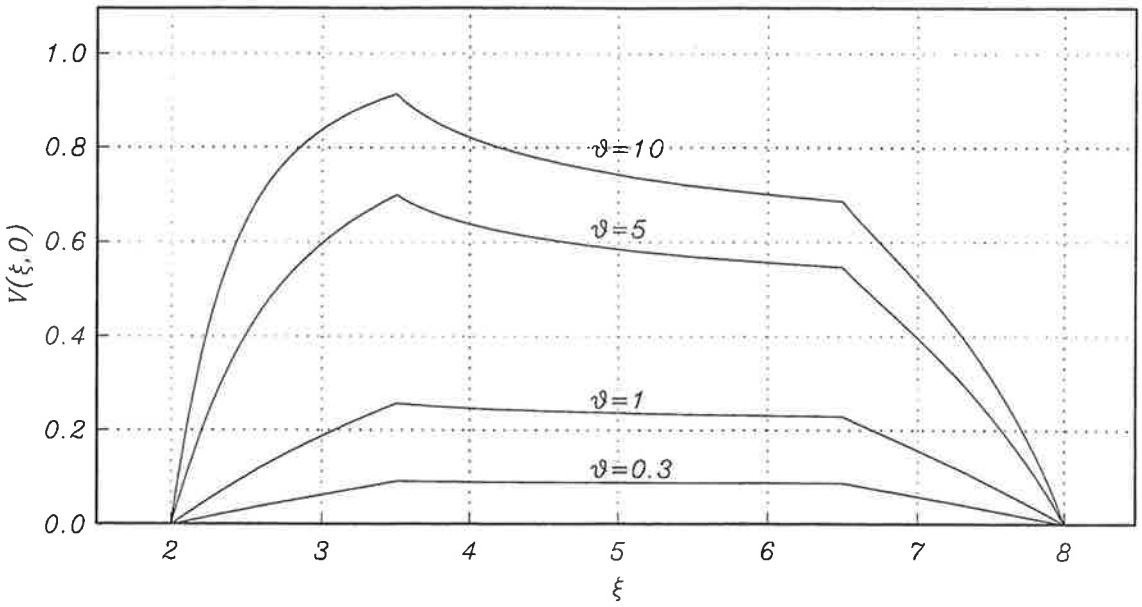

Figure 6.8: The vertical velocity $V(\xi, \eta)$ at the permeable surface ($\eta = 0$), for the case of diffusion driven flow at $\xi_{le} = 2$, $l = 3$ and $\epsilon = 1.5$.

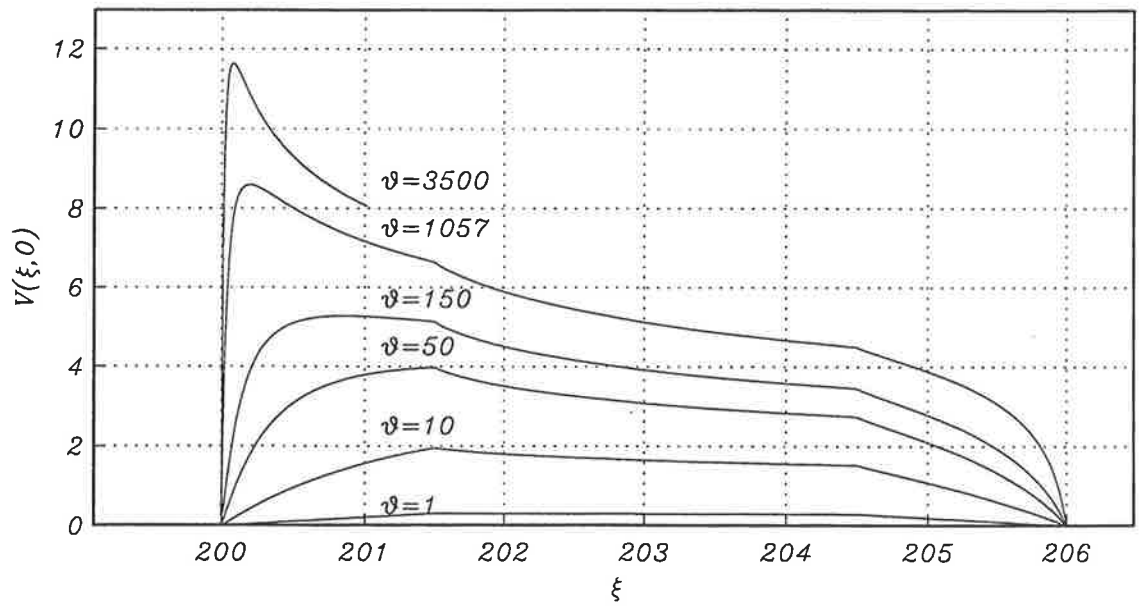

Figure 6.9: The vertical velocity $V(\xi, \eta)$ at the permeable surface ($\eta = 0$), for the case of diffusion driven flow at $\xi_{le} = 200$, $l = 3$ and $\epsilon = 1.5$.

sure gradient is prescribed, then the boundary-layer separation will result in a Goldstein separation. In our numerical calculations the "blowing" velocity is prescribed as a regular function of the distance and the the concentration gradient along the surface, which is calculated from the solution of the concentration equation. This we conjecture leads to flow separation without the occurrence of a singularity. In order to verify this further

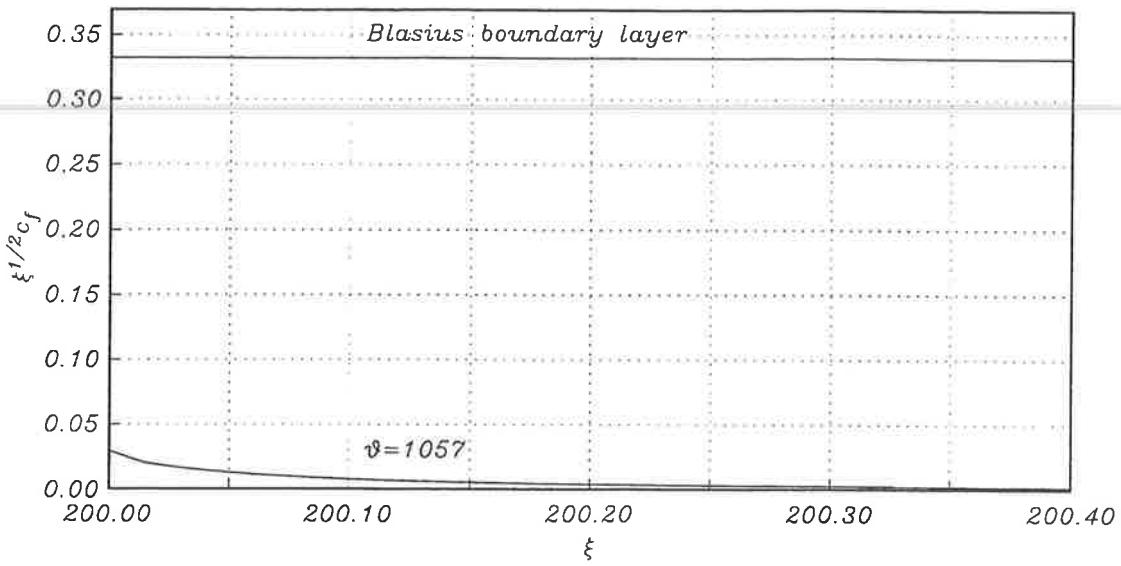

Figure 6.10: The skin friction as a function of ξ for "large-slot", located far-downstream ($\xi_{le} = 200$, $l = 30$ and $\epsilon = 1.5$).

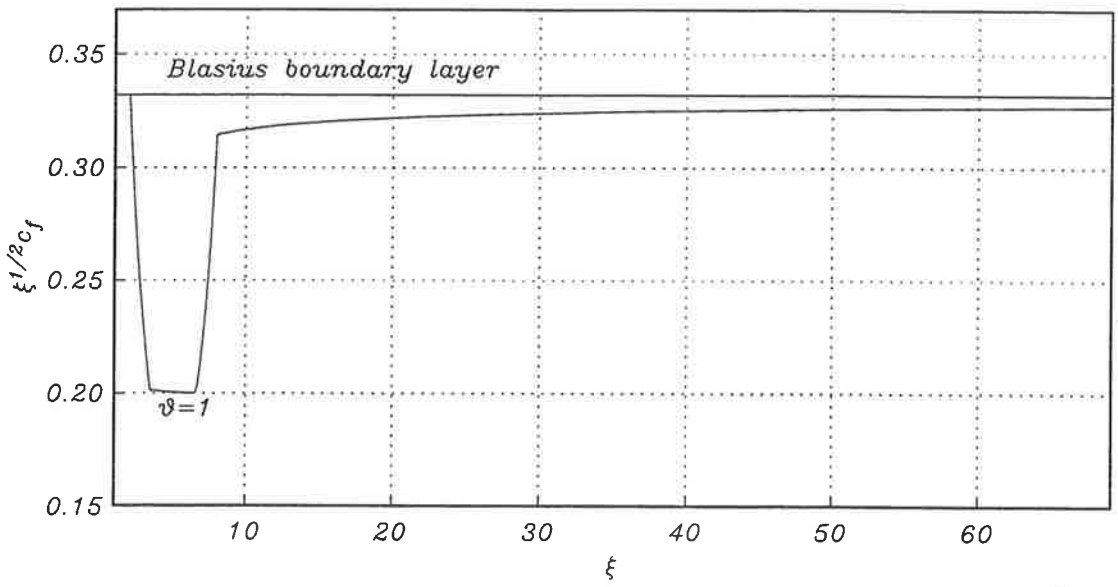

Figure 6.11: The recovery of skin friction downstream of the slot ($\xi_{le} = 2$, $l = 3$ and $\epsilon = 1.5$).

analytical studies must be undertaken.

The velocity profiles F, V, the concentration profile G and the second derivative of F with respect to η at the surface $F''(0, \eta)$ are given in Figures 6.12 and 6.13 at different streamwise locations $\xi = 2$, 3.5, 4.5, 6.5 and $\vartheta = 1$, $l = 3$, $\epsilon = 1.5$ and $\xi_{le} = 2$. It is clearly seen from these figures that at streamwise locations $\xi = 3.5$, 4.5, 6.5 the velocity profile F has an inflection point. This in turn suggests that the action of diffusion may

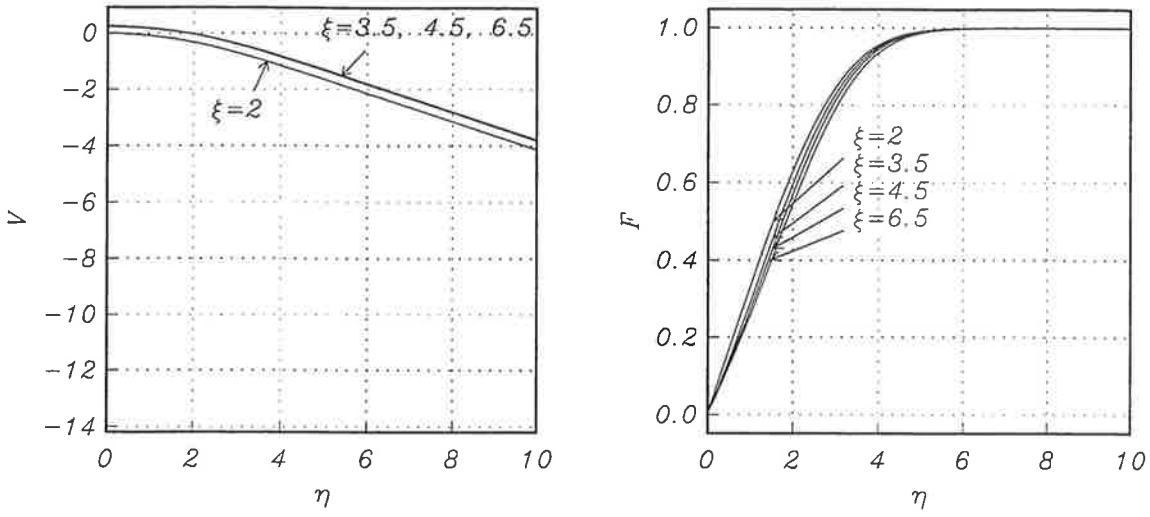

Figure 6.12: The velocity profiles F and V at different downstream locations ξ = 2, 3.5, 4.5 and 6.5, for the case of diffusion driven flow at $\xi_{le} = 2$, $l = 3$, $\epsilon = 1.5$ and $\vartheta = 1$.

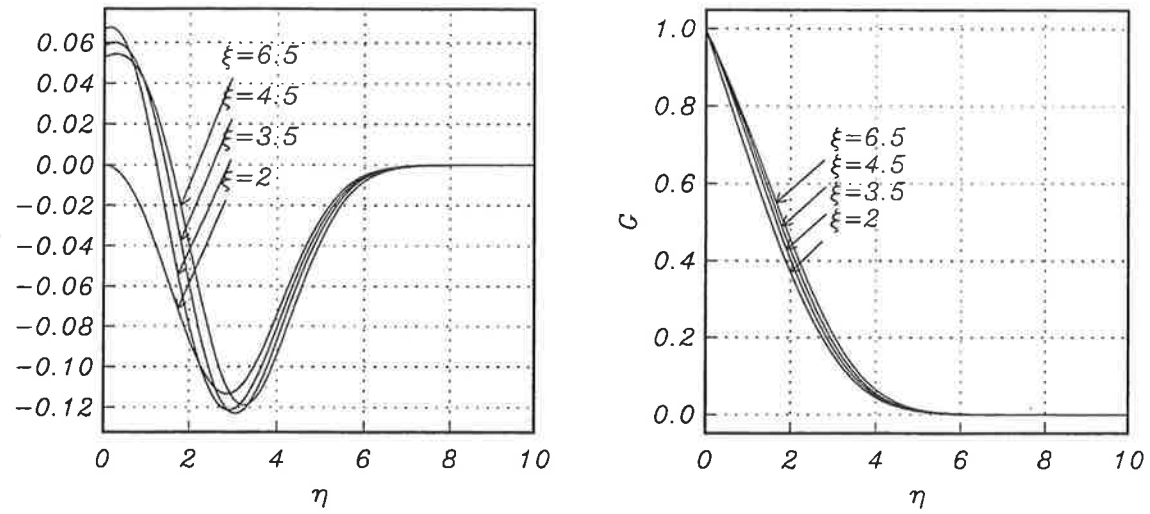

Figure 6.13: The concentration profile G and the second derivative of F with respect to η at the surface $F''(0,\eta)$ at different downstream locations ξ = 2, 3.5, 4.5 and 6.5, for the case of diffusion driven flow at $\xi_{le} = 2$, $l = 3$, $\epsilon = 1$ and $\vartheta = 1$.

lead to a potential early transition-to-turbulence due to the flows susceptibility to short scale, high frequency, Rayleigh waves. This is the subject of the next section.

6.4 Growth rates curves

We now turn our attention to the question of the inviscid instability of the diffusion slot-boundary-layer flow. The growth rate $\sigma_i = \alpha\omega_i$ was calculated by solving the eigenvalue

problem (6.11) with boundary conditions (6.12). This was done at different values of the mass-transfer parameter θ, at several streamwise locations over the slot. The results are shown in Figures 6.14 - 6.16.

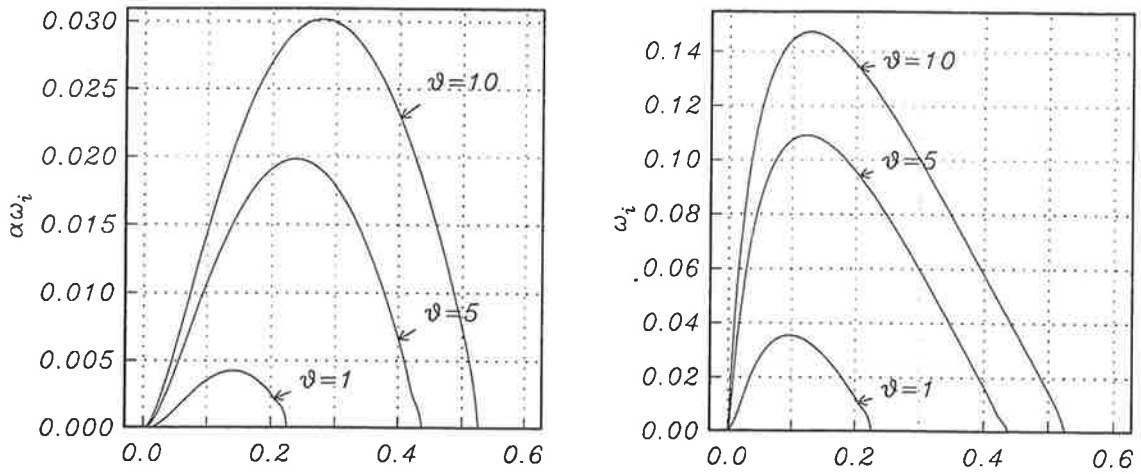

Figure 6.14: Graphs of the imaginary part of the wave-speed ω_i and growth rate σ_i with respect to the wave number α in the unstable regime for a diffusion driven boundary-layer flow for several values of the magnitude of the mass-transfer parameter θ over the "slot" at $\xi = 3.5$.

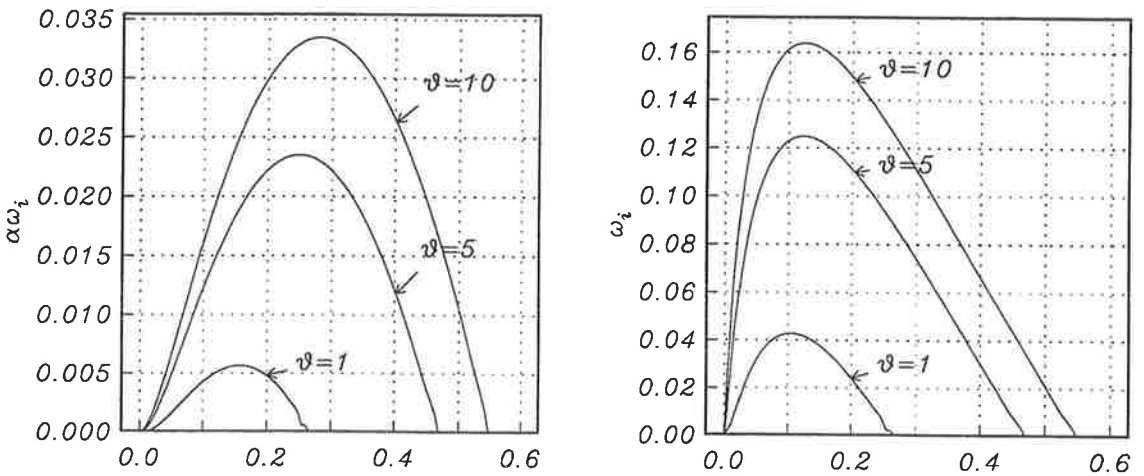

Figure 6.15: Graphs of the imaginary part of the wave-speed ω_i and growth rate σ_i with respect to the wave number α in the unstable regime for a diffusion driven boundary-layer flow for several values of the magnitude of the mass-transfer parameter θ over the "slot" at $\xi = 4.5$.

In Figures 6.14 - 6.16 we present plots of the dimensionless imaginary part of the wave-speed ω_i and dimensionless growth rate σ_i for the unstable normal modes. These results demonstrate that at a fixed streamwise location ξ, increasing the level of mass transfer

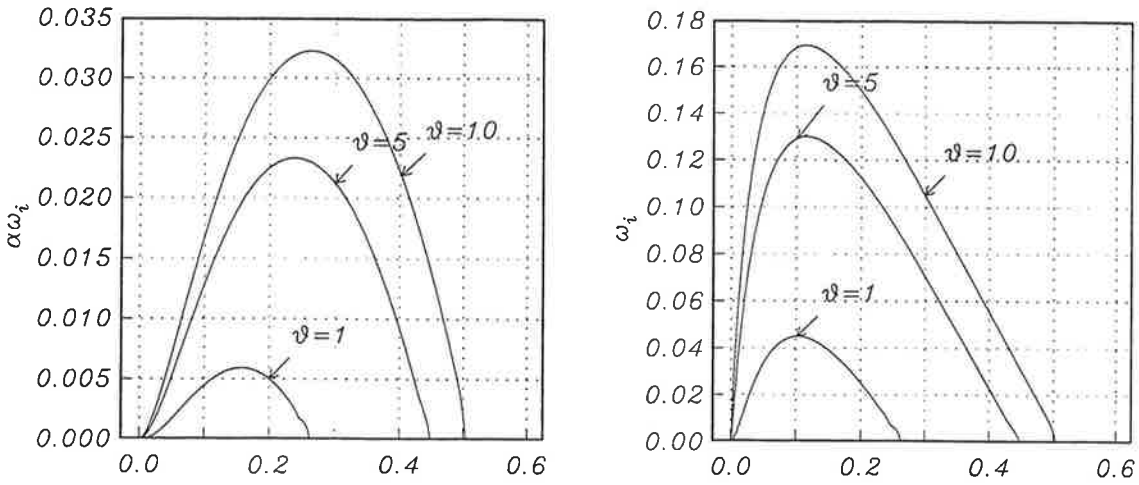

Figure 6.16: Graphs of the imaginary part of the wave-speed ω_i and growth rate σ_i with respect to the wave number α in the unstable regime for a diffusion driven boundary-layer flow for several values of the magnitude of the mass-transfer parameter θ over the "slot" at $\xi = 6.5$.

leads to an increase in the maximum of the dimensionless imaginary part of the wave-speed, dimensionless growth rate and wave number α respectively. For instance, at $\xi = 3.5$ in the case of "blowing" with mass-transfer parameter $\vartheta = 1$ the maximum growth rate is 0.00425 at wave number 0.1408, while for $\vartheta = 10$ the maximum growth rate is 0.03016 at wave number 0.2780. The growth rate curves were calculated at different streamwise locations at a fixed value of the mass-transfer parameter and going downstream the maximum value of the dimensionless imaginary part of the wave-speed and dimensionless growth rate increases. For example at $\xi = 6.5$ and $\vartheta = 10$ we have $\sigma_{i\,max} = 0.03226$. The unstable bandwidth increases at fixed location as we increase the level of mass transfer, i.e. at $\xi = 3.5$ and $\vartheta = 1$ it is 0.2292, while at $\vartheta = 5$ the unstable bandwidth is 0.44. At small, fixed values of the mass-transfer parameter the unstable bandwidth increases downstream: at $\vartheta = 1$ and $\xi = 3.5$ the unstable bandwidth is 0.229, while at $\vartheta = 1$ and $\xi = 6.5$ it is 0.2555. At large, fixed values of mass-transfer parameter we observe the reverse effect: at $\vartheta = 10$ and $\xi = 3.5$ the unstable bandwidth is 0.540, while at $\vartheta = 10$ and $\xi = 6.5$ it is 0.516.

It is clearly seen that even at small levels of mass transfer ($\vartheta = 1$) the boundary-layer flow becomes unstable. Results for the second and third modes yield growth rates that are sufficiently small to allow us to conclude that the instability of the boundary-layer flow will be dominated by the first mode.

Graphs of the wave-speed ω_r versus the wave number α in the unstable regime for a diffusion driven boundary-layer flow for several values of the mass-transfer parameter ϑ over the "slot" at different streamwise locations ξ are presented at Figures 6.17 - 6.19.

Note that our results do demonstrate some grid dependency, as the comparison of the graphs of the growth rate $\sigma_i = \alpha\omega_i$ with respect to the wave number α for different

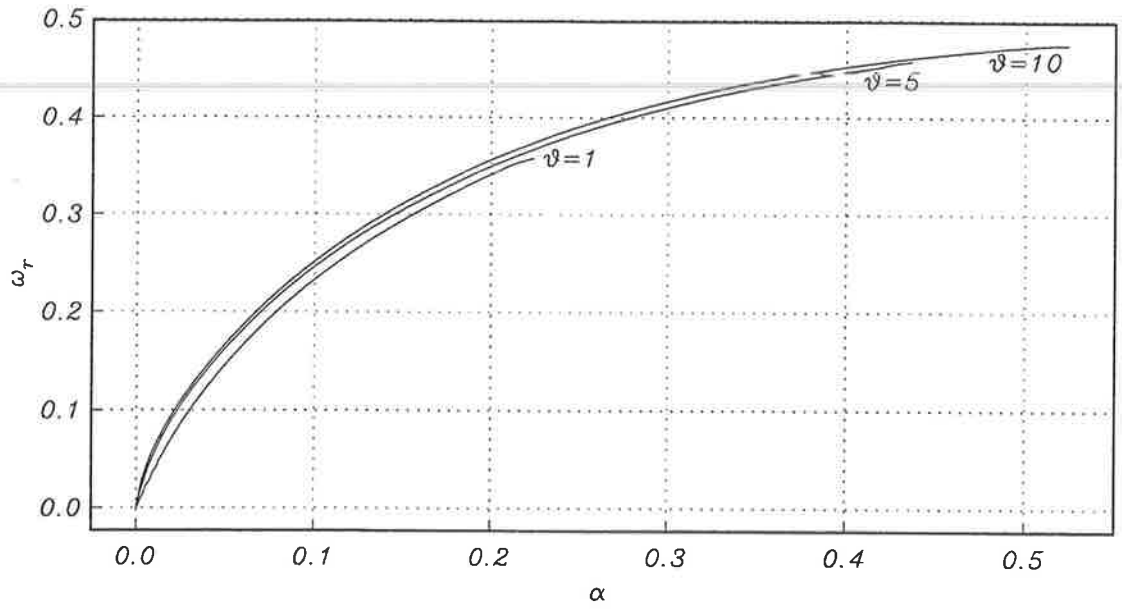

Figure 6.17: Graphs of the wave-speed ω_r with respect to the wave number α in the unstable regime for a diffusion driven boundary- layer flow for several values of the magnitude of the mass-transfer parameter θ over the "slot" at $\xi = 3.5$.

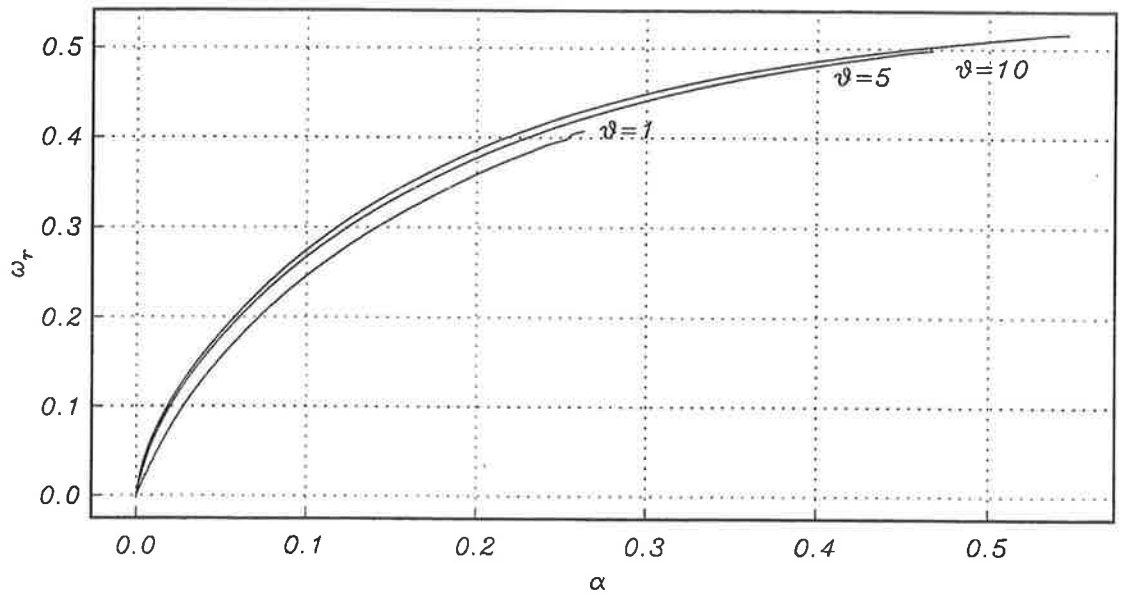

Figure 6.18: Graphs of the wave-speed ω_r and with respect to the wave number α in the unstable regime for a diffusion driven boundary-layer flow for several values of the magnitude of the mass-transfer parameter θ over the "slot" at $\xi = 4.5$.

values of the vertical step size $\Delta\eta$ at $\xi = 3.5$ and $\vartheta = 1$ plotted in Figure 6.20 show. This

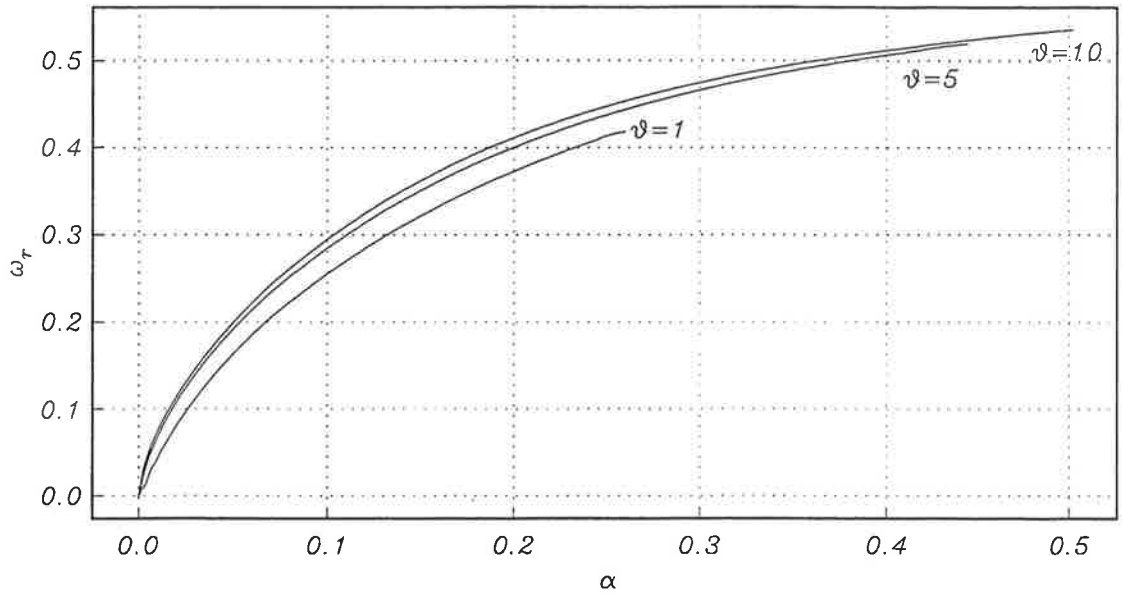

Figure 6.19: Graphs of the wave-speed ω_r with respect to the wave number α in the unstable regime for a diffusion driven boundary-layer flow for several values of the magnitude of the mass-transfer parameter θ over the "slot" at $\xi = 6.5$.

is, however, confined to the vicinity of the point of neutral stability; the results for the maximum growth rate showing little variation with step-size $\Delta\eta$. The results presented in Figures 6.14 - 6.19 were obtained using $\Delta\eta = 0.05$ with 200 grid points.

For completeness the growth rate curves were calculated for the case when the diffusion region is located far-downstream at $\xi = 203$. The results are analogous to the slot located upstream for the growth rate curves (see Figures 6.21 and 6.22). The results for the wave-speed ω_r presented in Figure 6.22 show that it has maximum, whose value increases as we increase the level of the mass transfer (at $\xi = 203$ and $\vartheta = 150$ the maximum is $\omega_{r\,max} = 0.24911$ at $\alpha = 0.663$, while at $\xi = 203$ and $\vartheta = 1057$ it is 0.26696 at $\alpha = 0.697$).

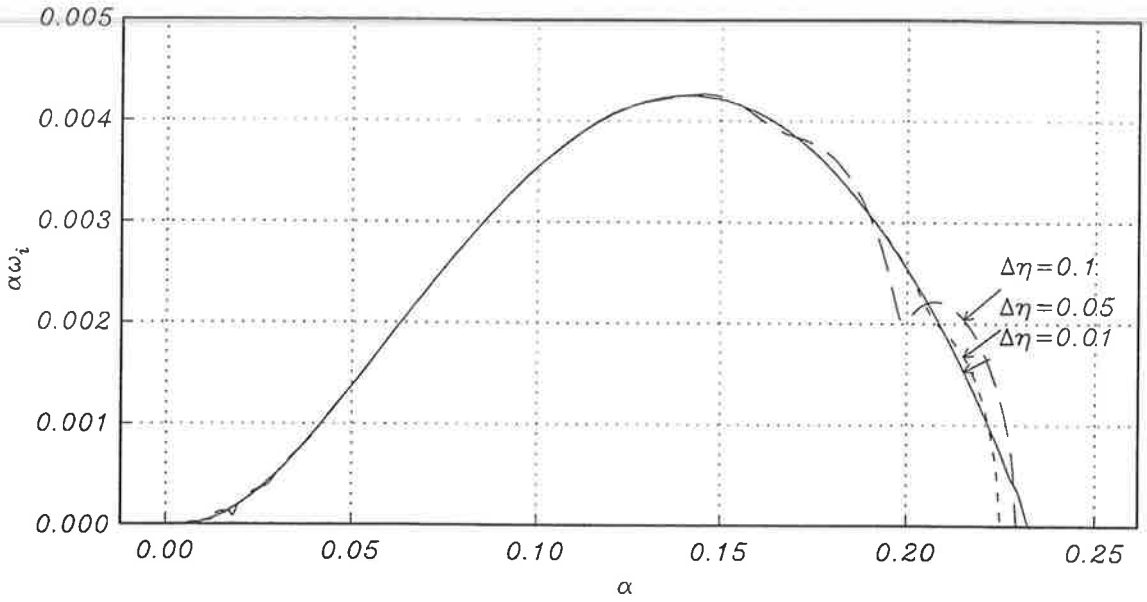

Figure 6.20: Comparison of the graphs of the growth rate σ_i with respect to the wave number α for different values of the vertical step size $\Delta\eta$ at $\xi = 3.5$ and $\vartheta = 1$.

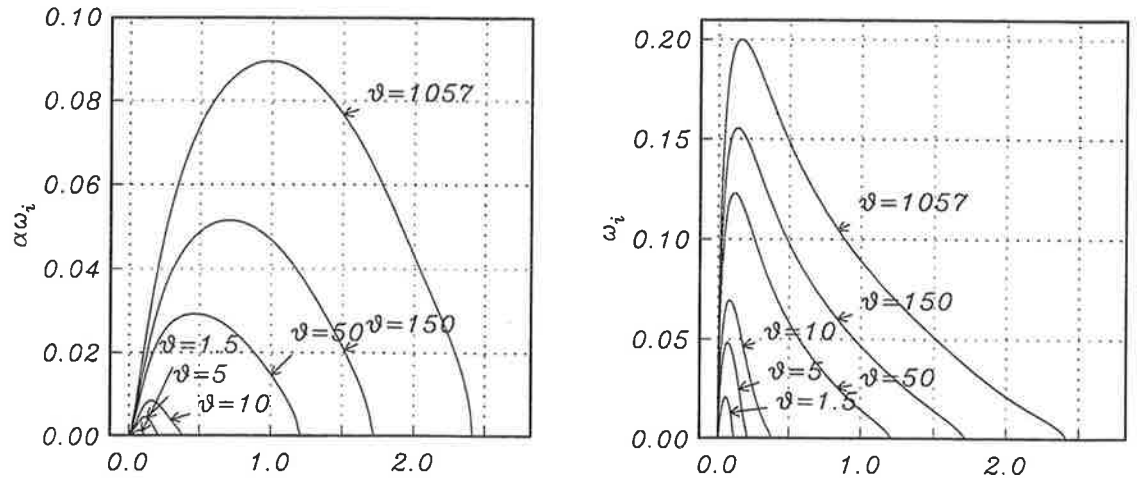

Figure 6.21: Graphs of the imaginary part of the wave-speed ω_i and growth rate σ_i with respect to the wave number α in the unstable regime for a diffusion driven boundary-layer flow for several values of the magnitude of the mass-transfer parameter θ over the "slot" at $\xi = 203$.

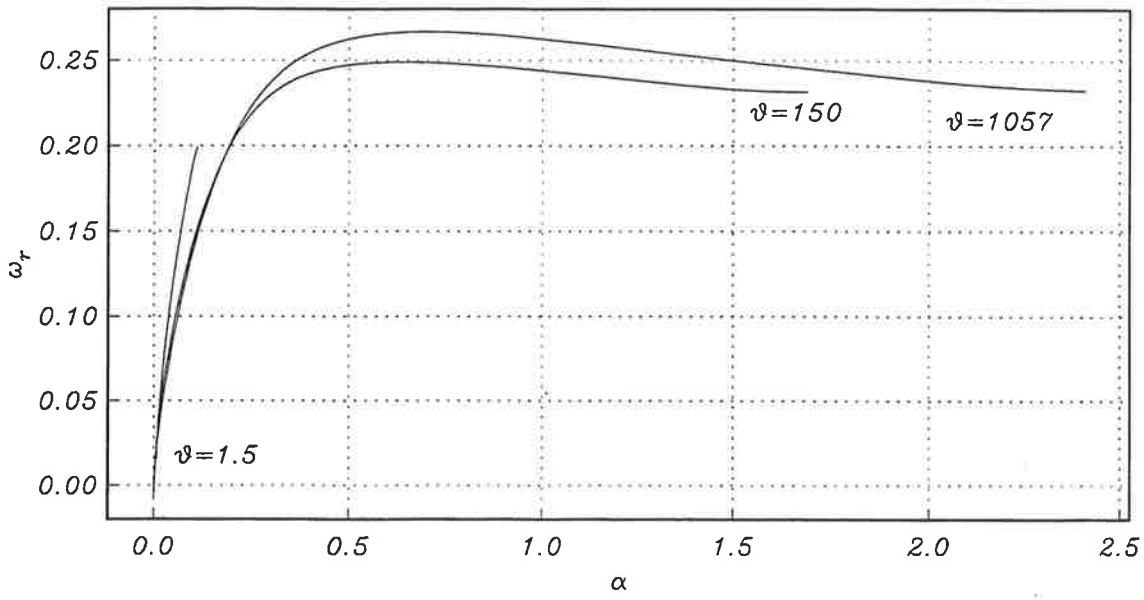

Figure 6.22: Graphs of the wave-speed ω_r with respect to the wave number α in the unstable regime for a diffusion driven boundary-layer flow for several values of the magnitude of the mass-transfer parameter θ over the "slot" at $\xi = 203$.

Conclusions

The crucial assumption made in the present research is that separation occurs downstream of the slot leading edge. With increasing rates of injection it is probable that the separation first occurs upstream of the slots' leading edge and the proposed boundary-layer equations, and consequently the numerical scheme, break down. It was for this reason that our study of the slot-injection problem was carried out within the weak or moderate injection regime.

Diffusion induced boundary-layer separation can occur far-downstream at high mass-transfer parameters θ. However the levels of the interfacial mass transfer at which boundary-layer separation is observed are very large and hardly achievable in practice. In the case when the slot is located upstream, separation does not occur. It is important to draw attention to the different physical mechanism of "blowing" for the diffusion driven boundary-layer flows, where the velocity and concentration fields are coupled in the boundary conditions over the slot length, which in turn serves to inhibit flow separation.

The higher the mass-transfer rate, the nearer the separation point is to the leading edge of the slot. Increasing the length of the slot leads to flow separation at a lower level of mass transfer. There is a distinct similarity between the simple "injection" induced separation and the diffusion forced one.

There is no evidence of a Goldstein singularity at the point of separation, i.e. a smooth separation is observed, due to the fact that the boundary layer can adjust so as to remove or inhibit the singularity. We have not attempted to obtain a detailed mathematical description of the flow in the vicinity of the separation point. This does, however, provide an interesting avenue for future work. A more rigorous mathematical treatment is necessary in order to clarify this point.

Diffusion leads to an inflection point in the velocity profile F at some local station ξ_{cr} and the boundary-layer flow becomes unstable. The results of this work demonstrate that, although moderate levels of mass transfer can induce flow separation, the flow will become susceptible to inviscid instabilities well before separation has occurred.

The question of the separation marginality is still open and it will be the subject of future work on this problem.

Future Work

Linear analysis of two-fluid systems

The linear stability analysis of two-fluid systems considered in the Introduction and Chapter 1 was restricted to a stable interface (i.e. one which is not deformable) and the criteria for flow instability of a horizontal interface between two liquids was not firmly established. The problem of laminar boundary layers on either side of a plane, stable interface was first studied by Potter (1957), the hydrodynamic conditions are represented in Figure 7.1. There have been several approaches, from the hydrodynamic point of view, to examine some aspects of the boundary-layer flow instabilities in the cases of gas–liquid

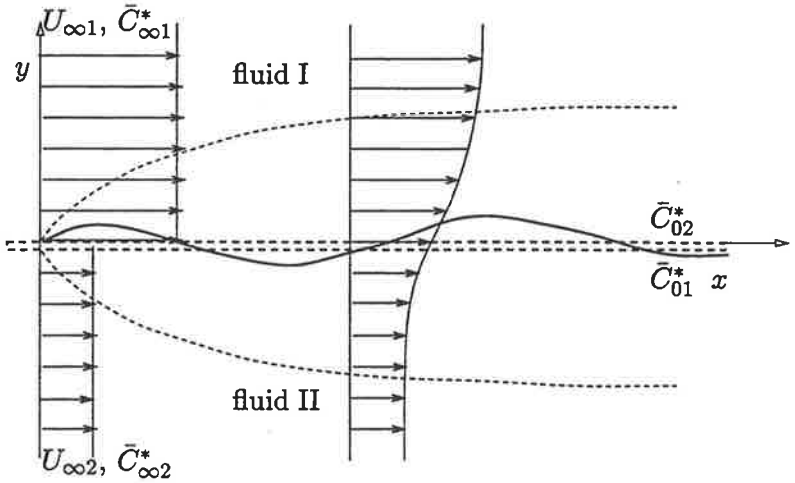

Figure 7.1: Schematic representation of momentum boundary layers at the interface between two co-current fluids.

(see Boyadjiev & Halatchev (1996b)), liquid–liquid (see Halatchev & Boyadjiev (1996)) and gas–liquid film–solid surface systems (see Boyadjiev & Halatchev (1996c)). Unfortunately these studies only provide a partial solution to the problem as they took the interface to be rigid and non-deformable. These studies have therefore considered only the effect of mass transfer upon the purely shear (viscous) modes of instability and have not considered the important question of interfacial instabilities. A detailed study of this problem is outside the scope of this thesis, however, we briefly consider the changes in the boundary conditions connected with coupling of the disturbances equations in two-fluid

systems.

The instability analysis of a variety of steady two-layer flows has been examined numerically as well as asymptotically (see Joseph & Renardy (1993)). Different configurations of bi-component flows, i.e. coupled flows of a fluid and another constituent, have been studied, such as rotating flows of two fluids, two-layer Bénard convection problems, plane channel flows, drops and miscible liquids, core-annular flows in vertical pipes, to mention just a few of them. An excellent survey of these studies can be found in Renardy, Coward, Papageorgious & Sun (1996). Here we wish to focus our attention on the problem of the stability of laminar boundary-layer flows, under conditions of intense interfacial mass transfer, when high mass fluxes through the gas–liquid interface induce secondary flows. The interaction between the flow in the fluid I (gas, phase 1) and fluid II (liquid, phase 2) is considered in the case of a movable interface (see Figure 7.1). A very conservative approach to the problem will be undertaken in the first stage of this final section on possible directions for future research. The flow stability under these conditions is not only of theoretical interest, but also of practical interest in view of the fact that it defines the rate of a number of industrial absorption and desorption processes.

Let us consider a transition layer between two uniform streams, which is the diffusing sheet vortex (see Batchelor (1970)) under conditions of interfacial mass transfer between two phases. The pressure is uniform throughout the flow and consequently inside the layer. When these fluids are in co-current flow, the shear stress resulting from their relative motion results in a velocity distribution near the interface and this will affect the mass-transfer rate between the two phases (see Skelland (1974)). The governing equations for steady laminar flow, for the two phases, consists of the Navier-Stokes equations coupled to the convection-diffusion equations in each phase

$$\begin{aligned}
\frac{\partial U_{0j}^*}{\partial x^*} + \frac{\partial V_{0j}^*}{\partial y^*} &= 0, \\
U_{0j}^* \frac{\partial U_{0j}^*}{\partial x^*} + V_{0j}^* \frac{\partial U_{0j}^*}{\partial y^*} &= -\frac{1}{\rho_{0j}^*} \frac{\partial P_{0j}^*}{\partial x^*} + \nu_j \left(\frac{\partial^2}{\partial x^{*2}} + \frac{\partial^2}{\partial y^{*2}} \right) U_{0j}^*, \\
U_{0j}^* \frac{\partial V_{0j}^*}{\partial x^*} + V_{0j}^* \frac{\partial V_{0j}^*}{\partial y^*} &= -\frac{1}{\rho_{0j}^*} \frac{\partial P_{0j}^*}{\partial y^*} + \nu_j \left(\frac{\partial^2}{\partial x^{*2}} + \frac{\partial^2}{\partial y^{*2}} \right) V_{0j}^*, \\
U_{0j}^* \frac{\partial C_{0j}^*}{\partial x^*} + V_{0j}^* \frac{\partial C_{0j}^*}{\partial y^*} &= D_j \left(\frac{\partial^2}{\partial x^{*2}} + \frac{\partial^2}{\partial y^{*2}} \right) C_{0j}^*.
\end{aligned} \tag{7.1}$$

Here the index $j = 1, 2$ denotes the upper/lower fluid respectively (see Figure 7.1). The system (7.1) is subject to the boundary conditions

- At the start of the interface $x^* = 0$

$$(U_{0j}^*, V_{0j}^*) = (U_{\infty j}, 0),\ C_{0j}^* = \bar{C}_{\infty j}^*; \tag{7.2}$$

- At the interface $y^* = h_0^*(x^*, t^*)$ we have the requirement of continuity of velocity, the kinematic boundary condition on the interface, continuity of shear stress, the jump in the normal stress which is balanced by the surface tension, continuity of

concentration and mass flux due to concentration gradient. These can be written as

$$\frac{\partial h_0^*}{\partial t^*} + U_{0j}^* \frac{\partial h_0^*}{\partial x^*} - \frac{MD_j}{\rho_{0j}^*} \frac{\partial C_{0j}^*}{\partial y^*} = V_{0j}^*, \tag{7.3a}$$

$$U_{01}^* = U_{02}^*, \;\; \mu_1 \left(\frac{\partial U_{01}^*}{\partial y^*} + \frac{\partial V_{01}^*}{\partial x^*} \right) = \mu_2 \left(\frac{\partial U_{02}^*}{\partial y^*} + \frac{\partial V_{02}^*}{\partial x^*} \right), \tag{7.3b}$$

$$C_{01}^* = \chi C_{02}^*, \;\; 2\mu_1 \frac{\partial V_{01}^*}{\partial y^*} - P_{01}^* = S^* \frac{h_0^{*\prime\prime}}{\left(1 + h_0^{*\prime 2}\right)^{3/2}} + 2\mu_1 \frac{\partial V_{02}^*}{\partial y^*} - P_{02}^*, \tag{7.3c}$$

$$\frac{D_1 \rho_1^*}{\rho_{01}^*} \frac{\partial C_{01}^*}{\partial y^*} = \frac{D_2 \rho_2^*}{\rho_{02}^*} \frac{\partial C_{02}^*}{\partial y^*}; \tag{7.3d}$$

- In the free-stream as $y^* \to \infty$ and $y^* \to -\infty$

$$\begin{aligned} y^* \to \infty: \;\; U_{01}^* = U_{\infty 1}, \; C_{01}^* = \bar{C}_{\infty 1}^*; \\ y^* \to -\infty: \;\; U_{02}^* = U_{\infty 2}, \; C_{02}^* = \bar{C}_{\infty 2}^*. \end{aligned} \tag{7.4}$$

Here S^* is the dimensional surface tension coefficient, the subscript j denotes the different phases and an asterisk is used for dimensional variables. The interfacial mass transfer, due to the concentration difference, is taken into account with the coupling of the Navier-Stokes equations with the convection- diffusion equations in both phases through the kinematic free surface interfacial condition (7.3a). The conditions at the interface are posed at the unknown position $h_0^* = h_0^*(x^*, t^*)$.

The system prescribed by (7.1) - (7.4) can be non-dimensionalised using a typical length scale L (for example, the distance from the start of the interface), the free-stream speeds $U_{\infty j}$ and the concentrations $\bar{C}_{0j}^*$ and $\bar{C}_{\infty j}^*$ as follows:

$$(x^*, y^*) = L(x, y), \;\; h_0^* = L h_0, \;\; t^* = \frac{Lt}{U_{\infty j}}, \;\; (U_{0j}^*, V_{0j}^*) = U_{\infty j}(U_{0j}, V_{0j}), \tag{7.5}$$

$$C_{0j}^* = \bar{C}_{\infty j}^* + (\bar{C}_{\infty 1}^* - \chi \bar{C}_{\infty 2}^*) C_{0j} \;\; P_{0j}^* = \rho_{0j}^* U_{\infty j}^2 P_{01}, \;\; S = \frac{S^*}{\mu_2 U_{\infty 2}}.$$

The resulting non-dimensional equations are

$$\begin{aligned} \frac{\partial U_{0j}}{\partial x} + \frac{\partial V_{0j}}{\partial y} &= 0, \\ \frac{\partial U_{0j}}{\partial t} + U_{0j} \frac{\partial U_{0j}}{\partial x} + V_{0j} \frac{\partial U_{0j}}{\partial y} &= -\frac{\partial P_{0j}}{\partial x} + \frac{1}{Re_j} \left(\frac{\partial^2}{\partial x^2} + \frac{\partial^2}{\partial y^2} \right) U_{0j}, \\ \frac{\partial V_{0j}}{\partial t} + U_{0j} \frac{\partial V_{0j}}{\partial x} + V_{0j} \frac{\partial V_{0j}}{\partial y} &= -\frac{\partial P_{0j}}{\partial y} + \frac{1}{Re_j} \left(\frac{\partial^2}{\partial x^2} + \frac{\partial^2}{\partial y^2} \right) V_{0j}, \\ \frac{\partial C_{0j}}{\partial t} + U_{0j} \frac{\partial C_{0j}}{\partial x} + V_{0j} \frac{\partial C_{0j}}{\partial y} &= \frac{1}{Sc_j Re_j} \left(\frac{\partial^2}{\partial x^2} + \frac{\partial^2}{\partial y^2} \right) C_{0j}, \;\; j = 1, 2, \end{aligned} \tag{7.6}$$

with the following boundary conditions:

$$x = 0: \quad (U_{0j}, V_{0j}) = (1, 0),\ C_{0j} = 0; \tag{7.7a}$$

$$y = h: \quad U_{01} = \theta_2 U_{02},\ \frac{\partial h_0}{\partial t} + U_{0j}\frac{\partial h_0}{\partial x} - \frac{\theta_{3j}}{Sc_j Re_j}\frac{\partial C_{0j}}{\partial y} = V_{0j}, \tag{7.7b}$$

$$\frac{\partial U_{01}}{\partial y} + \frac{\partial V_{01}}{\partial x} = \theta_1\theta_2\left(\frac{\partial U_{02}}{\partial y} + \frac{\partial V_{02}}{\partial x}\right), \tag{7.7c}$$

$$2\frac{\partial V_{01}}{\partial y} - Re_1 P_{01} = S\frac{h_0''}{\left(1 + h_0'^2\right)^{3/2}} + 2\theta_1\theta_2\left(\frac{\partial V_{02}}{\partial y} - Re_2 P_{02}\right), \tag{7.7d}$$

$$1 + C_{01} = \chi C_{02},\ \frac{\partial C_{01}}{\partial y} = \epsilon_0\frac{\partial C_{02}}{\partial y}; \tag{7.7e}$$

$$y \to \infty: \quad U_{01} = 1,\ C_{01} = 0; \tag{7.7f}$$

$$y \to -\infty: \quad U_{02} = 1,\ C_{02} = 0, \tag{7.7g}$$

where $Re_j = U_{\infty j}L/\nu_j$ are the respective Reynolds numbers for each phase, $Sc_j = \nu_j/D_j$ are the Schmidt numbers in each fluid, $\epsilon_0 = (D_2/D_1)(\rho_2^*/\rho_1^*)(\rho_{01}^*/\rho_{02}^*)$ is the diffusivity-density ratio, $\theta_1 = \mu_1/\mu_2$ is the viscosity ratio, $\theta_2 = U_{\infty 2}/U_{\infty 1}$ is the ratio between the free-stream speeds of the two phases and $\theta_{3j} = M(\bar{C}_{\infty 1}^* - \chi\bar{C}_{\infty 2}^*)/\rho_{0j}^*$ is a parameter which characterises the intensity of the mass transfer across the interface.

To pose the general problem of stability of such flows perturbations to the velocity, pressure and concentration fields are denoted by (u_j, v_j, p_j) and interface position h_0 is considered as a small disturbance.

$$\begin{aligned}(U_j, V_j, P_j, C_j) &= (U_{0j}, V_{0j}, P_{0j}, C_{0j}) + \epsilon(u_j, v_j, p_j, c_j) + \cdots, \\ h_0 &= \epsilon h,\end{aligned} \tag{7.8}$$

where ϵ $(0 < \epsilon \ll 1)$ is a small perturbation parameter.

The governing equations for two-dimensional disturbance follow from the Navier-Stokes equations and the convection-diffusion equation in both phases by linearisation about the basic steady flow and concentration state. This yields the equations

$$\begin{aligned} u_{jx} + v_{jy} &= 0, \\ u_{jt} + U_{0j}u_{jx} + u_j U_{0jx} + v_j U_{0jy} + V_{0j}u_{jy} &= -p_{jx} + Re_j^{-1}\left(u_{jxx} + u_{jyy}\right), \\ v_{jt} + U_{0j}v_{jx} + u_j V_{0jx} + V_{0j}v_{jy} + v_j V_{0jy} &= -p_{jy} + Re_j^{-1}\left(v_{jxx} + v_{jyy}\right), \\ c_{jt} + U_{0j}c_{jx} + u_j C_{0jx} + V_{0j}c_{jy} + v_j C_{j0y} &= Re_j^{-1}Sc_j^{-1}\left(c_{jxx} + c_{jyy}\right), \quad j = 1, 2. \end{aligned} \tag{7.9}$$

The boundary conditions for the total field (U_j, V_j, P_j, C_j) have the same form as (7.7). Since the interface position $h_0(x, t)$ is assumed to be small we can expand the interfacial boundary conditions in Taylor series about $y = 0$ and truncate at $O(\epsilon)$. The disturbance boundary conditions then become:

On $y = 0$

$$h\frac{\partial U_{01}}{\partial y} + u_1 = \theta_2 \left(h\frac{\partial U_{02}}{\partial y} + u_2 \right), \tag{7.10a}$$

$$\frac{\partial h}{\partial t} + U_{0j}\frac{\partial h}{\partial x} - \frac{\theta_{3j}}{Sc_j Re_j}\left(h\frac{\partial^2 C_{0j}}{\partial y^2} + \frac{\partial c_j}{\partial y} \right) = h\frac{\partial V_{0j}}{\partial y} + v_j, \tag{7.10b}$$

$$\begin{aligned} &h\frac{\partial^2 U_{01}}{\partial y^2} + h\frac{\partial^2 V_{01}}{\partial x \partial y} + \frac{\partial u_1}{\partial y} + \frac{\partial v_1}{\partial x} \\ &= \theta_1\theta_2\Big(h\frac{\partial^2 U_{02}}{\partial y^2} + h\frac{\partial^2 V_{02}}{\partial x \partial y} + \frac{\partial u_2}{\partial y} + \frac{\partial v_2}{\partial x} \Big), \end{aligned} \tag{7.10c}$$

$$2h\frac{\partial^2 V_{01}}{\partial y^2} + 2\frac{\partial v_1}{\partial y} - Re_1 p_1 = Sh'' - 2\theta_1\theta_2 \left(h\frac{\partial^2 V_{02}}{\partial y^2} + \frac{\partial v_2}{\partial y} - \frac{1}{2}Re_2 p_2 \right), \tag{7.10d}$$

$$h\frac{\partial C_{01}}{\partial y} + c_1 = \chi \left(h\frac{\partial C_{02}}{\partial y} + c_2 \right), \tag{7.10e}$$

$$h\frac{\partial^2 C_{01}}{\partial y^2} + \frac{\partial c_1}{\partial y} = \epsilon_0 \left(h\frac{\partial^2 C_{02}}{\partial y^2} + \frac{\partial c_2}{\partial y} \right); \tag{7.10f}$$

and in the far field

$$u_1 \to 0,\ c_1 \to 0 \ \text{ as } \ y \to \infty; \tag{7.11a}$$

$$u_2 \to 0,\ c_2 \to 0 \ \text{ as } \ y \to -\infty. \tag{7.11b}$$

For the basic flow field, in the limit of large Reynolds number, the two flows will develop boundary layers of thickness $O(Re_j^{-1/2})$. We then introduce the following boundary-layer variables:

$$y = Re_j^{-1/2} Y_j,\ U_{0j} = U_{Bj},\ V_{0j} = Re_j^{-1/2} V_{Bj},\ C_{0j} = C_{Bj}, \tag{7.12}$$

where y is physical coordinate and Y_j the boundary-layer coordinate appropriate to the jth phase. Note that these are two different scales and the two Reynolds numbers are connected as $Re_2 = r\theta_1\theta_2 Re_1$, where $r = \rho_{02}^*/\rho_{01}^*$. Introducing (7.12) into (7.6) and the corresponding boundary conditions (7.7) reduces the problem to a system of Prandtl equations coupled with concentration equations for both phases.

The linear stability analysis of two-fluid systems can now be posed by considering a small wave-like disturbance

$$\begin{aligned} u_j(x,y) &= F_j'(y)\exp\left[i\alpha(x-ct)\right], \\ v_j(x,y) &= -i\alpha F_j(y)\exp\left[i\alpha(x-ct)\right], \\ c_j(x,y) &= i\alpha G_j(y)\exp\left[i\alpha(x-ct)\right], \\ h(x,y) &= H\exp\left[i\alpha(x-ct)\right], \end{aligned} \tag{7.13}$$

where $F_j(y)$ and $G_j(y)$ are the amplitudes of the disturbances, α is a real quantity and $c = c_r + ic_i$ is complex; they are the wavenumber and phase speed respectively, and H is an unknown constant.

The disturbance equations (7.9) and their boundary conditions (7.10) - (7.11) can be reduced to a standard form in a similar fashion as in Chapter 4. Substituting (7.13) into (7.9) - (7.11) then yields an eigenvalue problem in the form of a two-point boundary-value problem, which serves to determine the complex wave-speed c as a function of the system parameters α, Re_j, S, Sc_j, θ_j, etc. The numerical solution of this system will be the subject of future work.

Appendix A

Some Mathematical Derivations

A.1 Discretisation of the Orr-Sommerfeld and concentration equations - matrix forms

The system (4.22)

$$\begin{pmatrix}
d_1 & \mu_4 & \mu_5 & & & & & & & \\
\mu_2 & \mu_3 & \mu_4 & \mu_5 & & & & & & \\
\mu_1 & \mu_2 & \mu_3 & \mu_4 & \mu_5 & & & & & \\
 & \mu_1 & \mu_2 & \mu_3 & \mu_4 & \mu_5 & & & & \\
 & & \ddots & & & & & & & \\
 & & & \mu_1 & \mu_2 & \mu_3 & \mu_4 & \mu_5 & & \\
 & & & & \ddots & & & & & \\
 & & & & & \mu_1 & \mu_2 & \mu_3 & \mu_4 & \mu_5 \\
 & & & & & & \mu_1 & \mu_2 & d_2 & d_3 \\
 & & & & & & & d_4 & d_5 & d_6
\end{pmatrix}
\begin{pmatrix}
\tilde{\varphi}_1 \\ \tilde{\varphi}_2 \\ \tilde{\varphi}_3 \\ \tilde{\varphi}_4 \\ \vdots \\ \tilde{\varphi}_k \\ \vdots \\ \tilde{\varphi}_{N-2} \\ \tilde{\varphi}_{N-1} \\ \tilde{\varphi}_N
\end{pmatrix}
=
\begin{pmatrix}
r_1 \\ r_2 \\ 0 \\ 0 \\ \vdots \\ 0 \\ \vdots \\ 0 \\ 0 \\ 0
\end{pmatrix}$$

The system (4.23)

$$\begin{pmatrix}
\mu_7 & d_7 & & & & & & & \\
\mu_6 & \mu_7 & \mu_8 & & & & & & \\
 & \mu_6 & \mu_7 & \mu_8 & & & & & \\
 & & \ddots & & & & & & \\
 & & & \mu_6 & \mu_7 & \mu_8 & & & \\
 & & & & \ddots & & & & \\
 & & & & & \mu_6 & \mu_7 & \mu_8 & \\
 & & & & & & \mu_6 & \mu_7 & \mu_8 \\
 & & & & & & & d_7 & d_8
\end{pmatrix}
\begin{pmatrix}
\tilde{\sigma}_0 \\ \tilde{\sigma}_1 \\ \tilde{\sigma}_2 \\ \vdots \\ \tilde{\sigma}_k \\ \vdots \\ \tilde{\sigma}_{N-2} \\ \tilde{\sigma}_{N-1} \\ \tilde{\sigma}_N
\end{pmatrix}
=
\begin{pmatrix}
q_0 \\ q_1 \\ q_2 \\ \vdots \\ q_k \\ \vdots \\ q_{N-2} \\ q_{N-1} \\ q_N
\end{pmatrix}$$

In their compact storage forms:

$$\begin{pmatrix} & & d_1 & \mu_4 & \mu_5 \\ & \mu_2 & \mu_3 & \mu_4 & \mu_5 \\ \mu_1 & \mu_2 & \mu_3 & \mu_4 & \mu_5 \\ \mu_1 & \mu_2 & \mu_3 & \mu_4 & \mu_5 \\ \vdots & & & & \\ \mu_1 & \mu_2 & \mu_3 & \mu_4 & \mu_5 \\ \vdots & & & & \\ \mu_1 & \mu_2 & \mu_3 & \mu_4 & \mu_5 \\ \mu_1 & \mu_2 & d_2 & d_3 & \\ d_4 & d_5 & d_6 & & \end{pmatrix} \quad \text{and} \quad \begin{pmatrix} & \mu_7 & d_7 \\ \mu_6 & \mu_7 & \mu_8 \\ \mu_6 & \mu_7 & \mu_8 \\ \vdots & & \\ \mu_6 & \mu_7 & \mu_8 \\ \vdots & & \\ \mu_6 & \mu_7 & \mu_8 \\ \mu_6 & \mu_7 & \mu_8 \\ d_7 & d_8 & \end{pmatrix}$$

respectively.

A.2 Keller's technique for eigenvalue problems on infinite domains

The matrices $\mathbf{D}(\eta; \hat{A}, R_\delta, \hat{C})$ and $\mathbf{G}_\infty^+$ respectively

$$\begin{pmatrix}
0 & 1 & 0 & 0 & 0 & 0 \\
\hat{A}^2 + \frac{i\hat{A}R_\delta}{1.72}(f' - \hat{C}) & \frac{1}{2}(\eta f' - f) & -\frac{i\hat{A}R_\delta}{1.72} f''' & -\frac{1}{2}(\eta f''' + f'') & 0 & 0 \\
0 & 0 & 0 & 1 & 0 & 0 \\
1 & 0 & \hat{A}^2 & 0 & 0 & 0 \\
0 & 0 & 0 & 0 & 0 & 1 \\
0 & 0 & -\frac{i\hat{A}R_\delta Sc}{1.72} g' & 0 & \hat{A}^2 + \frac{i\hat{A}R_\delta Sc}{1.72}(f' - \hat{C}) & \frac{1}{2}Sc(\eta f' - f)
\end{pmatrix}$$

$$\begin{pmatrix}
-\frac{1}{4}k + \frac{1}{4}\sqrt{k^2 + 16\beta_0^2} & 1 & 0 & 0 & 0 & 0 \\
\hat{A} - \frac{1}{2}k & 1 & -\frac{i\hat{A}^2 R_\delta}{1.72}(1 - \hat{C}) - \frac{1}{2}\hat{A}^2 k & -\frac{i\hat{A}R_\delta}{1.72}(1 - \hat{C}) - \frac{1}{2}\hat{A}k & 0 & 0 \\
0 & 0 & 0 & 0 & -\frac{1}{4}kSc + \frac{1}{4}\sqrt{k^2 Sc^2 + 16\beta_1^2} & 1
\end{pmatrix}$$

A.3 Central differences coefficients

The coefficients appearing in (4.22) - (4.23) are

$$\begin{aligned}
d_1 &= \mu_3 - \mu_1, \\
d_2 &= \mu_3 + \mu_5\Omega_1, \\
d_3 &= \mu_4 - \mu_5\Omega_2, \\
d_4 &= \mu_1 + \mu_5, \\
d_5 &= \mu_2 + \mu_4\Omega_1 - 2\mu_5(\zeta_1 - \zeta_3\Omega_1), \\
d_6 &= \mu_3 - \mu_4\Omega_2 + 2\mu_5(\zeta_2 - \zeta_3\Omega_2), \\
d_7 &= \mu_6 + \mu_8, \\
d_8 &= \mu_7 - \mu_8\zeta_7,
\end{aligned}$$

$$\begin{aligned}
r_1 &= -\bar{\alpha}D - \mu_1(2\bar{\alpha}D + h^2), \\
r_2 &= -\mu_1\bar{\alpha}D,
\end{aligned}$$

$$\begin{aligned}
q_0 &= (\bar{\alpha}\mu_9 + 2\mu_6 h)D, \\
q_1 &= \mu_9\varphi_1, \\
q_2 &= \mu_9\varphi_2, \\
&\vdots \\
q_k &= \mu_9\varphi_k, \\
&\vdots \\
q_{N-2} &= \mu_9\varphi_{N-2}, \\
q_{N-1} &= \mu_9\varphi_{N-1}, \\
q_N &= \mu_9\varphi_N,
\end{aligned}$$

where

$$\begin{aligned}
\gamma &= \frac{i\hat{A}R_\delta}{1.720}, \\
\bar{\alpha} &= \frac{1.720\theta}{R_\delta Sc},
\end{aligned}$$

$$
\begin{aligned}
\mu_1 &= -\frac{1}{h^3}\left(\frac{1}{2}a_1 - \frac{1}{h}\right), \\
\mu_2 &= -\frac{1}{2h}a_3 + \frac{1}{h^2}a_2 + \frac{1}{h^3}a_1 - \frac{4}{h^4}, \\
\mu_3 &= a_4 - \frac{2}{h^2}a_2 + \frac{6}{h^4}, \\
\mu_4 &= \frac{1}{2h}a_3 + \frac{1}{h^2}a_2 - \frac{1}{h^3}a_1 - \frac{4}{h^4}, \\
\mu_5 &= \frac{1}{h^3}\left(\frac{1}{2}a_1 + \frac{1}{h}\right), \\
\mu_6 &= -\frac{1}{h^3}\left(\frac{1}{2}b_1 - \frac{1}{h}\right), \\
\mu_7 &= \frac{1}{h^2}\left(b_2 - \frac{2}{h^2}\right), \\
\mu_8 &= \frac{1}{h^3}\left(\frac{1}{2}b_1 + \frac{1}{h}\right), \\
\mu_9 &= \frac{1}{h^2}b_3,
\end{aligned}
$$

$$
\begin{aligned}
\chi_1 &= \frac{1}{4}\sqrt{k^2 + 16\beta_0^2} - \frac{1}{4}k, \\
\chi_2 &= \hat{A} - \frac{1}{2}k, \\
\chi_3 &= \beta_0^2 + \frac{1}{2}\hat{A}k, \\
\chi_4 &= \frac{1}{4}\sqrt{Sc^2k^2 + 16\beta_1^2} - \frac{1}{4}Sck,
\end{aligned}
$$

$$
\begin{aligned}
\zeta_1 &= \frac{1}{2}h^2\hat{A}^2 + h\chi_1 + 1, \\
\zeta_2 &= h\chi_1(h^2\hat{A}^2 + 2), \\
\zeta_3 &= \frac{1}{2}h^2\hat{A}^2 - h\chi_1 + 1, \\
\zeta_4 &= \frac{1}{2}h^2\chi_3 + h\chi_2 + 1, \\
\zeta_5 &= h(h^2\hat{A}\beta_0^2 + 2\chi_2), \\
\zeta_6 &= \frac{1}{2}h^2\chi_3 - h\chi_2 + 1, \\
\zeta_7 &= 2h\chi_4,
\end{aligned}
$$

$$
\begin{aligned}
\Omega_1 &= \frac{\zeta_1 - \zeta_4}{\zeta_3 - \zeta_6}, \\
\Omega_2 &= \frac{\zeta_2 - \zeta_5}{\zeta_3 - \zeta_6}.
\end{aligned}
$$

A.4 The integrals H_j and terms ξ_0, Ai_0, Ai_0' and k

The integrals H_j and terms ξ_0, Ai_0, Ai_0' and k appearing in sections 5.5 and 5.6

$$\delta_1 = \left.\frac{\partial C_1}{\partial \xi}\right|_{\xi=\xi_0},$$

$$\hat{D} = \frac{4}{3}i + \frac{2}{3}\left(\beta_1 Ai_0/k\Delta^{2/3}\right) D,$$

$$D = 1 + k\xi_0/Ai_0',$$

$$\hat{I} = \int_{\tilde{\lambda}}^{0} U_B^{-2}(Y_1)\,\mathrm{d}Y_1,$$

$$\tilde{I} = \int_{\tilde{\lambda}}^{0} U_B^{-3}(Y_1)\,\mathrm{d}Y_1,$$

$$H_1 = \int_0^Y U_B^2(x,Y_1)\,\mathrm{d}Y_1,$$

$$H_2 = \int_{\tilde{\lambda}}^{Y} U_B^{-2}(x,Y_1)\,\mathrm{d}Y_1,$$

$$H_3 = \int_0^Y U_B^2(x,Y_1) \int_{\tilde{\lambda}}^{Y_1} \frac{\mathrm{d}Y_2\,\mathrm{d}Y_1}{U_B^2(x,Y_2)},$$

$$H_4 = \int_0^Y U_B(x,Y_1)\,\mathrm{d}Y_1,$$

$$H_5 = U_B(x,Y) \int_0^Y U_B^{-2}(x,Y_1) \int_0^{Y_1} U_B^2(x,Y_2)\,\mathrm{d}Y_2\,\mathrm{d}Y_1,$$

$$H_6 = \int_{\tilde{\lambda}}^{Y} U_B^{-3}(x,Y_1)\,\mathrm{d}Y_1 + \int_{\tilde{\lambda}}^{Y} U_B^{-2}(x,Y_1) \frac{\partial U_B}{\partial Y_1}(x,Y_1) \int_{\tilde{\lambda}}^{Y_1} U_B^{-2}(x,Y_2)\,\mathrm{d}Y_2\,\mathrm{d}Y_1,$$

$$H_7 = \int_0^Y U_B^{-2}(x,Y_1) \int_0^{Y_1} U_B^2(x,Y_2) \int_{\tilde{\lambda}}^{Y_2} U_B^{-2}(x,Y_3)\,\mathrm{d}Y_3\,\mathrm{d}Y_2\,\mathrm{d}Y_1,$$

$$H_8 = 2\int_0^Y U_B^{-2}(x,Y_1) \int_0^{Y_1} U_B(x,Y_2)\,\mathrm{d}Y_2\,\mathrm{d}Y_1 + U_B^{-1}(x,Y) \int_0^Y U_B^{-2}(x,Y_1) \int_0^{Y_1} U_B^2(x,Y_2)\,\mathrm{d}Y_2\,\mathrm{d}Y_1$$
$$-2\int_0^Y U_B^{-3}(x,Y_1) \int_0^{Y_1} U_B^2(x,Y_2)\,\mathrm{d}Y_2\,\mathrm{d}Y_1,$$

$$
\begin{aligned}
H_9 &= 2\int_{\tilde{\lambda}}^{Y} U_B^{-2}(x,Y_1)\frac{\partial U_B}{\partial Y_1}(x,Y_1)\int_{\tilde{\lambda}}^{Y_1} U_B^{-3}(x,Y_2)\,\mathrm{d}Y_2\,\mathrm{d}Y_1 + \int_{\tilde{\lambda}}^{Y} U_B^{-4}(x,Y_1)\,\mathrm{d}Y_1,\\
H_{10} &= \int_{0}^{Y} U_B(x,Y_1)\int_{\tilde{\lambda}}^{Y_1} U_B^{-2}(x,Y_2)\,\mathrm{d}Y_2\,\mathrm{d}Y_1,\\
H_{11} &= \int_{0}^{Y} U_B^{2}(x,Y_1)\int_{0}^{Y_1} U_B^{-2}(x,Y_2)\int_{0}^{Y_2} U_B^{2}(x,Y_3)\,\mathrm{d}Y_3\,\mathrm{d}Y_2\,\mathrm{d}Y_1,\\
H_{12} &= \int_{0}^{Y} U_B^{2}(x,Y_1)\left[\int_{\tilde{\lambda}}^{Y_1} U_B^{-2}(x,Y_2)\frac{\partial U_B}{\partial Y_2}(x,Y_2)\int_{\tilde{\lambda}}^{Y_2} U_B^{-2}(x,Y_3)\,\mathrm{d}Y_3 + \int_{\tilde{\lambda}}^{Y_1} U_B^{-3}(x,Y_2)\right]\mathrm{d}Y_2\,\mathrm{d}Y_1,
\end{aligned}
$$

$$
\begin{aligned}
H_{1Y}|_{Y\to 0} &= 0,\\
(U_B H_2)_Y\Big|_{Y\to 0} &= U_{BY}\Big|_{Y\to 0}\hat{I},\\
H_{3Y}|_{Y\to 0} &= 0,\\
H_{4Y}|_{Y\to 0} &= 0,\\
H_{5Y}|_{Y\to 0} &= 0,\\
(U_B H_6)_Y\Big|_{Y\to 0} &= 2U_{BY}\Big|_{Y\to 0}\tilde{\tilde{I}},\\
H_{7Y}|_{Y\to 0} &= 0,\\
H_{8Y}|_{Y\to 0} &= 0,\\
(U_B H_9)_Y\Big|_{Y\to 0} &= 2U_{BY}\Big|_{Y\to 0}\tilde{\tilde{I}},\\
\xi_0 &\sim (-1.9893,-1.1485),\\
Ai_0 &= (0.7248,-0.9569),\\
Ai_0' &= (1.2677,1.2250),\\
k &= (1.7096,0.4266).
\end{aligned}
$$

A.5 The full system of governing equations for the triple-deck

In order to obtain the full set of neutral stability parameters β_i and K_i we apply a rather different approach. In the lower deck we have ten unknown parameters $A_i = A_i(x)$, $P_i = P_i(x)$ $(i = 1, \ldots, 4)$ and A_{4L}, P_{4L}, representing the pressure and negative displacement perturbations respectively. We can solve the lower deck system of equations numerically; in order to do this, it is necessary to eliminate these unknown functions.

Matching the main deck disturbance velocities u_i $(i = 1, \ldots, 4)$ (5.23) - (5.27) with the lower deck ones U_i $(i = 1, \ldots, 4)$ as $Y \to 0$ and $Z \to \infty$ gives

$$\begin{aligned} u_1 &= U_1 = \mathcal{B}_1 A_1, \\ u_2 &= U_2 = \mathcal{B}_1 A_2 + \mathcal{B}_2 A_1, \\ u_3 &= U_3 = \mathcal{B}_1 A_3 + \mathcal{B}_2 A_2 + \mathcal{B}_3 A_1, \\ u_4 &= U_4 = \mathcal{B}_1 A_4 + \mathcal{B}_2 A_3 + \mathcal{B}_3 A_2 + \mathcal{B}_4 A_1, \end{aligned} \tag{A.1}$$

where A_i $(i = 1, \ldots, 4)$ are unknown functions of x. The operators $\mathcal{B}_i$ $(i = 1, \ldots, 4)$ are defined as follows:

$$\begin{aligned} \mathcal{B}_1 &= \lambda, \\ \mathcal{B}_2 &= -\lambda(\mathcal{P}_1 \hat{I} + K_2 K_1^{-1}), \\ \mathcal{B}_3 &= -\lambda(\mathcal{P}_2 \hat{I} + 2\beta_1 \tilde{I} - K_2^2 K_1^{-2} + K_3 K_1^{-1}), \\ \mathcal{B}_4 &= -\lambda(2\beta_1 \mathcal{P}_2 \tilde{I} - 2\beta_1 K_2 K_1^{-1} \tilde{I} - 6\beta_1^2 K_1^{-1} \tilde{I} + 2\beta_2 \tilde{I} - \\ &\quad K_2 K_1^{-1} + K_4 K_1^{-1} + K_2^2 K_1^{-2} - K_3 K_2 K_1^{-2} + \mathcal{P}_3 \hat{I}) + i\lambda K_1^{-1} A_{1x}/A_1, \end{aligned} \tag{A.2}$$

where $\hat{I}$, $\tilde{I}$ and the integrals $H_j = H_j(x, Y)$ $(j = 1, \ldots, 12)$ which are functions of x and Y, are defined in Appendix B.4.

The unknown functions P_i $(i = 1, \ldots, 4)$ in equations (5.16) can be rewritten considering (5.31) as follows:

$$\begin{aligned} P_1 &= \mathcal{P}_1 A_1, \\ P_2 &= \mathcal{P}_1 A_2 + \mathcal{P}_2 A_1, \\ P_3 &= \mathcal{P}_1 A_3 + \mathcal{P}_2 A_2 + \mathcal{P}_3 A_1, \\ P_{4L} &= \mathcal{P}_1 A_{4L}, \\ P_4 &= \mathcal{P}_1 A_4 + \mathcal{P}_2 A_3 + \mathcal{P}_3 A_2 + \mathcal{P}_4 A_1, \end{aligned} \tag{A.3}$$

where the operators $\mathcal{P}_i$ $(i = 1, \ldots, 4)$ are defined as follows:

$$\begin{aligned}
\mathcal{P}_1 &= K_1, \\
\mathcal{P}_2 &= K_1^2(H_{1\infty} - H_{2\infty}) - 2\beta_1, \\
\mathcal{P}_3 &= K_1^3(H_{2\infty}^2 - H_{1\infty}H_{2\infty} - H_{3\infty} + H_{5\infty}) + \beta_1 K_1(3H_{2\infty} - 2H_{4\infty} - H_{6\infty}) \\
&\quad + K_2K_1(H_{1\infty} - H_{2\infty}) + 2\beta_1 K_2 K_1^{-1} + \beta_1^2 K_1^{-1} - 2\beta_2, \qquad \text{(A.4)} \\
\mathcal{P}_4 &= K_1^4(H_{11\infty} - H_{7\infty}) + K_2^2(H_{1\infty} - H_{2\infty}) - \beta_1 K_1^2(H_{5\infty} + H_{8\infty} - H_{10\infty} + H_{12\infty}) \\
&\quad + 2K_3K_1(H_{1\infty} - H_{2\infty}) - 3K_2K_1^2(H_{3\infty} - H_{5\infty}) + \beta_1 K_2(H_{2\infty} + 2H_{4\infty} - H_{6\infty}) \\
&\quad + \beta_2 K_1(H_{2\infty} - 2H_{4\infty} - H_{6\infty}) + \beta_1^2(H_{6\infty} - H_{9\infty}) \\
&\quad - \mathcal{P}_2\left[K_1^2 H_{3\infty} + 2K_2H_{2\infty} + K_3K_1^{-1} - \beta_1(H_{2\infty} - H_{6\infty})\right] \\
&\quad - \mathcal{P}_3(K_1H_{2\infty} + K_2K_1^{-1}) + 3\beta_1\beta_2 K_1^{-1} - \beta_1 K_3 K_1^{-1} - \beta_1^2 K_2 K_1^{-2} - 2\beta_3 \\
&\quad - iK_1^{-1}(K_1A_1)_x/A_1 + iP_{1x}K_1^{-1}/A_1.
\end{aligned}$$

Following the same procedure as before, matching the disturbance concentrations solutions from the main and lower decks we obtain the following boundary conditions for C_i $(i = 1, \ldots, 4)$ as $Z \to \infty$:

$$\begin{aligned}
c_1 &= C_1 = \mathcal{C}_1 A_1, \\
c_2 &= C_2 = \mathcal{C}_1 A_2 + \mathcal{C}_2 A_1, \qquad \text{(A.5)} \\
c_3 &= C_3 = \mathcal{C}_1 A_3 + \mathcal{C}_2 A_2 + \mathcal{C}_3 A_1, \\
c_4 &= C_4 = \mathcal{C}_1 A_4 + \mathcal{C}_2 A_3 + \mathcal{C}_3 A_2 + \mathcal{C}_4 A_1,
\end{aligned}$$

where

$$\begin{aligned}
\mathcal{C}_1 &= \mu, \\
\mathcal{C}_2 &= -\mu\left(K_1H_2|_{Y\to\infty} + K_2K_1^{-1} + K_2K_1^{-1}\right), \qquad \text{(A.6)} \\
\mathcal{C}_3 &= -\mu\left(K_3K_1^{-1} + K_1\mathcal{P}_2H_2|_{Y\to 0} - K_2^2K_1^{-2}\beta_1 H_6|_{Y\to 0} - \beta_1\left(U_B^{-1}H_2\right)\Big|_{Y\to 0}\right).
\end{aligned}$$

Because of the nature of the coupling between normal disturbance velocity and the disturbance concentration gradient along the surface we shall limit our expansions to the third-order term.

The same procedure can be adopted for the disturbance velocity field. Using the above presentations we can rewrite the disturbance velocity terms in the lower deck in the following form, for the x-component:

$$\begin{aligned}
U_1(x, Z; A_1, A_2, A_3, A_4) &= U_{11}(x, Z; A_1), \\
U_2(x, Z; A_1, A_2, A_3, A_4) &= U_{21}(x, Z; A_2) + U_{22}(x, Z; A_1), \\
U_3(x, Z; A_1, A_2, A_3, A_4) &= U_{31}(x, Z; A_3) + U_{32}(x, Z; A_2) + U_{33}(x, Z; A_1), \qquad \text{(A.7)} \\
U_4(x, Z; A_1, A_2, A_3, A_4) &= U_{41}(x, Z; A_4) + U_{42}(x, Z; A_3) + U_{43}(x, Z; A_2) \\
&\quad + U_{44}(x, Z; A_1),
\end{aligned}$$

for y-component:

$$\begin{aligned}
V_1(x,Z;A_1,A_2,A_3,A_4) &= V_{11}(x,Z;A_1),\\
V_2(x,Z;A_1,A_2,A_3,A_4) &= V_{21}(x,Z;A_2)+V_{22}(x,Z;A_1),\\
V_3(x,Z;A_1,A_2,A_3,A_4) &= V_{31}(x,Z;A_3)+V_{32}(x,Z;A_2)+V_{33}(x,Z;A_1),\\
V_4(x,Z;A_1,A_2,A_3,A_4) &= V_{41}(x,Z;A_4)+V_{42}(x,Z;A_3)+V_{43}(Ax,Z;A_2)\\
&\quad +V_{44}(x,Z;A_1),
\end{aligned} \tag{A.8}$$

and disturbance concentrations terms as follows:

$$\begin{aligned}
C_1(x,Z;A_1,A_2,A_3,A_4) &= C_{11}(x,Z;A_1),\\
C_2(x,Z;A_1,A_2,A_3,A_4) &= C_{21}(x,Z;A_2)+C_{22}(x,Z;A_1),\\
C_3(x,Z;A_1,A_2,A_3,A_4) &= C_{31}(x,Z;A_3)+C_{32}(x,Z;A_2)\\
&\quad +C_{33}(x,Z;A_1),
\end{aligned} \tag{A.9}$$

where a column separator in the arguments denotes a parametric dependence.

Taking into account the linearity of the equations, the above separation, the form of the corresponding solutions in the main deck and the idea of the asymptotic expansions we can subtract from the system of equations (5.16) - (5.17) the terms depending only on A_1 and after normalisation of U_{ii}, V_{ii} and C_{ii} with A_1 $(i=1,\ldots,4)$ we end up with the following system of equations:
continuity:

$$\begin{aligned}
\mathcal{L}_1(U_{11},V_{11}) &= 0\\
\mathcal{L}_1(U_{22},V_{22}) &= -iK_2U_{11},\\
\mathcal{L}_1(U_{33},V_{33}) &= -i(K_2U_{22}+K_3U_{11}),\\
\mathcal{L}_1(U_{44},V_{44}) &= -i(K_2U_{33}+K_3U_{22}+K_4U_{11})+U_{11x}/A_1;
\end{aligned} \tag{A.10}$$

***x*-momentum**:

$$
\begin{aligned}
\mathcal{L}_2(U_{11},V_{11},\mathcal{P}_1) &= 0,\\
\mathcal{L}_2(U_{22},V_{22},\mathcal{P}_2) &= i\beta_2U_{11}-\lambda ZiK_2U_{11}-iK_2\mathcal{P}_1+\theta Sc^{-1}\lambda\mu Z\Big(\frac{1}{2}ZiK_1U_{11}+V_{11}\Big)\\
&\quad -\theta Sc^{-1}\mu U_{11Z},\\
\mathcal{L}_2(U_{33},V_{33},\mathcal{P}_3) &= i(\beta_2U_{22}+\beta_3U_{11})-\lambda Zi(K_2U_{22}+K_3U_{11})-i(K_2\mathcal{P}_2+K_3\mathcal{P}_1)\\
&\quad +\frac{1}{2}\theta Sc^{-1}\lambda\mu Z^2i(K_1U_{22}+K_2U_{11})-\frac{1}{2}\theta^2Sc^{-2}\lambda\mu^2Z^2\big(\frac{1}{3}ZiK_1U_{11}\\
&\quad +V_{11}\big)-\theta Sc^{-1}\mu U_{22Z}+\theta Sc^{-1}\lambda\mu ZV_{22},\\
\mathcal{L}_2(U_{44},V_{44},\mathcal{P}_4) &= i(\beta_2U_{33}+\beta_3U_{22}+\beta_4U_{11})-\lambda Zi(K_2U_{33}+K_3U_{22}+K_4U_{11})\\
&\quad -i(K_2\mathcal{P}_3+K_3\mathcal{P}_2+K_4\mathcal{P}_1)+\frac{1}{2}\theta Sc^{-1}\lambda\mu Z^2i(K_1U_{33} \qquad \text{(A.11)}\\
&\quad +K_2U_{22}+K_3U_{11})-\frac{1}{6}\theta^2Sc^{-2}\lambda\mu^2Z^3i(K_1U_{22}+K_2U_{11})\\
&\quad +\frac{1}{48}\lambda x^{-1}Z^4iK_1U_{11}+\frac{1}{24}\theta^3Sc^{-3}\lambda\mu^3Z^4iK_1U_{11}\\
&\quad -Z(\lambda U_{11})_x/A_1-P_{1x}/A_1+\frac{1}{6}\theta^3Sc^{-3}\lambda\mu^3Z^3V_{11}\\
&\quad +\frac{1}{12}\lambda x^{-1}Z^3V_{11}-\frac{1}{2}\theta^2Sc^{-2}\lambda\mu^2Z^2V_{22}\\
&\quad +\theta Sc^{-1}\lambda\mu ZV_{33}+\frac{1}{2}\lambda_xZ^2U_{11Z}-\theta Sc^{-1}\mu U_{33Z};
\end{aligned}
$$

and
concentration:

$$
\begin{aligned}
\mathcal{L}_3(C_{11},V_{11}) &= 0,\\
\mathcal{L}_3(C_{22},V_{22}) &= i\beta_2C_{11}-\lambda ZiK_2C_{11}+\frac{1}{2}\theta Sc^{-1}\lambda\mu Z^2iK_1C_{11}-\theta Sc^{-1}\mu C_{11Z}+\theta\mu^2ZV_{11},\\
\mathcal{L}_3(C_{33},V_{33}) &= i(\beta_2C_{22}+\beta_3C_{11})-\lambda Zi(K_2C_{22}+K_3C_{11})+\frac{1}{2}\theta Sc^{-1}\lambda\mu Z^2i\big(K_1C_{22}\\
&\quad +K_2C_{11}\big)-\frac{1}{6}\theta^2Sc^{-2}\lambda\mu^2Z^3iK_1C_{11}-\theta Sc^{-1}\mu C_{22Z}-\frac{1}{2}\theta^2\mu^3Z^2V_{11}\\
&\quad +\theta\mu^2ZV_{22}, \qquad \text{(A.12)}\\
\mathcal{L}_3(C_{44},V_{44}) &= i(\beta_2C_{33}+\beta_3C_{22}+\beta_4C_{11})-\lambda Zi(K_2C_{33}+K_3C_{22}+K_4C_{11})\\
&\quad +\frac{1}{2}\theta Sc^{-1}\lambda\mu Z^2i(K_1C_{33}+K_2C_{22}+K_3C_{11})+\frac{1}{12}Sc\lambda\mu x^{-1}Z^4iK_1C_{11}\\
&\quad -\frac{1}{6}\theta^2Sc^{-2}\lambda\mu^2Z^3i(K_1C_{22}+K_2C_{11})+\frac{1}{24}\theta^3Sc^{-3}\lambda\mu^2Z^4iK_1C_{11}\\
&\quad -Z\lambda C_{11x}/A_1-\mu_xZU_{11}+\frac{1}{2}\lambda_xZ^2C_{11Z}-\theta Sc^{-1}\mu C_{33Z}+\frac{1}{6}\theta^3\mu^4Z^3V_{11}\\
&\quad +\frac{1}{12}Sc\lambda\mu x^{-1}Z^3V_{11}-\frac{1}{2}\theta^2\mu^3Z^2V_{22}+\theta\mu^2ZV_{33}.
\end{aligned}
$$

We have omitted the critical layer equations for U_{4L}, V_{4L} and C_{4L}, the same can be done for them but it is easier to normalise with A_{4L}. The resulting system can be solved

independently knowing the values of K_1 and β_1. We will note that the first eigenrelation (defining K_1 and β_1) and that one defining K_{4L} and β_{4L} are unmodified and their values are known.

The set of boundary conditions for the system (A.11) - (A.12) considering (5.19) and (A.1) - (A.9) is

$$\begin{aligned}
Z = 0: \quad & U_{11} = U_{22} = U_{33} = U_{44} = 0, \\
& V_{11} = 0, V_{22} = \frac{\partial C_{11}}{\partial Z}, V_{33} = \frac{\partial C_{22}}{\partial Z}, V_{44} = \frac{\partial C_{33}}{\partial Z}, \\
& C_{11} = C_{22} = C_{33} = 0; \\
Z \to \infty: \quad & U_{11} = \mathcal{B}_1, U_{22} = \mathcal{B}_2, U_{33} = \mathcal{B}_3, U_{44} = \mathcal{B}_4, \\
& U_{11Z} = U_{22Z} = U_{33Z} = U_{44Z} = 0. \\
& C_{11Z} = C_{22Z} = C_{33Z} = 0.
\end{aligned} \tag{A.13}$$

A.6 The matrix form of Rayleigh equation

The matrices **A** and **B** in equation (6.30)

$$\mathbf{A} = \begin{pmatrix} b_1 & a_1 & & & & & & & \\ a_2 & b_2 & a_2 & & & & & & \\ & a_3 & b_3 & a_3 & & & & & \\ & & \ddots & & & & & & \\ & & & a_i & b_i & a_i & & & \\ & & & & \ddots & & & & \\ & & & & & a_{N-3} & b_{N-3} & a_{N-3} & \\ & & & & & & a_{N-2} & b_{N-2} & a_{N-2} \\ & & & & & & & 2a_{N-1} & q_{N-1} \end{pmatrix}$$

and

$$\mathbf{B} = \begin{pmatrix} d_1 & c_1 & & & & & & & \\ c_2 & d_2 & c_2 & & & & & & \\ & c_3 & d_3 & c_3 & & & & & \\ & & \ddots & & & & & & \\ & & & c_i & d_i & c_i & & & \\ & & & & \ddots & & & & \\ & & & & & c_{N-3} & d_{N-3} & c_{N-3} & \\ & & & & & & c_{N-2} & d_{N-2} & c_{N-2} \\ & & & & & & & 2c_{N-1} & p_{N-1} \end{pmatrix},$$

where

$$\begin{aligned} a_i &= F_i, \quad i = 1, \ldots, N-1, \\ b_i &= -2F_i - h^2(F_i\alpha^2 + F_i''), \\ c_i &= 1, \\ d_i &= -2 - \alpha^2 h^2, \\ q_{N-1} &= b_{N-1} - 2\alpha h a_{N-1}, \\ p_{N-1} &= d_{N-1} - 2\alpha h. \end{aligned}$$

List of Tables

List of Figures

BIBLIOGRAPHY

Abramowitz M. and Stegun I. A., (1972), *Handbook of Mathematical Functions*, Dover Publications, Inc., 877.

Astarita G., (1967), *Mass Transfer with a Chemical Reaction*, Elsevier, New York.

Bassom A. P., (1989), Weakly nonlinear lower-branch stability of fully developed and developing free-surface flows, *IMA J. Appl. Math.*, **42**, 269–301.

Batchelor G. K., (1970), *An Introduction to Fluid Dynamics*, Cambridge University Press.

Berzin I. S. and Zhidkov N. P., (1965), *Computing Methods*, Vol. II, Pergamon, Oxford.

Bird R. B., Stewart W. E. and Lightfood E. N., (1966), *Transport Phenomena*, John Wiley and Sons, Inc., 564–565.

Blottner F. G., (1975), Investigations of some finite-difference techniques for solving the boundary layer equations, *Comp. Meth. App. Math. Engin.*, **6**, 1–30.

Boyadjiev C. B., (1982), Non-linear mass transfer in falling films, *Int. J. Heat Mass Trans.*, **25**, (4), 535–540.

Boyadjiev C. B., (1984), Influence of some non-linear effects on the mass transfer kinetics in falling liquid films, *Int. J. Heat Mass Trans.*, **27**, (8), 1277–1280.

Boyadjiev C. B., (1990a), Asymptotic theory of non-linear transport phenomena. II. Heat transfer, *Hung. J. Ind. Chem.*, **18**, 1–7.

Boyadjiev C. B., (1990b), Asymptotic theory of non-linear transport phenomena. III. Multicomponent mass transfer, *Hung. J. Ind. Chem.*, **18**, 7–13.

Boyadjiev C. B., (1990c), Non-linear mass transfer between gas and liquid film flow. I. Numerical analysis, *Journal of Eng. Physics*, **59**, 92–98.

Boyadjiev C. B., (1990d), Non-linear mass transfer between gas and liquid film flow. II. Asymptotic analysis, *Journal of Eng. Physics*, **59**, 277–286.

Boyadjiev C. B., (1992), On the kinetics of the intensive interphase mass transfer, *Russian J. Eng. Thermophysics*, **2**, (4), 289–297.

Boyadjiev C. B., (1996), On the theory of non-linear mass transfer in systems with intensive inter-phase mass transfer, *Hung. J. Ind. Chem.*, **24**, 35–39.

Boyadjiev C. B., (1998), Non-linear interphase mass transfer in multi-component gas–liquid systems, *Hung. J. Ind. Chem.*, **26**, 33.

Boyadjiev C. B. and Babak V. N., (2000), *Non-linear Mass Transfer and Hydrodynamic Stability*, Elsevier Science, Amsterdam.

Boyadjiev C. B. and Beshkov V., (1984), *Mass Transfer in Following Liquid Films*, Publ. House Bulg. Acad. Sci., Sofia.

Boyadjiev C. B., Halatchev I. A. and Tchavdarov B., (1996a), The linear stability in systems with intensive inter-phase mass transfer–I. Gas(liquid)–solid, *Int. J. Heat Mass Trans.*, **39**, (12), 2571–2580.

Boyadjiev C. B. and Halatchev I. A., (1996b), The linear stability in systems with intensive inter-phase mass transfer–II. Gas–liquid, *Int. J. Heat Mass Trans.*, **39**, (12), 2581–2585.

Boyadjiev C. B. and Halatchev I. A., (1996c), The linear stability in systems with intensive inter-phase mass transfer–IV. Gas–liquid film flow, *Int. J. Heat Mass Trans.*, **39**, (12), 2593–2597.

Boyadjiev C. B. and Halatchev I. A., (1998a), Non-linear mass transfer and Marangoni effect in gas–liquid systems, *Int. J. Heat Mass Trans.*, **41**, (1), 197–202.

Boyadjiev C. B. and Halatchev I. A., (1998b), The mass transfer and stability in systems with large concentration gradients - I. Mass transfer kinetics, *Int. J. Heat Mass Trans.*, **41**, (6-7), 939–944.

Boyadjiev C. B. and Toshev E., (1989), Asymptotic theory of non-linear transport in boundary layers. I. Mass transfer, *Hung. J. Ind. Chem.*, **17**, 457–465.

Boyadjiev C. B. and Vulchanov N. L., (1988), Non-linear mass transfer in boundary layers. 1. Asymptotic theory, *Int. J. Heat Mass Trans.*, **31**, (4), 795–800.

Boyadjiev C. B. and Vulchanov N. L., (1990), Influence of the intensive inter-phase mass transfer on the rate of mass transfer – 1. The system "solid-fluid(gas)" *Int. J. Heat Mass Trans.*, **33** (9), 2039–2044.

Brown S. N., (1996), *Laminar Boundary Layers and Separation*, Research Trends in Fluid Dynamics, American Institute of Physics (1996) 43–54.

Brian P. L., Vivian J. E. and Matiatos D. C., (1967), Interfacial turbulence during the

absorption of carbon dioxide into monoethanoaline, *AIChE J.*, **13** (1), 28–36.

Catherall D. and Mangler K. W., (1966), The investigation of the two-dimensional laminar boundary-layer equations past the point of vanishing skin friction, *J. Fluid Mech.*, **26**, 163–182.

Catherall D., Stewartson K. and Williams P. G., (1965), Viscosity flow past a flat plate with uniform injection, *Proc. R. Soc. Lond.*, A, 284, 370–396.

Chang P. K., (1970), *Separation of Flow*, Pergamon Press Inc., 5.

Cole J. D. and Aroesty J., (1968), The blowhard problem–inviscid flows with surface injection, *Int. J. Heat Mass Trans.*, **11**, 1167–1183.

Drazin P. G. and Reid W. H., (1981), *Hydrodynamic Stability*, Cambridge University Press, 311-317.

Emmons H. W. and Leigh D., (1954), Transition of the Blasius function with blowing and suction, *Aero. Res. Counc. Current Paper*, 157.

Feron P. and Slot G. S., (1991), The influence of separators on hydrodynamics and mass transfer in narrow cells: flow visualisation, *Distillation*, **84**, 137-152.

Fletcher C. A. J., (1988), *Computational Techniques for Fluid Dynamics*, Volume II, Springer-Verlag, 200–247.

Gadd G. E., Jones C. E. and Watson E. J., (1963), *Laminar boundary layers*, Oxford University Press Ch. V.

Gaster M., (1974), On the effect of boundary-layer growth on flow stability, *J. Fluid Mech.*, **66**, 465–480.

Gebhart B., Bau H., Greif R., Jaluria Y., Mahajan R. L. and Viskanta R., (1996), *Thermal and Mass Diffusion Driven Flows*, Research Trends in Fluid Dynamics, American Institute of Physics, 77–91.

Golub G. H. and Van Loan C. F., (1982), *Matrix Computations*, John Hopkins University Press, New York/London.

Grassman P. and Anders G., (1959), Abhangigkeit des Stoffaustausche von der Austauschrichtung, *Chemie-Ing.-Techn.*, **31**, (3), 154–154.

Hadamard J., (1952), *Lectures on Cauchy's Problem in Linear Partial Differential*

Equations, Yale University Press, New Haven, 133–141.

Halatchev I. A. and Boyadjiev C. B., (1996), The linear stability in systems with intensive inter-phase mass transfer–III. Liquid–Liquid, *Int. J. Heat Mass Trans.*, **39**, (12), 2587–2592.

Halatchev I. A. and Boyadjiev C. B., (1998), The mass transfer and stability in systems with large concentration gradients - II. Hydrodynamic stability, *Int. J. Heat Mass Trans.*, **41**, (4-7), 945–949.

Halatchev I. A. and Denier J. P., (2000), Stability of boundary-layer flows under conditions of intensive interfacial mass transfer: the effect of interfacial coupling, *Int. J. Heat Mass Trans.* (*accepted*).

Halatchev I. A. and Denier J. P., On diffusion induced separation and inviscid instabilities, *Int. J. Heat Mass Trans.* (*to be submitted*).

Hartnett J. P. and Eckert E. R. G., (1957), Mass-transfer cooling in a laminar boundary layer with constant fluid properties, *Trans. of ASME*, **79**, 247–254.

Hennenberg M., Bisch P. M., Vignes-Adler M. and Sanfeld A., (1979), Interfacial instability and longituidal waves in liquid–liquid systems, *Lecture Note in Physics*, Springler-Verlag, Berlin, **105**, 229.

Incropera F. P. and DeWitt D. P., (1990), *Fundamentals of Heat and Mass Transfer*, John Wiley & Sons, 312-369.

Jordinson R, (1970), The flat plate boundary layer. Part 1. Numerical integration of the Orr-sommerfeld equation, *J. Fluid Mech.*, **43**, 801–811.

Joseph D. D., (1976), *Stability of Fluid Motion*, Springer-Verlag, New York.

Joseph D. D. and Renardy Y. Y., (1993), *Fundamentals of Two-Fluid Dynamics. Part 1 and 2: Mathematical Theory and Applications*, Springer Verlag New York, Interdisciplinary Applied Mathematics Series vol. 3 and 4.

Keller H. B., (1976), *Numerical Solution of Two-Point Boundary Value Problems*, SIAM Regional Conference Series in Applied Mathematics, Philadelphia: Society for industrial and Applied Mathematics, 56-58.

Kerner W., (1989), Large-scale complex eigenvalue problems, *J. Comput. Phys*, **85**, 1–85.

Klemp J. and Acrivos A., (1972), High Reynolds number flow past a flat plate with

strong blowing, *J. Fluid Mech.*, **51**, 337–356.

Kundu P. K., (1990), *Fluid Mechanics*, Academic Press, Inc.

Levich V. G., (1962), *Physiochemical Hydrodynamics*, Prentice-Hall, Inc., Englewood Cliffs, N.J.

Lin C. C., (1955), *The Theory of Hydrodynamic Stability*, Cambridge University Press.

Linde H., Schwartz E. and Gröeger K., (1967), Zum auftreten des oszillatorischen regimes der Marangoni-instabilität biem stoffübergang, *Chem. Eng. Sci.*, **22**, 823–836.

Linde H., Schwartz E. and Wilke H., (1979), Dissipative structures and nonlinear kinetics of the Marangoni-instability, *Lecture Note in Physics*, Springler-Verlag, Berlin, **105**, 75.

Mauss J., (1994), Asymptotic modelling for separating boundary layers,*Lecture Note in Physics*, Asymptotic Modelling in Fluid Mechanics, Proceedings, 239–254.

Na T. Y., (1979), *Computational Methods in Engineering Boundary Value Problems*, Academic Pres, Inc, New York, 30–51.

Napolitano M. and Messick R. E., (1980), On strong slot-injection into a subsonic laminar boundary layer, *Comput. Fluids*, **8**, 199–212.

Pereyra V., (1979), An adaptive finite-difference Fortran program for first order nonlinear, ordinary boundary problems, In: *Codes for Boundary Value Problems in Ordinary Differential Equations - Lecture Notes in Computer Science*, **76**, 64–77.

Porter K. E., Cantwell A. D. C. and McDermott C., (1971), Absorption and desorption accompanied by a reversible reaction, *AIChE J.*, **17**, 536–541.

Potter O. E., (1957), Mass transfer between co-current fluid streams and boundary layer solutions, *Cem. Eng. Sci.*, **6**, 170–182.

Prandtl L., (1904), Über Flüssigkeitsbewegung bei sehr kleiner Reibung, *Proc. 3rd Int. Math. Congr.*

Ramm V. M., (1976), *Gas Absorption*, Himia, Moscow.

Reid W. H., (1965), *Basic Developments in Fluid Dynamics*, vol. 1, New York Academic Press.

Renardy Y. Y., Coward A. V., Papageorgiou D. and Sun S. M., (1996), *Advances in Multi-Fluid Flows*, Society for Industrial and Applied Mathematics Proceedings in Applied Mathematics **86**.

Roy S. M., (2000), Nonuniform slot injection (suction) into a compressible flow, *Acta Mechanica*, **139**, 43–56.

Ruckenstein F. and Berbente C., (1964), The occurence of interfacial turbulence in the case of diffusion accompanied by chemical reaction, *Chem. Eng. Sci.*, **19**, 329–347.

Sanfeld A., Steinchen A., Hennenberg M., Bisch P. M., Van Lamswerde D. and Dall-Vedove W., (1979), *Mechanical and Electrical Constants and Hydrodynamic Interfacial Instability, Lecture Note in Physics*, Springler-Verlag, Berlin, **105**, 168.

Sapundjiev T. N. and Boyadjiev C. B., (1993), Non-linear mass transfer in liquid-liquid systems, *Russian J. Eng. Thermophysics*, **3**, (2), 185–198.

Savistowski H., (1981), Interfacial convection, *Ber. Bunsenges Phys. Chem.*, **85**, 905.

Schetz J. A., (1984), *Foundations of Boundary Layer Theory for Momentum, Heat and Mass Transfer*, Prentice-Hall, Inc., Englewood Cliffs, New Jersey, 75–78.

Schlichting H., (1979), *Boundary-Layer Theory*, McGraw-Hill, Inc., 467.

Sherwood T. K., Pigford R. L. and Wilke C. R., (1975), *Mass Transfer*, McGraw-Hill, New York.

Skelland A. H., (1974), *Diffusional Mass Transfer*, John Wiley & Sons, Toronto.

Smith F. T., (1979a), On the non-parallel flow stability of the Blasius boundary layer, *Proc. R. Soc. Lond.*, A, **366**, 91–109.

Smith F. T., (1979b), Nonlinear stability of boundary layers for disturbances of various sizes, *Proc. R. Soc. Lond.*, A, **368**, 573–589.

Smith F. T., (1982), On the high Reynolds number theory of laminar flows, *IMA J. App. Math.*, **28**, 207–281.

Smith F. T. and Stewartson K., (1973), Plate-injection into a separated supersonic boundary layer, *J. Fluid Mech.*, **58**, 143–158.

Sorensen T. S., (1979), *Lecture Note in Physics*, Springler-Verlag, Berlin, **105**, 1–74.

Sorensen T. S. and Henennberg M., (1979), Instability of a Spherical Drop with Surface Chemical Reaction and Transfer of Surfactants, *Lecture Note in Physics*, Springler-Verlag, Berlin, **105**, 276.

Sterling C. V. and Scriven L. E., (1959), Interfacial turbulence: hydrodynamic instability and the Marangoni effect, *AIChE J.*, **5**, 514–523.

Stewartson K., (1974), Multi-structured boundary layers on flat plates and related bodies, *Adv. Appl. Mech.*, **14**, 145–239.

Stuart J. T., (1963), *Laminar Boundary Layers*, Oxford University Press, Ch. 9.

Sychev V. V., Ruban A. I., Sychev V. V., and Korolev G. L., (1998), *Asymptotic theory of separated flows*, CUP.

Thomas W. T. and Nicholl E. Mc K., (1969), Interfacial turbulence accompanying absorption with reaction, *Trans. Inst. Chem. Eng.*, **47**, 325–331.

Ting L., (1959), On the mixing of two parallel streams, *J. Math. and Phys.*, **38**, 153–165.

Tollmien W., (1929), Nachr. Ges. Wiss. Göttingen, *Maths. Phys. Klasse*, **22**, (44), (Translated by *N.A.C.A. tech. Memo.* **609**).

Van Stijn T. L., (1982), On the stability of almost parallel boundary-layer flows, *Comput. & Fluids*, **10**, 223–241.

Van Stijn T. L., (1983), *Stability of Almost Parallel Boundary Layer Flows*, PhD Thesis, Royal University of Groningen.

Vulchanov N. L. and Boyadjiev C. B., (1988), Non-linear mass transfer in boundary layers - 2. Numerical investigation, *Int. J. Heat Mass Trans.*, **31**, (4), 801–805.

Vulchanov N. L. and Boyadjiev C. B., (1990), Influence of the interphase mass transfer on the mass transfer rate – 2. The system "gas–liquid", *Int. J. Heat Mass Trans.*, **33**, (9), 2045–2049.

Zierp J. and Oertel H., (1981), *Convective Transport and Instability Phenomena*, Braun Verlag, Karalsruhe.